THE OPTOGALVANIC EFFECT IN MOLECULAR DISCHARGES AND THE STABILIZATION OF CO_2 LASERS

S. Moffatt

A Thesis Submitted for the Degree of PhD
at the
University of St Andrews

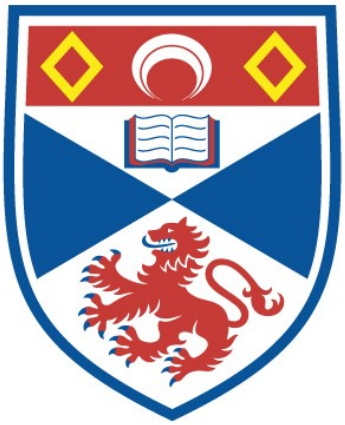

1983

THE OPTOGALVANIC EFFECT IN MOLECULAR DISCHARGES AND THE STABILIZATION OF CO_2 LASERS

- A thesis prepared for the Degree of Doctor of Philosophy for the University of St. Andrews.

S. Moffatt
5.2.83

- ABSTRACT -

The optical perturbation of discharge current voltage characteristics (optogalvanic effect or OGE) has been investigated for CO_2 and CO laser discharges. A quantitative power perturbation model is constructed and a series of experiments show a close agreement for changes of all the major operating parameters of the CO_2 laser. The theory consists of an evaluation of the microscopic kinetic relaxation processes leading to the changes in thermal balance of the discharge that occur due to the absorption and amplification of the resonant laser radiation. A generation of compact and efficient cw CO_2 lasers has been developed which produces higher stable output powers per unit length than previously reported, and these have been actively stabilized by OGE to provide a high degree of frequency stability ($\lesssim$ 50 kHz) and amplitude stability ($\lesssim$ 0.5%) which is a six orders and two orders of magnitude improvement over the passive resonator capability, respectively. New optogalvanic effects have been discovered both at high frequencies (up to 100 kHz) and for sequence (00^02) laser transitions in CO_2 and also in the cw CO laser. Preliminary investigation of optogalvanic detection of standing wave saturation resonances in low pressure discharged CO_2 have been carried out and some analysis of discharge noise has been necessary to evaluate the ability of such a narrow band detector for laser stabilization.

The empirical evidence provided by the temporal response of OGE combined with the gas composition dependence (including N_2 free mixtures) proves conclusively that no major ionization mechanism described so far can be responsible for the effect. A thermal explanation of the effect due to modified kinetic cooling of the laser gas has been developed from existing qualitative explanations. This proposed "gas temperature" power perturbation model provides for the first time, an accurate ($\sim$ 20%) prediction of perturbations (amplitude, phase, and frequency) due to the resonant interaction of a CO_2 laser beam over a wide range (up to 4 orders of magnitude) of detailed parametric changes, with a CO_2 or laser mixture discharge.

BIOGRAPHICAL NOTE

Stephen Moffatt is a physicist with Applied Implant Technology, a subsidiary of Applied Materials Inc. of Santa Clara, California and Horsham, Sussex. He received a B.A. in Physics and an M.Sc. in Optoelectronics from the University of Essex in 1975 and 1977 respectively. During this period he concentrated on laser and solid state projects including CO_2 laser modulation with Ge and far infrared laser research.

Prior to this Ph.D. work he had worked in UK industry for Shell Research Ltd., Decca Radar, EMI Varian and Gresham Lion Ltd., on a variety of projects including arc phenomena and wideband amplification. Recently he has worked at the universities of Strathclyde and Surrey as a Research Fellow in laser physics and the interaction of laser, electron and ion beams with materials including $LiNbO_3$, Si, GaAs and InP.

Born in 1954 in the north of England, he spent a large part of his childhood in Canada. He is married with one daughter and his leisure interests include the foundations of language, oil painting, Jaguar cars and tennis.

- "Would it be correct to say, 'it is difficult to say what real exactness is, for all we know is only rough approximations'?"

Ludwig Wittgenstein, The Brown Book I(4) (1934-35)

PREFACE

The experimental physics carried out and described in this thesis took place between 1977 and 1981. The majority was performed in the Department of Physics at the University of St. Andrews and a part of the work (mainly described in chapters 8 and 9) was undertaken in the Natural Philosophy Department of the University of Strathclyde, Glasgow. During the period of the experimental work, optogalvanic laser spectroscopy became a subject of considerable interest, and I found that I was working in a 'fashionable' and exciting area. The subject of concern, here, is a molecular discharge optogalvanism as distinct from the ionization optogalvanic effects which have been studied in great detail for atomic discharges. I would recommend any reader with little knowledge of the CO_2 laser to read Appendix I first.

The entire work represents the ideas, frustrations and satisfaction of experimental physics, a practice which I have adopted as a large fraction of my life. In this sense, despite its attempted objectivity, this is also a personal work.

S. Moffatt
Byfleet, Surrey
5.2.83

ACKNOWLEDGEMENTS

I would like to thank many people who have helped and encouraged this work; it is not possible to mention all of their names but I particularly want to extend my gratitude to the following who made significant contributions, Frits Akerboom, and Donald Cringean for their expert glassblowing in quartz without which the experimental work would not have been possible, N.F. Campbell for the precise mechanical engineering required in the construction of the lasers and M. Robertson and his colleagues for the construction and design of some of the electronic circuitry. I would also like to thank Edinburgh Instruments, particularly Peter Maggs, Roger Sandwell, Mike Bennett and John MacIntosh for assistance in all practical aspects of the work and for the loan of equipment. Thanks are also due to Professor S.D. Smith, Andrew Wood and Alec Vass of Herriot Watt University and P.G. Brown of Barr and Stroud Ltd., Glasgow, for the loan of facilities and equipment. The expert advice of G.E. Murray, B. Norris and H. Shields is gratefully acknowledged and the considerable assistance provided by John Mellis whose work forms an essential part of the overall pattern of the research of which this is a contribution.

I would like to acknowledge the long standing support of A.L.S. Smith, my supervisor, and the encouragement, efficient preparation and typing of the manuscript by my wife, Rosemary Chard. Finally, I thank the Science Research Council and Edinburgh Instruments for the financial support necessary for the experimental work and the Universities of Herriot Watt, Strathclyde and St. Andrews for the provision of facilities.

STATEMENTS AND DECLARATION

(i) I declare that this thesis has been composed by myself, that the original work of which it is a record has been done by myself, and that it has not been accepted in any previous application for a higher degree.

5.2.83 .....

(ii) This thesis is a record of the research work done by myself following admission as a research student, under ordinance general no.12, on October 12th, 1977, into the United College of St. Salvator and St. Leonard, of the University of St. Andrews, Scotland. I was admitted under resolution of the University Court, 1967, no.1 as a candidate for the Degree of Doctor of Philosophy on October 10th, 1978, after spending two terms as a full time research student in the Department of Physics under the supervision of Professor A.L.S. Smith.

.....5.2.83.....

(iii) I have supervised Stephen Moffatt as a research student for the Physics Department, University of St. Andrews, and to my knowledge all the conditions of the resolution and regulations have been fulfilled.

.....5.2.83.....

CONTENTS

1.0 INTRODUCTION

Perturbations of the electrical parameters of gases due to irradiation with light have been studied for over fifty years and with the availability of intense, coherent and sometimes tunable light from lasers, a resurgence of interest in several mechanisms, leading to optically induced discharge perturbation has occurred during the last fifteen years. This has resulted in direct electrical detection of electromagnetic radiation in molecular and atomic discharges with a high resolution capability, now known as the optogalvanic effect.

Of the many available cw lasers, the CO_2 and CO molecular lasers are of primary importance (due to high efficiency, low cost and convenient size and construction) for two major applications. These lasers are used for localized heating in industrial/medical applications (higher power) and as coherent sources for infrared laboratory and field applications (lower power), including pollution monitoring, radar, absorption and flourescence spectroscopy, and pumping FIR lasers (a representative list which is by no means complete). Many of these applications require frequency (and amplitude) stability considerably better than is available by the use of a stable cavity only and active cavity stabilization using a frequency reference and a closed loop servomechanism is required.

Stabilization is a major technological application of the optogalvanic effect (OGE) requiring the frequency selectivity of this mechanism (which results in a detected electrical signal with a high signal to noise ratio) with the consequent calibration of laser wavelength to the OGE detected transition. The requirements for active stabilization of both the electrical detection of laser beam fluctuations and an absolute reference frequency are satisfied by OGE; a free-running laser oscillator can be locked with a suitable feedback system.

1.1 CO_2 LASER AND THE STABILIZATION PROBLEM

Almost all laser applications require intensity stability ($\lesssim$5%) beyond

that available from a simple passive resonator (e.g. semiconductor and metal surface treatment) and many require a considerable degree ($\sim$ 1 MHz) of frequency stability (e.g. pumping FIR lasers). Three parameters of stability are (a) stability of frequency, (b) stability of amplitude (or intensity) and (c) phase coherence. Frequency and amplitude are related in a laser oscillator in at least two ways: (i) amplitude modulation (by spontaneous emission or otherwise) causing generation of AM sidebands in the frequency domain and (ii) the precise oscillating frequency (set by the resonator) resulting in a particular gain and generating an amplitude which depends on that frequency. Phase coherence is a stringent requirement which is a useful measure of stability for holography, but for the majority of applications it can be seen as homogeneous frequency broadening.

Every laser has at least two frequency selective components: (a) the laser gain profile (usually broad) and (b) the resonator, i.e. the optical cavity set up to provide sufficient positive feedback for oscillation (usually narrow). In addition to this, dispersive optical components can be inserted into the resonator (such as gratings, prisms, etalons, etc.) which introduce a deliberate further degree of frequency selection.

In the CO_2 laser case, a laser line gain profile at 20 torr is broadened to approximately 150 MHz (full width half maximum) and a series of such laser lines occurs in the 9 to 11 μm infrared region due to the $(00^01 \rightarrow 10^00, 02^00)_{I,II}$ vibrational-rotational transitions of the molecule in 4 bands (2P, 2R). Each adjacent pair of lines is $\sim$ 55 GHz apart and these are conventionally discriminated by using a blazed diffraction grating (resolution $\sim$ 3 GHz) as one of the resonator reflectors.[1]

For short ($\lesssim$ 1 m) CO_2 laser cavities the longitudinal resonator mode frequency spacing is approximately equal to the width of the laser gain profile; for lengths 1 m to 1.5 m a transitional case occurs where either one or two modes can oscillate (see Figure 1.11). In the short case as long as only <u>one</u> cavity mode exists, which is frequency coincident with the gain profile then either no oscillation (if feedback is insufficient) or else single longitudinal

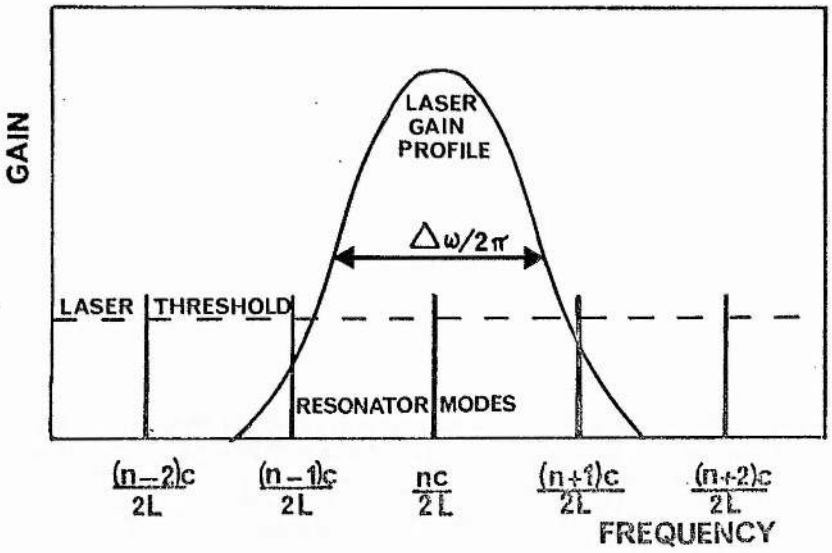

Fig. 1.11 Frequency diagram showing resonator modes and one CO_2 laser gain profile. The transitional situation displayed here represents $L \sim 1.3$ m (for laser pressure $\sim$ 25 torr). If one mode is not held at line centre then two modes can be above threshold and oscillate simultaneously.

Stable Sources	S value
1 MHz Wein Bridge Oscillator	10^4
1 MHz Crystal Oscillator	10^5 to 10^8
Primary Kr. Length standard	10^8
Primary Cs. Time standard	10^{13}
CO_2 laser (multiline)	8×10^2
CO_2 gain profile (single line)	3×10^5
CO_2 laser actively stabilized	10^8 to 10^{10}
HeNe (methane stabilized) NBS	10^{13}

Fig. 1.12 Comparison of the stability (S) of laser and other stable sources.

Laser System	M value
HeNe (3.39 μm)	6
CO_2 (10 torr)	4
Ar ion	10^{-1}
CO_2 (1 atm)	0.07
HeNe (633 nm)	0.015
Dye Rh6G	10^{-3}
Nd^{3+}:Glass	10^{-4}

Fig. 1.13 Comparison of M criteria for various laser systems.

mode oscillation will occur. The resonator feedback is supplied by reflectors supported by a mechanical structure enclosing the amplifying medium which gives rise to the high Q cavity modes represented as δ -functions in Figure 1.11. A 'perfect' cavity would suffer length changes due to Brownian motion only, giving a cavity stability factor $S \sim 10^{12} - 10^{15}$ (the frequency stability is defined carefully in Chapter 4 and is simply the oscillator frequency f_o divided by the drift (Δf)). If the CO_2 laser is constrained to oscillate on one vibrational-rotational (V-R) transition only then $S \sim 3 \times 10^5$. Although no resonator is near perfect, the (short term $\sim$ 1 s) cavity mode width is always very much less than the gain profile, and the Figure 1.11 representation (modes as δ -functions) is suitable. In order to illustrate the order of optical stability Figure 1.12 compares stability values of some useful electromagnetic sources.

In practical terms the cavity mode width is typically 10 Hz to 1 kHz for short observation times ($\lesssim$ 1 μs) whereas the gain profile is $\sim$ 150 MHz wide. Laser active stabilization consists, in the main part, of controlling the frequency of the cavity mode by referring its frequency to some absolute optical calibration frequency which could be another very stable cavity or a fine spectral feature of gas absorption or the laser gain profile itself. Initially the laser resonator is carefully constructed in order to reduce alignment and length changes (high passive stability) which result in frequency shifting of the laser mode.

A necessary and sufficient strategy for actively stabilizing a laser to provide a stable source ($S \sim 10^8$ to 10^{10}) and to fulfill the requirements is

1. Choose a cw laser which is suitable for the application and also for practical stabilization (wavelength, gain, linewidth, size, efficiency, etc.)
2. If multi-transition system then select one line (in CO_2 case one V-R transition)
3. Select one transverse mode (usually axial modes, TEM_{oon} or suitable waveguide mode)

4. Either (i) select one longitudinal resonator mode and keep it
   or (ii) use a few longitudinal modes sequentially and switch between them at suitable pre-determined times
5. Lock single resonator mode by a servomechanism to
   (i) laser line-centre or Lamb dip
   or (ii) spectral feature in (a) external cell
   (b) intra-cavity cell
   possibly tuning this transition (Stark or otherwise)
   or (iii) very stable external cavity.

The choice of the particular laser medium to be used with active stabilization depends largely upon the subsequent use; HeNe (methane stabilized 3.39 μm) and CO_2 (CO_2 stabilized 10.6 μm) have dominated for metrological purposes. One criterion of laser medium choice is set by the single mode requirement (4). The cavity must be kept short in order to keep the mode frequency spacing sufficiently wide. The axial mode frequency f_{mode} is

$$f_{mode} = \frac{nc}{2L} \quad \ldots\ldots\ldots\ldots\ldots\ldots \quad (1.1)$$

where n is the longitudinal mode number and L is the optical length of the resonator. Therefore, for a mode spacing (Δf_{mode}) greater than the laser line width ($\Delta f_0 = \Delta\omega_0/2\pi$)

$$\Delta f_{mode} = \frac{c}{2L} \geq \Delta f_0 \quad \ldots\ldots\ldots\ldots\ldots \quad (1.2)$$

The laser length, however, cannot be shortened beyond a certain lower limit determined by the saturated gain (i.e. to oscillate, gain > losses). For laser oscillation the round trip gain $e^{2\alpha L}$ must exceed the losses, ξ

$$e^{2\alpha L}/\xi > 1 \quad \ldots\ldots\ldots\ldots\ldots\ldots \quad (1.3)$$

which expresses the laser threshold condition (ξ is the losses factor defined in Chapter 7, equation (7.14), α is the laser gain coefficient and L is the laser amplifier length). The simultaneous

satisfaction of these two requirements gives a criterion for laser medium selection, by eliminating L

$$\frac{2\pi\alpha c}{\Delta\omega_o} > \log_e \xi \quad \ldots\ldots\ldots\ldots\ldots\ldots \quad (1.4)$$

The RHS of this equation lies in the range 0 to 1 (the range of $\log_e \xi$) and the LHS (to be called M) is just related to the quotient of gain and the line width.

$$M = \frac{2\pi c\alpha}{\Delta\omega_o} \quad \ldots\ldots\ldots\ldots\ldots\ldots \quad (1.5)$$

Now M is a figure of merit for the active stabilization of systems, Figure 1.13 shows M values for various lasers and HeNe (3.39 μm) and CO_2 (∿ 20 torr cw) are good choices with high M values. This criterion favours lasers with a high gain per unit length and narrow line width. The length restriction can be overcome by using a Fox Smith resonator[2] which uses three reflectors, two of which form a suitably short cavity. These resonators generally have a lower passive stability due to the increased complexity. The relaxation of this restriction is most important for some applications such as visible lasers (i.e. cw dye lasers) which frequently require several methods of restricting the laser bandwidth so that only a few modes can oscillate.

The selection of one line (of a multiline medium such as CO_2) is conventionally achieved by an extra dispersive element but when the oscillator is sufficiently short and if strong line competition occurs, then the 'signature' effect is observed. If a short cavity ($\lesssim$ 50 cm) is used, single mode operation occurs if off-axis modes are suppressed (Chapter 4) and line competition succeeds in producing all the laser intensity in one spectral line, without the need for an extra dispersive element. Gratings introduce losses (R ∿ 93 to 96%), have irregular figure (curvature), require complex mechanical mounts which have poor mechanical stability, and are expensive. As the cavity length is changed, due to drift, or with deliberate perturbation, a successive array of several individual high gain laser line segments occurs producing a laser signature[3] which can be predicted by geometrical optics

and knowledge of the line shapes and line gain ratios.[4] Figure 1.14 shows a typical CO_2 laser signature measured during this present work and investigation has shown[3] that in most discharge configurations 10P(20) occurs in every $\lambda/2$ portion of the signature (the spectroscopic notation for CO_2 transitions is explained in Appendix 1).

Schiffner[4] uses approximate (parabolic) lineshapes (identical for each transition) and takes into account the dispersive nature of Brewster windows in order to make good predictions of line occurrences in signatures. The resonator equation,[5,6] where n is the medium index of refraction and d is the distance between the curved reflector (radius of curvature R_1 and R_2), was used in the prediction

$$nd = (q + 1 + B)\frac{\lambda c}{2} = q'\frac{\lambda c}{2} \quad \ldots\ldots\ldots \quad (1.6)$$

where

$$B = \pi^{-1}(1+r+s) \arccos\{(1-d/R_1)(1-d/R_2)\}^{\frac{1}{2}} \quad \ldots \quad (1.7)$$

and

$$q' = q + 1 + B \quad \ldots\ldots\ldots\ldots\ldots\ldots \quad (1.8)$$

where λ_c is the resonant laser transition vacuum wavelength, q is the longitudinal mode number and r and s (integers) are the transverse mode numbers (i.e. mode defined TEM_{rsq}). Schiffner assumed that at the equal gain point (e.g. where say $\alpha_{10P(20)} = \alpha_{10P(16)}$ for d_1) the laser would instantaneously change oscillation of one transition to another (this phenomenon will be explained subsequently) and a simple computer programme yielded the results shown in Figure 1.15.

Signature line selection has been shown experimentally to be capable of rejection of the other available laser lines for sufficiently short devices and has become an elegant and cost effective technique for cw CO_2 lasers. Single transverse mode operation is, however, essential for selection and this is usually achieved in CO_2 lasers by judicious choice of tube diameter or by insertion of an intracavity iris (see Chapter 3).

The first three requirements for the stabilization strategy can be satisfied by a short cw CO_2 laser with signature line selection and suitable

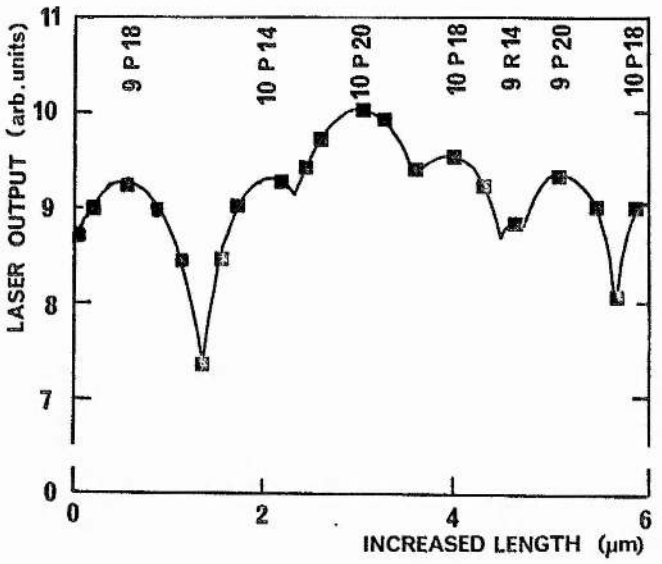

Fig. 1.14 A laser signature for $\gtrsim \lambda/2$ for the compact CO_2 laser used for this work. Arbitrary laser power was measured with a pyroelectric detector and the laser transition was identified with an Optical Engineering spectrum analyzer. The length was tuned by applying 0 to $\sim$ 500 volts manually to a Lansing PZT supporting the output coupler. The nomenclature for line designation is given in Appendix 1.

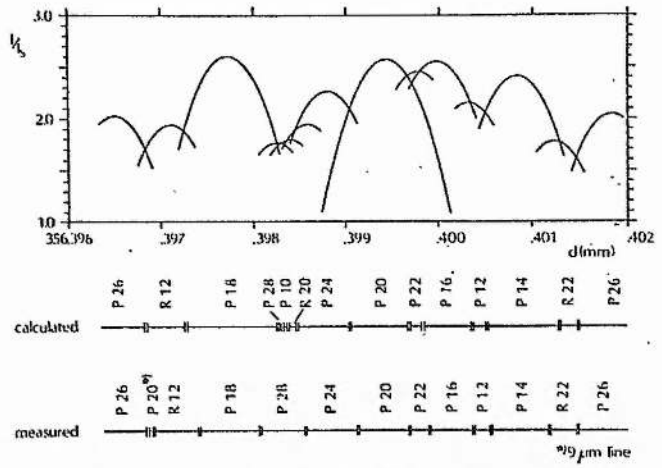

Normalized intensity versus cavity length d for the laser described. Only those parabolas are shown contributing to the envelope of the intensity profile. A large portion of the $P(20)$ parabola can be seen. From the curve crossings, the regions of oscillation were determined and are presented below (see "calculated"). The regions of oscillation from Fig. 2 (lower trace) are shown for comparison (see "measured").

Fig. 1.15 The successful prediction by geometrical optics of an empirical CO_2 laser signature, reproduced from Schiffner.[4]

aperture selection of mode. One longitudinal mode is ensured for a given operating point by making the frequency mode spacing exceed the full width half maximum (FWHM) gain profile, i.e.

$$\frac{c}{2L} > (40 + 5\,p) \times 10^6 \text{ MHz} \quad \ldots\ldots\ldots\ldots \quad (1.9)$$

This approximate relation where p is gas pressure (torr), requires the optical length L to be sufficiently short to make the mode spacing c/2L exceed the pressure broadened CO_2 line shape (approximately 40 MHz + 5 MHz/torr). This requires for 25 torr pressure, the cavity length $L \lesssim 90$ cm; if this criterion is exceeded then not only does single longitudinal mode operation cease but signature rotational selection also becomes inadequate.

In order to lock the single laser mode to some reference frequency some form of control system is required to drive the freerunning laser mode to some maximum, minimum or inflection point of a detected error signal. This has been achieved in many ways but the commonest form of active stabilization involves locking the laser to the line centre of the oscillating transition, which in the case of the CO_2 laser is a maximum at pressures above $\sim$0.5 torr (below which a Lamb dip minimum is observed). Obviously before cavities are stabilized a considerable degree of passive stability is desirable (low thermal expansion, high stiffness and rigidity, damping, offset of thermal coefficients, low recrystallization), although this is less necessary as cavity correction techniques have improved (electronic development); this subject (passive stability) and the trade-off with increasingly complex servo-electronics will be discussed later.

Active stabilization, operationally, consists of compensating for any length change so that a well-defined optical length is maintained to yield a precise frequency cavity mode which is referred to some absolute reference (e.g. gain profile centre). Typical well-constructed CO_2 lasers with signature selection (such as Edinburgh Instruments PL1) have medium term (1 s) stability of $\sim 1:10^7$ and long term (10^3 s) of $\sim 1:10^5$. A feedback system is required initially to bring the long term stability into line with

the medium term (i.e. to correct for drift ∿10 s) and possibly to improve the medium term stability (∿0.1 to 5 s). The short term stability (0.1 to 1 ms) is usually observed to be approximately ∿1:10^9 to 1:10^{10} and the ultimate aim of active stabilization is to make use of this precision over a longer timescale. Length adjustment of up to 20 μm can be made with a piezoelectric translator (PZT). Figure 1.16(a) shows a simple stabilizer consisting of a laser oscillator (L) fitted with a PZT element and using an optical detector (D) to measure the beam power emitted. The cavity length is dithered (at audio frequencies within the detector bandwidth) giving rise to a frequency modulation

$$\frac{\Delta L}{L} = \frac{\Delta f}{f} \qquad \ldots\ldots\ldots\ldots\ldots\ldots\ldots \quad (1.10)$$

which results in an intensity fluctuation (Figure 1.16(b)). The ac component of intensity is detected by the square law optical detector (voltage ∝ intensity) and the phase of this component resolves the length sign ambiguity. Detection of phase can be achieved with a suitable lock-in amplifier (PSD) and some degree of post-detector integration (INT) is required. The resulting dc correction signal is fed (often via further integration) to a high voltage dc amplifier (HVA) to drive the PZT in order to bring the laser mode to the peak intensity point by seeking a null in the detected ac signal. Frequency stability of 1:10^8 to 1:10^9 in the long term can be achieved by this technique, however, the ac dither frequency modulates the laser by a known amount ∿0.1 to 10 MHz reducing the absolute stability to $\lesssim$ 1:10^8.

1.2 SCOPE OF THIS WORK

The primary objective of this work is to fully describe the construction, optimization and performance of OGE active stabilization of CO_2 lasers (in the cw power range 1 W to 50 W) to a laboratory stability standard (frequency stability ∿1:10^9), the investigation of the microscopic kinetic processes leading to OGE signal generation in CO_2 oscillators and external absorbers/amplifiers, and a full predictive theoretical model of the phenomenon.

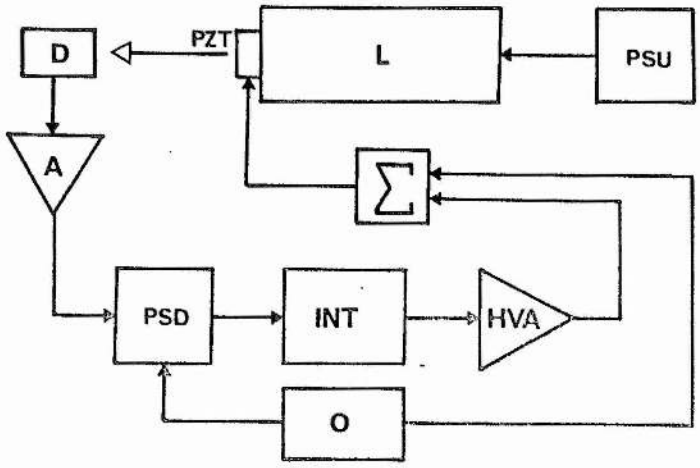

Fig. 1.16 (a) A schematic diagram of a simple feedback laser stabilizer.

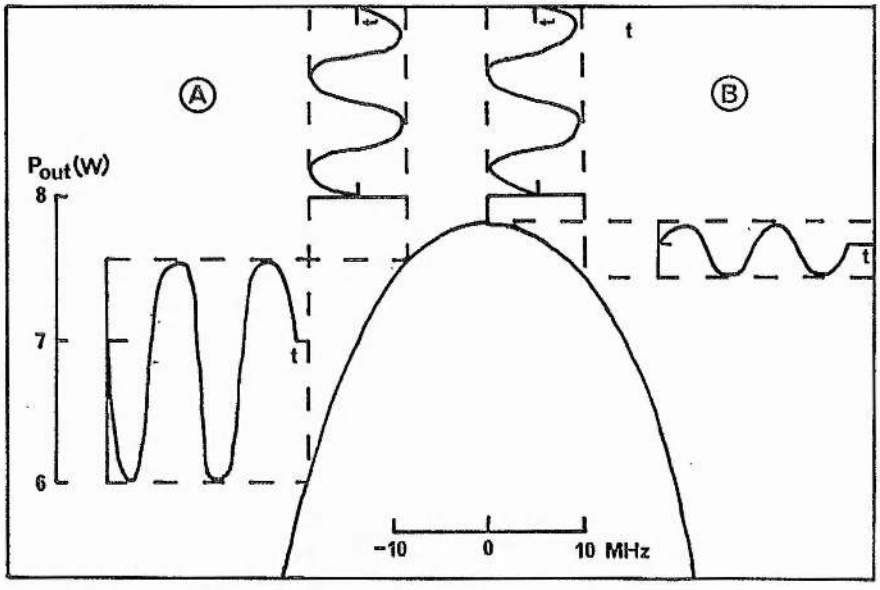

Fig. 1.16 (b) The output power variations with time due to periodic length modulation which is equivalent to laser frequency modulation. Two cases are represented (A) where the laser mode is - 10 MHz with respect to the laser line centre. The power variation is large and is out of phase with the modulation voltage. Case (B) shows the laser mode at + 7 MHz with respect to laser line centre. The power variation is smaller and in phase with the modulation. The stabilizer drives the laser mode either high frequency or low frequency (depending on signal phase) until the minimum signal is returned.

In practical terms, this means the use of optically induced current changes in the laser excitation discharge to detect the off-line centre error signal required for active control of the laser mode by a phase locked loop. The elegance of this method (optogalvanic effect) coupled with signature selection is evident: a simple, rugged and cost effective improvement of up to 4 orders of magnitude in frequency stability and 2 orders of magnitude in intensity stability combining well with the simplicity and efficiency of the CO_2 molecular laser.

The main subsidiary systematic investigations are the stabilization and optogalvanic studies of the CO_2 sequence ($00^02 \rightarrow [10^01, 02^01]_{I,II}$) laser and the CO molecular laser. The generation of high frequency OGE signals up to 100 kHz in CO_2 laser discharges is demonstrated and the new mechanisms elucidated; previous investigations were limited to < 5 kHz. Investigation of low pressure standing wave saturation resonances with Lamb dip OGE detection is also presented and the feasibility of using CO_2 Lamb dip reference to stabilize the CO_2 waveguide laser (which has inherently a wide tuning range) is analyzed.

Further investigations of this technique (OGE) to discharges spatially separated from the main laser amplifier was undertaken and this has shown the generality of OGE detection. Optogalvanic detector discharges of this type (outwith the laser amplifier) with various non-lasing gas compositions and pressures (either physically outside or within a laser cavity) were used to make measurements of gain, absorption, and the dependency of the optogalvanic effect on the discharge operating parameters. Investigations of the variation of excitation, pressure, composition, temperature, length and geometry were made and the magnitude and phase of the resulting OGE detected signals is accurately predicted by the power perturbation theory given in Chapter 7.

2.0 PREHISTORY - PHOTOELECTRIC EFFECTS IN GASES

Following the discovery by Lenard and revolutionary description due to

Einstein of the photoelectric effect in solids, at the beginning of this century and, due to the vigorous development effort devoted to the thermionic valve (tube) and discharge tubes, interest in 'photoelectric' effects in gases grew both from the point of view of physical understanding of microscopic processes (mainly ionization) and from the photometric applications required by spectroscopy. At this time also great achievements in the theoretical understanding of atomic gas discharges in breakdown and pre-breakdown conditions occurred (notably by Penning and Townshend) and the use of light as a diagnostic probe was a novel extension to existing experimental diagnostic apparatus (such as probes, etc. to measure charge). Initially, studies of photoelectricity in metal vapours were made and the early efforts of Foote and Mohler[7] consisted of studying photoelectric detection not with a sustained discharge, but using a thermionic diode which was current limited by the electron space charge. Cesium vapour was used and a diode operating potential of 0.5 V employed to avoid electron impact ionization of the gas; absorbed photons produced ions which were detected by the partial neutralization of the space charge giving an increased diode current. In these experiments, the 3180 Å photoionization limit for the cesium ground state was observed (electrically) but the apparatus wavelength resolution was not sufficient to observe individual transitions; previous attempts to observe photoelectricity in metal vapours gave ambiguous results due to insufficient apparatus which had been improved to include hard vacuum, quartz envelope and Pt electrodes for the tube and a monochromator for filtering the light source. This work also showed that the long wavelength limit of ionization by radiation or electronic impact was not sharply discontinuous but that intertomic collisions (translational energy supplied by the heater which was varied) could contribute significantly to the energies of atoms and as a result ionization occurred beyond the long wavelength side of the (theoretical) limit. Therefore, unlike a solid X-ray limit the photoionization effect for a valence electron was not sharply discontinuous at the calculated threshold.

It required the investigation, in 1927, of Meissner and Graffunder[8] to

show that the irradiation of rare gas sustained discharges (neon and argon) by resonant visible radiation (from neon and argon lamps) perturbated the v-i characteristic of low pressure (few torr) discharges and they offered a qualitative explanation requiring the decrease of population and lifetime of metastable atoms due to irradiation.

A critical dialogue developed in 1931 between F.M. Penning and L.G.H. Huxley resulting in an interesting paper by Penning,[9] where in attempting to prove the purity of the Ne used to investigate starting potentials, he irradiated the neon discharge tube with a helical neon positive column glow tube to change the v-i characteristic of the test tube. The starting potential of a Ne Ar mixture was increased by a factor of 2 with illumination. This provided a sensitive measure of purity; excepting helium, all other gases have ionization potentials smaller than $V_{metastable}$ for neon (16.6 V). Hence small traces of impurities (10^{-6} to 10^{-3} concentration) cause an increase of starting potential due to irradiation, but if no increase of starting potential occurs then the neon must be very pure. Apart from this diagnostic use for measuring purity (two patents were issued in 1934 and 1937 concerning pure rare gases) and noting that at high irradiances the effect can be very large, Penning shows little scientific interest in it. Figure 2.01 shows part of Penning's explanation. This effect was first seen in pure helium in 1930 by Meissner and Pierson.[10]

To summarize, this rare gas effect requires the depletion of a metastable population by radiative absorption into a level which can radiatively decay to the ground state. In many discharge systems (notably rare gases) metastable states dominate in ionization mechanisms and this results in a higher electron temperature to maintain the discharge and the discharge voltage (for a given i) rises; it is this effect that was seen by Penning[11] and Meissner[8,10] in rare gas discharges and Kenty[12] in the Hg vapour lamp during irradiation by similar discharges in the same gases.

Conversely, if the absorbed radiation causes transitions to higher levels which are more easily ionized then the discharge voltage will decrease because

When the discharge-tube is not irradiated the metastable states can be destroyed in two ways: first by collision with a neon atom they can be brought into the $1s_4$-state [12], from which they return to the normal level with emission of the resonance line 736 Å [14]; secondly they can ionize an argon atom. When the discharge-tube is irradiated by intensive light from a neon column the metastable atoms can be raised by this light to the $2p$-states, and from there return, at least partly, *via* the $1s_4$-level into the normal state. The result of this irradiation therefore

Fig. 1.

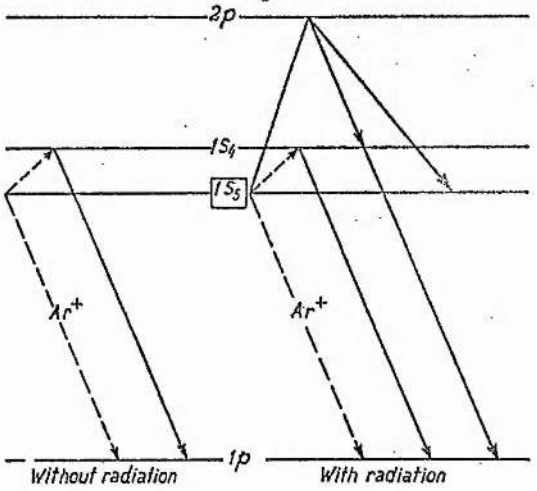

is that fewer argon atoms are ionized and that the starting potential increases. Indeed, this conclusion was confirmed experimentally [15]. The effect reaches high values with large light intensities; not yet published measurements showed that under suitable conditions the starting potential of a Ne–Ar mixture could be increased by irradiation with neon light from 550 v. up to 900 v. It is difficult to see how this irradiation could cause such a large increase if the ionization were not due to metastable atoms.

Fig. 2.01 Extract from Penning[9] (1931).

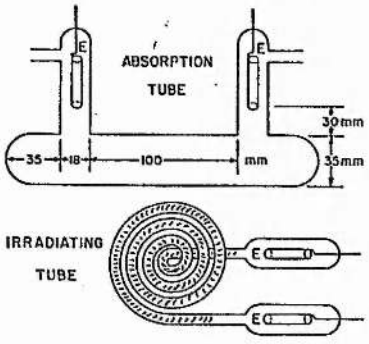

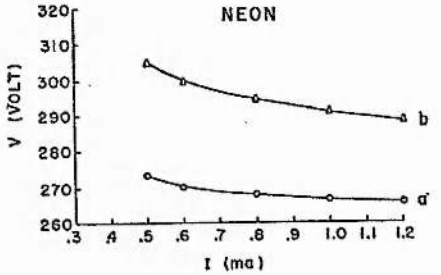

Characteristics of neon (pressure 2.8-mm Hg). (a) without irradiation, (b) with irradiation.

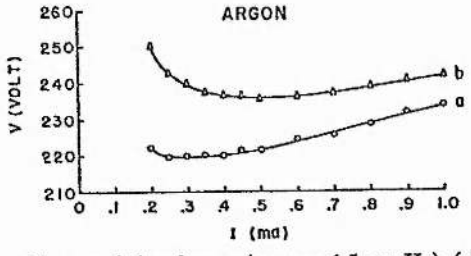

Characteristics of argon (pressure 1.5-mm Hg), (a) without irradiation, (b) with irradiation produced by imaging the removed irradiating tube on the positive column of the absorption tube.

Fig. 2.02 Apparatus and v-i characteristic perturbations of neon and argon, reproduced from Meissner and Miller[17].

the electron temperatures required to maintain the discharge is decreased; for a lucid description see Bridges.[13]

However, it was possible by this time (1930) to compute the concentration of excited atoms and their mean lifetimes in a Townshend discharge[14] from the known electronic properties of neon using the mean lifetimes as adjustable parameters. A comparison of Penning's direct optical perturbation measurements allowed Pike (whilst a Ph.D. student)[15,16] to provide absolute numerical values (at 36 torr Ne) of lifetime of $^3P_2$ metastable state of $2 \times 10^{-3}/P$ seconds of and 2 $^3P_1$ resonance states $4 \times 10^{-5}/P$ seconds (where P is the pressure in torr).

The study of Hg (+Ar, Kr, Xe) rare gas mixtures, used for lighting purposes, brought an interesting result from Kenty[12] who noted that strong Hg vapour radiation (through glass, long wavelength) resulted in doubling the discharge voltage of an Hg test tube at 1 mA and that this illumination could suppress the striations at pressures of a few torr. This effect could only be observed at temperatures below 16°C.

By 1953 Meissner and Miller had examined the optically induced v-i characteristic perturbations (see Figure 2.02) in some detail[17] for Ne, He, Ar, Kr and Xe and the spectroscopic power of this effect was becoming realized and that its main advantage was the frequency selectivity of the detection mechanisms. Some large rare gas perturbations (10% typical) were being seen and careful filtering of nonmonochromatic discharge lamps was required for detailed analysis of particular level population perturbations, etc.

2.1 RECENT HISTORY - LASER OPTOGALVANIC STUDIES OF VISIBLE ATOMIC TRANSITIONS

Although early work of researchers like Meissner was limited by poor monochromaticy and the low irradiance per unit bandwidth and solid angle, of the available light sources such as arcs, discharge tubes, etc., some significant discharge perturbations due to strong transitions were detected. The rebirth of these optically induced effects came with the availability of the laser and the name optogalvanic (OGE) spectroscopy came into common usage

by the middle 1970's due to Green and co-workers' revival of interest in visible rare gas transitions.[18] It was the tunability of the cw dye laser over the visible spectrum and the subsequent illumination of the rare gases that were intensively studied in discharges which were characterized by relatively high electron temperatures (0.2 to 10 ev); in this situation significant population of many excited levels exist. In addition atomic ions, molecular ions, molecular free radicals with relatively low concentrations were studied not only in discharges but also in the pre-breakdown condition[19] and in flames.[20] Figure 2.11 shows a typical optogalvanic detection system as described by Goldsmith and Lawler[21] and figure 2.12 shows a representative laser optogalvanic spectrum obtained using a dye laser (Rhodamine 6G) to probe an HeNe discharge.[22] An optical absorption curve is also given for comparison which shows some of the stronger transitions. Phase sensitive detection is usually used although it is not necessary on strong transitions and the positive or negative value of the OGE signal depends on the precise kinetics of the levels involved in the absorption process (a simple description has been given in 2.0).

2.11 LASER DISCHARGE PERTURBATIONS

More important to this present work are the optogalvanic effects that have been demonstrated in the amplifying discharges of gas laser oscillators. Garscadden et al,[23] Garscadden and Adams[24] and Weaver and Freiberg[26] observed decreases of current of HeNe discharges undergoing laser action; Schiffner and Seifert,[25] Weaver and Freiberg[26] and Weaver[27] reported that a typical laser on/off current change is ≈ 2%; previously Bennett[28] had noticed increased electric current noise during laser amplification in a pulsed argon discharge and Waksberg and Carswell[29] measured laser induced sidelight fluctuations in HeNe discharges and obtained some kinetic information by using phase lock techniques. The favoured explanation of this effect is that the laser action depletes Ne $3S_2$ (3.39 μm or 0.6328 μm transition) or $2S_2$ (1.15 μm transition) upper laser levels and this increases the reduction of the corresponding

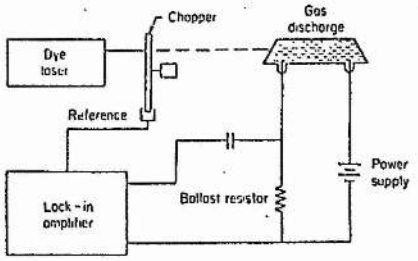

Fig. 2.11 Typical experimental apparatus for studying optogalvanic atomic transitions using a tunable dye laser and phase sensitive detector, reproduced from Goldsmith and Lawler.[21]

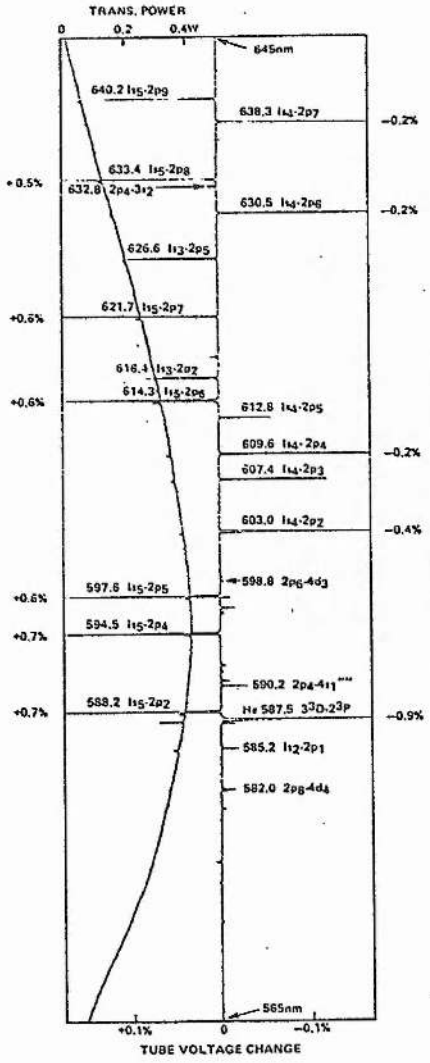

Broadband optogalvanic-effect spectrum of a helium-neon discharge in the tuning range of rhodamine 6G. Signal strengths are measured as percentage changes in tube voltage; numbers at right and left are end points of off-scale readings. The dye-laser power transmitted through the tube is indicated by the superimposed curve at left

Fig. 2.12 OGE spectrum of HeNe discharge and comparison of absorption spectrum reproduced from King and Schenck.[22]

collision coupled He metastable population (2^1S or 2^3S) and consequently the optogalvanic effect follows the Meissner description. Smaller decrease ≈ 0.02% in pure Xe discharge lasers has been reported by Freiberg and Weaver.[30]

Perturbations of Argon Ion laser discharges were anticipated, predicted and later observed by Klein,[31] and Dunn and Maitland;[32] reduction of discharge voltage of ∿ 1 V in 500 V was observed during laser action. The suggested mechanism is that stimulated emission increases the 723 and 745 Å spontaneous emission from the lower laser level to the ion ground state and that this radiation increases the photoionization of neutral argon (ionization limit 780 Å).

Early investigation of the CO_2 laser discharge showed very large perturbations of discharge parameters and these experiments will be described in 2.4. The CO_2 laser induced current perturbations originated from the thermal considerations of the molecular discharge rather than the electronic (ionization) description of the atomic laser perturbations. The epistemology of the optogalvanic effect is split into twin streams (i.e. atomic and molecular) and in general, the atomic side has been more thoroughly investigated and better theoretically described. In this work the molecular case (particularly for CO_2 and CO lasers) is investigated experimentally and detailed theoretical kinetic modelling given, but for both historical completeness and for pedagogical purposes a study of all optogalvanic perturbation is undertaken in this chapter.

2.2 MODERN OGE THEORY OF ATOMIC DISCHARGES

The prelaser optogalvanic theory consisted of qualitative description of atomic level perturbations and the work of Pike[15] is notable for the use of rate equations (very simplified) in order to quantify metastable and resonant state mean lifetimes; the analysis required many assumptions of which some are dubious. Modern approaches (after 1976) have largely consisted of two major approaches at different levels:

1. Rigorous Rate Equation Models such as the work of Pepper[33] and Lawler[34] in principle allow detailed quantified prediction, unfortunately they suffer from the majority of crossections being not sufficiently well known and the subsequent numerical solutions are multivalued with adjustable parameters. These models are a more detailed attempt than prelaser analyses but the approach is essentially similar, and the method relies on the non-equilibrium approach and linear analysis of a restricted set of rate equations.
2. Simplified Phenomonological Models such as the work of Erez et al,[35] which are successful in predicting sign changes at particular discharge excitations (unlike the rate equation models) and relative magnitude and time evolution of OGE signals. Several parameters (rather like transistor equivalent circuit parameters) are introduced and essentially quasisteady state analysis is used; unfortunately, precise prediction is not possible with the model offered so far.

This work will, in chapter,[7] provide a predicative perturbation model for molecular V-R transition OGE effect in the CO_2 laser which is different from cases (1) and (2) but the CO_2 laser molecular discharge restrictive case allows an accurate and quantitative model to be constructed which cannot be generalized to the atomic case because the mechanism is fundamentally different; it is in this light that the modern atomic OGE theories will be discussed.

Pepper[33] calculated magnitude and sign for the effect in sodium vapour by a rate analysis technique with a modified Schottky approximation for glow discharges, the specific technological application under consideration was isotope separation. Lawler[34] has split the analysis into two parts and developed a semi-empirical model by experimentally measuring the v-i characteristic to avoid calculating dZ/di; consequent calculations (similar to Pepper's) result in prediction of the OGE amplitude (for a known He transition) with constant voltage excitation (see 3.2).

The normal Schottky model considers only two states of an atomic system: the ground state and the ionization state, no excited state is allowed. Pepper, in order to analyze optical perturbations modified this formalization by considering an intermediate state as two, two level 'atomic systems'. An iteration procedure was set up (see Figure 2.21) to provide a numerical solution of the coupled rate equations (for the 'two' resonant atomic gases and the buffer) and the electron temperature T_e is calculated for the non-irradiated case; unfortunately, no exact closed form solution is possible. This routine was repeated for the irradiated case and the calculated change of electron temperature was used to predict the discharge voltage perturbation for a constant excitation current. Pepper only considered the increase in upper level population on absorption and this always leads to an optogalvanic decrease in tube voltage. Additionally, in order to satisfy the criterion of conservation of energy the electron density must change with illumination (as well as temperature) and this would lead to an increase ($\sim$ 15%) in the ionization density which would consequently decrease the optogalvanic response; this second order effect was not considered.

The change of electron temperature alters the dissipation of electrical power in the discharge (due to irradiation) and using standard approximate expressions for discharge power[37] and substituting for the ambipolar diffusion coefficient

$$D^{+} = \left[\frac{r}{2.4}\right]^2 \sum_{i=1}^{3} N_i S_{ij} \qquad \ldots\ldots\ldots\ldots\ldots\ldots \quad (2.1)$$

where S_{ij}, the electron collision rate is calculated using a Maxwellian electron distribution, changes in the input discharge power (v i) can be calculated.

Pepper subsequently obtains an expression for the fractional voltage change at constant current as

$$\frac{\Delta V}{V} = \sum_{i=1}^{3} \left[\frac{(\varepsilon_{iI} + 5kT_e^{o})\ \Delta(N_i S_{iI}) + 5k(N_i S_{iI})^{o}\ \Delta T_e}{(\varepsilon_{iI} + 5kT_e^{o})\ (N_i S_{iI})^{o}} \right] \qquad \ldots\ldots \quad (2.2)$$

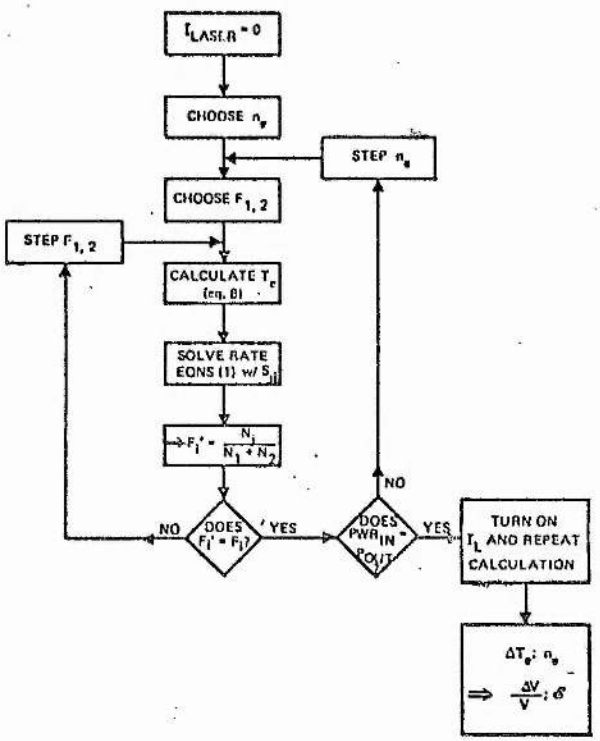

Fig. 2.21 Modified Shottky solution for optogalvanic effect due to Sodium Atomic Transitions. The calculated perturbation of electron temperature ΔT_e determines the change of discharge input power, reproduced from Pepper[33]. The figure shows the flowchart of the iterative technique used to solve for T_e.

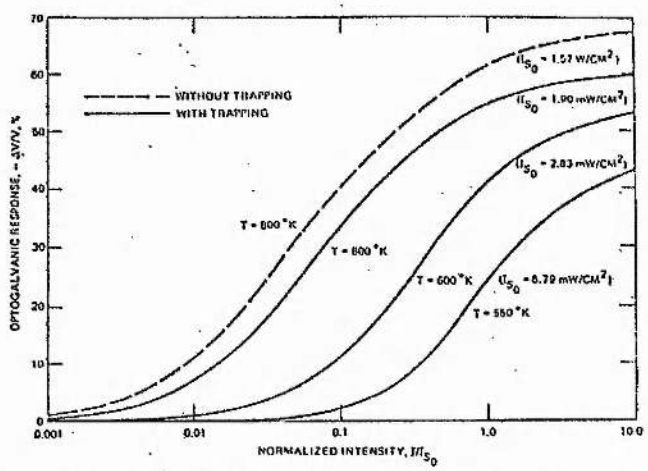

Optogalvanic effect versus (normalized) laser intensity for various temperatures in a sodium discharge (with and without radiation trapping). External illumination is at the Na "*D*" line, argon pressure = 10 torr; $n_e = 10^{13}$ cm^{-3}; tube diameter = 1 cm.

Fig. 2.22 Calculated optogalvanic response $\Delta v/v$ for sodium with irradiation of sodium 'D' line for various sodium temperatures, reproduced from Pepper.[33]

where o superscript indicates parameter without irradiation and $\Delta(...)$ means the difference in parameter brought about by irradiation. The summation is over the three species in the discharge ("Atom no. 1", "Atom no. 2", i.e. three state single system and buffer gas).

The assumptions are that D^+ is independent of position and longitudinal ambipolar diffusion and thermal diffusion is small; volume recombination is not considered and complete ion neutralization at the walls is assumed. Uniform radiation at line centre frequency over the full tube diameter and length is assumed.

The case of sodium vapour in Argon buffer gas is considered at 10 torr for 1 cm diameter tube. Figure 2.22 shows the predicted saturation of the optogalvanic response at high intensities for different sodium temperatures. This saturation has been observed in cesium by Bridges[13] and the close agreement is considered to be fortuitous by Pepper due to the increased complexity of the Cs system and vastly different operating parameters.

In contrast the simpler phenomonological model of Erez, Lavi and Miron[35] depends only on the consideration of a parameter which is the electron multiplication factor (α) namely the number of electrons generated at the cathode by the avalanche caused by a single electrode emitted from the cathode. For steady state $\alpha = 1$, if $\alpha < 1$ then current decreases and if $\alpha > 1$ then the current increases. The case of constant voltage excitation plus ballast was considered (see later chapter) rather than constant current so that, for example, a current increase leads to a voltage increase across the ballast which results in a current decrease and consequently a decrease in α; Erez et al[35] refer to this negative feedback effect as 'self-regulation' of α.

Only quasi-steady state variation in the small signal regime was considered and in this restricted case $\alpha = 1$ and $d\alpha = 0$ and, therefore,

$$d\alpha = \left[\frac{\partial \alpha}{\partial v}\right]_{n_i} \Delta v + \left[\frac{\partial \alpha}{\partial n_i}\right]_{v, n_{jj \neq i}} \Delta n_i = 0 \quad \ldots\ldots\ldots (2.3)$$

where v is the tube voltage, Δv is the optogalvanic signal, n_i are the various atoms and ionic populations and Δn_i are the respective population deviations from steady state. Erez et al[35] next made the assumption that a voltage increase leads to an ionization probability increase and by summing all levels j and treating them collectively as a bath, certain characteristic energy relaxation times (after radiation is switched off) are all that is required to complete the analysis giving

$$\frac{d(\Delta n_1)}{dt} = \frac{\Delta n_1}{T_1} - (n_1 - n_2)\sigma_{12}I_{12} \quad \ldots\ldots\ldots (2.4)$$

$$\frac{d(\Delta n_2)}{dt} = \frac{\Delta n_2}{T_2} - (n_2 - n_1)\sigma_{12}I_{12} \quad \ldots\ldots\ldots (2.5)$$

where the laser illumination is resonant with the transition $1 \leftrightarrow 2$ and n_1 and n_2, T_1 and T_2 are the population and relaxation times of the lower and upper levels respectively. I_{12} is the laser irradiance and σ_{12} is the optical cross-section of the transition.

The temporal consequences of this theory are interesting and predict at least two time constants operating for every OGE signal and most importantly for the cw case the following predictions, assuming 1 to be the lower level and $n_1 > n_2$

1. Optogalvanic signal, Δv is negative with respect to I_{12} unless excitation from a metastable level occurs whence it is positive. Detailed sign changes can be predicted (due to current or pressure changes).[35]
2. Time profile of optogalvanic signal, Δv follows the profile of ΔI_{12} as long as changes are slow compared with relaxation (chopped mode).
3. The optogalvanic signal Δv is proportional to $(n_1 - n_2)$ and $\sigma_{12}I_{12}$ in the small signal limit.

Empirical optogalvanic signals in Argon were compared by Erez to the phenomenological theory; the transient behaviour of dye laser, very short

(< relaxation times) pulses illuminating an Argon discharge and the OGE signal (relaxation time limited) was in good agreement with the theory and useful measurements of the relaxation times were made. This technique (and similar methods) is a well established method of establishing molecular relaxation times, and the subject will be covered for CO_2 subsequently.

2.3 MOLECULAR LASER OPTOGALVANIC PERTURBATIONS

The introduction of molecular lasers[38,39] in the early 1960's provided for the first time, intense light sources in the middle infrared spectral region (10 to 100 μm); unlike the visible spectrum where arcs, etc. provided relatively intense sources, no bright infrared sources were available (filaments, globar, plasmas and mercury discharges) and consequently no optically induced v-i perturbations due to irradiation with infrared radiation of molecular discharges were reported prior to the arrival of the molecular laser.

The earliest observation of an optogalvanic effect in a molecular discharge was due to the pioneering laser work of Rigden and Moeller[40] which is noteworthy because of the observation that the voltage (and current) of the CO_2 laser amplifying discharge changed when the optical feedback was supplied (i.e. when the laser was oscillating); this detection scheme where the optogalvanic element is the laser amplifier discharge is, in many ways, optimum (i.e. the beam irradiance is very high and an efficiently large volume is filled with the light). Previously, Schiffner and Seifert[26], Waksberg and Carswell[30] and Parks and Javan[41] had reported measurements of the very strong coupling of some discharge parameters (particularly sidelight intensity) and the resonant electromagnetic field, but Rigden and Moeller gave the first quantitative measurements and suggested a possible mechanism for the optogalvanic effect in CO_2 laser discharges.

The changes of discharge parameters were given as variation of impedences which had magnitude up to 50% (constant voltage, cv, excitation); figure 2.31 shows the measured plasma impedance with and without laser irradiation at ∿ 50 W in an external cell filled with pure CO_2 and laser mixture. The

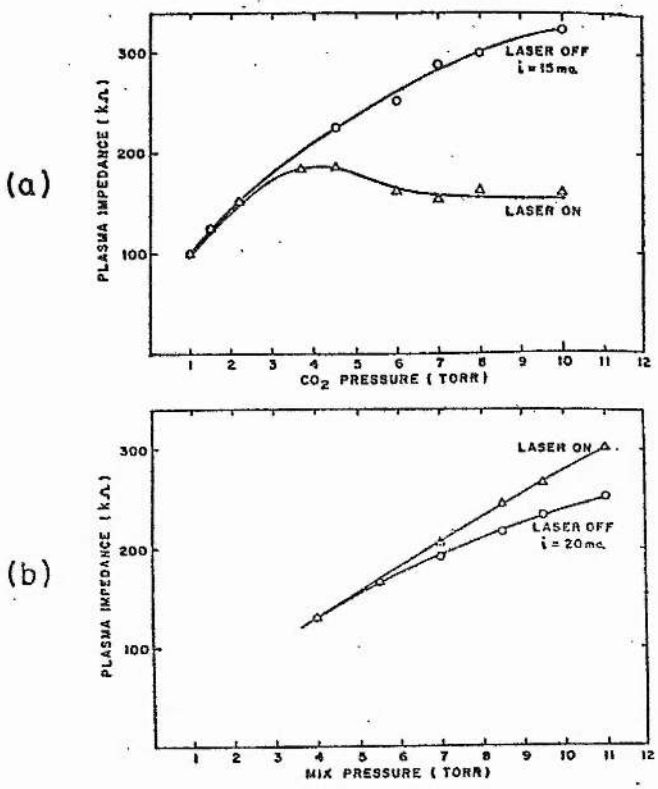

Fig. 2.31 First measurement of an optically induced impedance variation in a molecular discharge. Changes of typically 10% (and up to 50% in extreme CO_2 absorption cases) were seen with intense laser irradiation of $\sim$ 200 Wcm^{-2}.[40]

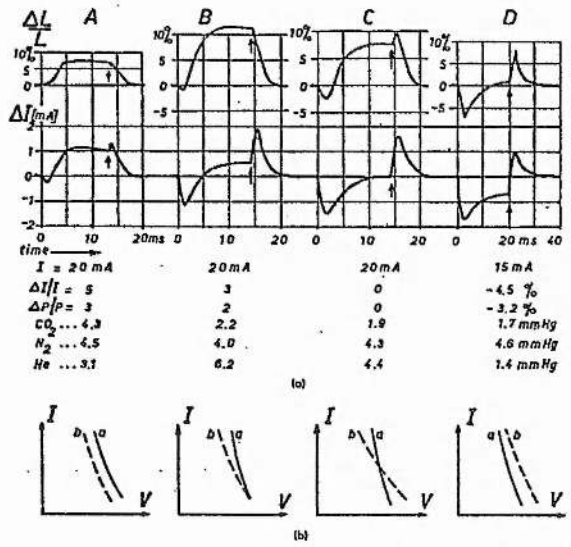

Fig. 2.32 (a) Discharge current fluctuations (ΔT) and sidelight fluctuations (ΔL/L) induced by switching off laser radiation. Gas composition is shown.

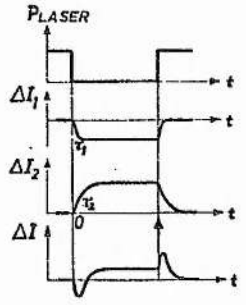

(b) The hypothesis that two time constants τ_1 and τ_2 could approximate the temporal behaviour.[43]

explanation provided by Rigden and Moeller uses a 'gas temperature' photon current coupling mechanism; the hypothesis states that because a large proportion of electrical input power (~10%), is coupled out of the discharge by stimulated emission into the output beam, the discharge is substantially cooled. The gas cooling effect is large because the CO_2 laser is particularly efficient. Rigden and Moeller measured impedance changes brought about by changing the cooling wall temperature. If the walls were heated the discharge impedance decreased, as was also seen by switching off the 10.6 μm stimulated emission (with a shutter).

A more thorough investigation of the discharge perturbations in CO_2 laser mixtures brought about by the generation of the laser beam was made, in 1967, by Carswell and Wood;[42] broadband sidelight intensity, discharge impedance, electron density and probe measurements of electron temperature were studied. The switched beam induced perturbations in all these parameters were measured as a function of discharge current and the primary mechanism of optically induced current changes (OGE) isolated. This first order change is subsequently amplified by the negative differential v-i characteristic when conventional constant voltage (cv) and ballast excitation is used. At low currents when the discharge impedance is strongly dependent on current, the current changes are amplified by a large factor, and the secondary resultant sidelight, electron density, electron temperature and impedance changes are also amplified. The "true" impedance change (neglecting circuit amplification which depends on ballast value, etc.) was found by Carswell and Wood to be ~1.5% for full on/off laser perturbation (whereas at low currents where the tube discharge impedance is approximately equal to the ballast resistance the discharge could be distinguished when the laser field was set up, i.e. > 100% impedance change). The precise nature of sidelight changes showed some complicated behaviour but no results were given and a reactive component (phase change) of the current perturbation was described but not measured.

Kindl, Leeb and Schiffner[43] investigated gas compositional and pressure changes of the optogalvanic effect in CO_2 laser discharges. Conventional cw

excitation was used and an intracavity chopper switched the laser beam on/off. Current changes of ∿5% were measured and the beam chopped at a rate of 30 Hz. Unfortunately, the gas compositional dependence was not conclusive and showed some anomalous v-i perturbations which subsequently have not been observed by repeated experiments by other authors. The interesting observation of this particular work was, however, the temporal nature of the induced current changes. Figure 2.32 shows (in the upper half) some of the current fluctuations brought about by switching the laser field (∿ 30 Hz). At least two time constants can be seen to operate and the lower part of Figure 2.32 shows how the sum of two different temporal responses can qualitatively explain the complicated temporal behaviour. For the operating conditions of 20 mA discharge in 10 torr total pressure the authors observed that two major mechanisms were present, one causing a current decrease and one causing a current increase when laser action is stopped. The second time constant was seen to "distinctly exceed" the rate of the first (time constants ∿ 1 ms and ∿ 5 ms were suggested although poor signal to noise of this technique is given by authors to imply the accuracy of this result to be order of magnitude). The mechanism explanation is an ionization theory (rather like Penning, Meissner, etc.) and the authors briefly suggest that this would require that the ion density is raised by increasing the population of the $00^0 1$ upper laser level and lowered by decreasing the population of the lower laser level (when the laser field is switched off). Reasonable agreement with measurements of lifetimes[44] were noted and an attempt at more exact analysis would require either at least three independent mechanisms, or else gross non-linearity between level populations and discharge current.

Schiffner[45,46] also recorded CO_2 laser signatures (the array of V-R transitions that oscillate in turn with adjusted cavity length, see 3.1) and measured the frequency response of the current perturbations up to 10 kHz; this was achieved not by chopping but by length modulating the laser with a piezoelectric element (PZT) driving one mirror. Figure 2.33 shows the amplitude and phase response of OGE as a function of frequency and Figure 2.34

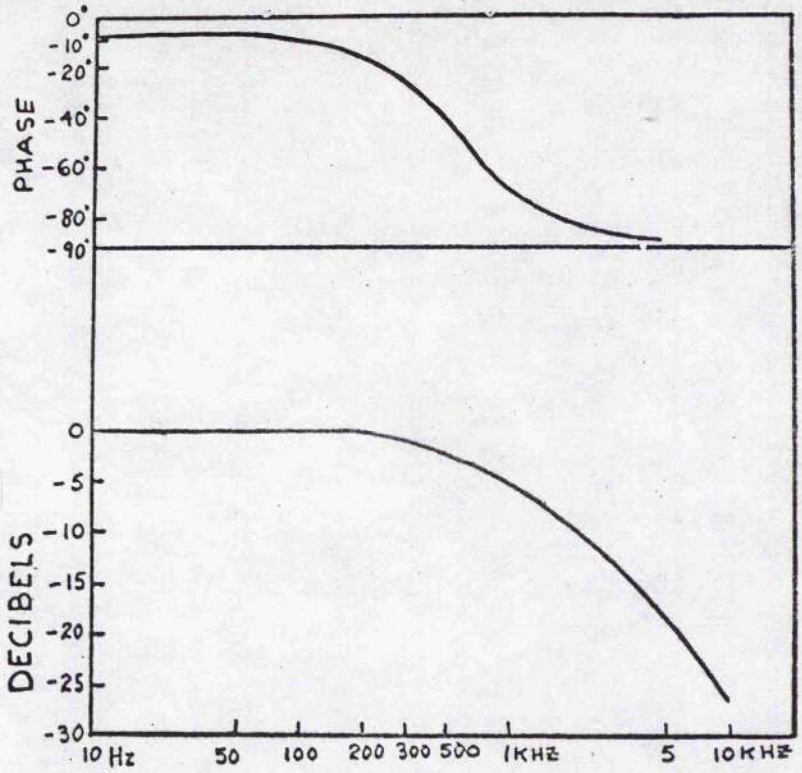

Fig. 2.33 Amplitude and phase response of CO_2 laser optogalvanic effect as measured by Schiffner.[45,46]

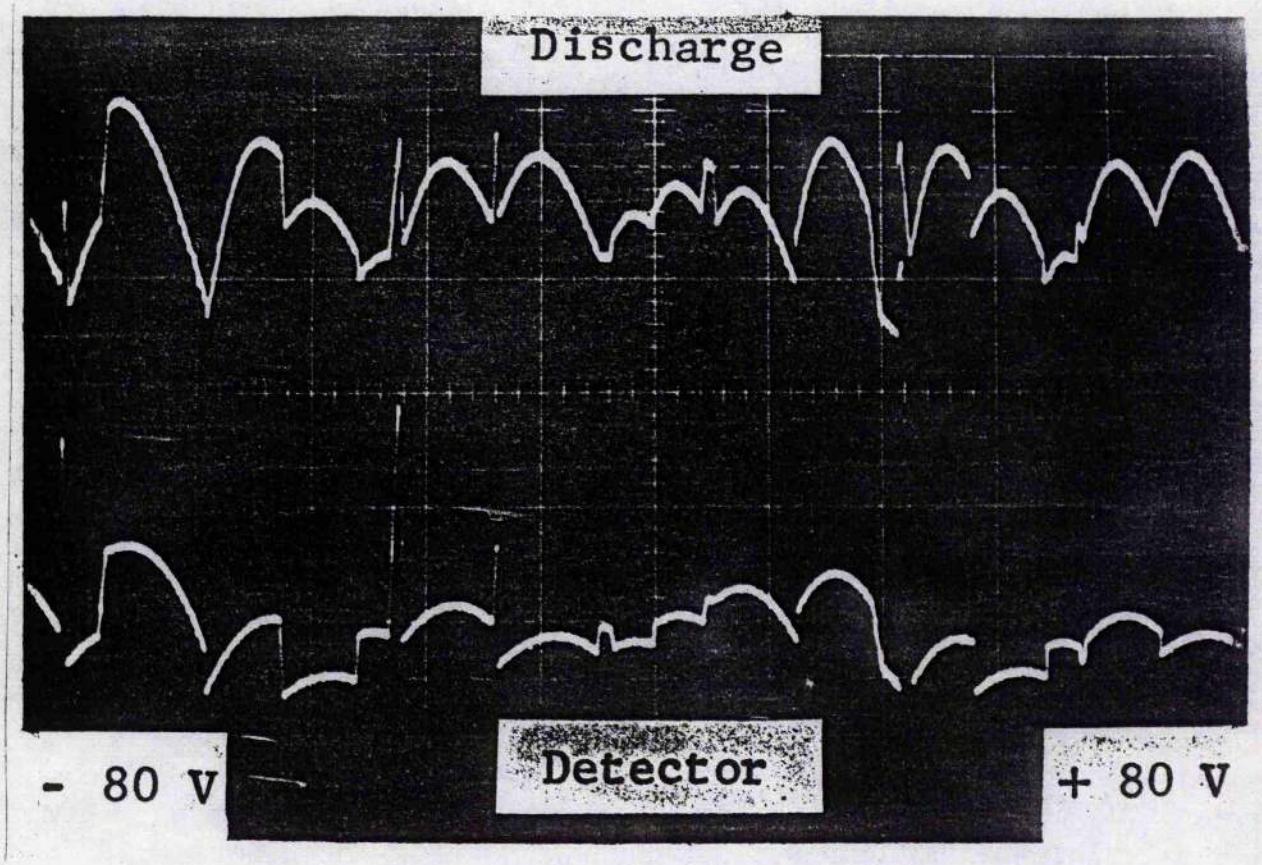

Fig. 2.34 Laser signature (length selected line pattern) recorded by optical detector (lower), conventionally (using HgCdTe detector) and optogalvanic detection (upper) from 'CO_2 Laser Signatures: Calculations and Experiments' by Schiffner.[45,46]

shows a comparison of a signature showing parabolic line segments as detected optically and with tube voltage perturbation technique.

Pulsed CO_2 laser perturbation of laser discharges has been studied by Gower and Carswell[47] using a TEA CO_2 laser to provide short intense 10 μm pulses to probe a low pressure CO_2-N-He continuous discharge. Discharge current perturbations (OGE) as well as sidelight spontaneous emission fluctuations were studied. Data from these relaxation experiments was used to augment known relaxation rates from shock tube, ultrasonic dispersion and spectrophonic techniques.[48] Current fluctuations (temporal information) gave rise and fall times (τ_1 and τ_2 respectively) predicted to be

$$\tau_1^{-1} \simeq k_{10}\, p + n_e r_{10} \ (s^{-1}\ torr^{-1}) \quad \ldots\ldots\ldots \quad (2.6)$$

$$\tau_2^{-1} \simeq a_{11} \simeq k_{21}\, p + n_e(r_{21} + r_{20}) \quad \ldots\ldots \quad (2.7)$$

where k is a molecular collision rate and r denotes an inelastic electron collision rate and p is pressure for a pure CO_2 discharge (see Figure 2.35). When reciprocal OGE rise time is compared to the partial pressure of H_2O or CO in the CO_2 discharge only a narrow range of pressure gave straight line behaviour. The slopes of these lines (Figure 2.36) give the average molecular V-T rates from levels 1 and 2 in the discharge. Extrapolation to zero gave information about the electron deactivation rate which was found by this method and from sidelight perturbations to be $\sim 10^{-6}\ cm^3\ s^{-1}$ (not previously measured for CO_2). Detailed information on the role of H_2O in laser discharges was analyzed showing that for pure CO_2

1. $P_{H_2O} < 0.4$ torr; τ_1^{-1} increases linearly with partial H_2O pressure
2. $P_{H_2O} > 0.4$ torr; τ_1^{-1} does not increase significantly.

In case (1) the lower complex V-T process

$$CO_2\ (01^10) + M \overset{km}{\rightarrow} CO_2\ (000) + M \quad \ldots\ldots\ldots \quad (2.8)$$

$$CO_2(10^00) + CO_2(00^00) = 2CO_2(01^10) + 53.2\ cm^{-1} \quad \ldots \quad (2.9)$$

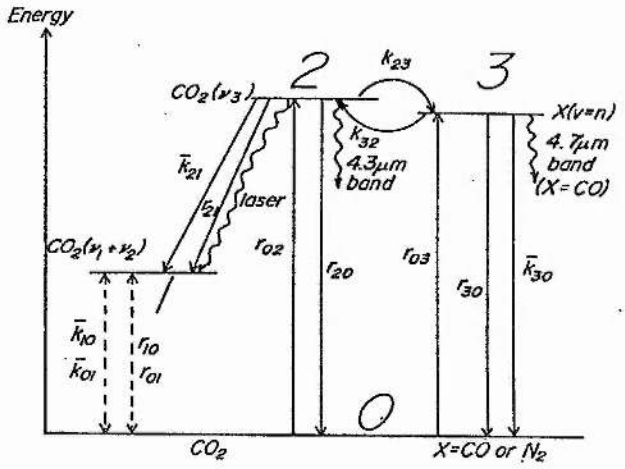

Fig. 2.35 Four level kinetic model of CO_2 discharge showing notation of rates etc.[50]

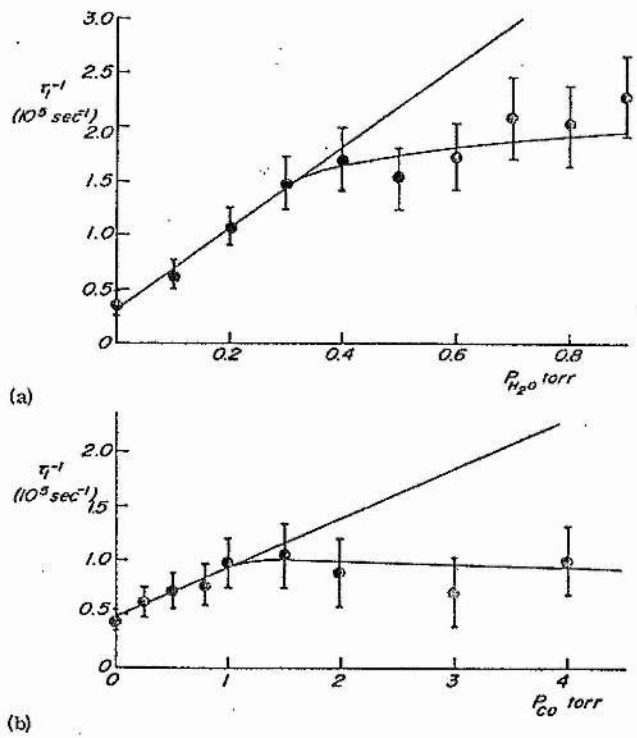

Fig. 2.36 Reciprocal current perturbation rise time as a function of H_2O and CO partial pressure at 10 torr and 20 mA.[50]

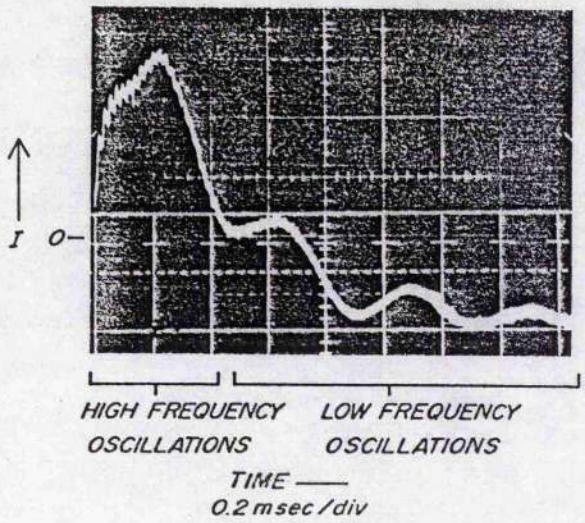

Fig. 2.37 Laser pulse excitation of current oscillations in CO_2:N_2:He amplifying mixture as described below, occurs in two frequency regimes 30 to 50 kHz and 2 to 3 kHz.[50]

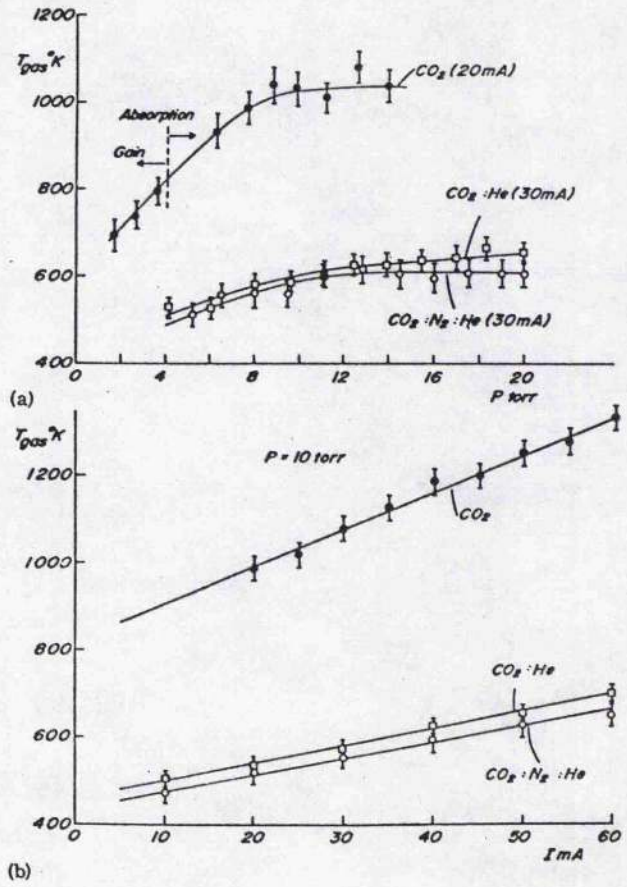

Fig. 2.38 Discharged gas temperature (spatially averaged) measured by radial propogation of acoustic waves generated by short laser pulses as a function of pressure and current for a mixture CO_2:He (1:4) and CO_2:N_2:He (9.5:12.5:78).[50]

must dominate the rate.[48]

Gower and Carswell also reported for the first time observations of periodic damped oscillations after pulse absorption/gain in both sidelight and discharge current and these effects were most pronounced immediately after the receiving discharge was switched on (minimized ∿ 1 minute after switch on). No such oscillations in He or N_2 were seen, therefore, induced (second order) CO_2 population fluctuations seem a likely explanation. Figure 2.37 shows that these oscillations occurred at low (2 to 3 kHz) frequency and high (30 to 50 kHz) frequency following excitation with a short laser pulse; 50 kHz oscillations were observed also by Aoki[49] and attributed to radially propogating acoustic waves. Gower and Carswell[50] utilized this phenomenon to measure the average gas temperature (see Figure 2.38), as a function of discharge current and pressure for 'pure' CO_2 and laser mixtures. By winding a sensing coil around the discharge tube and moving this from cathode to anode the authors found an antiphase relationship between induced EMF and sidelight for the 2 to 3 kHz oscillations which could not be attributed to acoustic waves. The following possible explanations were proposed

1. Variations in electron density proposed by Vesley[51] for HeNe (similar to moving striations).
2. Plasma 'wobbling' at the cathode and resultant current fluctuation possibly due to above.
3. Ringing in excitation/load circuit (unlikely as ballast was changed by factor of 10).
4. Unidentified longitudinal acoustic wave (unlikely as length was changed).

Another possible explanation in the light of this work will be given in 6.3. The authors also note that striation noise in OGE measurements was troublesome particularly at currents above 20 mA in pure CO_2.

2.4 SUMMARY OF PROPOSED MECHANISMS - OPTOGALVANIC EFFECT IN CO_2 LASER DISCHARGES

This brief survey of the proposed explanations of this effect is an overview of the last fifteen years and detailed discussion and comparison will be made in several parts of this work, particularly in Chapter 7 where a full quantitative theory of this effect is presented.

The extensive investigations of Brooks[52] and Smith and Brooks[53] have helped clarify the evidence available which allows discrimination of the three main theories, two of which have been briefly given treatment so far; the three major proposed mechanisms can be named

1. Ionization theory
2. Gas temperature theory
3. Momentum exchange theory.

The ionization theory dates back to Penning and Meissner and assumes that the ionization rates during discharge, for the laser levels are different; this explanation for electronic transitions in atomic discharges is both well developed and documented. As the laser radiation perturbs directly some of the level populations and subsequently coupled levels, then the overall ionization of the gas changes and, as a result, the discharge v-i characteristic is altered. This mechanism was first proposed for the CO_2 laser effect by Kindl et al[43] and further described by Kerecman et al[54]. The required assumptions are that the ionization of the laser levels ($00^0 1$, $02^0 0$, $10^0 0$) and <u>closely</u> coupled levels is adequately large compared to ground state ionization and that the upper and lower laser levels (or selectively coupled levels) have significantly different rates of ionization. If this requirement is satisfied then positive/negative perturbation brought about by gain/absorption can be qualitatively described. These requirements are satisfied in most atomic systems where (a) the role of metastables in gross ionization is dominant, (b) where the laser transition is not much below the ionization limit and (c) there are other very closely coupled levels

(i.e. metastable) which have very different ionization rates. Explanation of the CO_2 laser molecular discharge by this theory is problematic: the ionization limit is almost two orders of magnitude above the laser levels in energy (0.2 and 13.7 eV); there are many vibrational-rotational coupled levels to analyze and there is no evidence to suggest that the upper and lower laser levels have substantially different ionization rates. Crane[55] has suggested that excited N_2 levels close to the ionization limit may be collisionally mixed with the metastable (vibrational ground state) $X\,^1\Sigma_g^+$ levels of N_2 and would be subsequently perturbed, but Bleekrode[56] demonstrated that the lifetime of these electronic levels is approximately three orders of magnitude smaller than the vibrational metastable levels; therefore, mixing is improbable.

Recently Nowicki[57] has attempted to determine a sufficient coupling route from the $00^0 1$ upper laser level to the ionized population in order to implement an ionization explanation for the changes of sidelight and discharge current in CO_2 laser discharges. The analysis consists of a complete set of rate equations (nine populations) for which a stationary solution is found by elimination of most variables. Use is made of experimental v-i measurements (after Lawler[36]) during the simplification process. Little experimental evidence was given and the calculated correlation of discharge current with laser output power is the same as given by Lobov (momentum exchange theory) and the gas temperature explanation;[53] the conclusion of Nowicki is that after surveying many likely energy levels, the nitrogen $N_2(B\,^3\Pi_g)$ level dominates in the ion creating process. All other significant levels have rates two orders of magnitude or more lower. The conclusion[57] follows Crane[55] in asserting that this excited N_2 level which can collisionally mix with the $X\,^1\Sigma_g^+$ metastable vibrational level results in ionized population changes coupled to vibrational energy level changes.

There are three reasons why this explanation is not adequate to explain the empirical evidence for CO_2 optogalvanism:

1. When CO is substituted for N_2 the optogalvanic effect is unchanged (within 5%). This is demonstrated in Figure 8.16.
2. The relevant lifetimes for N_2 ($B^3\Pi_g$) and $X^1\Sigma_g^+$ states are $\sim 9 \times 10^{-6}$s [52] and $\sim 10^{-2}$s [56]. The frequency response of CO_2 OGE should decay at $\sim$ 100 Hz. All authors[45,50,52,53] have found responses up to $\sim$ 1 to 5 kHz and although the $N_2(B^3\Pi_g)$ lifetime is sufficiently fast to support the optically induced ionization changes up to the high frequency ($\sim$ 100 kHz) demonstrated in this work the $X^1\Sigma_g^+$ ionized level time constant is not comparable. In principle, ionization population changes (if they can occur) should produce current changes at rates $\sim$ 1 μs. If another route was contemplated then the upper frequency limit of OGE should be 1 to 2 orders of magnitude higher than that observed.
3. At low currents the OGE signals can be larger for a given optical change and Smith and Brooks[53] and Carswell and Wood[42] have observed this effect; it is presented in detail in Chapter 8 of this work. The ionization explanation predicts an OGE signal turnover at low/medium currents $\sim$ 10 mA. This signal reduction has not been observed in these or any previous investigations. The gas temperature explanation, however, does predict the observed behaviour.

The gas temperature theory originates with the first observation of the CO_2 laser OGE by Rigden and Moeller[40] and begins with the idea that the generation of an intense laser beam is a major energy loss process (10 to 25% efficiency) and, therefore, considerable cooling of amplifiers (and heating of strong absorbers) should occur, substantially altering the thermal balance of the discharge. By changing the discharge tube wall temperature similar changes of discharge impedance were observed. Aoki et al[58] have investigated this theory in some detail using an intracavity CO_2 absorption cell in a Q-switched CO_2 laser (a pulsed rather than cw experiment). The proposed explanation was that for a gain medium the upper CO_2 laser level

($00^0 1$) population is reduced and the lower laser level ($10^0 0$) population is increased (and vice versa for absorption). Normal relaxation from the $00^0 1$ level is via V-T processes which result in heating the gas (by providing a translational energy fraction) and this relaxation process is in direct competition with the laser transition (which also depletes the $00^0 1$ population). Therefore, as the laser gives up vibrational energy to photon generation, energy is taken away from the heating process and the gas is cooled (kinetic cooling). The time constant for the relaxation of this level population is the V-T lifetime $\sim$ 0.5 ms depending on pressure, mixture, temperature, etc.

Conversely, as the ($10^0 0$) lower laser level population increases (with laser action, in gain) then the normal V-T relaxation from this level is increased, resulting in more translational energy supplied to the gas (kinetic heating). The time constant for the relaxation of this level population by V-V-T and V-T relaxation is $\sim$ 10 μs. Overall, there is a net loss of translational energy (i.e. cooling) because $\sim$ 10 to 25% is given up to the beam. Previously Kindl et al[43] had recognized two different time constants and Aoki et al[58] studied this in some detail and found a reasonable correlation with the predicted relaxation times. The gas temperature theory does account for positive and negative perturbations for gain and absorption, but Aoki et al and Rigden and Moeller did not explain how the discharge current was modified by these changes in thermal balance.

Smith and Brooks[53] suggested that a change of gas translational energy (temperature) would cause a localized number density change (in the radiating/irradiated volume) and that this would lead to a gross pressure change in a sealed laser tube (optoacoustic effect - Gebhardt and Smith[59]). For a decreasing temperature (laser in gain) an increase in number density would occur which results in a decrease of electron mean free path and electron mobility.

The momentum exchange theory is due to Lobov et al[60] and proposes no changes in ionization and no density change, but only perturbations of the energy exchanged per inelastic collision of molecules with electrons.

The electron mobility (b_e) depends on this process and any change of exchange momentum would result in a change of electron mobility and subsequently discharge v-i characteristics. The electron mobility is given by

$$b_e = C\,(e\lambda/mE)^{\frac{1}{2}}\,(X)^{\frac{1}{4}} \quad \ldots\ldots\ldots\ldots \quad (2.10)$$

where C is a constant depending on the electron distribution factor, e, λ and m are the electron charge, mean free path and mass; E is the accelerating electric field and X is the average energy imparted by an electron to a molecule per collision. Lobov[60] considered no change of λ or number density and predicts well the change in discharge voltage of 10 mV/W when a CO_2 amplifier was used as an external detector, which was measured as 8 mV/W. This correspondence was probably fortuitous, bearing in mind that the irradiated volume and laser beam parameters were not measured (or known) and various processes were ignored.

Smith and Brooks[53] used an external cell of similar dimensions to a conventional amplifier (see Figure 2.41) and measured pressure changes in the cell as well as current and sidelight changes. Changes in pressure were measured by a fast response MDC capacitance manometer coupled to the discharge reservoir volume. The pressure fluctuations were corrected for the volume factor (the ratio of irradiated to non-irradiated volume). Good agreement of experimental results with the gas temperature theory was found (see Figure 2.42) for currents > 10 mA (20 mA/cm^2) and the number density changes were found to provide a sufficient mechanism in this pressure regime. From the electron mobility equation the discharge current is just

$$i = n_e AeEb_e = C^1(E\lambda)^{\frac{1}{2}}(X)^{\frac{1}{4}} \quad \ldots\ldots\ldots\ldots \quad (2.11)$$

provided λ and X changed due to perturbations of the CO_2 vibrational populations; n_e is the electron density; A is the tube area and C^1 another constant dependent upon the electron distribution factor. Assuming that the optically induced current fluctuation Δi depends only on X and λ by taking increments and using $\lambda \propto p^{-1}$ (where p is gas pressure)

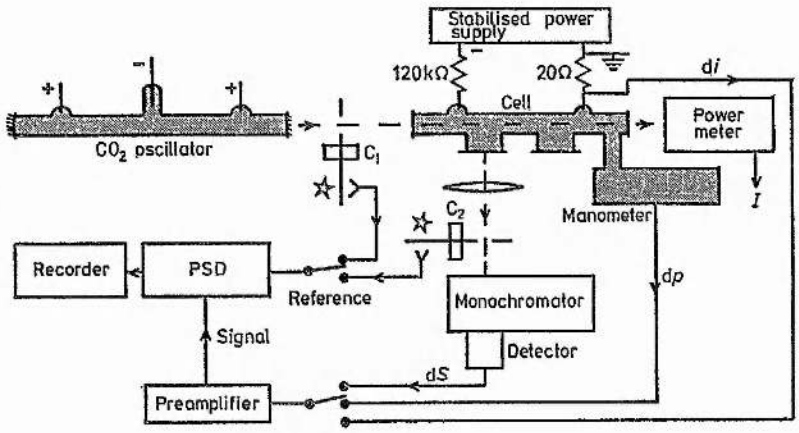

Fig. 2.41 Apparatus used by Smith and Brooks to measure changes of sidelight (spontaneous emission), discharge current and gas pressure in a sealed 'laser like' discharge of pure CO_2 or CO_2, N_2, He, Xe, H_2.[53]

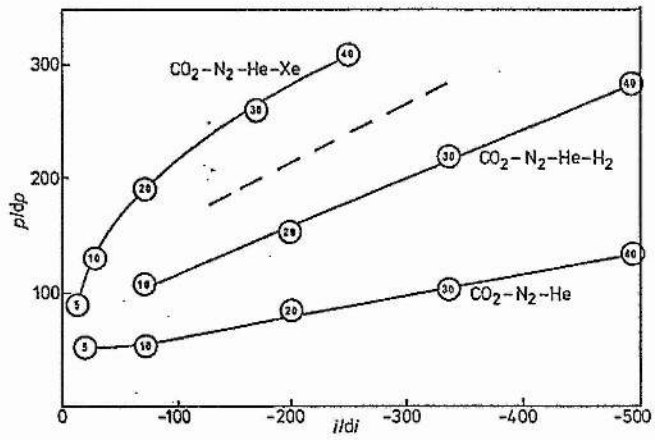

Fig. 2.42 Gas temperature theory predicts that i/di ∿ - 2 p/dp shown as dotted line compared with experimental results of Smith and Brooks.[53]

$$\frac{\Delta i}{i} = \frac{1}{4}\frac{\Delta X}{X} - \frac{1}{2}\frac{\Delta p}{p} \quad \ldots\ldots\ldots\ldots\ldots\ldots \quad (2.12)$$

Figure 2.41 shows some experimental results of Smith and Brooks; provided $i > 10$ to 20 mA then the slope of p/dp vs i/di is close to -2, as would be predicted by the previous equation if $\Delta X/X \ll \Delta p/p$; Smith and Brooks conclude that at higher currents the number density fluctuation is the primary mechanism producing current fluctuations. Additionally, it was found that particularly for mixtures including Xe and H_2 that at low currents another mechanism was significant, and because the ionization mechanism should be most important at higher current densities it is concluded that this other mechanism is likely to be the momentum exchange mechanism (as proposed by Lobov et al[60]). It was not determined whether this effect was due to electron collisions with 00^01 or 10^00 populations (or both) and closely coupled populations, or if the altered momentum exchange was a direct consequence of the pressure fluctuation but, because time constant limitations of OGE at low currents were comparable with the 00^01 V-T relaxation rate then the final hypothesis seemed most likely. The decisiveness and elegance of the Smith and Brooks experiments (which included a vast study of sidelight perturbations[53]) resulting in strong evidence in favour of the gas temperature mechanism as the dominant process, was largely due to the use of a constant current PSU for dc excitation, which removes many ambiguities in measurement which had become a characteristic (if notorious) feature of the literature on this subject; a detailed discussion of excitation will be given in 3.2.

To summarize, the gas temperature explanation was favoured by Smith and Brooks as the primary optogalvanic mechanism in CO_2 laser discharges for the following reasons:

1. Pressure fluctuations were known to occur with radiation field changes (optoacoustic effect) and have been carefully measured. The sign and slope of $\Delta i/i$ vs $\Delta p/p$ agrees well.
2. The decay of the OGE signal at $\sim$ 1 kHz is commensurate with the upper laser level relaxation time (i.e. the V-V-T process is closely related).

3. The ionization rate of the laser levels is not significantly different from the other levels in the system.
4. Ionization limit is very much higher energy than laser levels and selective coupling channels are not known to exist.

The momentum exchange mechanism probably contributes significantly at low currents and the sign of the contribution is opposite to the ionization prediction.

2.5 OPTOGALVANIC MOLECULAR LASER STABILIZATION - PREVIOUS WORK

Following the observation of a molecular V-R transition optogalvanic effect in pure CO_2 and CO_2 laser mixture discharges by Rigden and Moeller[40], a CO_2 laser was first actively stabilized by utilizing this effect by Skolnick[61] in 1970. Previously, CO_2 lasers had been actively stabilized, by using an optical detector, to the laser line centre or to a spectral feature in an absorbing gas,[62,63] and the technique of frequency modulating externally[64] later resulted in a stabilized beam without dither. By 1970 Freed and Javan[65] had observed the low pressure Lamb dip in the 4.3 μm ($00^0 1$ to $00^0 0$) transitions of CO_2 in an external cell which has become a major stabilization scheme for the CO_2 laser.[66]

The optogalvanic stabilization system used by Skolnick was electronically conventional; it used the change of laser output power/intracavity intensity in order to generate the frequency error signal (frequency shift from oscillating line centre) with phase information to distinguish if the oscillating mode frequency was high or low. As the single laser mode (see Chapter 4) is tuned across the laser line gain profile, the laser intracavity power changes and this results in a current change.[40] Skolnick set up a phase locked loop by feeding an ac modulation signal (500 Hz) to a linear PZT element which subsequently dithered one of the laser mirrors and this generated an ac fluctuation of laser intensity. The resultant ac voltage changes were capacitatively coupled from the discharge tube and fed to a lock-in amplifier referenced to the modulation frequency. The 45 cm long

sealed laser was fitted with four NaCl Brewster prisms to ensure single line operation. The laser produced 2 W output beam from 8 mm diameter tube and a 9 kV potential sustained the CO_2, N_2, He, H_2 discharge. The frequency modulation due to dither was calculated to be ∿ 2 MHz excursion. The maximum gain slope signal was ± 10 V (with the above modulation) or 0.25% fluctuation with a cv supply. Simple passive filtering and dc amplification were required before the error signal could be applied to the PZT and this simple servoloop (when closed) produced a stable lock to line centre and, although no detailed performance figures of the system were measured, an estimated 50 kHz/hour drift rate (ignoring modulation) was given.

Thomason and Elbers[67] described a similar but simplified system (with simply constructed PSD and amplification etc.) without extra dispersive elements, other than the laser cavity itself, for actively stabilizing a commercial Silvania 948 CO_2 laser. By eliminating the need for prisms, gratings, infrared detector, or commercial lock-in amplifier these authors stress the great improvement of long and short term amplitude and frequency stability obtained inexpensively (< \$150),[67,68] (see Figure 2.51).

The Thomason and Elbers system allowed off-line centre stabilization by locking the laser mode to line centre and adding into the integrator (where the error is stored) input a dc voltage to offset the zero-error locking point. This optogalvanic system unfortunately was not performance tested although the damping time of the servo was measured to be 1 to 1.4 s and using this passive error observation, a longer than 1 s response to frequency drift step should be ∿ 0.5 MHz; another limitation noted was that a 2% total change of modulation oscillation, gain of servo amplifier and laser power (realistic estimation of operating variations) would imply a < 1 MHz drift when line centre stabilized.

Several experimenters have used similar stabilization schemes for CO_2 laser stabilization without publication. Notable amongst them is Hart[69] for investigations into different and novel detection coupling methods.

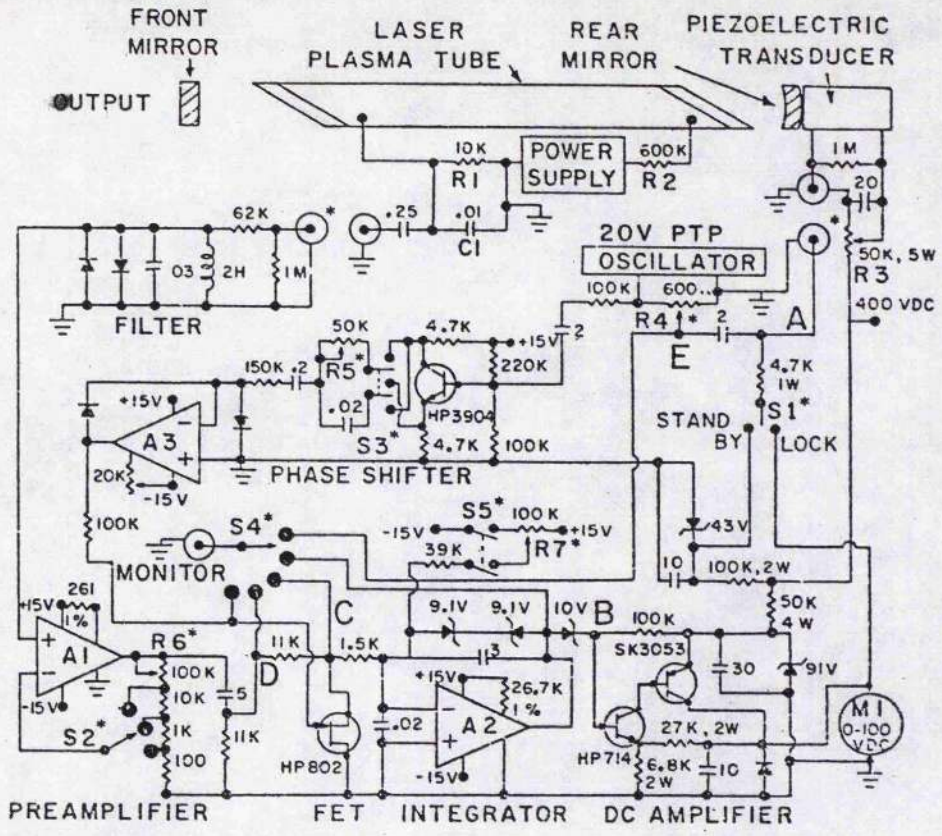

Fig. 2.51 Schematic of OGE laser stabilizer for an 'inexpensive' system to stabilize a Sylvania 948 CO_2 laser.[67]

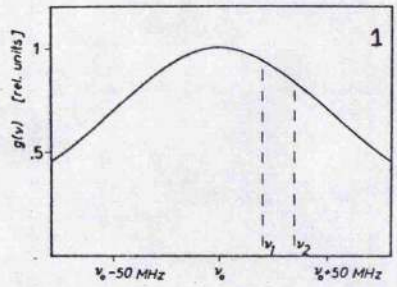

a b

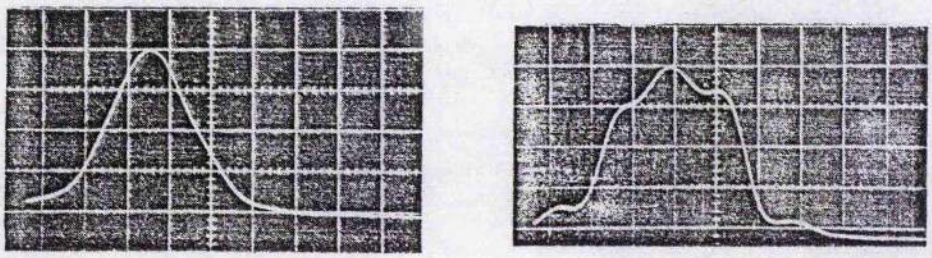

Fig. 2.511 (1) How the transverse mode can have a lower gain away from line centre. If both transitions are near line centre then the gains will be almost equal. (b) Intensity profiles (by rotating mirror technique) of (a) OGE stabilized offset mode control and (b) conventional iris mode control.[70]

2.51 OTHER TECHNOLOGICAL APPLICATIONS

The earliest applications include Penning's neon purity measurement system, previously discussed, striation suppression and easier starting by Kenty.[12] With respect to molecular discharges the earliest published application is due to Carswell and Wood[42] who suggested that the laser beam control of discharge current in a cell could be used in a similar fashion to the grid control of current in a thermionic triode; the additional large circuit amplifications (due to the negative differential impedance) may be useful for this application or used alone as a two terminal amplifier (rather like a varactor diode, etc.). Jacobs et al[71] also suggested in 1967 that these discharges could make suitable radiation detectors. Pepper[33] has recently introduced the idea of isotope separation by OGE.

Stefanov[72] first suggested that current changes could be used for detection of laser action (near thresholds) and optimization of mirror alignment. This work shows that for a low gain laser transition initialization of laser action is most easily achieved with two total reflectors and, as a result, no optical output is available and a v-i perturbation is simply observed and has a fast time response (compared to pyroelectric and thermopile detectors). A mechanical chopper ($\sim$ 300 Hz) and a very high stability PSU ($\sim$ 2 mV/kV) was used as the measurement system.

Stefanov notes that no alignment or refrigeration is necessary for IR detection and that an OGE signal was strongly observed at 3.39 μm in HeNe. Early gain investigations were made in waveguides ($\sim$ 2 mm diameter English Electric tubes) filled with various mixtures and excited at differing currents. With two total reflectors, losses $\sim$1% (half round trip) are claimed and, therefore, laser gains $\sim$1% were observed and were compared by studying current changes; mirror alignment in this case was manual but extension to an automated system is easily visualized.

A Thomason and Elbers stabilization system was used in 1976 by Massig[70] to stabilize a CO_2 laser off laser line centre, not to improve frequency stability, but in order to suppress transverse modes. Many laser

applications require single frequency operation and in order to select one line a grating is normally chosen or the cavity is kept short (see Chapter 4.1) as the signature effect adequately selects one laser line which best matches the length conditions. Simultaneous oscillation on several longitudinal modes is also suppressed by shortening the laser cavity by increasing the mode separation to greater than the transition linewidth. Higher order transverse modes are usually suppressed with an intracavity iris which increases the diffraction losses of these modes and gives preference to the axial (TEM_{00}) modes. Massig reports that for the particular experiment in consideration (forward scattering) the iris reduced output power considerably and resulted in a non-Gaussian diffraction pattern for the lowest order single mode output beam, and resulting sidelobes produced greatly increased beam divergence.

In some resonators not including concentric and planar/planar (i.e. many cases) it is in principle feasible to discriminate spectrally the different transverse modes because the transverse mode frequencies are not the same. Figure 2.511(a) shows how the small signal gain of one mode will excede the other mode as long as the modes are shifted away from line centre. For the system described by Massig the TEM_{00} and TEM_{01} mode frequency difference is $\sim$ 15 MHz (typical) and an offset of 20 MHz of the TEM_{00} mode was sufficient to suppress the TEM_{01} mode. The exact offset can be calculated by taking into account the gains and losses of the two or more modes being considered.[73] Figure 2.511(b) shows a comparison of the active offset (optogalvanic stabilizer) technique and the iris technique noting that the intensity profile approaches Gaussian much more closely than the iris technique.

Massig used a different offset circuit (to Thomason and Elbers): an ac signal at modulating frequency was injected into the input along with the OGE signal. Adjusting the amplitude of this ac input varies the offset by generating a fixed dc point at the integration (alternatively, it can be seen as subtracting from the allowed non-zero error signal at the input).

This mode improvement technique was found to be superior to any other

method and Massig suggests a shortening of the cavity (beyond 80 cm) in order to increase the transverse-axial mode frequency difference.

2.6 FUNDAMENTAL REASONS FOR FAVOURING OPTOGALVANIC EFFECTS

There are many reasons why OGE detection is preferred to conventional optical methods, i.e. solid state photon detectors, and these fall into two broad categories: fundamental and technological. Some major fundamental reasons are listed below with brief explanations.

1. OGE is a resonant detector. Only signals with wavelengths resonant with the chosen transitions of the detector are measured. This has important consequences for the detection of low power narrow band signals in the presence of intense signals detuned from the narrow detection band. This is a major reason for using OGE as a stabilization error detector.
2. OGE is not necessarily fundamentally wavelength sensitive; most optical detectors are i.e. CO_2 10P(20) and 10P(12) radiation can be compared in power directly.
3. The detector bandwidth may be adjusted. For example, by adjusting the pressure of the receiving gas the bandwidth of the CO_2 V-R transitions can be adjusted (in principle) from $\sim$ 1 MHz (0.2 torr Lamb dip) to $\sim$ 5 THz ($\sim$ 12 atmospheres) when the CO_2 lines coalesce. This consideration will be made in Chapter 9.1.
4. Linearity of electrical signal with beam intensity often exists over a very wide range. It is this major property along with the inability to damage the detector which makes the effect suitable for stabilizing high power CO_2 lasers (including TEA lasers).
5. The quantum efficiency is theoretically and practically high. In the configuration used in these experiments

almost every photon that is absorbed (or amplified) should produce an electrical change. In practice, the amount of energy lost or gained during gain or absorption determines the numbers of photons being used in the detection process. The energy lost (or gained) by these photons directly changes, to the first order, the temperature of the gas being discharged. The relation between discharge temperature and the v-i characteristic depends on the properties of the discharge and the excitation scheme. In some cases, signal amplification of 10 to 1000 times can occur.

In addition to these fundamental reasons supporting OGE techniques, there are several important technological advantages which are listed below.

2.61 TECHNOLOGICAL ADVANTAGES OBTAINED WITH OGE TECHNIQUES

1. OGE is a direct electrical technique. In most radiation detection schemes there is an intermediate stage, e.g. the Golay detector, where radiation is converted into gas pressure changes which are subsequently changed into electrical signals by a moving coil transducer mounted on a flexible diaphragm.
2. OGE is particularly vibrationally insensitive and not microphonic. This is due both to the distributed nature of the detection element and because of the spatial coincidence with the light source (in the case of the oscillator). Many optical detectors, e.g. pyroelectrics, are also piezoelectric and very susceptible to microphony.
3. Wide electric bandwidths can easily be achieved. In these CO_2 experiments ac detection up to frequencies

of 100 kHz was achieved. Many thermal detectors (due to their high capacitance) are slow when large areas and powers are being detected. For example, a 0.5 cm^2 pyroelectric element would be unusable, typically at frequencies above 500 Hz.

4. The OGE detector is rugged and cannot be damaged by very intense optical beams due to the gaseous nature. This factor may be essential when TEA pulses must be shared by the same optical system.
5. The OGE detector is both simple and cheap. In addition the properties should not age. For stabilizing oscillators the discharge already exists and intensity detection costs no extra.
6. The OGE detector is optically thin or 'transparent'. Conventional optical detectors must remove some power from the laser beam resulting in either degradation of beam quality (geometry) or reduction of output power available from the system.
7. For laser stabilization the detector reliability can be assured as long as the laser oscillates.

From the preceding stated technological and fundamental advantages it can be seen that there is a strong case for the utilization of OGE detection in laser systems; there are also some disadvantages, including the separation of the low ac signal from the high dc excitation voltage (Chapter 3.22) and the channel noise associated with dc discharges (Chapter 9.1). Detailed discussion of the advantages and disadvantages are presented with the experimental results in Chapters 4, 5, 6, 8 and 9.

2.7 OTHER SIMILAR DETECTION SCHEMES

Various experimental techniques, other than OGE, are used today which depend on optically induced electrical changes with resonant or broadband radiation. This family of electrical detectors is a member of a wider class of gas/light interaction schemes, including opto-acoustic spectroscopy[74,75] where microphonic rather than electrical detection is used,[76,77] thermal lensing[78,79] where another probe beam monitors the optically induced changes in the gas refractive index, and photothermal deflection spectroscopy (PDS)[80] which also uses a probe beam; PDS is finding increasing applications in studying absorption/reflection in solids, liquids and gases, particularly where the absorption is very low[81] $\lesssim 10^{-8}\text{cm}^{-1}$. A new technique, photoacoustic ranging[82] has recently been developed using acoustic detection of laser induced soundwaves over long distances.

The electrical schemes (other than conventional OGE) of detection can be broadly classified as follows:

1. Optogalvanic detection in hollow cathode lamps
2. Optogalvanic detection in flames
3. Space-charge limited diode detection
4. Photoionization detectors: notably light and microwave detection with commercial neon and argon miniature lamps
5. Prebreakdown regime detection.

Cases (1) and (2) have both been used extensively[18] for spectroscopic purposes with tunable dye laser probes operating in the visible. Hollow cathode lamps operated in OGE mode have provided an important and powerful means of frequency locking cw dye lasers to a very large number of atomic transitions (e.g. Ne, Na, Ba)[83] and the ability to stabilize at frequencies corresponding to excited states should be useful in analytic chemistry, spectroscopy and isotope separation. Stabilization to weak transitions is feasible with this technique due to no scattering and collection problems, unlike flourescence techniques. Other species have been detected including impurities present in the cathode (rare metals, alloys, etc.) and parallel

investigation of atoms and molecular ions in flames is feasible in order to study ionization during combustion. Chemical analysis of trace metals using dye laser induced OGE in analysis flames has been reported,[22] see Figure 2.71 and an application for U.S. patent made by Green.[20] Low concentrations of less than 1 p.p.b. have been measured[85] and this sensitivity of detection is equal or just better than other existing methods.

Space charge limited diode detection dates back to early photoionization studies and the early work of Foote and Mohler[7] has been described in 2.0. Lawrence and Edlefsen,[86] Mohler and Boekner[87] and Freundenberg[88] have all used this technique to study ion formation in Cs. This optical detection technique was reintroduced in 1966 by Popescu,[89,90] and Marr and Wherret[84] in 1972 studied Cs_2 molecular ions using essentially the same apparatus with a Hg lamp and monochromator as a source (see Figure 2.72).

The detection capabilities of dc discharges in normal and abnormal glow have been discussed by many authors for microwave frequencies,[91,92,93] millimeter wave frequencies[94,95] and optical frequencies;[96] these commercial indicator glow lamps (Penning mixture) provide cheap, rugged, wide dynamic range and microsecond rise time detection.

The extensive work of Kopeika[97] had included by 1977 various mechanism studies and by using HeNe, HeCd, Ar ion, lasers as well as broadband sources, many processes have been explained. The primary mechanism given is gas breakdown enhancement by the electromagnetic field (from the radiation) augmenting the fixed dc bias. At short wavelengths where detectivities can be as good as photomultipliers[98] breakdown is enhanced by direct photoionization. At long wavelengths (microwave) the breakdown is explained as a cascade ionization process where the incident EM wave enhances the electron velocity and hence increases the collision rate and ionization.[99] The amplified change description then follows the optogalvanic phenomenological theory of Erez et al[35] however, the interesting feature of this work is the temporal behaviour of these discharge detectors.

Parasitic reactance (mostly inductive) has been studied in great detail

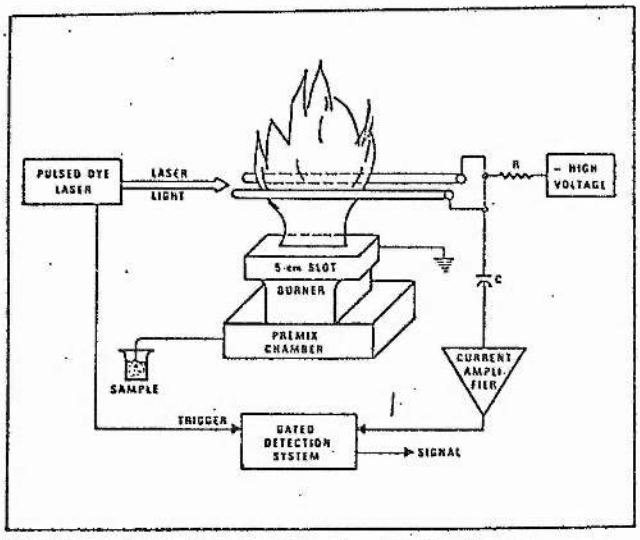

Fig 4 *Optogalvanic detection of atomic species in a flame*

Fig. 2.71 Typical OGE flame detection system using a pulsed dye laser and gated detection system for signal enhancement, reproduced from King and Shenck.[22]

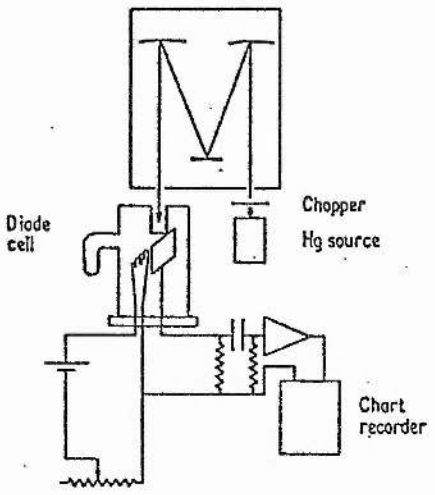

Figure 1. Schematic diagram of the apparatus.

Fig. 2.72 Conventional space charge detection apparatus used to study molecular ion formation in CO_2 (no phase sensitive detection), reproduced from Marr and Wherret.[84]

and the intrinsic mechanisms have been shown to be very fast ($\sim$ 1 to 100 ps) in low pressure subminiature tubes; the other feature of these devices to have been extensively investigated is the gain of the device due to the negative differential impedance. Typical operating characteristics of a miniature indicator lamp (not designed for this purpose) are a tuned ac detector response (video detector response) of 10 to 100 kHz with a Q of $\sim$ 10 which is a strong function of current and device construction and a typical gain of 100 times a gas filled photodiode in the prebreakdown mode (internal gain is $\sim$ 10 dB). An important consequence of this work is that device construction rather than fundamental time constants (of the gas) controls the high frequency response. Penning ionization spectroscopy has recently been achieved[100] using the optogalvanic effect in calcium-neon discharges to show that the Penning ionization process, lowest Ne metastable ionization of Ca, exists and that the effect is useful in such studies. The experiments utilized a pulsed dye laser to stimulate a quasiresonant transition. Penning ionization by neon metastables is shown to be readily achieved but no efficient Penning ionization was seen from the Ne $^1P_1$ level owing to the strong allowed dipole transition to the ground state. Temporal signal behaviour was found to change significantly with voltage and current and consists of two or three spikes (with possible sign changes) over a timescale $\sim$ 0.1 to 0.5 ms and the authors promise a 'detailed theoretical model' as these effects are not predicted by Erez et al[35] or Shuker.[101]

In the prebreakdown regime extensive investigation of the transient behaviour of discharges using pulsed light sources,[102,103] and the first study of ionization growth due to laser induced ionization showed some important advantages of working in this mode.[19]

Interpretation of the prebreakdown OGE perturbations is simplified because the electron energies are well defined and a near uniform field exists. Figure 2.73 shows the apparatus used by Kravis et al to investigate prebreakdown OGE and Figure 2.74 shows an optogalvanic signal due to irradiation by dye laser at 6143 $\mathring{A}$, corresponding to the Ne $1_5 \rightarrow 2p_6$

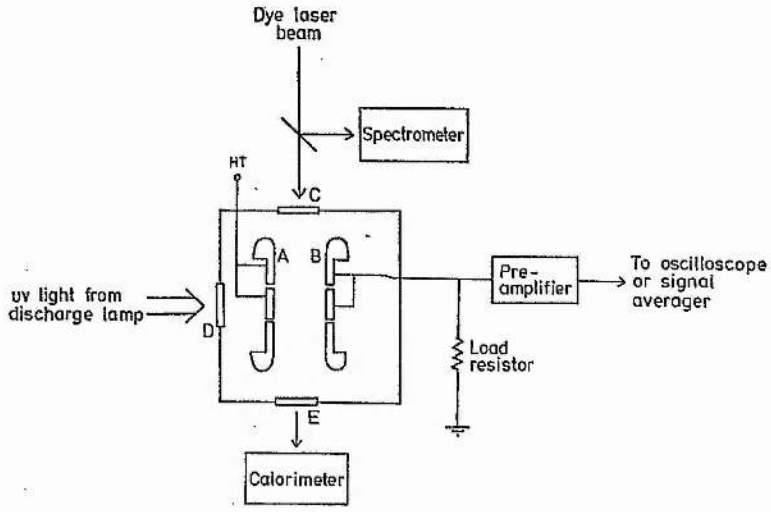

Fig. 2.73 Apparatus used to measure prebreakdown optogalvanic effects in neon. Temporal growth of ionization was made with uv source and optical perturbation measurements with dye laser at 6143 Å reproduced from Kravis and Haydon.[19]

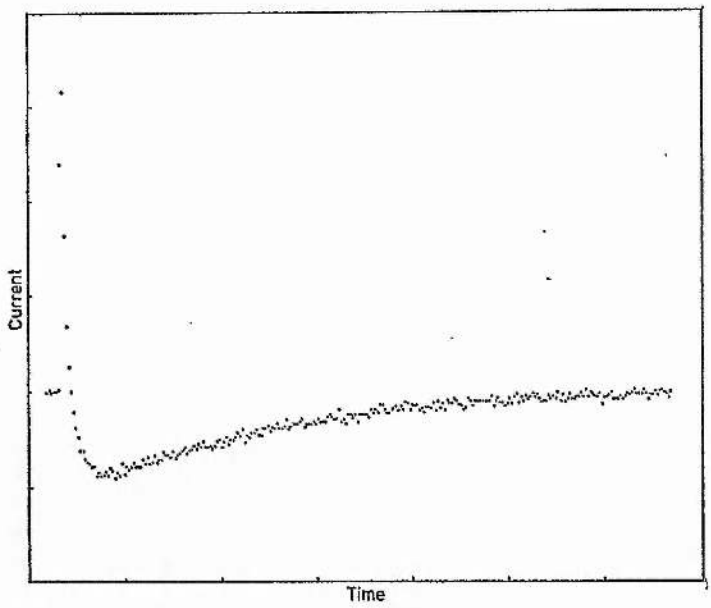

Optogalvanic signal produced by irradiation at 6143 Å ($1s_5 \rightarrow 2p_6$ transition). Vertical scale 1 nA div^{-1}, horizontal scale 0·5 ms div^{-1}. Discharge conditions, V= 180 V, d=1·8 cm, Cu cathode. The total ionisation current was 14 nA.

Fig. 2.74 Prebreakdown optogalvanic signal observed by Kravis and Haydon with fast critical spike and slow exponential decay, reproduced from Kravis and Haydon.[19]

transition. Detuning of the laser showed rapid decay so this is a resonant absorption process unlike in the case of the uv photoionization detection in neon lamps (which corresponds to a transition to the ionization continuum). The slow negative component ($\sim$ 10 ms) has been shown (by varying electrode distances) by Krish[104] and Haydon and Williams[105] to be due to diffusion of metastable atoms. A positive fast spike 30 to 60 μs is observed and several mechanisms have been suggested to explain this component, including

1. Laser excitation of more highly excited states (metastables)[106]
2. Direct photoelectron generation at the cathode[19]
3. Upper excited state relaxation[35].

Explanation (1) seems improbable because semi-empirical prediction of electron ionization rates from excited levels[107] gives the cross-section ratio for ionization of states $2s_6$ and $1s_5$ to be 3. Also the average electron energy is > 11 ev[108] at suitable values of E/N and, therefore, only a small number of electrons $\sim$ 10% can exceed the threshold energy for ionization from each level. As a result, the increased ionization rate (due to irradiation) of the $2P_6$ level is not more than 3.5 times the rate for the $1s_5$ level. Only $1:10^{10}$ atoms are in a metastable level, and the increase in ionization would cause a very small perturbation of total ionization which is dominated by ground state-electron collisions.

The cathode photoelectron explanation would predict a $\sim$ 30 ms spike related to the drift time for an electron pulse in the device. High energy photons originating from decay of He $1s_2/1s_4$ resonance states are required and it might be possible that the spike is an unresolved train of successive pulses generated by positive ion impact (transit time $\sim$ 4.5 μs). This explanation is consistant with Kravis' observation of the lengthening of the spike very near to breakdown.

According to the theory of Erez et al the upper level decay time should dominate the OGE decay time ($\sim$ 50 ms) and a combination of cathode effects and upper laser relaxation may be a suitable explanation.

3.0 EXPERIMENTAL APPARATUS

The laser apparatus constructed for these experiments consisted of five passively stable CO_2 lasers shown schematically in Figure 3.01 and described in 3.11, 3.12 and 3.13, two intracavity discharge tubes, two multianode separate discharge cells and a 4.3 μm $00^0 1$ sidelight flourescence cell (described in Chapters 8 and 9). Different discharge tubes were fitted to each laser frame. Several stabilizer servomechanisms were constructed for stabilizing these lasers (described in 3.23) and a heterodyne detection system for studying the beat frequency of two or more lasers assembled (described in 3.42). Additionally, CO lasers constructed by G.A. Murray of St. Andrews University, Edinburgh Instruments and Heriot Watt University, were used for the CO optogalvanic measurements.

Additionally, beam profile monitoring with a commercial (Delta Developments) 50 element self-scanning pyroelectric array was used to evaluate laser mode quality and a suitable beam telescope was constructed for these experiments (see 3.41).

3.1 CO_2 LASER DESIGN, DEVELOPMENT AND CONSTRUCTION

Five CO_2 lasers were constructed during these investigations and they underwent considerable development during use; all lasers and discharge tubes were constructed of stainless steel and glass, sealed with a stainless steel bellows valve and were refillable. A gradual development towards a modular construction was followed in order to facilitate simple modification for experimental purposes (such as discharge tube changing). All the lasers used either a 3 rod (25 mm diameter) or 4 rod (19 mm diameter) invar framework and the smaller systems used aluminium 25 mm and 12 mm material mounting plates for the optical stages and for mechanical construction and the final developed system, used 25 mm stainless steel construction (see Figure 3.131). No intentional magnetic screening or temperature control of the invar was used and the lasers were not built into a soundproofed cabinet for acoustic (audio frequency) insulation. The lasers were mounted to the

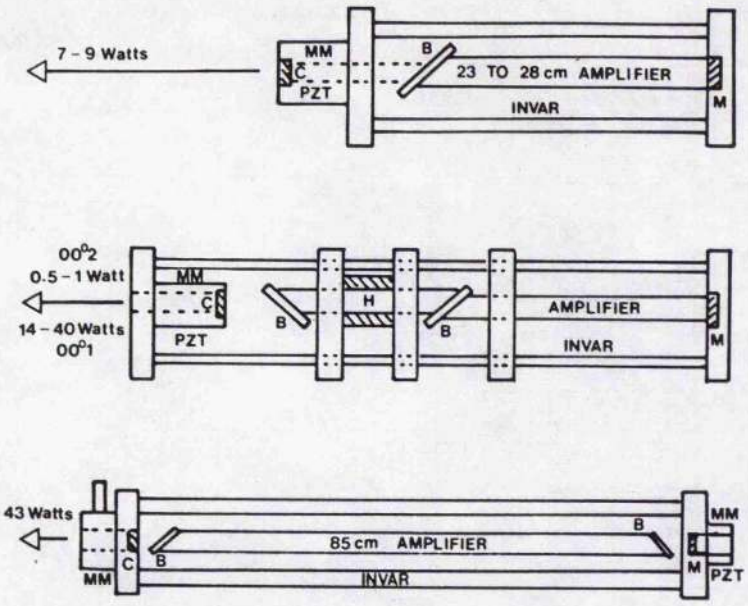

Fig. 3.01 Schematic diagrams of (a) the compact 8 W sealed lasers described in 3.11, (b) the sequence band CO_2 lasers described in 3.12 and 5.1 and (c) the high power laser developed to produce output powers > 40 W described in 3.13.

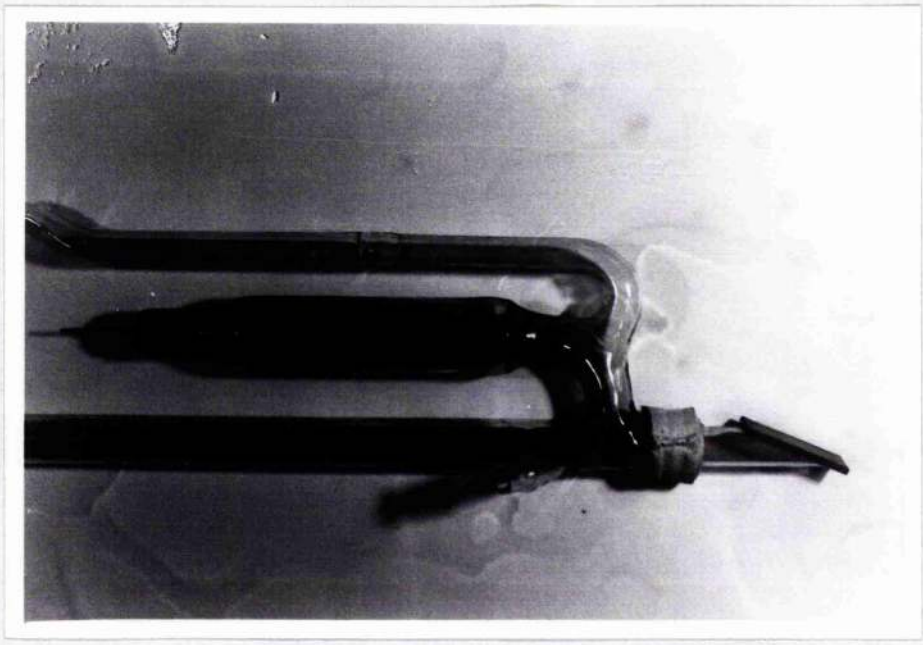

Fig. 3.11 7 mm diameter, 25 cm quartz laser tube showing ZnSe Brewster window, Pt cathode, gas inlet and water jacket. Note dark deposits in cathode inner bore after ∿ 1500 hours use.

Ealing table by clamping (with PTFE coated slides) to keep alignment with each other and with the other optical components; this mounting also reduced the tendency of the structures to flex.

The quartz (clear silica) discharge tubes (other than the small system described in section 3.11) had integral ballast volumes concentric with the optical axis and tubes longer than 500 mm had split discharges (up to a maximum length of 850 mm). Care was taken to select straight bore tubes and they were subsequently straightened in a glass lathe, but precision bore tube was not used. The silicon oxide deposit was chased off the surface with a hot working flame. The tubes were sometimes HF (concentrate) etched for ten minutes prior to construction in order to clean off oxide deposits, cleaned with propanol, and acetone dried. Care was taken to avoid dust and foreign matter entering the tube before final assembly by keeping the tube closed with rubber stoppers; dust is known to be disadvantageous in stable laser tubes.

The electrical feedthroughs were tungsten wire (1 mm to 2.5 mm diameter) passing through pyrex and graded sealed with GS20 then GS10 glass to the quartz; in some cases the anodes were sharpened to a point; no difference in discharge stability was noticed between the point and blunt anodes; ring anodes were not used. Platinum sidearm cathodes were manufactured by using a quartz sputter shield which entered into the cathode cylinder to limit material sputtering into the main bore. Two tubes (both platinum cathodes) were examined after over 18 months' daily use ($\tilde{<}$ 1500 hours) with Xe, CO_2, N_2 and He mixtures (1.5 Xe, 3 CO_2, 4 N_2, 14 He torr) and after breaking, careful observation showed (see Figure 3.11) the following surface changes.

1. The sputter shield had become silvered with a heavy coating of platinum and the electrical resistance across the tube neck was 8 Ω. The platinum film was easily removed from the glass by scraping.
2. The inside surface of cathode Pt sheet showed the discharge area which exhibited a white haze to grey

film with boundaries of flared density of colour which were rough white and brown in appearance.

3. The side arm connection with the laser tube main bore showed a heavy dark brown deposit which was non-conducting and easily removed.
4. The main bore showed a light yellow deposit along half its length (12 cm) on the cathode side.
5. The Brewster window (ZnSe) and tube mounting point showed no discolouration or visible deposits.
6. The side arm showed a scaley metallic deposit (half silvered) which was of very high resistivity ($\geq 10^7$ Ω).

The hot platinum cathode (along with sputtered material) appears effective in heterogeneous catalysis in reforming CO_2[109] and no intentional alternative catalysis was used other than that due to residual H_2. The relevant processes for these two schemes are:

$CO + O$ (or O_2) $\rightarrow CO_2$ at hot platinum surfaces.[110,111]

$CO + OH \rightarrow CO_2 + H$ in the gas volume due to OH radical.[112]

The residual H_2 may be useful also in depopulating the lower laser level[113] and the CO in resonant upper laser level vibrational excitation. Mass spectrometry measurements taken by Mellis[114] show that in this discharge configuration typical equilibrium CO_2 dissociation levels of ~50% occur. A 'burnt-in' cathode (after $\gtrsim$ 100 hours discharge) acts as a reservoir for CO_2 (as well as H_2) and a simple experiment was performed to demonstrate this. A tubular Pt cathode (2 cm diameter and 5 cm long) after 1000 hours' use was removed from a laser tube and heated in a pyrex bottle by a nichrome heater. In a control test the pyrex bottle alone was heated. The bottle was constructed so that the cathode was a close fit and the heater enclosed the

entire bottle. A mass spectrometer (AEI MS10) was used to observe the residual gases desorbed from the Pt surface with heating. The mean values of partial pressures are shown as a function of wall temperature in Figure 3.12 and a large quantity of CO_2 was desorbed; no H_2 concentration was measured and (there is an instrumental insensitivity of low mass numbers) H_2O concentration was not significantly large; no mass peaks 50 to 200 were observed. The operating cathode temperature was measured on the outside of the quartz envelope with a chromal alumel thermocouple, and this temperature is somewhat less than the Pt surface temperature. The temperature was measured, in the same manner, in an operating laser cathode, and the typical operating temperatures as a function of discharge current are shown in Figure 3.13. The actual value of the Pt surface temperature is unknown but because the heating bottles are of similar construction the outer wall temperature it is adequate to state that operating laser cathodes will typically (at $\gtrsim$ 15 mA) have temperatures > 125 C which is sufficiently high for significant quantities of 'stored' CO_2 from a 'burnt-in' cathode to be desorbed (Figure 3.12). When platinum cathodes are used in a CO_2 laser an equilibrium concentration of CO_2 is attached to the platinum surfaces. If parameters such as CO_2 partial pressure or discharge current (surface temperature) change then the platinum surfaces will either give up or accept CO_2 molecules.

3.11 COMPACT SEALED 8 W CW CO_2 LASERS

A generation of sealed, compact CO_2 lasers have been developed (the original design concept is due to A.L.S. Smith) to satisfy the requirements of small size (< 50 x 15 x 15 cm), high efficiency ($\gtrsim$ 10%), low cost and of a suitable rigidity and passive length stability to be actively stabilized with a phase locked loop; two invar frameworks have been constructed and a successive set of discharge tubes and optics fitted. The lasers were intended for long life sealed operation, the vacuum system consists of all stainless steel and quartz (clear silica) construction; basic design criteria for such

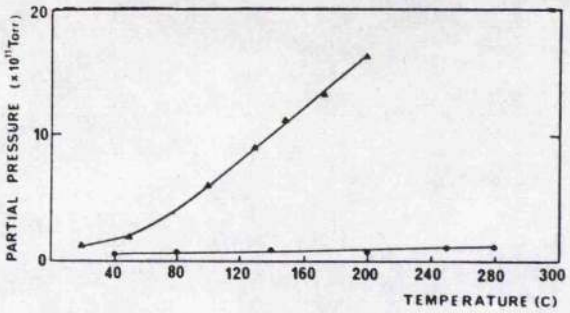

Fig. 3.12 Concentration of CO_2 desorbed (▲) from a 'burnt-in' Pt cathode during heating and a control test (●) of the pyrex container. The partial pressure scale shows relative partial pressure only.

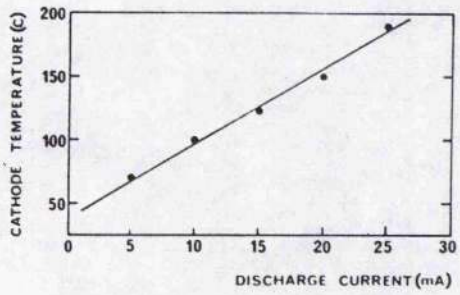

Fig. 3.13 Envelope temperature of Pt tubular cathode during operation in a compact CO_2 laser head. The temperature is measured by thermocouple in the same manner as in the apparatus used to obtain the results of Fig. 3.12. Gas mixture was 3 CO_2, 4 N_2, 16 He (torr) in a 9 mm internal diameter tube. The envelope temperature was $T_E \simeq 20 + 7i$ where i is the discharge current in mA.

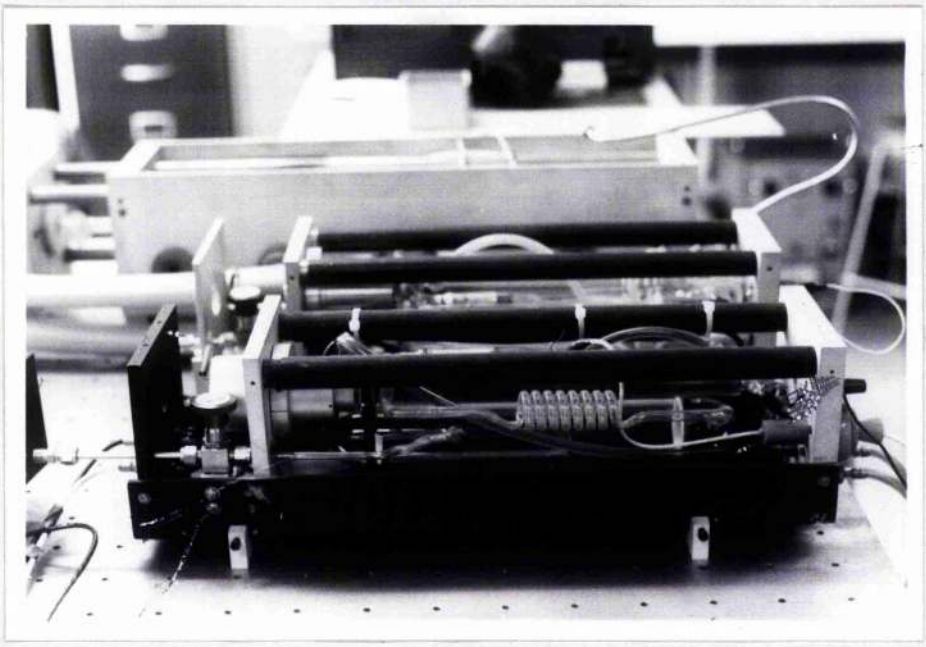

Fig. 3.111 Compact 8 W cw CO_2 lasers mounted on Ealing table with covers removed, tube, reservoir, draught shield and sealing valve can be seen.

lasers are well known.[115] The quartz laser discharge tubes fitted had internal diameters of 6.5, 7.0, 8.0, 9.0, 9.4 and 10 mm and lengths of 230, 250 and 280 mm have been used; two laser heads are shown in Figure 3.111. The internal tube surfaces have been modified for the purpose of off-axis mode suppression (see Figure 3.151). The optical cavities consist of a fixed 4 m radius gold coated, metal, total internal, reflector (∿97% reflecting at 10.6 μm) and a flat Ge or ZnSe output coupler (reflectivity in the range 70 to 98%, typically 90%). The total reflector is permanently aligned and fixed (by flexible epoxy resin - E7)[116] to the quartz tube in the expansion midplane of a machined 25 mm thickness, aluminium block; the other tube end is terminated with a ZnSe or KCl Brewster window directly attached with flexible epoxy resin to the discharge tube end cut at Brewster's angle and carefully ground flat. The output coupler is mounted on an elastically deformable 'one piece' metal mirror mount, mounted directly to a Lansing PZT stack for length adjustment. The stack is located on a 12 mm aluminium block secured to the total reflector block with three 25 mm diameter invar rods determining the optical cavity lengths of ∿ 350 mm; the PZT ceramic and aluminium components have their thermal expansions offset by a re-entrant design. A tubular, removable draught shield is fitted to closely enclose the laser beam outside the discharge; this has been found most necessary (see Chapter 4). The entire laser oscillator is housed in a massive U-channel aluminium piece with PTFE slides on the moving face to reduce sticking during differential expansion, with an aluminium cover which closes the laser head to reduce draughts, acoustic pickup and for HV safety.

These short cavities have a frequency mode spacing of 380 MHz and for the 15 to 30 torr pressures used, the laser signature is well defined, with only one optical CO_2 transition occurring for a specific length and with ∿ 10 transitions in any λ/2 length interval. It is a suitable alternative design procedure in a low cost stabilized system to use signature selection rather than inserting either a dispersive element (grating etalon, or prism)[1] or a selective absorber (thin film, gas tube, etc.).[117]

The optical cavity length, although largely determined by invar, varies in length over the range $\lambda/20$ to $\lambda/10$ for $1^{o}C$ ambient temperature change. The expansion offset is only effective if there are no thermal gradients existing in the system. The typical performance for a laser fitted with a 25 cm amplifier tube is 9 to 12% efficiency with an output power of 7 to 9 W on the available transition in the signature. Figure 3.112 shows how output efficiency is typically related to output power as a function of current (CO has been substituted for N_2 in one case), and Figure 3.113 shows the available output power and intracavity beam irradiance as a function of output coupler reflectivity for a typical mixture. For total pressures of 20 to 30 torr (useful range) the optimum gas mixture was found to be 4% Xe, 13% CO_2, 17% N_2 and 66% He with residual water vapour $\lesssim$ 0.2 torr (after diffusion pumping with 77 K cold trap to 10^{-4} torr with no baking). The emphasis of this work did not allow specific lifetime tests but everyday usage of up to ten months was achieved with less than 20% power degradation. Figure 3.114 shows two continuous run tests of a compact laser with a 28 cm active length tube (9.4 mm diameter profiled depth 0.5 mm). This laser suffered from some beam multimode effects but this test was meant primarily as a lifetime indication; realignment of the mirrors for maximum output power was performed once every week. The first run (new cathode) shows $\sim$30% power reduction in 1000 hours whereas the second filling shows $\sim$10% power fall off. This is consistant with an initial CO_2 loss from the gas to the cathode and Pt sputtered surfaces; the majority of loss seems to occur in the first 200 hours. The second run has improved sustained output power over the entire period and this may be due to the CO addition. Power increases are seen in the first few days in both cases; this could be due to some slow desorption of H_2O from walls which is beneficial in CO_2 catalysis.

The laser mode quality (see Chapter 3.15) is dependent on the ratio of tube radius to beam radius and the table in Figure 3.115 gives a guide to the judicious choice (maximum power single mode) of non-profiled tube $\sim$ 8.0 mm for the cavity described. Unstabilized laser performance was monitored for

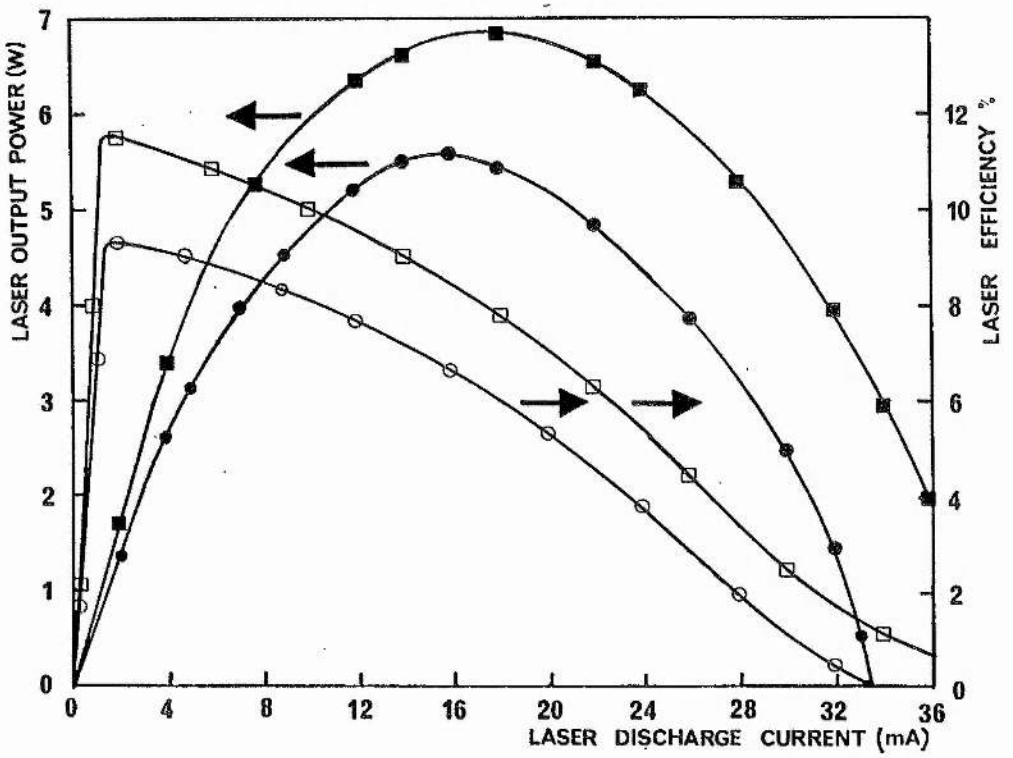

Fig. 3.112 Laser output power and efficiency for compact laser head with 25 cm active length, 8 mm diameter tube and 90% Ge output coupler for (■□) 1 Xe, 3 CO_2, 4 N_2, 16 He (torr) and (●○) 1 Xe, 3 CO_2, 4 CO, 16 He (torr).

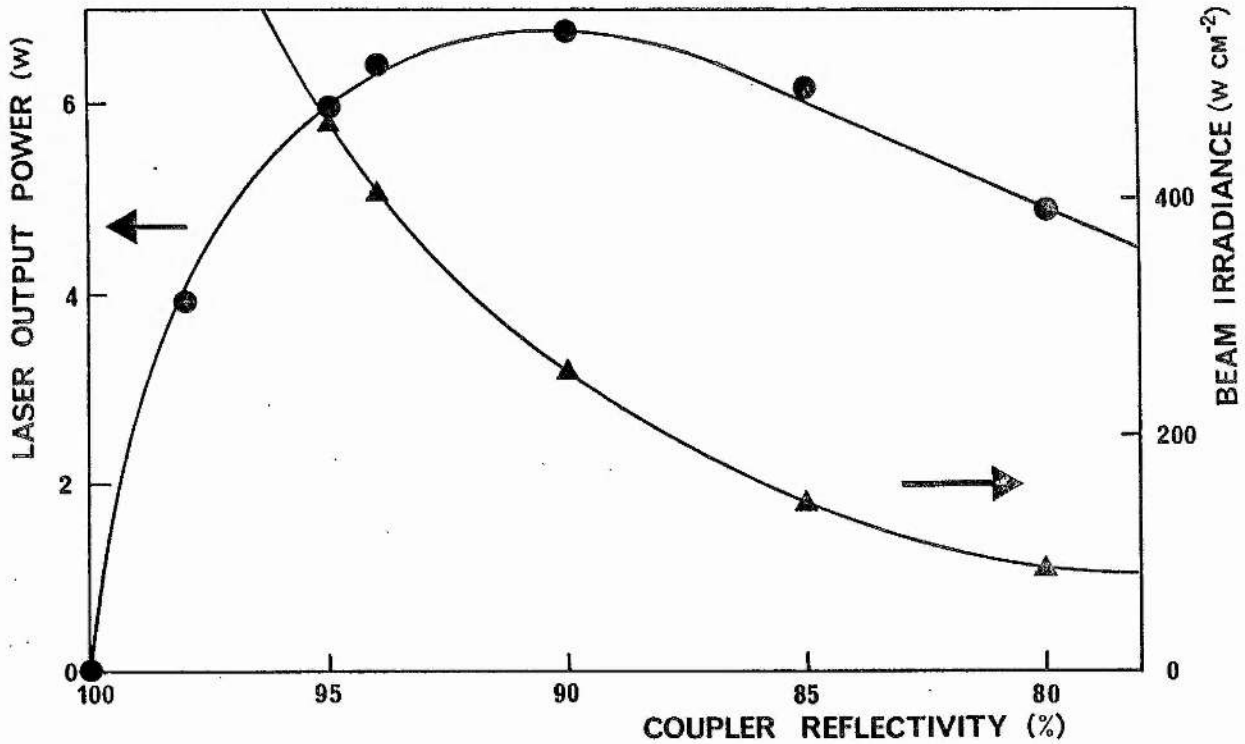

Fig. 3.113 Laser output power and intracavity beam irradiance as a function of output coupler reflectivity for 25 cm active length, 8 mm diameter tube fitted in compact laser head filled with 3 Xe, 3 CO_2, 4 N_2, 16 He (torr).

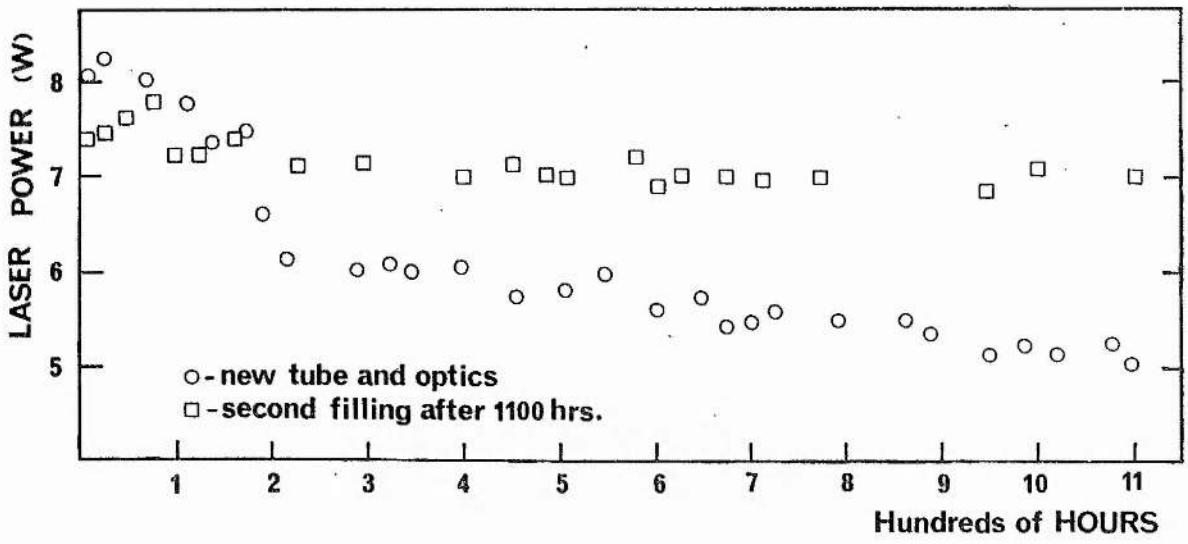

Fig. 3.114 Continuous run test for compact laser with 28 cm length new profiled tube, Pt cathode, with new ZnSe Brewster window, total reflector and 90% Ge output coupler filled with gas 1 Xe, 3 CO_2, 4 N_2, 16 He (torr) and run for 1100 hours, and a second filling of 1 Xe, 2 CO, 3 CO_2, 4 N_2 and 16 He.

TABLE OF OUTPUT POWER AND MODE QUALITY

Mean Tube Diameter (mm)	Maximum Laser Output Power	Mode Quality (Far Field)
6.5 *	3.5	Axial only
7.0 *	5.2	Axial only
8.0	8.1	Axial dominant some off-axis with misalignment
9.0 *	8.5	Axial operation over narrow range otherwise off-axis modes dominate
9.4	9.2	Off-axis dominant. Very narrow range of axial only
10.0	8.7	Off-axis only

Fig. 3.115 Table of laser mode quality and output power for compact CO_2 laser fitted with quartz 28 cm (or 25 cm * corrected values assuming output power directly proportional to length), active length discharge tube for 10P(20) line centre operation with a fresh fill of 1 Xe, 3 CO_2, 4 N_2, 16 He (torr). The total reflector had 4 m radius of curvature and the output coupler was flat; the cavity length was 35 cm. Mode quality assessed with scanning pyroelectric beam monitor and optical engineering image plates.

long periods (see Chapter 4) using a calibrated radiation thermopile (CRL laser power meter) and a Mullard TGS pyroelectric detector for power measurements along with an Optical Engineering CO_2 spectrum analyzer for wavelength measurements. Relative frequency measurements were made by the two similar independent system heterodyne technique (see Chapter 3.42). For tubes $\leq$ 8.0 mm single line oscillation is always seen from switch-on whereas for tubes > 9.0 mm dual line oscillation is always seen and tubes of diameter 9.0 > d > 8.0, can have multiline oscillation during the initial (15 to 30 minutes) warm-up period. After this period single mode oscillation is always seen, with careful manual alignment, for tube diameters < 9.0 mm and oscillation on one particular line can occur for hours (good thermal case) or always longer than 15 minutes as long as shocks, etc., are avoided and a slow drift of output power corresponding to the single laser mode slowly scanning through a gain profile segment in the signature occurs; this causes output power fluctuations of $\sim$10%. In section 3.41 where beam profile monitoring is described, some spatial mode stability evidence is presented.

3.12 CO_2 SEQUENCE BAND LASERS

The two sequence band lasers were constructed in a sealed, invar stabilized format similar to the compact laser but constructed with four invar rods situated on a 100 mm square. Figure 3.121 shows the earlier laser which was fitted with a 50 cm long amplifier (on right side of photograph) with fixed internal 6 m radius gold (evaporated) mirror and a heated palladium tube (Jencons JHDT5) for control of H_2 content. One KCl Brewster window isolates the quartz amplifier from the quartz hot CO_2 cell (centre of photograph), which acts as a selective absorber of fundamental ($00^0 1$ upper level) laser lines. The hot cell is terminated with another KCl Brewster window enclosed in a carefully sealed draught shield (left side of photograph), the 98% reflecting ZnSe 1" output coupler is mounted in an elastically deformable mirror mount attached to a commercial (Lansing serial no. 21.938) twin PZT for modulation and length correction.

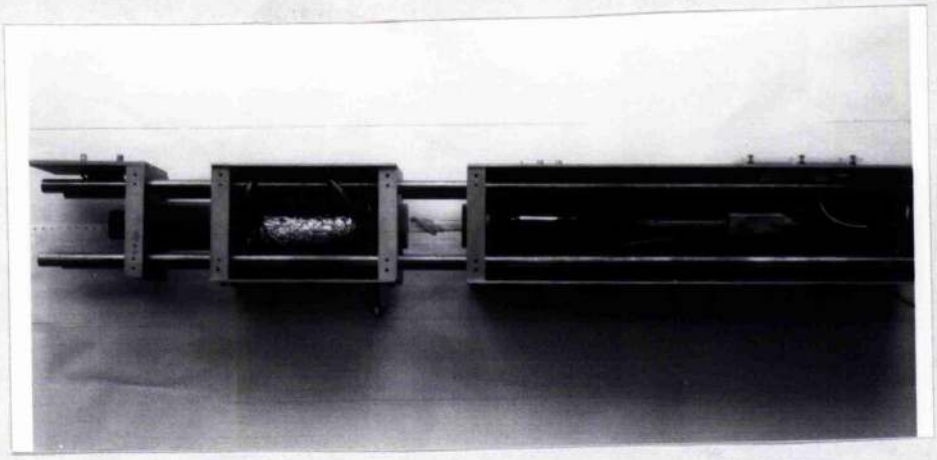

Fig. 3.121 First CO_2 sequence laser with four invar rod construction, 50 cm laser tube with integral coaxial gas ballast, hot cell (wrapped in Al foil) and output stage with two element stack PZT.

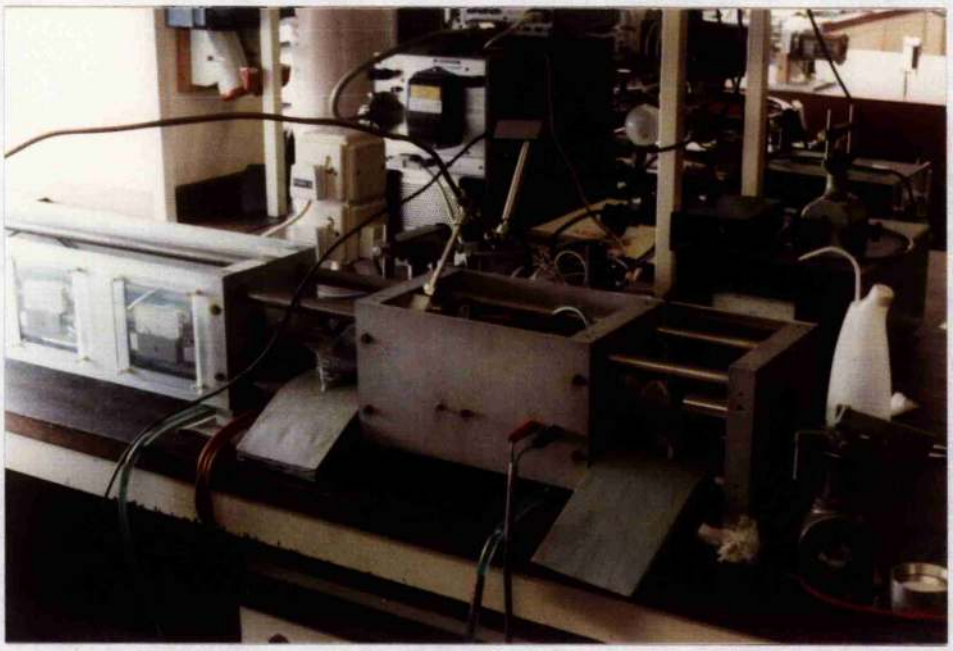

Fig. 3.122 Second CO_2 sequence laser showing similar four invar rod construction, hot cell housing with cooled Brewster window mounts, deformable metal (invar and stainless steel) mirror mount and part of the 85 cm (split discharge) amplifier housing.

Description, operating parameters and performance of the CO_2 sequence band laser is given in Chapter 5.1. One of these lasers (larger shown in Figure 3.122) has been used to accurately measure vibrational temperatures of the CO_2 assymetric stretch mode.[118]

3.13 SEALED HIGH POWER CW CO_2 LASER

A larger (85 cm active length) CO_2 laser was constructed to assess optogalvanic stabilization of larger systems and to provide a more intense probe beam for external cell studies of OGE and flourescence phenomena. This laser featured a 3 rod invar design with tube carriers/frame stiffeners split at 45^o so that the laser tube could be simply removed. The tube was mounted in the supports with nylon screws to align the tube axis to the optical axis of the invar frame; this proved most useful when demounting and changing the tube due to glass manufacturing tolerances. The complete laser head (100 x 10 x 10 cm) is shown in Figure 3.131 mounted on the Ealing antivibration table. Electrically driven micrometers (Motor Mike) aligned the output coupler (70% reflecting ZnSe) and the PZT was mounted in an elastically deformable mirror mount and thermally compensated PZT assembly described in detail in 3.14. Construction of the discharge tube was similar to the sequence lasers utilizing an integral ballast volume, platinum cathode and two tungsten point anodes. ZnSe Brewster windows were attached to both ends of the tube and machined blackened stainless steel heatsinks were used to dissipate the heat generated by material absorption and reflection (see Figure 3.132, the total reflector PZT end), and the intervening air space was carefully draught shielded (see Figure 3.13 which shows the output coupler end) with sliding facility for tube alignment and movement.

The invar rod ends were located by screws to the 25 mm stainless steel endplates and very carefully machined; it has proved possible for an operator to remove the endplates and replace them without losing sufficient alignment for immediate laser action on replacement.

Fig. 3.131 Stable sealed 50 W cw CO_2 laser, mounted on antivibration table showing output coupler mount (with motormike adjustment) and mounted quartz laser tube with integral concentric ballast.

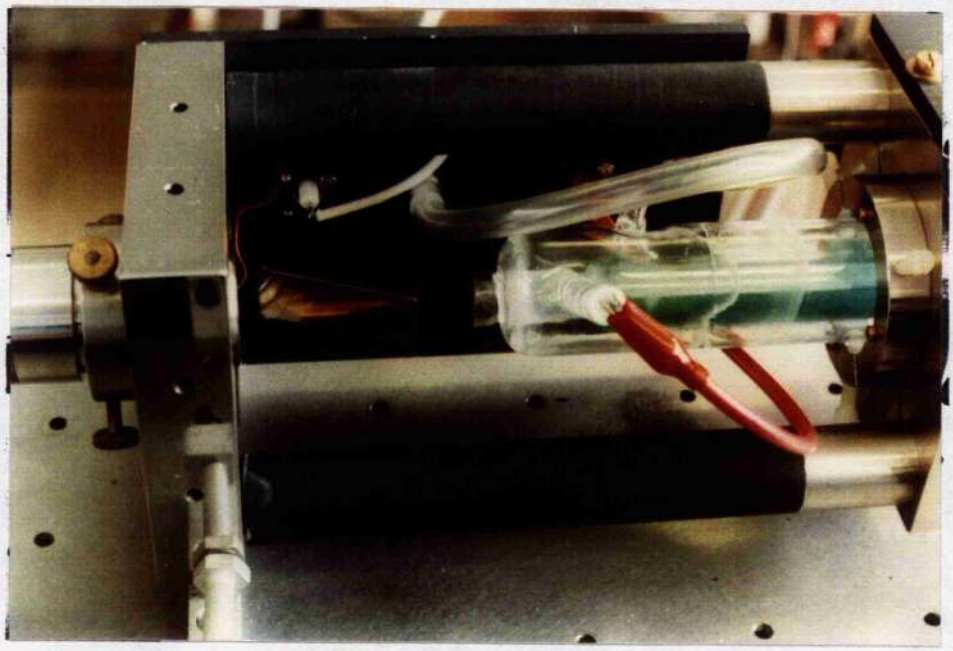

Fig. 3.132 PZT/total reflector end showing ZnSe mounted on blackened stainless steel heatsink. A repaired tube fracture can be seen next to the anode.

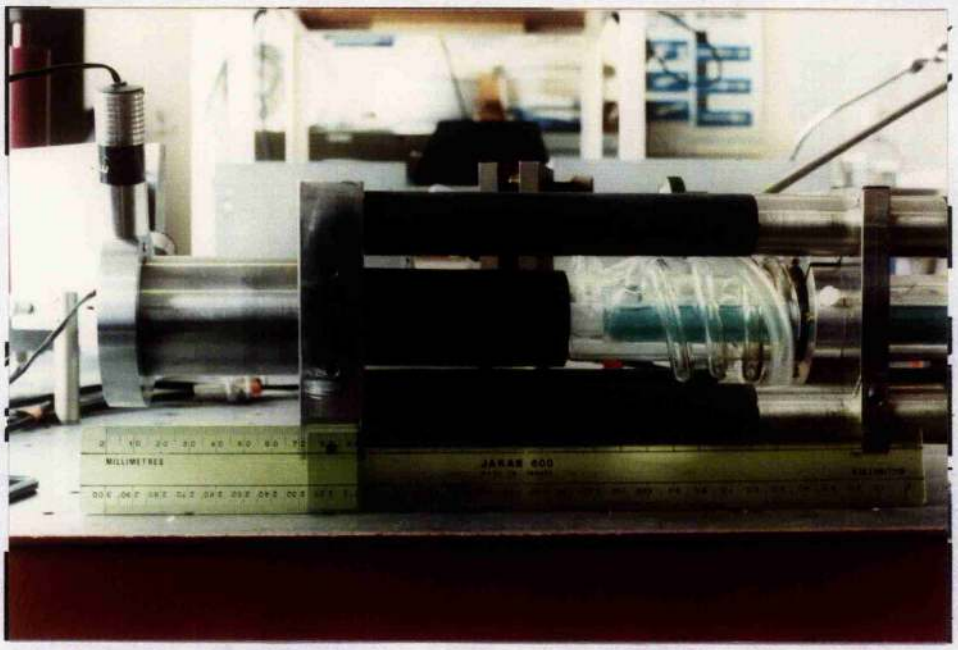

Fig. 3.133 The output coupler end showing glass flexible coupling to sealing valve, split tube mounts with screw adjustment of tube centre, and a fixed draught shield.

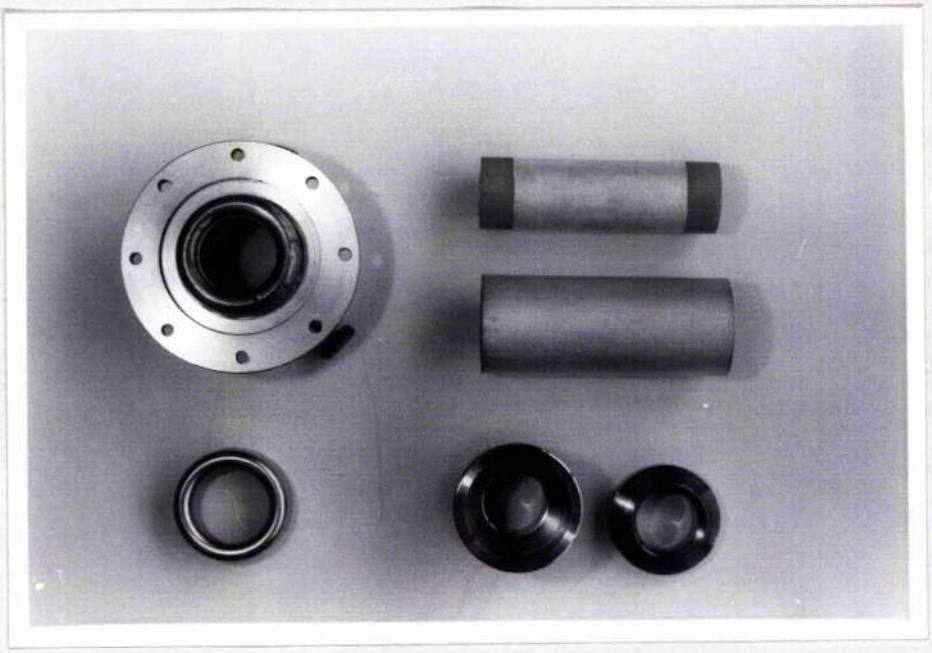

Fig. 3.141 Components of fabricated PZT assembly. Finished mirror mount (upper left) with invar cup component beneath. Two PZT - 5 H (Vernitron) tubes and mounting rings carefully fitted for tube alignment.

3.14 PZT CONSTRUCTION AND CALIBRATION

All lasers constructed were fitted with PZT length translators for cavity tuning. Commercial units (Lansing 21.333 and 21.938) single and double element, were used as well as constructed translators,[119] (lead zirconate titanate) and initially, deformable mirror mounts were attached to the moving face. In order to improve mechanical frequence response and rigidity the final systems used PZT tubes to directly drive the laser mirrors.

Figure 3.141 shows the components before assembly of the mirror mount/PZT assembly. The variable angle mount consists of an invar (or stainless steel) pressed or spun cup (lower left) which is silver soldered to support the moving inner cylinder which is screw controlled from the main body. Two tubes of PZT material (PZT-5H) are used, one inside the other, to both compensate thermally and provide twice the amount of length translation. Figure 3.142 shows the outer tube mounted to the threaded flange in the moving support tube and the inner PZT tube (without mirror which is attached by glue to the upper surface). The inner tube (plus mirror) is then inverted and inserted into the outer tube (Figure 3.143), carefully aligned and the mating ring glued to the ceramic material. The mirror front surface is now located in the zero expansion plane (i.e. the ceramic expansion and stainless steel expansion is compensated) where the flange attaches to the laser.

Accurate dc (and low frequency ac) translation sensitivities are both given for the materials and supplied by the manufacturers (Lansing) of the commercial units. However, for these investigations ac mechanical response up to 100 kHz was used and careful calibration was required. The problems of electrically driving PZT's at high frequency will be further discussed in Chapter 6. Traditional measurement of change in length per unit drive voltage uses interferometry and recently Varwig et al have used acousto-optic modulation and heterodyning.[120] Calibration of the individual translators with/without mirror mount load was achieved successfully by a CO_2 laser heterodyning technique as follows. One laser, after warmup, was used as a reference frequency and another frequency modulated by applying a sine wave

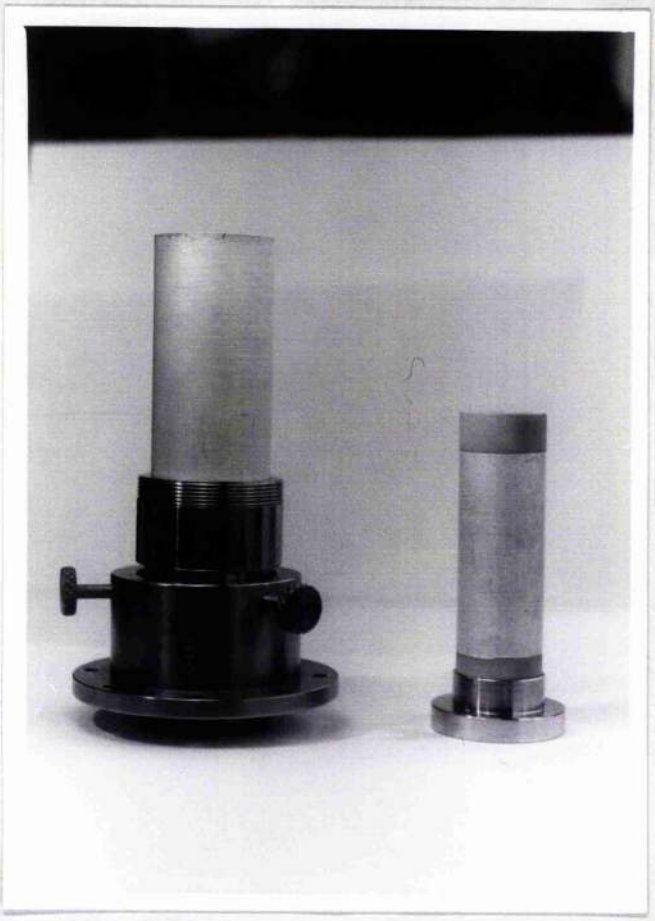

Fig. 3.142 First assembly step of mirror mount/PZT assembly. Mirror is glued to top surface of smaller tube and inserted into larger.

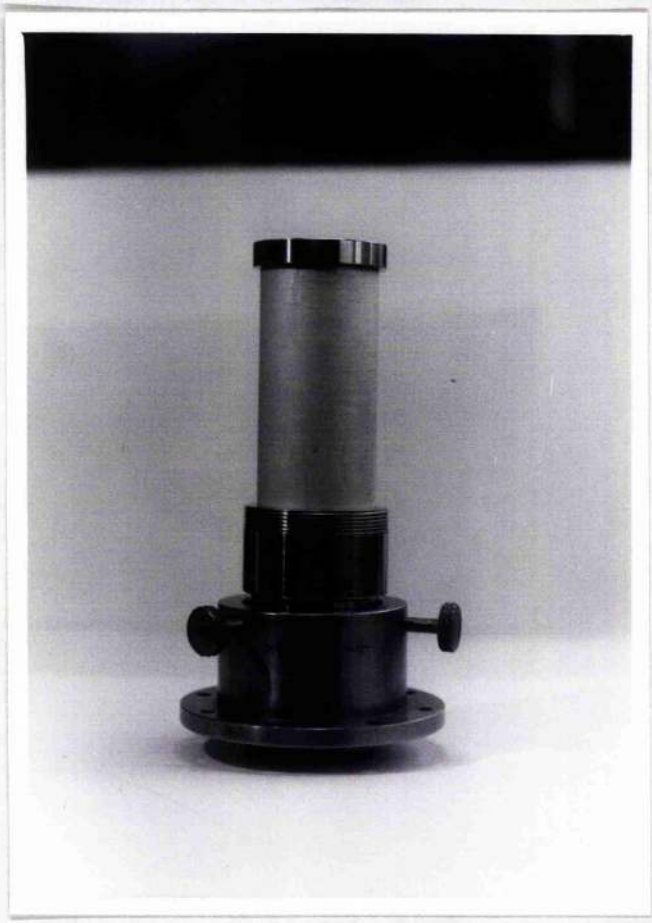

Fig. 3.143 Fully assembled mirror mount/PZT assembly. Mirror lies in zero expansion plane.

voltage after suitable amplification to the PZT (see Figure 4.27). The laser difference frequency spectrum (viewed on an RF spectrum analyzer) gives the excursion of the laser frequency due to length modulation. Then frequency excursion Δf is simply related to the length excursion ΔL

$$\frac{\Delta f}{f} = \frac{\Delta L}{L} \quad \ldots\ldots\ldots\ldots\ldots\ldots \quad (3.1)$$

where f is the laser frequency and L is the optical length of the cavity.

Figure 3.144 shows the frequency response of three translators used and all show considerably decay at frequencies > 1 kHz. The Lansing translators are stacks of rings (which have electric fields parallel to the expansion direction) mounted together with insulating glue. This produces a less rigid structure with an unknown temperature coefficient, and it also appears that these systems have more resonances than the cylinder type (which have electric fields perpendicular to the expansion direction), but this could be due to the attached metal mirror mounts. Both stacks show a broad resonance at $\sim$ 12 kHz and the double stack shows a large resonance at 45 kHz. Typical stack (with mirror mount load) characteristics are a falling HF response - 10 dB at 1 kHz, - 30 dB at 10 kHz, - 40 dB at 20 kHz and - 50 dB at 60 kHz. The direct driven twin tube assembly produced greater excursions over most of the tested frequency range.

It is possible to use this method with suitable drive amplification up to $\gtrsim$ 200 kHz but the accuracy of measurement (> 20 kHz) is low. The error sources are

1. Stability of lasers (least important)
2. The ac drive falls with frequency due to high element capacitance requiring $\gtrsim$ 100 W drive with a suitable matching network
3. The mechanical response is falling rapidly > 10 kHz so that signal to noise is decreasing (most important).
4. Waveform of the drive is a matching problem.

Typical frequency response calibration accuracies are ± 5% for dc - 3 kHz,

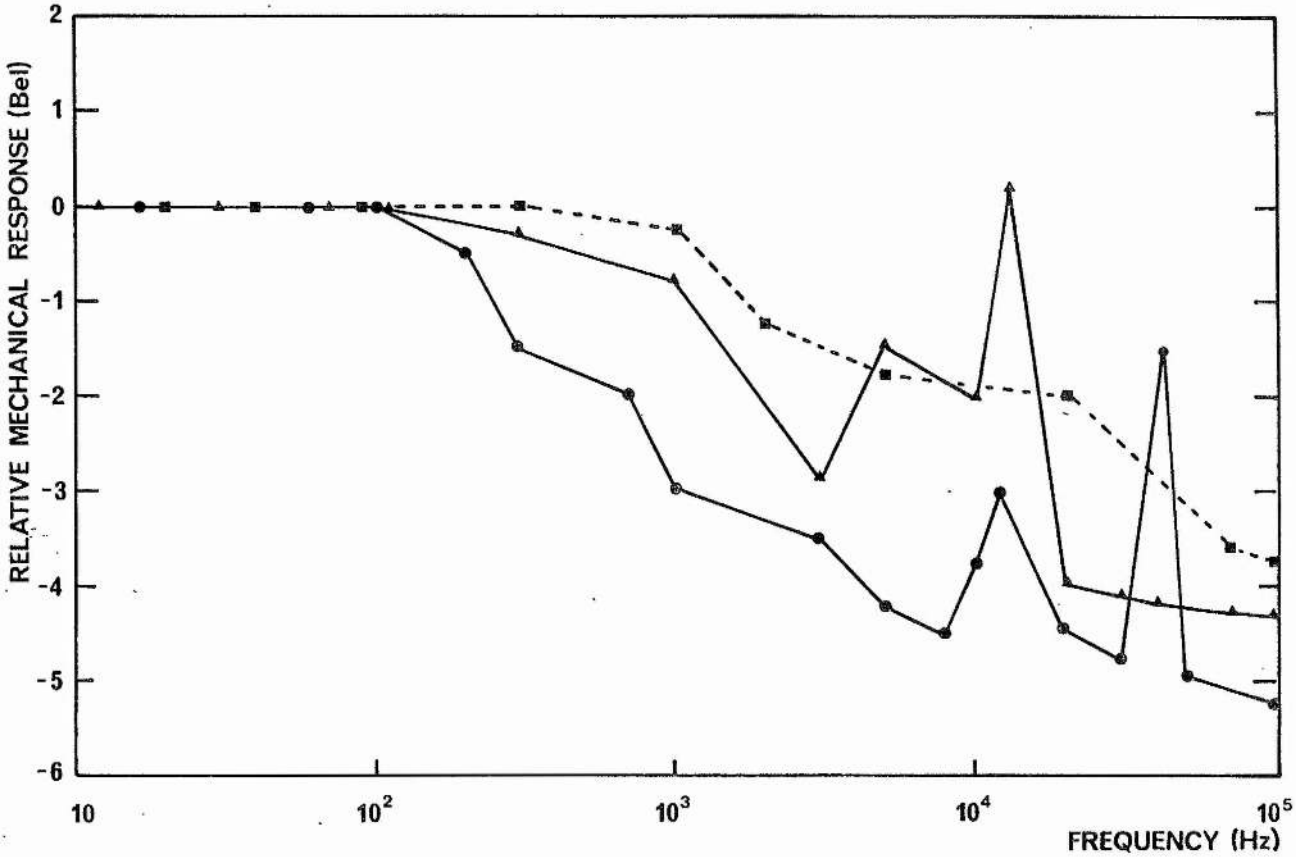

Fig. 3.144 The frequency response of three PZT/mirror mount assemblies: Lansing 21.333 translator with deformable mirror mount (▲), Lansing 21.938 double translator with deformable mirror mount (●) and twin tube translator shown in Figures 3.141 to 3.143 (■).

± 10% for 3 - 10 kHz, ± 20% for 10 - 100 kHz and ± 50% for frequencies 100 kHz for the particular laser system used. Investigation of the polarity equivalence showed that small amplitude length changes (± 20 V) provided equivalent frequency shifts (to within 10%) which infers that ac drive at zero bias should produce symmetrical excursions (LF and HF).

3.15 LASER TUBE PROFILES AND OFF-AXIS MODE SUPPRESSION

There has been some evidence that low angle, tube wall reflections from the glass laser tube produce secondary power lobes in the far field pattern of a nominally TEM_{oo} free space mode laser beam and some CO_2 laser manufacturers (Silvania and Edinburgh Instruments) have introduced distributed apertures within the amplifying tube in order to reduce the tendency of off-axis lobe production.

Visual inspection of a straight glass tube shows concentric rings of reflection for a point source and this was verified by illuminating tube walls with HeNe and CO_2 laser beams and examining the emerging beam with the eye (by projection) and thermal image plates respectively. Wall reflection appears to be a sufficient mechanism for extra lobe generation.

The following tube processing was undertaken (and some sample tubes are shown in Figure 3.151) in order to reduce this effect in working 25 cm, 50 cm and 85 cm active length lasers:

1. HF acid etching of the inner bore surface produced a ribbed profile with a depth of 0.5 mm and a spatial frequency along the tube of one cycle per cm. Heated nylon was attached to the inner walls to resist etching and two fills (30 minutes each) of maximum strength of HF were used. This produced $\lesssim$ 1 mm deep etching in pyrex tubes and $\lesssim$ 0.5 mm deep etching in quartz tubes. Both circular bands and spiral shaped profiles were fabricated.
2. HF etched random spot profiles with a depth of 0.5 mm were constructed with a mean spot size of $\sim$ 2 mm. To produce a

random distribution of projecting fingers into the tube a resist of paraffin wax was used; small pellets of 2 to 4 mm in diameter were vibrated by shaking the tube whilst heating by flame. After the wax had hardened, two fills of HF were used as above, and less sharp edges were attained but with similar etched depth.

3. Deformation of surface while hot by pressing pointed calipers into the tube.
4. Shot blasting of the inner surface with large particle sand was used and although the quartz was roughened visibly little effect at 10 μm was observed. The quartz tube was very much weaker after this method and fractured easily.
5. Carborundum roughening of the inner surface with coarse powder resulted in greater depth variations than the shot blasting and although the quartz was initially fragile after a conditioning etch of 30% HF and heating the tube was sufficiently robust for laser construction.

In order to interpret the effectiveness of this technique suppression of major higher order (non axial) transverse modes must be achieved and tube diameters for the compact laser > 9.5 mm showed no improvement in mode quality with processed over non-processed tubes. However, for tubes 8 to 9 mm diameter a noticeable lack of extra power lobes was observed and the self-heterodyne signal (single laser) showed less or no signal. These signals are due to the frequency shifting of slightly off-axis propagating modes and have been measured by Duxbury.[121]

Several test tubes of each fabrication method were constructed (with varying depth and frequency profiles) and these were investigated with both HeNe and CO_2 lasers by directing the beam along a processed tube at angles slightly off-axis. The emerging beam was studied by eye and thermal image

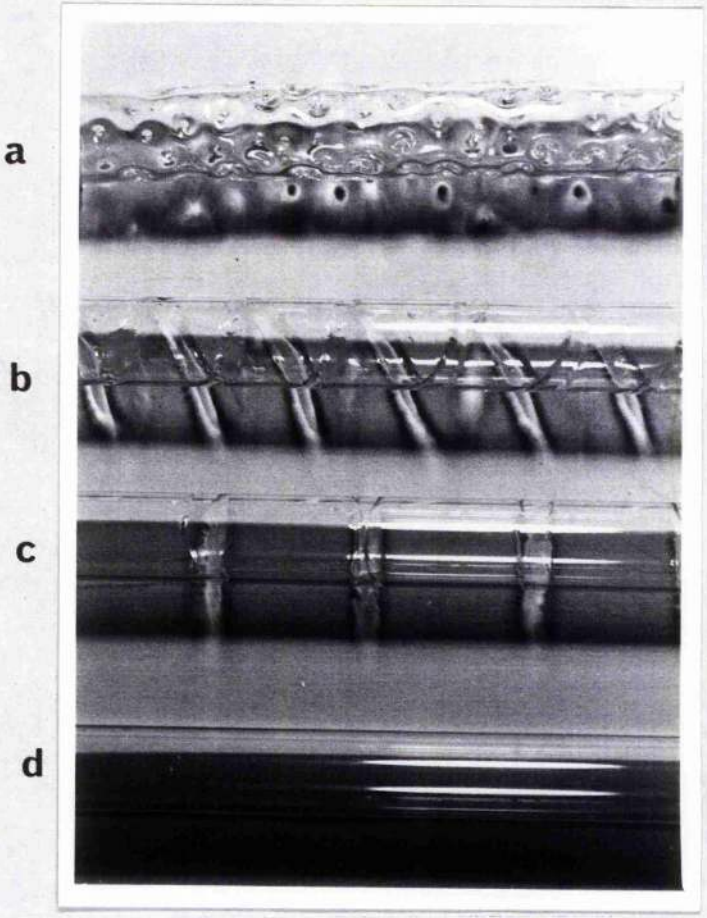

Fig. 3.151 Examples of tube surface processing for off-axis mode suppression. Tube (a) has been hot worked to produce protuberances in the bore. A similar effect was achieved by HF etching. Tubes (b) and (c) were etched using nylon resist and tube (d) is unmodified.

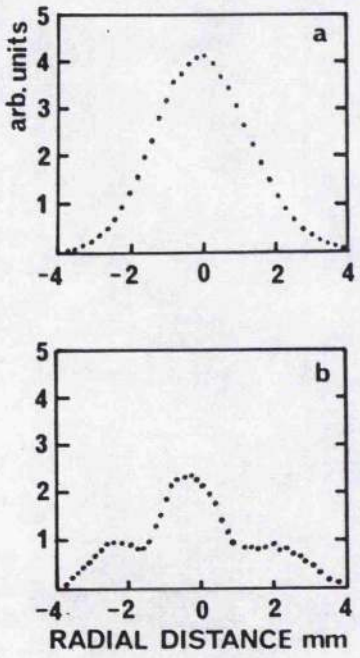

Fig. 3.152 Mode patterns of lasers fitted with tubes (a) with a spiral etch as shown in 3.151 (b), and (b) with no processing as shown in 3.151 (d).

plates respectively and while all fabrication techniques produced good randomization of the HeNe beam (0.6328 μm) only techniques (1) and (2) disturbed the 10 μm CO_2 beam substantially. The formation of crest-shaped focussed images occurred noticeably with unprocessed tubes and these patterns were strikingly similar to extra lobes generated by the CO_2 laser.

Figure 3.152 shows laser beam scans (see 3.41) which display beam power as a function of radius at 5 m from the laser output coupler for a compact laser with 8.5 mm diameter tube etched with a spiral pattern and a 8.0 mm diameter tube non-processed (optics, etc. otherwise identical). The non-processed laser tube can be carefully optically aligned to avoid extra power lobes and operation in this fashion can occur for 1 to 2 hours, but the off-axis lobes recur as the cavity drifts. The processed tube shows no tendency to produce off-axis power lobes with full misalignment. Some distortion of mode can be achieved with extreme misalignment.

Due to the linear increase of laser gain with length, problems of this kind are expected to increase with larger systems. No direct evidence of this was found, but random etched pattern 50 cm tubes (9 mm diameter) produced very stable pure TEM_{oo} mode operation suitable for low noise heterodyne reception. The technique of deforming (by pinching) the discharge tube to provide a distributed series of apertures was started (and this method looks promising and is now used by some manufacturers), but production difficulties (high stresses are generated in the quartz) resulted in no suitable tube being manufactured for these studies. The carborundum roughened tubes seemed less effective (perhaps due to the smaller dimension of disturbance) than the etched step tube and the random pattern etch seemed most effective of all the tested structures. The shot blasting technique weakened the quartz to the point that the fragility of the tube made construction difficult.

3.2 ELECTRONIC DESIGN AND CONSTRUCTION

In the design and development of a complete servo system such as this laser stabilizer, refinement during development can result in a particular electronic servomechanism 'tuned' to the particular laser being stabilized. The development of such a system for simple and general laser use and with sufficient flexibility to operate with very different lasers, power supplies and detector pick off configurations required several early electronic servo systems which were designed and constructed with many adjustable parameters (such as modulation frequency, depth, integration time constants, ac and dc gain, etc.) and only a brief summary is given in 3.23. An appreciation of the excitation power supply behaviour is essential for the explanation of this work and this is given in considerable detail in 3.21 and 3.22. The PSU generated noise was the major noise source in the optogalvanic system.

There was a substantial degree of freedom in the exact method of pick off used to extract the small optogalvanic signal from the larger dc excitation and different techniques are discussed in detail, particularly with respect to noise and ground loop considerations subsequently, and therefore a summary of pick off configurations will be given immediately in 3.22.

The exact electronic servomechanism constructed during this work will be described in 3.23 and some considerations for a universal system given in 3.3.

3.21 EXCITATION AND POWER SUPPLIES

CO_2 laser amplification occurs in the positive column of a molecular glow discharge of CO_2, N_2 and He (possibly including H_2, Xe, CO, etc.) and such a weakly ionized, wall dominated discharge has a positive valued, negative differential v-i characteristic. The continuous (rather than pulsed) excitation of these discharges for diameters $\sim$ 1 cm requires a potential of $\sim$ 200 V/cm at current densities of $\sim$ 30 mA cm^{-2} for filling pressures $\sim$ 20 torr. Ideally the electric supply should not introduce gross changes of

current (and voltage) which could modulate the laser output. RF, ac and dc excitation have been used for CO_2 lasers; in this case dc excitation was used exclusively. An ac supply usually results in undesirable beam modulation and RF excitation (particularly in a waveguide context) is a new technique which looks most promising for the future with electrodeless discharges which will have less contamination useful for small sealed volumes. The possibility of superheterodyne detection of optically induced vswr shifts analogous to OGE looks promising. The dc supplies used in these experiments were all commercial and are listed below.

1. Irvin C1096

   This supply was constant current or constant voltage regulated providing 10 kV, 50 mA maximum. It was single mains transformed, tetrode stabilized with ripple $\sim 2 \times 10^{-4}$ (peak to peak) constant voltage and $\sim 5 \times 10^{-3}$ (peak to peak) constant current, and has a current correction time $\lesssim 5$ ms. It was used for all external cell excitation and the more critical small signal applications due to the low noise capability.

2. Edinburgh Instruments 183

   Three units of this type were used; constant current only is available and one single 183S and a matched pair 183D, 4-20 mA, 13 kV maximum were used for both single and split discharges. Mains single phase transformed, they are both transistor regulated, and saturable reactor controlled. The single supply 183S was retrofitted to improve ripple specifications $\sim 5 \times 10^{-3}$ (peak to peak). Current correction time was $\lesssim 10$ ms.

3. Hivotronics 22/300/26

   This supply was a high power constant voltage unit providing 100 mA 25 kV. It was 3 phase mains transformed,

unregulated and produced a high ripple $\sim 1{:}10^2$ (peak to peak).

4. Hartley Measurements 421

This was a 20 mA, 20 kV, switched mode supply which was programmable and current regulated; it generated high ripple (1 to $8{:}10^2$) at variable frequency $\sim$ 1 kHz.

The Irvin C1096, HML 421, and Hivotronics 22/300/26 supplies were operated with 100 kΩ, 250 kΩ or 500 kΩ ballast. For 25 cm discharges 100 kΩ was found suitable for the mixtures/pressures used down to current $\sim$ 6 mA and for current $\sim$ 1 mA 500 kΩ was required. The ballast requirement is simply linear with discharge length (as is the discharge impedance) and ballasts of 10 kΩ + 4 kΩ/cm were suitable for these tubes.

Because of the negative slope of the impedance characteristic some care is required to avoid relaxation oscillations.[122] Presuming the laser current i_L is simply given by

$$i_L = \frac{V_L}{R} \quad \text{where R is the particular tube resistance at } i_o$$

when

$$R = \frac{V_o}{i_o} \qquad \ldots\ldots\ldots\ldots\ldots\ldots \quad (3.2)$$

and the differential impedance Z is just

$$Z = \frac{\Delta V}{\Delta i} \qquad \ldots\ldots\ldots\ldots\ldots\ldots \quad (3.3)$$

If shunt capacitance exists a further out of phase current flowing through this branch will exist

$$i_C = C \frac{dv}{dt} \qquad \ldots\ldots\ldots\ldots\ldots\ldots \quad (3.4)$$

The total current from the supply will be held constant (optimum case for cc supply) for small perturbations about i_o

$$-\frac{\Delta v}{Z} + C \frac{dv}{dt} = 0 \qquad \ldots\ldots\ldots\ldots\ldots\ldots \quad (3.5)$$

where the first term is a laser impedance perturbation and the second term is the capacitive current; this equation represents an unstable condition. The maximum rate of change of the laser current is constrained by the supply current maximum and the shunt capacitance. The limiting case consists of v_L rising and the capacitance charge current increases until more current is drawn in the capacitive branch than the laser branch and the discharge is lost. The voltage continues rising at the rate $dv/dt = i_0/C$ until the starting voltage of the discharge is reached and v_L starts to fall and the discharge current rises. At high currents the negative differential v-i characteristic decreases and at some current the total resistance becomes positive. This point is an unstable equilibrium and any perturbations starts the process off in the reverse direction. Oscillation between on/off or two discharge values usually occurs; sometimes one cycle to arc and then electrical failure can occur (with large capacitance). Reducing the stray capacitance results in increasing the oscillation relaxation frequency to a point where discharge cannot change fast enough to follow and an effective positive impedance results. The current is held but noisy operation occurs. Feeding the laser discharge via coaxial cable (earth screened) with a ballast resistor (as described) at the discharge end of the cable results in very stable operation; inductance may be introduced also, into the leads to modify time constants but this was not used in these experiments.

These considerations are important when considering ac v-i perturbations due to OGE because relaxation oscillations may be triggered or amplify the signal under investigation; capacitive coupling of voltage signals can be particularly problematic in this respect. A current value can be chosen which minimizes the power supply ripple noise and this current is not necessarily the highest laser output current. The exact noise minimum varies with tube length diameter and cathode .

A further discussion of discharge noise is given in Chapter 9; however, it is important to notice that the major noise contribution was from mains power supply harmonics. The treatment of this factor is necessary for the

explanation of stabilization performance. The Irvin C1096 cc and cv supply was used most extensively in these experiments and the noise detected by a 10 kΩ series resistor (see 3.22) is shown in Figure 3.211. The exact harmonic amplitude depended on current, gas pressure and composition, and ballast resistance volume; typical optimum laser parameters were used: 10 mA, 26 torr (1 Xe, 3 CO_2, 4 N_2, 18 He) and 250 kΩ respectively. All the harmonic noise (50 Hz to 1 kHz) is between one and two orders of magnitude lower for cv operation than cc operation. The long term current stability, however, important for constant excitation point, was typically one order of magnitude better during cc excitation, because ballast heating and drift is compensated in this case.

Figure 3.212 shows the harmonic noise generated by the Edinburgh Instruments 183 supplies both as manufactured and due to subsequent improvement.[123] The harmonic noise level is similar to the comparable Irvin supply when operated in the cc mode.

Figure 3.213 shows the noise spectrum from the HML supply which was the only switched mode supply used in these experiments. Along with substantial mains frequency harmonics from poorly regulated dc drive the main inverter operating frequency ∿ 640 Hz was observed to always dominate at a value of ∿ 6.5 V, two orders of magnitude greater than the E.I. 183 supplies and four orders of magnitude greater than the Irvin supply (in cv). The exact frequency of this noise changed with current setting and stabilization of lasers was just possible with modulation frequencies very different to this value (e.g. 16 Hz).

3.211 CONSTANT CURRENT AND CONSTANT VOLTAGE EXCITATION

When a laser discharge is excited with a constant current supply (Figure 3.2111) and the discharge impedance Z changes (say rises) due to optically induced effects then the potential difference across the discharge (v_Z) changes (increases).

Fig. 3.211 Noise generated by Irvin C1096 power supply during excitation of a CO_2 laser (discharge length ∿ 33 cm) at 10 mA. The fractional noise current $\Delta i/i$ was evaluated from the voltage developed across the 10 kΩ series resistor. The gas composition was 1 Xe, 3 CO_2, 4 N_2, 18 He (torr).

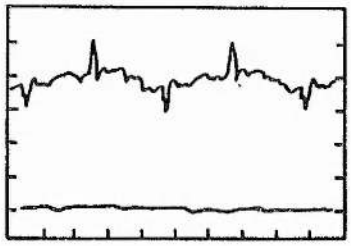

(a) Detected noise voltage (200 mV/div vertical scale) with 154 kΩ ballast resistance. The time scale (horizontal) is 5 ms/div. 200 mV corresponds to $\Delta i/i = 2 \times 10^{-3}$. The upper trace shows cc and the lower cv excitation.

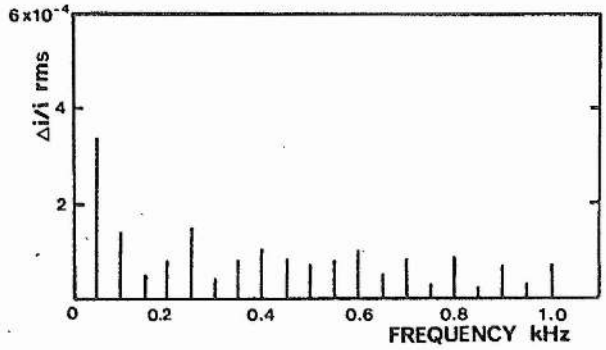

(b) The cc noise spectrum with 250 kΩ ballast as measured with a Dymar 771 RF wave analyzer.

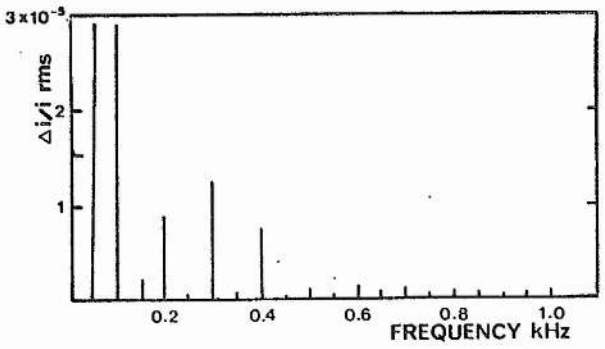

(c) The cv noise spectrum with conditions as above.

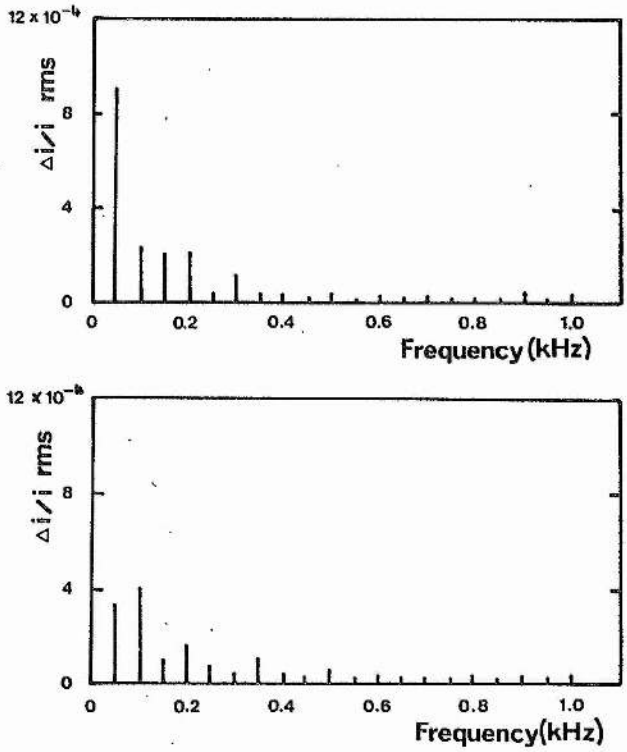

Fig. 3.212 Noise spectrum of EI 183 PSU with experimental conditions as described in Fig. 3.211. (a) shows the as-supplied unit and (b) after introducing modifications suggested by the manufacturer.

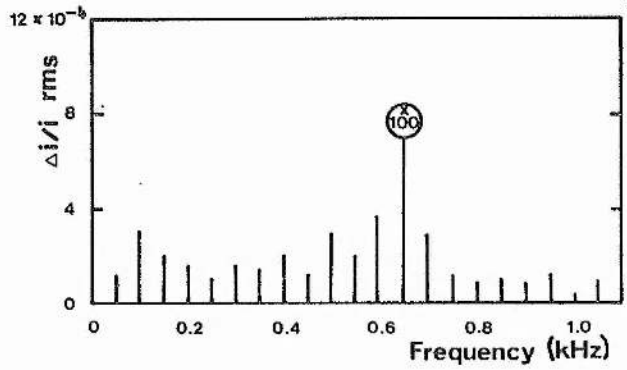

Fig. 3.213 The noise spectrum of the switched mode HML 421 PSU with the same experimental conditions as described in Fig. 3.21. The major noise peak at 650 Hz is shown reduced by 100 times. The rms noise fluctuation Δi/i was 8%.

$$v_Z = i_{const} Z \quad \ldots\ldots\ldots\ldots\ldots\ldots \quad (3.6)$$

and the total supply voltage v_T is related to current (where R is the ballast resistance) conventionally

$$v_T = (Z + R)\, i \quad \ldots\ldots\ldots\ldots\ldots\ldots \quad (3.7)$$

Now although the discharge impedance (Z) is a function of the current i, because i is kept constant the changes of discharge input power P_Z can be expressed

$$P_Z = i^2 Z \quad \ldots\ldots\ldots\ldots\ldots\ldots \quad (3.8)$$

or in differential terms

$$\frac{\partial P_Z}{\partial Z} = i^2 \quad \ldots\ldots\ldots\ldots\ldots\ldots \quad (3.9)$$

Because i is a constant the power input change ΔP_Z is directly proportional to the discharge impedance change

$$\Delta P_Z \propto \Delta Z \quad \ldots\ldots\ldots\ldots\ldots\ldots \quad (3.10)$$

Experimentally, this mode of detection requires sampling of the tube voltage (in ac case using suitable capacitive coupling) sometimes referred to as OVE (precise coupling schemes will be discussed in 3.22).

The alternative case, used in these experiments, is the most commonly reported scheme, namely constant voltage plus series ballast excitation where ballast (R) is slightly greater in value than the negative differential impedance of the discharge. If the discharge impedance changes (say rises) due to optical effects, then the voltage v_Z across the discharge initially rises and because the total supply voltage is limited

$$v_T = v_R + v_Z \quad \ldots\ldots\ldots\ldots\ldots\ldots \quad (3.11)$$

(where v_R is the ballast potential difference) when v_Z rises then v_R must reduce but because the ballast (R) is a simple Ohmic resistance

$$i = v_R/R \quad \ldots\ldots\ldots\ldots\ldots\ldots \quad (3.12)$$

then the circuit current falls, necessarily. Due to the negative differential v-i characteristic, this current fall results in a further tube voltage increase, which requires a further current reduction. The precise degree of this perturbation 'amplification' depends on the slope of the v-i (or more strictly Z-i) characteristic. This behaviour was first analyzed by Carswell and Wood[42] who considered the discharge to be considered of two parts: (a) the larger contribution which is current dependent, Z(i) and (b) the smaller contribution Z' which is optical intensity dependent. Initial optical changes of discharge impedance $\Delta Z'$ are circuit amplified by subsequent changes of i and Z(i). Relating current to impedance

$$i = v_T/Z_{TOTAL} \quad \ldots\ldots\ldots\ldots\ldots\ldots \quad (3.13)$$

where $Z_{TOTAL} = R + Z' + Z(i)$. Differentiating (remembering the current dependence of Z(i)) gives a current change Δi due to discharge impedance changes $\Delta Z'$

$$\Delta i = -\Delta Z' \; (v_T/Z^2_{TOTAL}) \left[1+(v_o/Z^2_T)\left(\frac{dZ(i)}{di}\right)\right]^{-1} \quad \ldots \quad (3.14)$$

Now dZ(i)/di is just the current dependence of impedance which is trivially measured but most difficult to accurately compute for wall dominated molecular discharges; the sign for these kind of discharges is negative and hence a circuit voltage gain factor (G) can be defined as

$$G = \left[1-(v_T/Z^2_{TOTAL}) \left|\left(\frac{dZ(i)}{di}\right)\right|\right]^{-1} \quad \ldots\ldots\ldots \quad (3.15)$$

which for all conditions where R > Z is greater than unity. Constant voltage with series ballast is the commonest form of excitation used for conventional OGE detection and the current changes which are induced are the primary parameters measured. Some quantitative measurements can still be made over a current interval as long as dZ(i)/di is measured (dynamically for ac signals) and Lawler[34] makes use of this half analytic, half empirical approach. The optically induced voltage change across the tube is now amplified by the

negative differential component and as the series ballast approaches the value of the discharge impedance the discharge can be switched off by small changes in beam intensity. Large amplifications occur at low currents where $dZ(i)/di$ is largest and as $(v_T/Z_T^2)\left|\frac{dZ(i)}{di}\right| \rightarrow 1$ then $G \rightarrow \infty$. Some measurements of discharge perturbations in this study (and many by others) have been made in this detection regime and these measurements generally show that noise increases as much or more than the signal gain factor. Operationally then there is little advantage of constant voltage plus series ballast excitation (other than its constructional simplicity) but the extra factor of long term laser power stability by current control favours the use of constant current supplies for optogalvanic detection in the laser discharge. Analysis of perturbation results is made simpler, $dZ(i)/di$ need not be known or accounted for, and ballast dependence does not occur.

Microscopically controlling current corresponds to compensating for the changes brought about (optically) due to changes in electron mean free path λ. However, due to the increased number density (caused by kinetic cooling) of all molecules (in the laser amplifying volume) the required potential difference for the discharge rises. In the constant voltage mode as the electron mean free path decreases the current decays and the reducing current increases the potential difference (secondary effect) as well as the primary effect.

The cases of parallel ballast and series plus parallel ballast were not investigated but simple consideration of the circuitry shows that very similar analysis is required to the series case. In the pure parallel case then no (or little) voltage change across the discharge tube is allowed but the current decays with increasing number density (amplification of laser beam) and the actual current change is analogous to the voltage change for constant current excitation with series ballast.

3.22 OPTOGALVANIC PICKOFF TECHNIQUES AND CIRCUITRY

There are several possible techniques for extracting the small optically induced electric perturbation (usually ac) from the larger (usually dc) discharge excitation current. The techniques used for stabilization were limited to the first four cases and the fifth technique has been previously investigated by Gower and Carswell[47] and Hart[69]; this particular scheme was investigated and found to be worse from the signal/noise respect by $\gtrsim$ 30 dB. The fourth case represents the scheme used for double discharges (high power laser) where all electrodes are at elevated potential.

1. Series Resistor R-C Coupling

   This scheme is shown in 3.221 and consists of sensing optically induced current changes (OGE) in a resistor R (value 50 Ω to 50 kΩ) which is in series with the discharge. If the excitation is constant voltage then (for an amplifying discharge) as the optical field increases then the impedance of the discharge increases and the current through the sensing resistor falls reducing the potential difference across the resistor. The fixed dc drop across the resistor (1 to 100 V) is blocked by the coupling capacitor C_1 and a roll-off filter circuit is established by C_2 and R to reduce the amplitude of fast risetime spikes during discharge switch on/off. Typical values used in these experiments were $R = 10 - 20$ kΩ, $C_1 = 0.5 - 1.0$ μF, $C_2 = 0.1$ μF, giving an upper roll-off $\sim$ 500 μs and a lower roll-off at $\sim$ 10 ms depending on the input impedance of the amplification circuitry. Alternatively, the current fluctuation may be sensed in the power supply current regulator[124] when a cc supply is used.

2. Parallel Capacitive Coupling

   This technique used by Scholtz and Schiffner[125]

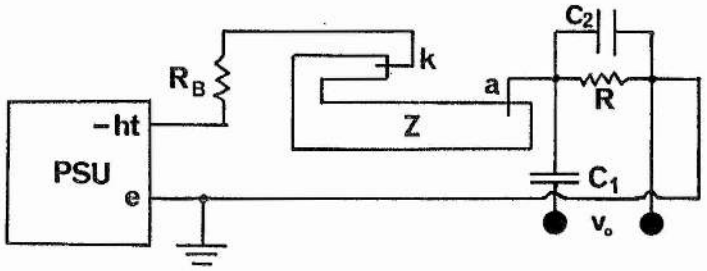

Fig. 3.221 Series resistor R-C coupling. This scheme was used conventionally for OGE detection with a cv power supply (PSU). The output voltage (V_o) is dependent on the value of R, R_B and the circuit gain G. Z represents the discharge impedance and the tube cathode (k) is supplied with the negative HT voltage.

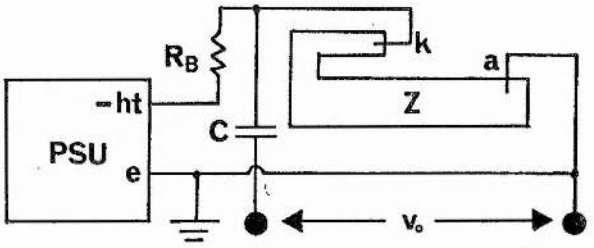

Fig. 3.222 Parallel capacitive coupling. Total voltage change signal is ac coupled out via the blocking capacitor C. A cc supply was used and the signal voltage is not fundamentally dependent on the circuit unlike the case in Fig. 3.221.

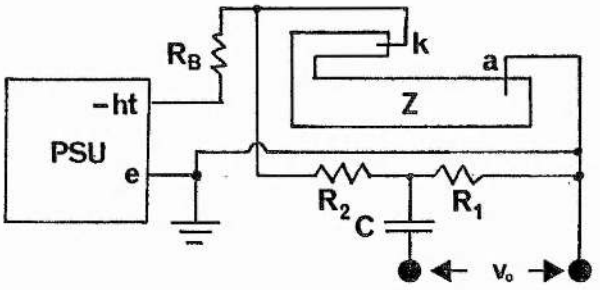

Fig. 3.223 Parallel R-C voltage potential divider coupling. This case is similar to 3.222 except the R_1 and R_2 potential divider reduces the dc (and ac) component. This coupling scheme was used frequently in these experiments particularly for the external sensing discharges.

directly senses ac tube voltage fluctuations (OVE) with constant current (or constant voltage excitation with consequent signal amplification) using a high voltage ($\sim$ 20 kV) dc blocking capacitor; the circuit is shown in 3.222. If the discharge current is held constant and optical perturbations occur, say for an amplifying discharge, then increased beam irradiance will cause an increased tube voltage. The whole voltage change is coupled into a high impedance input via C (typical value 0.01 to 0.1 μF). This mode gives results consistant with the theory prediction (Chapter 7) but discharge relaxation oscillation and capacitor breakdown frequently occurred with destruction of the subsequent electronic stage.

3. Parallel R-C Tube Voltage Potential Divider Coupling

This circuit shown in 3.223 consists of a high impedance parallel resistance sensing branch with a capacitive coupling from the earthed end of the discharge. As the tube voltage changes with constant current (or constant voltage excitation as above) then a small proportion $R_1/(R_1 + R_2)$ of this change is ac coupled via the dc blocking capacitor. This technique was found to be the most flexible and a chain of resistors could provide a varying proportion of pickoff. The total shunt resistance was set much larger than the discharge impedance ($R_1 + R_2 > 10$ Z); typical values were $R_1 = 9$ MΩ, $R_2 = 1$ MΩ and C = 1.0 μF.

4. Transformer Coupling

This technique shown in 3.224 is physically comparable

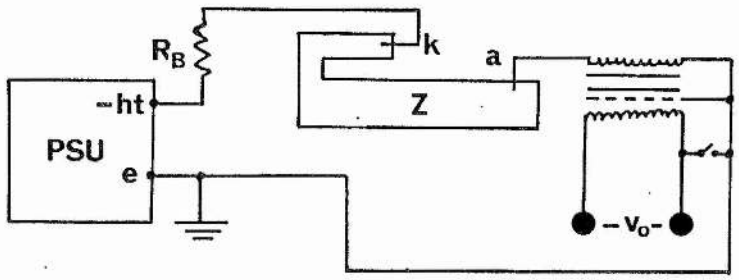

Fig. 3.224 Transformer coupling. This was developed in these experiments to avoid earth loop problems and was as useful as R-C coupling. The ac bandwidth is determined by the transformer. It required cv power supply (PSU) and the optically induced current fluctuations generate an OGE signal at the transformer secondary winding.

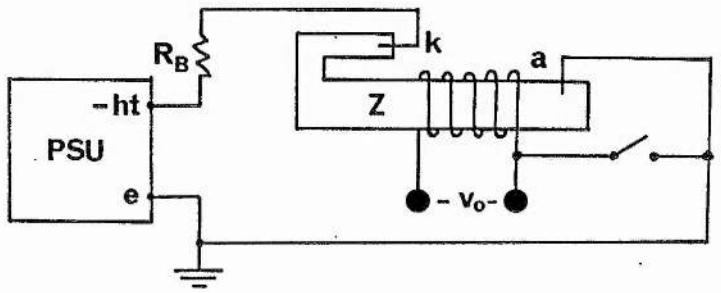

Fig. 3.225 Induction coupling. This was used to study the high frequency OGE and investigate the spatial dependence (within the positive column near to the anode, cathode, etc.).

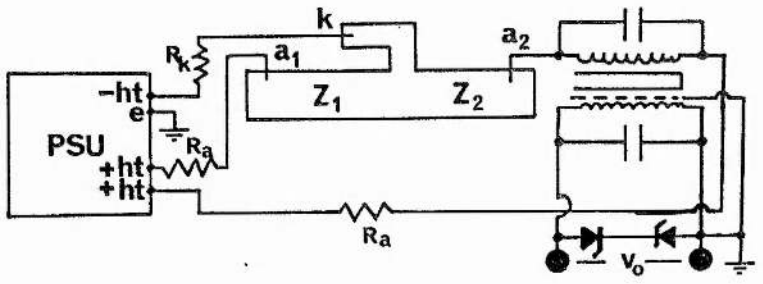

Fig. 3.226 Transformer coupling of twin discharge tube: required for split discharges where neither anode is earthed. R_a = 100 kΩ, R_k = 250 kΩ. Typical anode potential was 700 V - 1 kV.

to series resistor R-C coupling and is a constant voltage technique (OGE) sensing current changes. When the current changes in the transformer primary (due to optically induced impedance variation in the discharge), then so long as the variation occurs within the transformer passband (20 Hz to 20 kHz) then the secondary voltage will fluctuate with a voltage proportional to the turns ratio. Ratios between 1:2 and 2:1 were suitable; this corresponds to an impedance coupling from ∿ 100 kΩ (discharge and ballast resistance in parallel from the equivalent circuit) into the preamplifier and PSD inputs (∿ 50 kΩ).

This technique has one particular advantage, as long as the transformer has high voltage isolation then for split discharges none of the electrodes need to be earthed (Figure 3.226). This was the only method available for the EI PL3 laser and the high power laser constructed for these experiments. Any high quality audio transformer (preferably with screen) is generally adequate and for 10 kV isolation a Ferromag FM 3931 isolation transformer was used. With this method it is important that the transformer core is not saturated by the dc discharge current (10 to 20 mA) and that the primary resistance is not particularly high otherwise overdissipation can occur.

5. Induction Coupling

This technique suggested by Hart,[69] consists of monitoring current changes by winding a coil

around the discharge tube; the circuit is shown in 3.225. This method was found to have a wide passband and is useful for finding how the current was changing in different parts of the discharge by moving the sensing coil. Signal coupling efficiency rises with the oscillation frequency. At frequencies below 1 kHz very poor signal to noise ratio was measured (PSD time constants ∿ 10 to 30 s required to extract the signal ∿ 100 to 300 μV). At 3 kHz the detected signal peaked for ten turns of 18 swg tinned copper wire and with five turns the peak was shifted ∿ 10 kHz. The signal was ∿ 30 dB stronger at these frequencies than at 100 Hz and the high frequency reduction of the detected signal was consistant with the fundamental decrease in the efficiency of the high frequency OGE suggesting that either flat or increasing frequency response could be expected for frequencies > 50 kHz. This technique may be useful (and preferable) for OGE signal reception at much higher frequencies.

Another similar coupling scheme suggested by Hart and Siemsen[69] is a one turn closed winding of aluminium foil which consists of ∿ 10 cm long single Al loop; this was found to produce signal peaks ∿ 100 Hz coincident with the largest noise contributions from the excitation power supply and higher frequency detection was not observed so that cc excitation stabilization could not be achieved. Otherwise detection signal to noise (S/N) ratios were similar to the ten turn coil.

A careful comparative analysis of these techniques showed that the conventional series resistor R-C coupling was most flexible and useful for

laser stabilization, certainly for cv excitation and equivalent in all respects to parallel R-C tube voltage potential divider coupling during cc excitation. This has been observed by other researchers.[69,124] The latter choice allows good detection (large signal and good S/N) for both cv and cc cases whereas the former requires careful selection of the operating frequency (modulation) for the cc mode (see Figure 4.15). The parallel capacitive coupling method with cc excitation is equivalent to parallel R-C coupling in the cv case with a reducing low frequency response ($f < 500$ Hz) because of the impedance feedback gain (see equation 3.14) which is set to 1 by the psu current regulation at low frequencies. Transformer coupling was found to be equivalent in performance to R-C coupling so long as the transformer passband and the impedance matching was observed. The specific advantage of electrical isolation was required in some situations. Several pulse transformers were tried in order to receive high frequency signals with no success.

In summary, for optimum S/N consistant with a wide operating bandwidth and flexibility of use series R-C coupling and parallel R-C coupling were optimum and isolation was required for safety, circuit or other considerations. Transformer coupling was as effective with a reduced operating bandwidth. The induction coupling techniques are of physical interest for the investigation of the perturbation effects locally in the discharge but are not technologically useful for signal detection or stabilization (signal 30 to 40 dB less than series R-C case).

When the stabilizer electronics were situated in a remote position from the laser head preamplifiers were used to boost the OGE signal to $\sim$ 1 V (20 to 50 dB gain). This was largely to overcome noise generated in the co-axial signal cable; both hum and microphony can generate noise levels $\lesssim$ 0.1 V and several of the tuned preamplifiers were designed and constructed with bandpass frequencies in the range 16 Hz to 18 kHz. A high Q circuit is not desirable as this can introduce phaseshifts of the signal; it is phase information that is required to generate the sign of the correction ultimately fed back to the laser. By using several (typically four) low gain stages in

tandem useful preamplifiers were constructed with a $Q \sim 5$ and a gain $G \sim 100$.

3.23 FEEDBACK SYSTEMS FOR ACTIVE STABILIZATION

Individual electronic units which perform all the necessary functions required for active laser stabilization are available commercially; however, they are not intended specifically for servocontrol and many are not suitable. One multipurpose commercial stabilizer was used (Lansing 80.214) in some of these experiments. A simply constructed system has been well described by Shotton and Rowley[126] and Wallard and Wilson[127] and two units constructed to this design were used in this work; one is shown in Figure 3.231. In most cases the servo was required to drive the laser mode to the maximum power point and hold it there; a small sinusoidal modulation $v_m \sin(2\pi ft)$ is applied to the PZT in order to dither the laser frequency and generate an optogalvanic signal when the laser mode is not at line centre; Figure 3.232 shows how the modulation signal is added to the amplified error signal EG and fed to the length adjusting element PZT.

The length of the cavity is initially set (manually) for the laser line centre frequency f_0; any length change, due to vibration or thermal expansion results in a laser frequency drift to f_1 and an error signal E_1 is generated. This error signal drives the mirror back in order to return the laser frequency to f_0 (negative feedback). This is never achieved totally because some error is required $\Delta E \neq 0$ in order for correction to occur and the laser frequency takes a new value f_2 such that $|f_2 - f_0| < |f_1 - f_0|$. Any larger cavity perturbation will tend to increase $|f_2 - f_0|$ and the ratio factor $F = |f_1 - f_0| / |f_2 - f_0|$ is a measure of the servo's effectiveness in reducing frequency variations, proportional to the gain of the servoloop.

It is also important that the servo can respond sufficiently fast such that correction rate $\partial f/\partial t$ is greater than any likely drift rate. This requirement sets a lower limit on the servoloop bandwidth which must extend

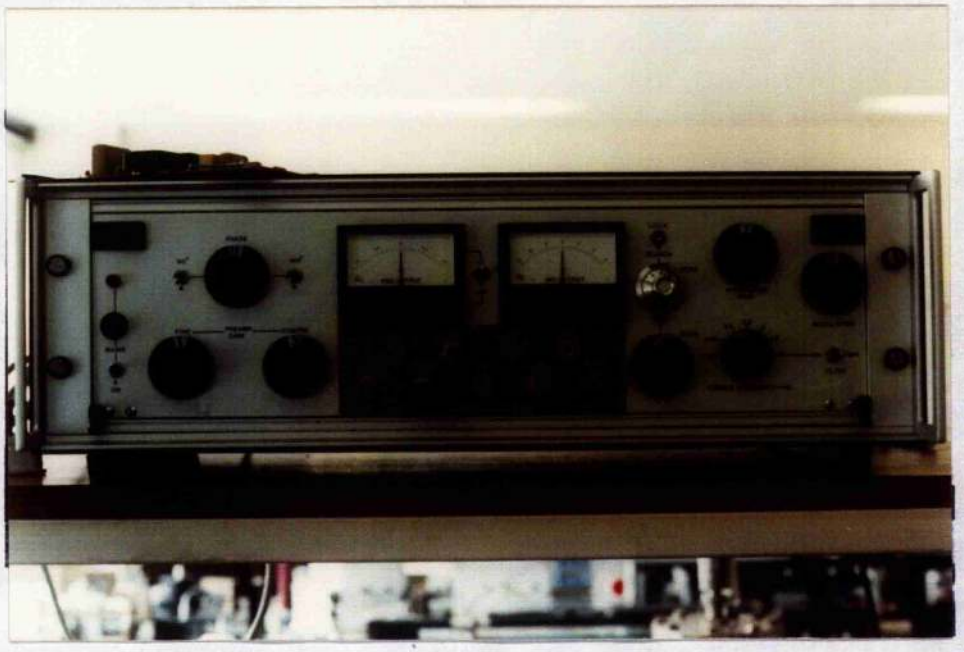

Fig. 3.231 Stabilization electronics consisting of switched ac preamplifier, PSD, integrators, modulation, switched dc amplifier, and high voltage amplifier to drive PZT. The circuitry was developed from Shotten and Rowley.[126]

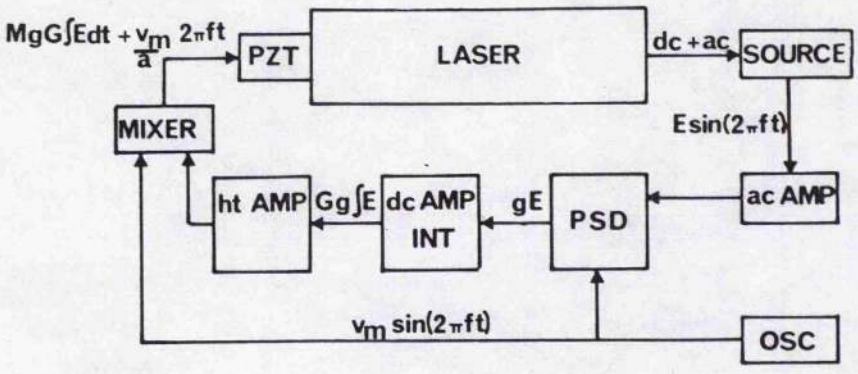

Fig. 3.232 The addition of modulation and the rectified, integrated and amplifier error signal.

down to dc to cope with slow drift associated with long term thermal cavity drift. The upper correction frequency limit is set by the necessity of phase integrity around the loop; at higher frequency phase changes occur and as the feedback becomes positive the system oscillates.

Two filter integrators were used in these systems (in a modified form after Shotten and Rowley[126] after the PSD which determines the sign of the error signal (to drive low or high frequency). The main integrator acts as a sample/hold circuit in the 'search' mode so that the laser can be manually frequency adjusted to near line centre and the dc voltage corresponding to this frequency is 'stored' in the capacitor. The time varying error E_1, etc. corrects this voltage.

Rather than amplifying the error signal and directly feeding it back the integrator delivers a steadily rising correction voltage (the rate varies with E_1). If and only if $E \equiv 0$ then the correction rate $\partial f/\partial t = 0$; in this respect the integrator has an infinite dc loop gain. Additionally, the main integrator provides post detector integration (PDI) which provides a time averaging of the noisy PSD output (rectified ac). In these experiments the value of the main integrator time constant was adjusted from 10 s (for 16 Hz modulation) to $\sim$ 50 ms for modulation frequencies > 10 kHz.

Despite integration, if the length is constantly changing ($\partial f/\partial t \neq 0$) then small, steady frequency offsets occur proportional to the time differential of frequency. A secondary integrator was inserted to reduce this effect and provide velocity feedback (rather than positional feedback). The time response of this integrator was made adjustable, in the first instance, over the range 100 s to 10 ms; it was intended that this would set an overall response rate restriction on the loop. It was found, however, that due to the large capacitance $\sim$ 0.2 μF of the PZT elements that the overall restriction below $\sim$ 3 s was due to the slewing rate of the high voltage amplifiers. Subsequently, a Burleigh PZ81 high voltage amplifier was installed which had a fast rise time capability.

The phase shifts at higher frequencies must never total π in order to

avoid oscillation. It is required that the gain of the system < 1 at this frequency. Any shift $\gtrsim \pi/2$ results in 'hunting' of the laser operating point; it was found that a unity gain frequency less than the $\pi/2$ shift frequency (and of course the modulation frequency) was required. The transfer function chosen by Shotten and Rowley was used to give both acceptable high frequency correction and hunting suppression (see Figure 3.233). The turnover point f_3 is set by the leakage resistance R_2 of the main integrating capacitor C and is just $f_3 = 1/2\pi R_2C$ and f_2 is chosen by the second integrator time constant.

3.3 ACTIVELY STABILIZED LASER SYSTEM CONSIDERATIONS

The general considerations in defining the detailed structure of OGE stabilization systems are

1. Type of laser (atomic-molecular, HeNe, CO_2, CO, etc.)
2. Discharge configuration (single, double, etc. earthed terminal, etc.)
3. Power supply type (ac, dc, rf) and noise factor
4. Passive cavity capability (mode stability, etc.)
5. Laser/control electronics interface (pickoff and single/double PZT, etc.).

The considerations specific to the subsequent application of the stabilized laser are

6. Degree of required stability (10%, 1%, 0.1% intensity stability for example)
7. Timescale of stability and operating bandwidth of the servomechanism. (Induced fm modulation may degrade the laser performance in some cases, etc.)
8. Dynamic performance of entire stabilized system (for example will a jolt cause a servo driven excursion in excess of the non-stabilized case and also can some hunting or oscillation be tolerated)

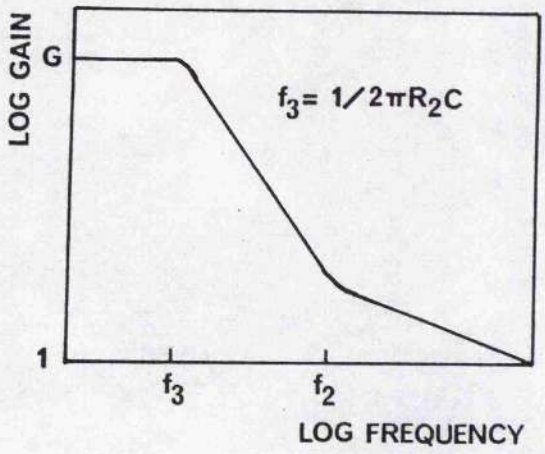

Fig. 3.233 Transfer function of dc amplifier and double integrator. G is set by the switched dc gain and f_2 is controlled by the secondary integrator time constant and f_3 is determined by the primary integrator capacitor and its leakage resistance R_2.

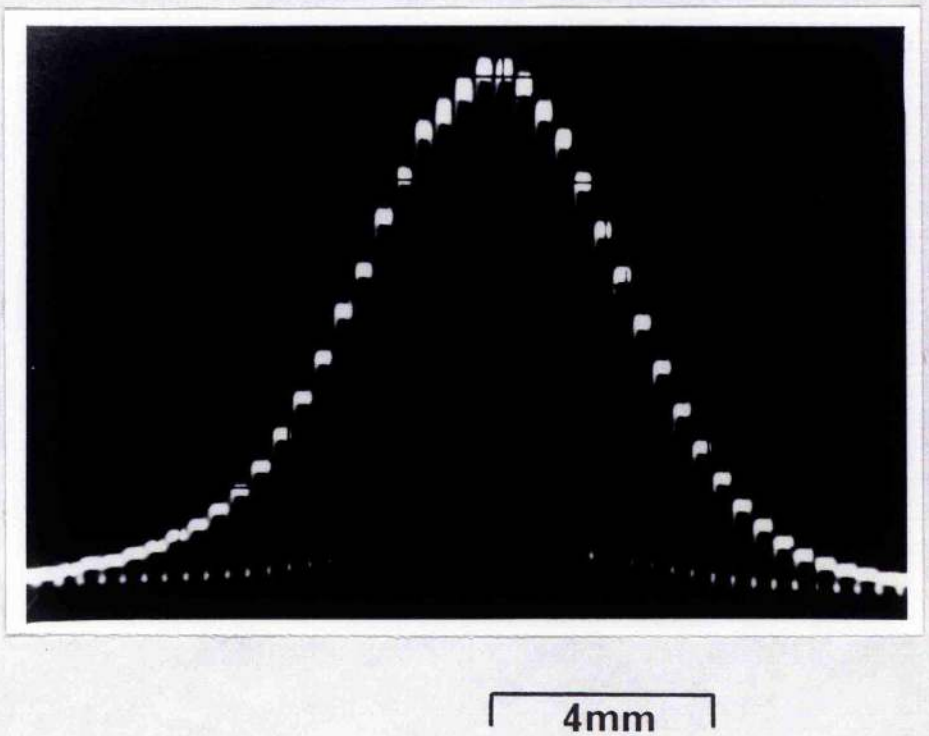

Fig. 3.411 Beam profile of a compact CO_2 laser fitted with a 9 mm diameter tube. The total output power was 5.2 W and the laser stabilized on 10P(20) at - 15 MHz with respect to line centre.

9. Expected drift rates due to environment
10. Other systematic factors including cooling considerations and vibration.

3.41 BEAM PROFILE MONITORING

It has been a difficult matter until recently to measure, quantitatively, laser beam power radial profiles. Several manufacturers now produce multi-element detector arrays suitable for the purposes of making these measurements (Spiricon, Plessey, Delta). Various techniques have been used previously with single detector, time resolution, of the beam profile. Massig[70], for example, used the rotating mirror method. It is difficult to calibrate this in terms of radial distance. For many years thermal image plates have been used for qualitative assessment.

A Delta Developments 50 element detector array was available for these experiments. As manufactured it was suitable only for pulsed laser measurements. In order to prevent overdissipation of the PVF_2 pyroelectric elements a chopper with a low mark to space ratio was inserted at the focus of a simple optical system. Because the array spanned 25 mm, some beam expansion was necessary in order to make maximum use of the spatial resolution. A simple variable magnification (x 2 to x 3) beam expanding telescope was designed and constructed using a ZnSe lens, circular Al apertures and a low frequency ($\sim$ 20 Hz) chopper.

Figure 3.411 shows a far field scan of a beam from a compact laser operating at 5.2 W. The beam was generally free from spatial modulation and had a half power diameter of $\sim$ 6 mm. The laser tube diameter was 9 mm and it was actively stabilized at - 15 MHz with respect to 10P(20) line centre with 1.5 MHz FM deviation. Over three hours the beam pointing stability and beam geometry stability were measured. The maximum change of power received by any one segment was < 7%. The peak shift was not more than two segments ($\sim$ 0.25 mm over a distance $\sim$ 4 m). This requires a pointing angle change of < 100 μrad. By measuring the half power width change, a measure of geometry

was made. This change was less than 8%.

When the laser was allowed to drift a series of off-axis mode patterns could be generated (see Figure 3.115). Figure 3.412 shows two such patterns when the laser was not actively frequency locked. A steady drift of the mode pattern towards a stable predominantly TEM_{01} mode occurred.

3.42 LASER HETERODYNE RECEPTION

The assessment of frequency stability was primarily achieved in these experiments by monitoring the difference frequency of two similar but independent laser systems. There are several experimental problems with this approach including systematic errors, such as the locking of one laser to the other, spuriously by the inadvertent mixing of one beam in the other amplifier and the physical non-independence of the systems. Freed[128] has used the reflection of a CO_2 beam from a satellite to try to avoid these problems. Unfortunately, both these systematic errors result in an improved stability being measured. In order to isolate the two lasers separate coolers, power supplies and tables were (sometimes) used. The details of these effects will be more carefully investigated in Chapter 4. The technique used in these experiments was to try to induce intentionally these errors and then remove them as far as possible. A novel beam mixing technique was developed using a diffuse reflector rather than a beam splitter and this was found to be most efficient at eliminating locking of one laser to the other.

The beam mixing technique consisted of using a rough (diffuse) reflector to scatter the beam energy over a wide angle. Several surfaces were tried including flame sprayed metals (aluminium and copper) and sand blasted aluminium. The flame sprayed surfaces had a surface roughness $\sim$ 1 mm and proved to be too rough. The sand blasted surfaces had a variable surface roughness $\sim$ 5 μm to 20 μm depending on grit size, workpiece distance from nozzle and pressure. The coarse sandblasted surfaces produced useful polar diagrams where $\lesssim$ 80% of the 10 μm beam power was reflected into the main lobe and the remaining $\gtrsim$ 20% scattered into the half hemisphere. Figure

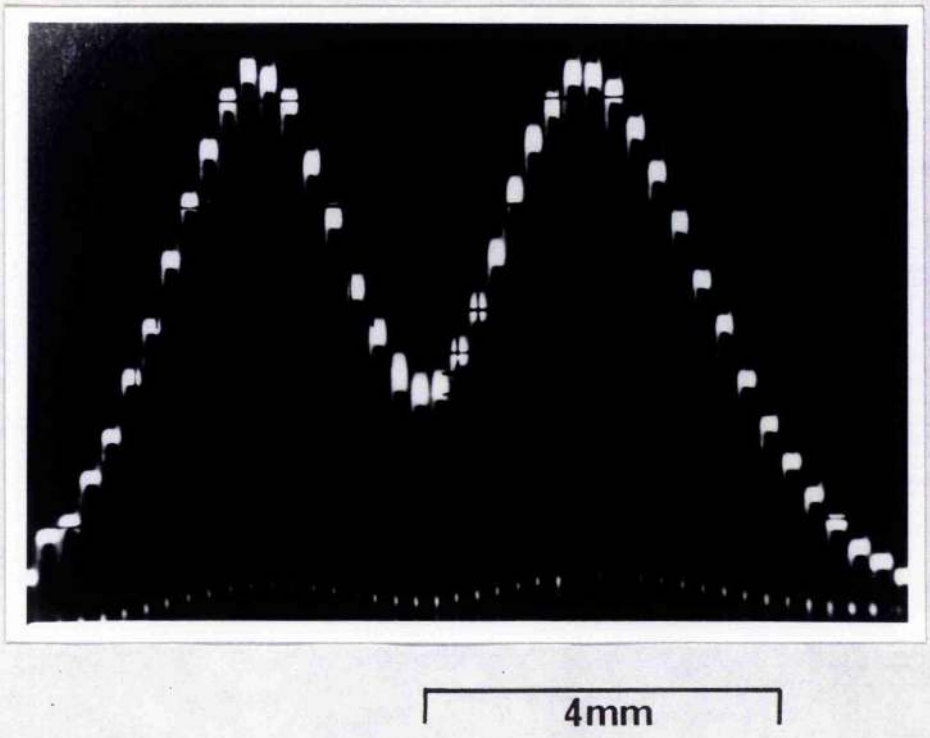

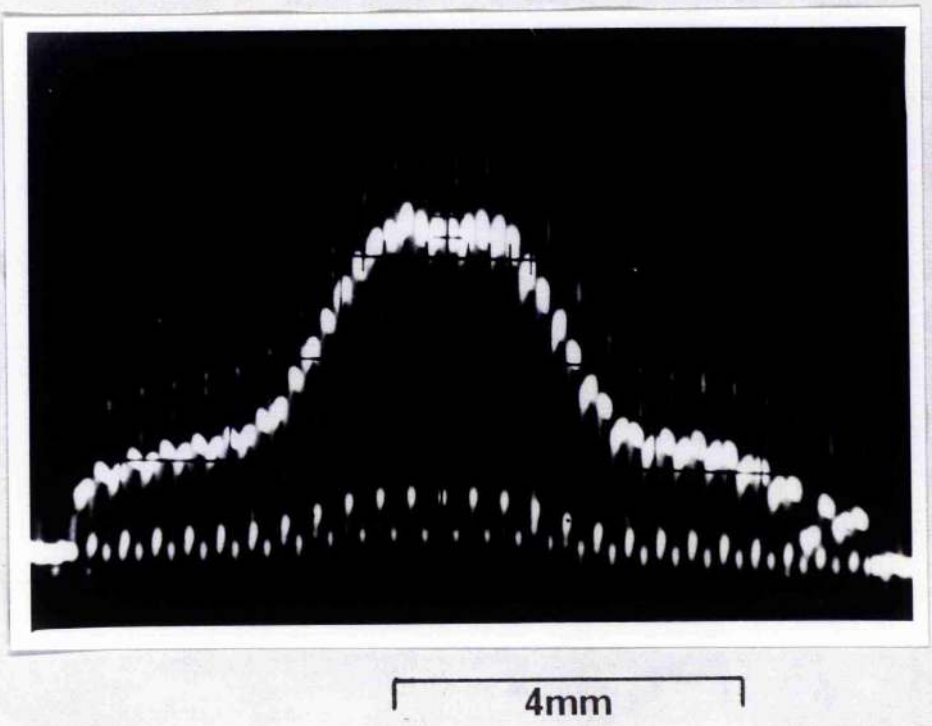

Fig. 3.412 With conditions as described in 3.411 but without active stabilization the laser drifts displaying an array of mode patterns such as these.

3.4212 shows the experimental situation where any two of the five lasers (LO, LS) could have beams set to a coincident point on the diffuse reflector (DR). The two beams (B_1 and B_2) were set to be at least 20^o apart and the diffuse reflector is angled at least 45^o off either of the beams. The major power lobe was dumped into bricks and the detector situated $\sim 30^o$ from B_1 and B_2. The detector area and distance determines the collection angle and a simple square law of received power was observed by moving the detector closer or farther from the reflector. By virtue of the small detector area only parallel parts of the two beams are selected and, therefore, the plane phase front criterion is automatically met. The detector itself was angled off axis. Reflection back along the beam path is a common source of systematic error. A typical distance of 10 to 100 cm was used in order to provide attenuation of $\sim$ 1000. It was not possible to produce three reflector effects or locking one laser with another by this method; a conventional beamsplitter layout was also used and some locking effects always occurred.

3.421 LTT DETECTORS AND SIGNAL PROCESSING

All the CO_2 laser mixing experiments were performed with Plessey Lead Tin Telluride (LTT) photo-detectors; two were used of the LXC 600 and LBC 600 series (serial nos. C280 and 262 respectively). These detectors were sensitive over an 8 to 14 μm wavelength window and operated in the photovoltaic mode at liquid nitrogen temperature (77 K). A matching Plessey preamplifier and autobias unit (CAA5345 serial no. 540) was used with the LXC detector and an amplifier and autobias circuit was constructed (to Plessey specification CA5100J) and used with the LBC detector. Additionally, both detectors were used in the unbiased non-amplified mode because very good signal to noise ratios existed in these experiments. The detectivity D^* was 6.2×10^{10} cm $Hz^{\frac{1}{2}}W^{-1}$ and the sensitive area was $\sim 6 \times 10^{-4}$ cm^2 with a 60^o field of view.

The detector frequency response was measured with a Tektronix 466 storage oscilloscope, Marconi TF2370 VHF spectrum analyzer and HP 8557A RF spectrum analyzer (with 8750A storage normalizer). Figure 3.4211 shows the

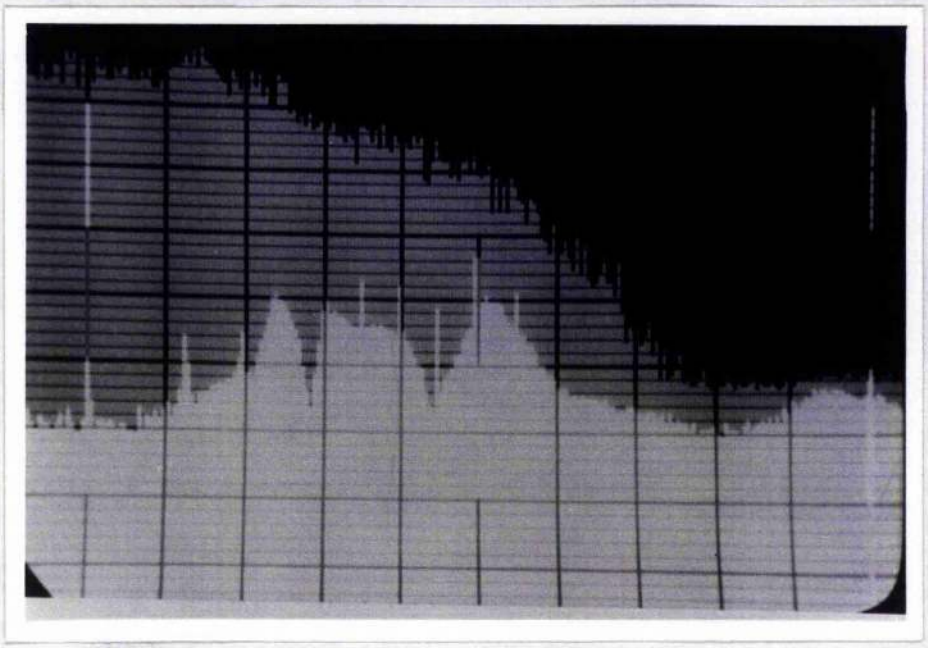

Fig. 3.4211 Frequency response of LTT detector/preamplifier. Noise (white) and signal + noise (grey) from LTT (Plessey LGC) detector and matched preamplifier obtained by wideband FM laser heterodyne technique (see below). The top line is - 10 dBM (relative to 1 mW into 50 Ω) and the vertical scale is 10 dB/major div. The horizontal frequency scale is 5 MHz per division with 5 kHz resolution. The spectra were averaged for 5 minutes and the zero marker is shown as a white line at the left and a 50 MHz marker is shown as a white line to the extreme right.

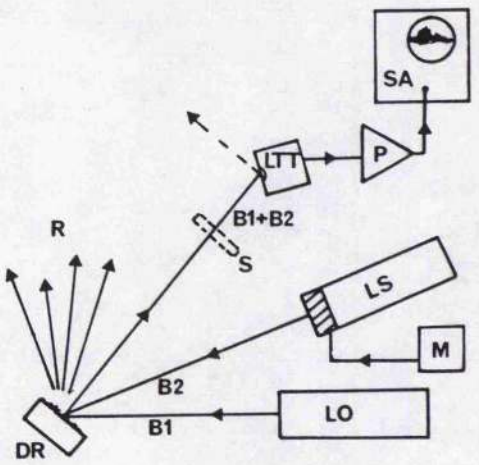

Fig. 3.4212 Experimental arrangement for FM laser technique to investigate the frequency response of LTT detectors. LO - local oscillator laser generating beam B1 at ∿ 5 W (5 mW incident on-detector), LS - signal laser (providing B2 at ∿ 1 W) modulated by PZT and modulation source M to provide > 50 MHz FM deviation, DR - diffuse reflector, S - shutter, R - majority of laser radiation, LTT - detector with preamp (P) and spectrum analyzer (SA). The detector is angled off normal to avoid back reflection into the laser and the distance from DR to LTT is adjusted to ensure sufficient attenuation (∿ 1:1000).

wideband spectra of the frequency difference signal detected by the LGC detector; a diffuse deflector was used to direct a small proportion of the beams from two CO_2 lasers (operating single line 10P(20)) onto the detector. One laser was frequency modulated across the entire line segment range by the PZT whilst the other was line centre stabilized (see Figure 3.4212). A spectrum analyzer (Marconi TF2370) average was taken over five minutes for the noise (no incident beam, shutter S in beam) and the signal plus noise for $\sim$ 5 mW and $\sim$ 1 mW of local oscillator laser beam and modulated signal beam. The noise spectrum is determined largely by the preamplifier. Several distinct noise spikes in the 5 to 25 MHz range were recurrent and due to parasitic behaviour of the preamplifier.

A 50 dB ($\sim$ 350 times) signal above noise is seen up to $\sim$ 10 MHz falling to $\sim$ 30 dB ($\sim$ 35 times) factor at 20 MHz. Some signal $\sim$ 3 dB above noise is detected up to 40 MHz and clearly this detection system offers a sufficient bandwidth capability for the investigation of beat frequencies of signature line selected CO_2 lasers.

A frequency response test was required in order to show that the detector/preamplifier combinations were adequate to receive any heterodyne signals generated by two same-line lasers. The LBC detector had a very similar bandwidth performance but the preamplifier was $\sim$ 10 dB noisier at low frequencies. Both detectors/amplifiers showed - 3 dB responses at the low frequency extreme of $\sim$ 20 kHz. This limit is determined by the preamplifier; the detectors will respond down to dc but 1/f noise dominates at low frequencies and this requires that the signal is attenuated for frequencies < 50 Hz for time domain signal reception (i.e. oscilloscope). These detectors behave as Johnson noise sources above 50 Hz and the effective resistance is $\sim$ 3Ω.

4.0 OPTOGALVANIC ACTIVE STABILIZATION OF CO_2 LASERS

It has been briefly outlined in Chapter 1 how a laser (CO_2 or otherwise) can be actively stabilized by a feedback loop. It has also been described

in Chapter 2 how optogalvanic (OGE) signals can be detected in gas discharges and how both amplitude and phase of the OGE signals can be utilized in a null seeking laser stabilizer. In this chapter the detailed description of active stabilization of CO_2 lasers by the optogalvanic effect will be given. The main emphasis will be on the anti-drift capability of passively stable oscillators frequency locked by this method. In Chapter 6 details of faster response feedback systems will be presented with an explanation of the high frequency optogalvanic effect in CO_2. In this chapter the discharge used as the OGE source is the main laser amplifying discharge positive column and unless otherwise stated, the servomechanism was locked to line centre of the 10P(20) transition with wavelength 10.59 μm. Sufficient description of the fundamental microscopic processes are given to explain the experimental stabilization results but the major theoretical treatment is presented in Chapter 7. This chapter also deals with the limitations, both fundamental and systematic, of the performance of the OGE stabilization of CO_2 lasers and the resolution of some of these limitations is explained in the succeeding chapters. Overall, the experimental results show that OGE active stabilization is a simple, efficient, cost effective and vibrationally insensitive stabilization method which brings considerable improvement in performance and which is ultimately capable of stabilization to a high degree.

When a CO_2 laser, which is dc constant current (cc) excited oscillates, it undergoes an increase of discharge voltage. Figure 4.01 shows in a simplified way, the voltage/current changes which have been observed by many authors (Skolnick[61], Schiffner[46], Stefanov[72], Smith and Brooks[53], etc.); these changes have sometimes been misinterpreted by both poor description and lack of care, in describing the type of supply (cc, cv, ballast, etc.), discharge condition changes (pressure, composition, etc.) and assumptions about phase changes.

Figure 4.01 shows the slow changing dc OGE signal obtained by the conventional series resistor R-C coupling method with cv excitation including

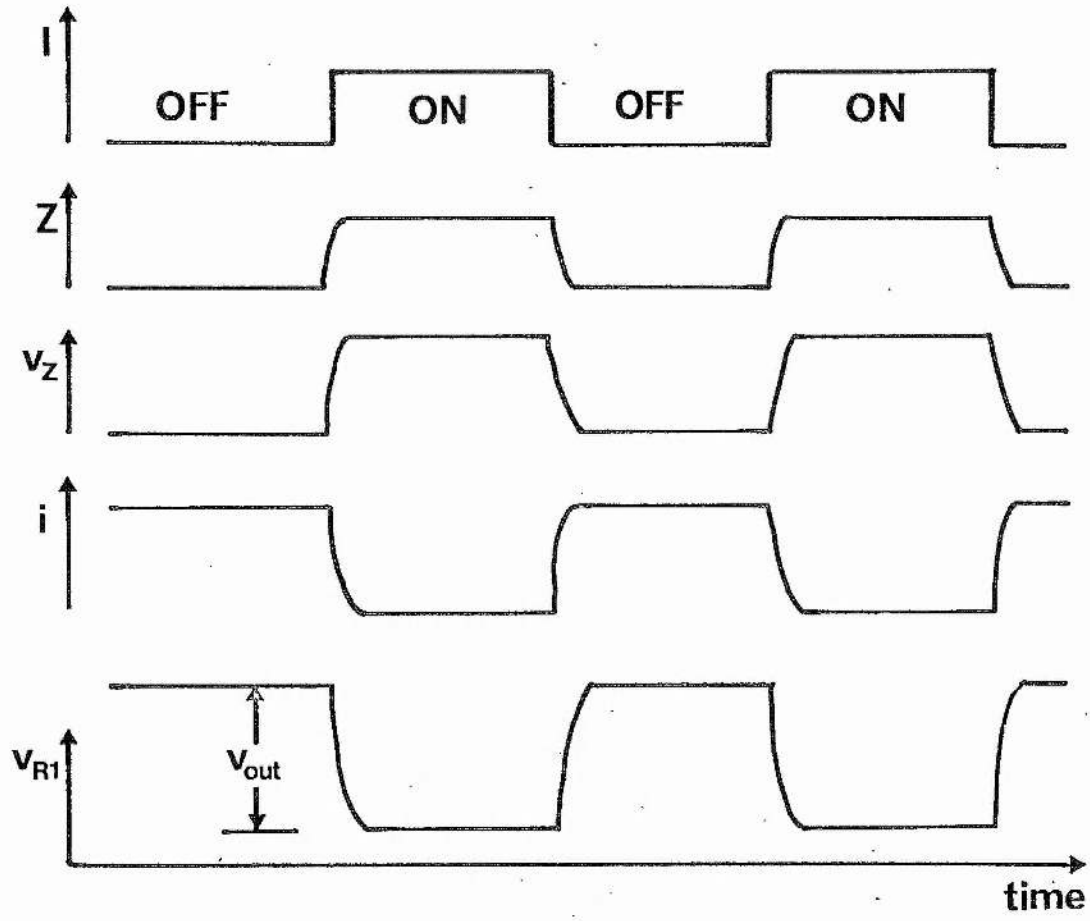

Fig. 4.01 The optogalvanic changes that occurred due to changing laser irradiance I, when cv plus series ballast excitation was used.

series ballast slightly larger in resistance than the discharge ($R_B > Z$). As the laser stimulated emission field increases (as mirrors are aligned) the discharge impedance (Z) rises and consequently the discharge voltage (v_Z) rises and the current (i) reduces due to the negative differential v-i characteristics. The precise amplitude of the change depends on the v-i characteristic which determines the circuit gain (see equations (3.11) to (3.15)). As a consequence of reducing current the series resistor potential difference (v_{R1}) falls. It is this reducing voltage (i.e. the step component V_{out} which is the conventional OGE signal) which reduces with the commencement of laser action. It is not particularly useful to measure the exact voltage changes for a given optical intensity for this mode of operation (as most previous authors have tried), because of the uncertainty in the circuit gain factor dependent upon power supply source resistance, circuit parameters (exact ballast value, etc.), gas pressure and composition and discharge tube details (diameter, length, cathode type, etc.). In this work initial consideration was given to cc excitation and the measurement of total discharge potential difference. Figure 4.02 shows the increase of discharge voltage at a cc of 15 mA for a compact laser discharge tube for the increase of laser output power (adjusted by partial misalignment of the laser output coupler). A detailed description of accurate measurement of OGE effects by this unambiguous technique is presented in Chapter 8 but here it is sufficient to notice the approximate linearity of the effect with some saturation at high output powers and see how a minimum change of discharge macroscopic parameters (e.g. voltage) will occur with length dither at laser line centre where the output power changes are minimum (flat top of gain profile).

The upper part of Figure 4.03 shows the set of vibrational rotational energy levels associated with infrared stimulated emission from CO_2, responsible for laser action. The asymmetric stretch mode first excited level is the upper laser level; it is situated $\sim$ 2500 cm^{-1} above the ground state. The whole set of similar levels (00^0n when n = 1, 2, 3, ...),

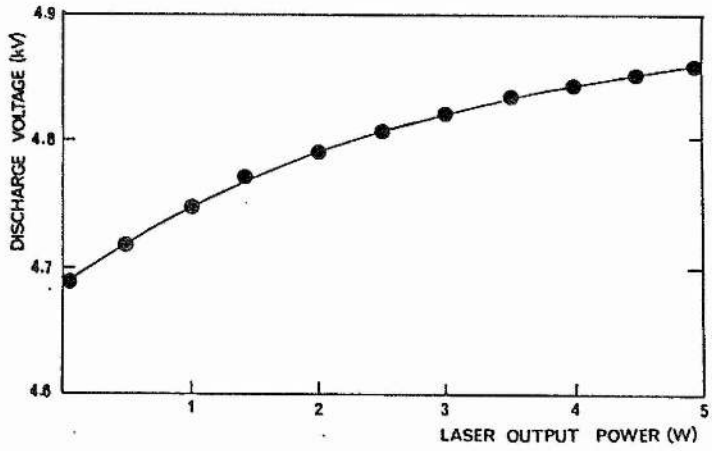

Fig. 4.02 Increased discharge voltage due to laser oscillation for compact CO_2 laser filled with 2 Xe, 2 CO_2, 4 N_2, 15 He and fitted with 90% reflecting output coupler.

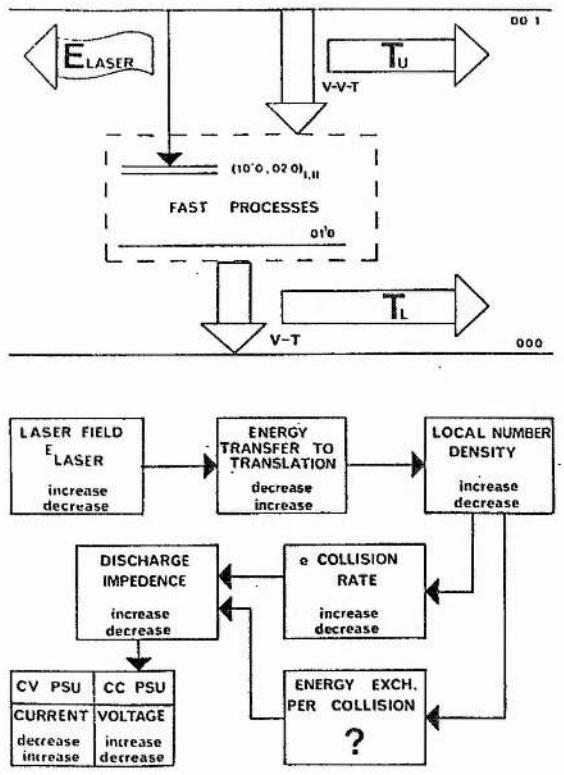

Fig. 4.03 A simplified diagram of the CO_2 kinetics relavent to the optogalvanic effect and (below) the sequence of changes leading to this effect.

which constitutes the asymmetric stretch mode population, is supplied by the discharge with vibrational energy from vibrationally excited N_2 molecules by near (energy) resonant collisions which exchange this energy (vibrational-vibrational collisions, V-V). N_2 molecules have a large cross-section for direct electron impact excitation and it is predominantly through this process that the energy from the electric current is transferred to the CO_2 asymmetric stretch mode. Other mechanisms of reasonable probability (all such are called pumping mechanisms) include direct electron impact of CO_2 molecules and vibrational energy exchange from vibrationally excited CO molecules which are abundant due to CO_2 dissociation in the discharge into O_2 and CO which is subsequently excited by electron impact in the same manner as nitrogen. A large proportion of this input discharge energy ($\lesssim$ 60%) is coupled into the CO_2 asymmetric stretch mode by these mechanisms[129] and it is the subsequent relaxation processes which are of immediate importance in the understanding of the gas temperature explanation of CO_2 OGE (reviewed in Chapter 2.4).

The largest proportion of energy is lost from the CO_2 asymmetric stretch mode by vibrational-vibrational-translational (V-V-T) process via the $00^0 1$ upper laser level; this relaxation process

$$CO_2\ (00^0 1) + M \rightarrow CO_2\ (n,m,o) + M + T_U$$

where M represents all the possible collision partners (CO_2, CO, O_2, N_2, He, Xe) transfers the surplus energy to kinetic energy (T_U) of all the molecules. This generalized exothermic process, shown by the bold arrow in Figure 4.03, has been considered in detail by several authors.[48,130] Normally, that is in a discharge which is not losing energy via stimulated emission, all relaxation from the $00^0 1$ level is by this route with a subsequent kinetic heating of the gas. An equilibrium temperature distribution is established across the diameter of the discharge tube with a resultant number density profile across the diameter.

The laser process (shown as the left hand arrow in Figure 4.03) competes

directly with the collisional relaxation process; both processes transfer the CO_2 excited population to a closely coupled group of levels (equilibriated by very rapid collisions) which are labelled (the lowest state) $01^{0}0$ for convenience. This $01^{0}0$ set rapidly relaxes to the ground state by exothermic V-T processes which transfer all the vibration energy to kinetic energy of the particles.

If the CO_2 discharge becomes a laser, by optical feedback, then energy is directly coupled out of the $00^{0}1$ level by 10 μm photons and a total energy of E_{LASER} (due to n photons) is lost from the relaxation system. At this stage the approximation of constant pumping will be made; this will need attention in 7.4. During an increase of laser field (E_{LASER}) a decrease of $00^{0}1$ population occurs which results in a first order decrease of V-V-T processes and a direct decrease of energy into translation (heating the gas). The lower part of Figure 4.03 shows the resulting sequence of changes taking place in the discharge. An increase in laser field results in a decrease of energy to translation (T_U). This reduced gas heating results in a reduced temperature of the gas. For a constant volume (some of which is radiating and some not) the radiating volume will have an increased number density of particles in the locally cooled part of the discharge (kinetic cooling). This increases the electron collision rate (more partners for collision) which is displayed macroscopically as a discharge impedance increase. Additionally, as suggested by Lobov[60] changes in the quantity of energy exchanged per electron-molecule/atom collision may occur.

The increased discharge impedance due to increased laser field for cv excitation results in a current decrease with a potential difference reduction across a series resistance. Alternatively, for cc excitation an impedance increase results in a discharge tube voltage increase. For a reduction of laser field the opposite result is obtained (see Figure 4.03).

4.1 DISCHARGE v-i CHARACTERISTIC CHANGES AND OGE SIGNATURE INVESTIGATIONS

The application of OGE processes for stabilization requires some consistent measurement of the magnitude of the effect; cc excitation and tube voltage changes were used for this reason and Figure 4.11 shows the manifestation of the optogalvanic effect in good qualitative correspondence to the gas temperature explanations given so far. For a particular laser discharge current (say 20 mA) as the laser output power is increased (by mirror alignment) then the discharge voltage rises (in an approximately linear manner) as shown in Figure 4.02. Also shown is the available laser power with discharge current. Reduced values of output power were obtained by misalignment of the laser output coupler. The voltage change at 5 mA is larger and at 20 mA much smaller, but when cv excitation is used many more parameters come into the analysis. This cc excitation measurement technique gives a consistent measure of magnitude for the effect. The one outstanding parameter of importance is the relationship between the laser field within the cavity (beam irradiance) and the laser output power (this is shown in equation 7.27).

A measure of the magnitude for laser on/off perturbations $\sim$ 5 to 10% was obtained (see Figure 4.11) and for stabilization typical variations of laser power due to modulation (for generation of an error signal) would be $\lesssim$ 1%, therefore the electronic circuitry must detect a discharge voltage perturbation of $\lesssim$ 0.05 to 0.1%. Figure 4.12 shows an optogalvanic signal (detected by R-C coupling and cv excitation) due to PZT length (with associated amplitude) laser modulation. The length modulation has been set to $\sim$ 150 times the typical stabilization case and, therefore, the laser field perturbation is the maximum available from the signature ($\sim$ 25% amplitude modulation depth). The modulation frequency of 520 Hz lies between the 500 Hz (10th) and 550 Hz (11th) power supply harmonics. The signal amplitude is $\sim$ 10 dB above these harmonics and this demonstrates that during the stabilization a typical <u>maximum</u> error signal may be 35 dB below adjacent power supply harmonics. Some detailed discussion of the signal recovery

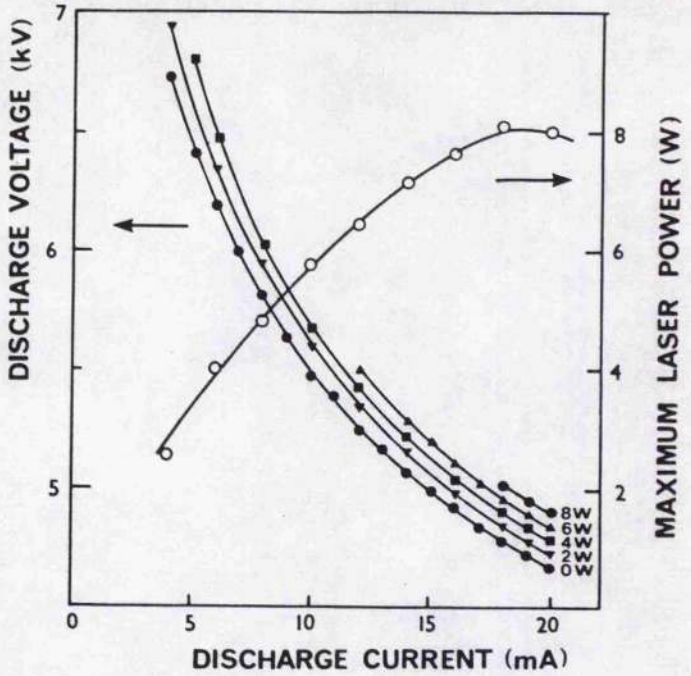

Fig. 4.11 Variation of laser discharge voltage with discharge current for laser output powers and variation of maximum laser output power with discharge current, for a compact CO_2 laser (33 cm discharge length, 25 cm active length) with a gas mixture 1 Xe, 3 CO_2, 4 N_2, 16 He (torr).

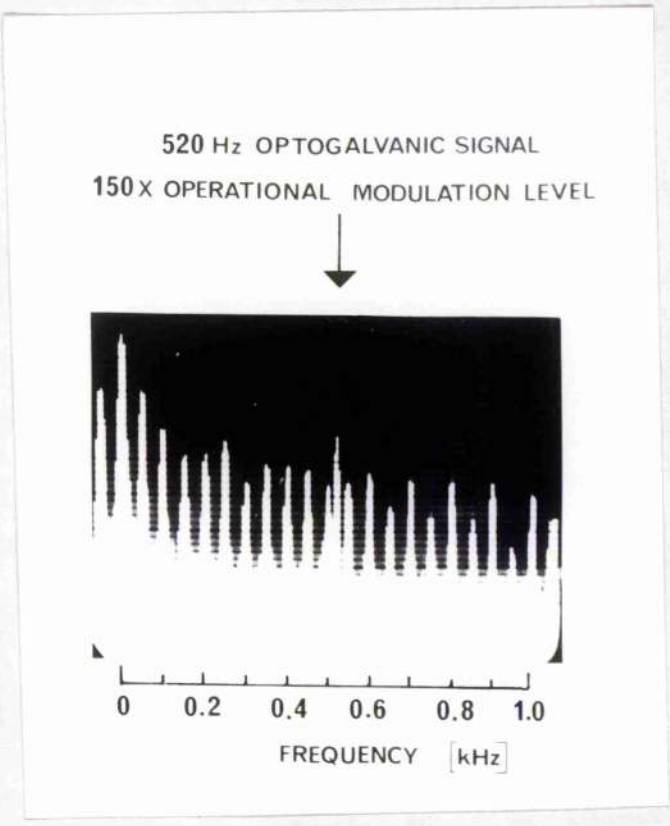

Fig. 4.12 Optogalvanic signal at 520 Hz detected by R-C coupling and with cv excitation. The PZT modulation is ~ 200 V which is typically 150 times the operating level for stabilization. This shows the dominance of the PSU mains harmonics in the noise spectrum; the vertical scale is relative 10 dB/ major division.

problem is given in 9.1.

The passively stable lasers used for these experiments (described in 3.11) were of simple construction, designed for efficiency and high output power per unit volume; as a result signature selection was used. The optogalvanic effect gives simple access to signatures[45,46] which are conventionally detected optically (see Figure 1.14). As the length of the laser cavity is adjusted with a slow ramp voltage the resonator selects a series of lines of greater or lesser gain which oscillate at various power levels. As the laser output power (and irradiance) vary an OGE signal can be obtained which due to the near linearity of the effect gives an electrical signal proportion to laser output which can be viewed on an oscilloscope directly; Figure 4.13 shows a tracing of an OGE signature taken by this method.

The OGE signature must be scanned slowly because the reception bandwidth (for small phase changes see Chapter 6.0) is limited to $\sim$ 800 Hz. Typical signatures (for $\sim$ 50 cm lasers) display an array of $\sim$ 8 lines per half wavelength interval or $\sim$ 16 maxima and minima (turning points). A suitable criterion for line resolution is the time $t_{\lambda/2}$ (second) for one half wavelength scan

$$t_{\lambda/2} > \frac{4n}{f} \quad \ldots\ldots\ldots\ldots\ldots\ldots \quad (4.1)$$

where n is the number of lines per half wavelength interval and f is the half power bandwidth of the OGE detection system. For the lasers under consideration

$$t_{\lambda/2} > 0.055 \text{ s} \quad \ldots\ldots\ldots\ldots\ldots\ldots \quad (4.2)$$

a criterion which was met with a 500 V scan of duration time 0.2 ms. OGE signatures can give an indication of the spatial mode pattern of the laser being monitored; this provides vital information for stabilization procedure (Chapter 1).

Figure 4.14 shows several optogalvanic signatures detected by series resistor R-C coupling with cv excitation. Photographs A and C show 'clean'

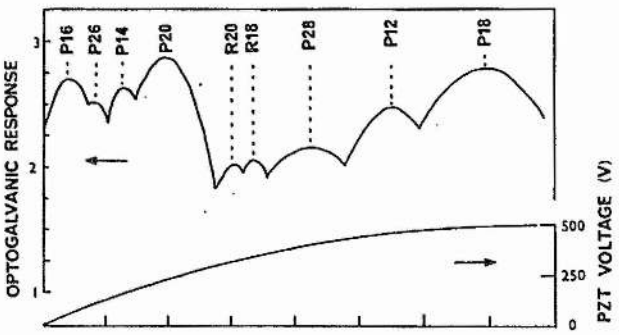

Fig. 4.13 A typical optogalvanic signature obtained with a 500 V ramp (4.4 μm length change) during 200 ms. The optogalvanic signal source was a 10 kΩ resistor in series with the discharge. All lines in this signature are $00^0 1 - 10^0 0$ band and were identified by an Optical Engineering spectrum analyzer; the peak laser output is 7 W.

(a) Single mode signature

(b) Multimode signature

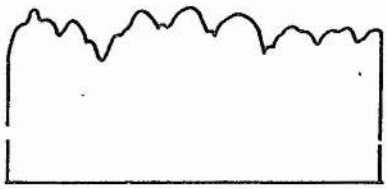

(c) Single mode signature

(d) Multimode signature

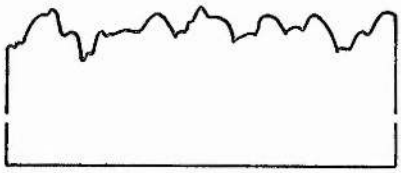

Fig. 4.14 Compact CO_2 laser (35 cm cavity) signatures with horizontal axis as distance ∿ 5 μm and vertical axis laser power (arbitrary units). Two single mode signatures are presented ((a) and (c)) and two multimode signatures ((b) and (d)). The single mode signatures have less turning points (n ∿ 20) and wider power fluctuations (∿ 30%) than the multimode (n ∿ 40 for two modes and power fluctuations ∿ 15%).

signatures with a shape that was reproducible over several hours, whereas photographs B and D show signatures with many more maxima and minima which deviate much less from the mean power level and change more quickly with time (seconds to minutes). By observing the laser beam profile with the scanning beam profile monitor these beams were found to be composed of at least two transverse modes; sometimes three or four modes could be identified by studying the far field pattern. Apart from the fundamental mode (TEM_{oon} in cylindrical co-ordinates) TEM_{o1n}, TEM_{1on} and TEM_{11n} modes were identified for lasers with insufficient spatial mode selection (see 3.11, 3.15 and 3.41). The number of maxima and minima increases because there are more possible $\lambda/2$ solutions for the resonator equation when several modes are present (see equation 1.6). The power level does not deviate as much because shorter excursions from a line centre start a new oscillation. Although this is a good qualitative method of assessing mode quality certain particular 'length' positions (all length changes induce some angular change) may bring about multimode operation which cannot be observed simply in the signature.

In order to determine the passband of the optogalvanic detection system experiments were performed initially up to a frequency of 2 kHz to establish the choice of optimum signal frequency; subsequently, experiments were performed with frequencies up to 100 kHz and these results are presented in Chapter 6. A compact laser was frequency modulated by applying a particular amplitude sine wave (determined by the PZT calibration, see section 3.14) in order to length modulate the cavity by 80 nm and the operating point on the signature chosen so that the OGE signal was maximum (maximum line profile slope). Figure 4.15 shows the OGE signal detected by a 10 kΩ series resistor obtained by sweeping the oscillation frequency over the range 10 Hz to 2 kHz. The small ($\sim$ 0.1%) discharge impedance change causes a current change in the cv excitation case (dependent on the gain profile) at low frequencies ($f < 100$ Hz) equal in value to the dc perturbation. As the period of the modulation frequency becomes comparable with the $00^0 1$ collisional relaxation time ($\sim$ 0.5 ms) the current fluctuation $\Delta i/i$ is attenuated as expected from

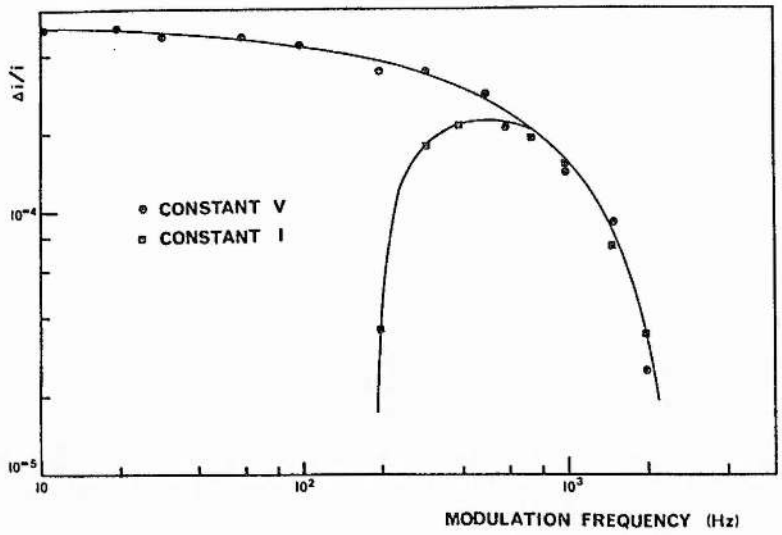

Fig. 4.15 Variation of optogalvanic signal ($\Delta i/i$), detected with a series 10 kΩ resistor, with a change of length modulation (fixed at 80 nm) frequency for a compact CO_2 laser. The cases of cc and cv excitation are distinguished; in the cc case the current fluctuations are attenuated, whereas OGE response increases with decreasing frequency (to the dc limit) for cv excitation (Irvin C23106 PSU).

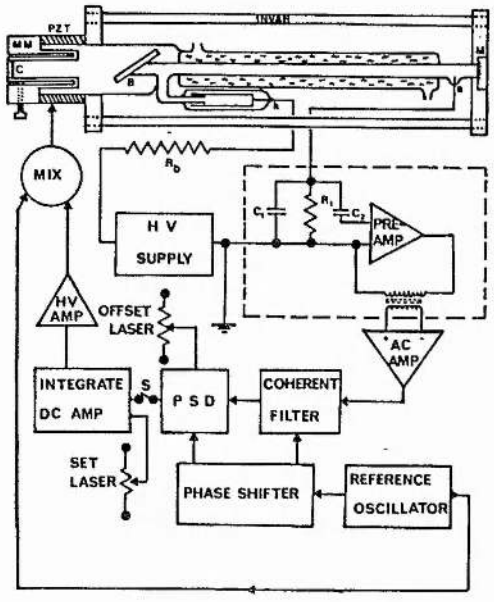

Fig. 4.21 Schematic diagram of an optogalvanic stabilized CO_2 laser where the OGE signal is RC coupled via R_1 and C_2. Facilities for offset locking and manual setting of the operating point were included. The integrator was a two stage circuit with adjustable time constants ∿ 1 s.

the gas temperature explanation.[53]

In the constant current case no variation of current occurs within the supply regulation bandwidth. Consequently, no OGE signal is observed at low frequencies, but a signal is detected at frequencies greater than the current regulator can compensate; for the Irvin C1096 supply the 50% regulation point was measured as 240 Hz; for the EI 183 supply it was 130 Hz. This result was achieved by using a variable speed chopper which switches the radiation field (10 μm) on to off and by measuring the voltage perturbation detected across the discharge (corrected due to the known OGE roll-off).

To summarize, a constant voltage rather than a current regulated supply permits current fluctuations whereas a cc supply suppresses these fluctuations within a fixed regulation bandwidth. Because it is usually advantageous to use a cc supply in stabilized laser systems to eliminate long term current drift, the OGE reference frequency (modulation) must lie outside the regulation band (typically ∿ 200 Hz) and, therefore, reference frequencies in the band 400 to 780 Hz were chosen so that power supply harmonics were avoided. (Alternatively, some restriction of the regulation bandwidth by altering the supply feedback loop time constant may be used with the proviso that a suitable minimum, 10 Hz is chosen so that the majority of current drifts are eliminated).

4.2 COMPACT SYSTEM PERFORMANCE

The schematic diagram of the OGE servomechanism used to stabilize the compact CO_2 lasers is shown in Figure 4.21. The feedback loop utilizes a series resistor (R_1) in the supply earth line as a signal detector. Either a tuned preamplifier or a broadband amplifier (100 Hz to 10 kHz) was included in the electrically screened laser head; transformer coupling to external circuitry ensured safety and reduced earth loop problems. The combination of R_1 and C_1 provided a low pass filter response to reduce power supply transients (∿ 1 kHz roll-off) and the coupling capacitor (dc blocking) C_2, was chosen for a low frequency roll-off ∿ 10 Hz.

The preamplified OGE signal was amplified by a switched gain wideband ac amplifier (situated in the external electronics) so that the input of the coherent filter/PSD was presented with a signal + noise voltage near saturation (8 V peak to peak). The PSD was locked by the reference oscillator and a variable quantity (of reference signal) was fed to the PZT (to dither the cavity length) by mixing either with the error signal or with the amplified error signal (as shown) by a capacitive mixer. The PSD was also fed with an attenuated signal at the reference frequency in order to offset the operating point from line centre. The error voltage derived from the PSD was fed to the integration and dc amplification circuitry (see 3.23) with a dc bias voltage (set laser) used to manually tune the laser initially to the required stabilization frequency. For offset locking the ac offset voltage (reference frequency) was added to reduce the integrator input to zero. Double integration was used with a limiting time constant of $\sim$ 1 s. The dc amplified (switched gain) error signal was fed to a stable high voltage amplifier with sufficient drive capability to drive the PZT from 0 to 1 kV in 1 to 2 seconds.

Measurement of the laser passive stability was required initially in order to

1. Optimize passive stability
2. Find operational criteria for feedback system
3. Find baseline values of instability and determine the improvement brought by stabilization.

Firstly, considerable understanding of factors contributing to instability was obtained by long term output power monitoring. Figure 4.22 shows the laser output powers over the first four hours of operation after the discharge was switched on. The worst case (A) was for a cavity with aluminium as the length defining material otherwise similar to the compact lasers constructed largely of invar (B) intended for stabilization. The invar cavities had a smaller amplitude power drift initially ($\sim$ 50%) and after $\sim$ 1½ hours greatly reduced power fluctuations; the number of output

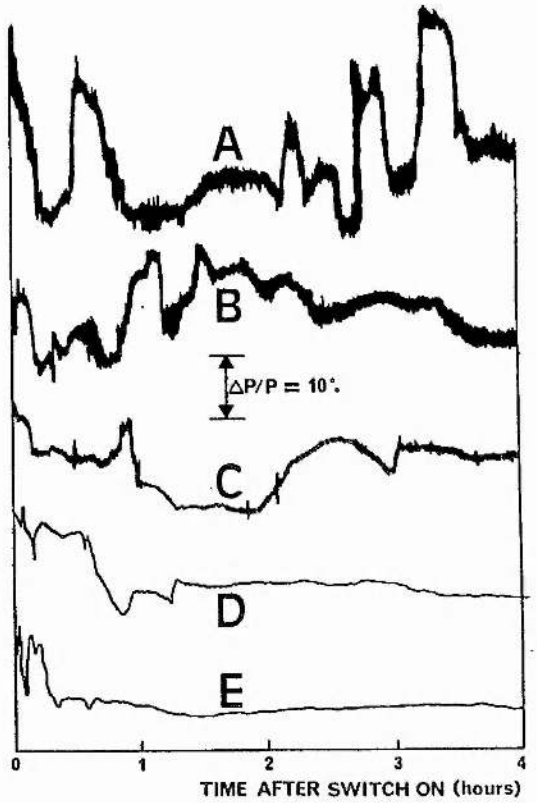

Fig. 4.22 Single mode laser power fluctuations (no active stabilization) for a compact CO_2 laser operating at 7 W for 4 hours after electrical switch on, for tap water cooling. Trace A: aluminium cavity construction, on wooden bench with no cover; B: invar cavity with part of optical axis open to draughts; C: as B but with laser cover fitted; D: as C but with close fitted draught shield; E as D but with laser mounted on Ealing antivibration table.

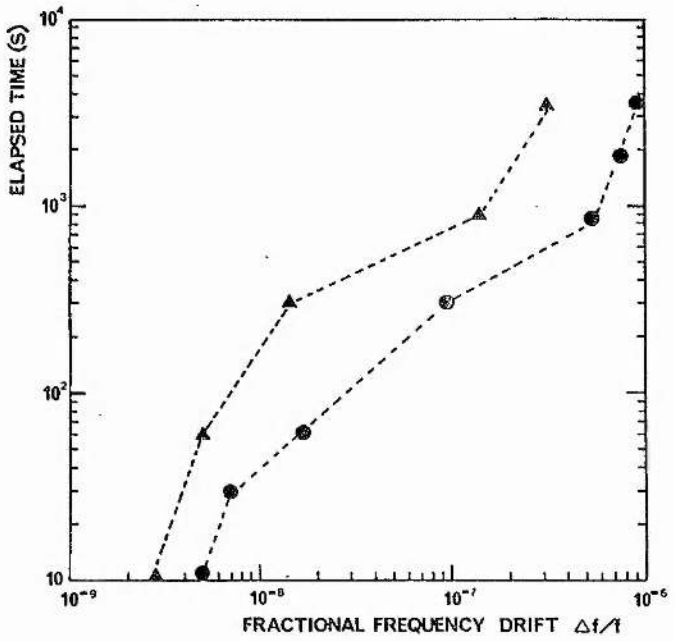

Fig. 4.23 Single mode 10P(20) fractional frequency drift (unstabilized) of a compact (40 cm cavity) CO_2 laser (●) and longer (120 cm cavity) laser (▲) designed for sequence band operation, after 30 minutes warm-up period and set initially to line centre.

power sign changes was always noticeably less. The third case (C) shows how some shielding from draughts (with the associated refractive index turbulence) by the complete enclosure of the laser head reduces the high frequency ($\lesssim$ 1 s) fluctuations by a factor of 4. By using a closely fitting (50 mm diameter tube) draught shield so that no part of the optical path is open to draughts (D) the high frequency amplitude noise is eliminated within the resolution of the power meter ($\sim$ 0.01 W in 7 W). Some serious long term fluctuations occur in the first 1½ hours but after this period an overall stability of $\sim$ 5% was measured (single line operation) for up to ten hours. When the laser head was mounted on the Ealing antivibration table (rather than a wooden bench) similar performance was observed with less discontinuous power shifts. The largest component of variation in power can be seen to occur in the first 20 minutes and after 1 hour 'warm up' complete immunity (for a working day) from rapid change occurs. The best passive amplitude stability is $\sim$ 4%. The 'warm up' phenomenon has been observed by other researchers[131] and it is postulated here that it is due to heating of the optical components (mirrors, Brewster windows and the tube) by the beam. A small amount of power $\sim$ 2% (about 2 W in these lasers) is dissipated in the optics and the time required for the output coupler to reach 99% of the asymptotic temperature due to this heat input would be $\sim$ 10 minutes. As the optical elements expand a first order frequency change occurs which is not cavity dependent and this could be the initial power decay (due to detuning) seen in all the traces in 4.22 (approximately 20 minutes); in all cases the cavity was set to optimize the output power at 10P(20) line centre. In cases (D) and (E) some structure is resolved within this period but it is masked by draught noise in (A), (B) and (C). There is a feedback effect due to this heating; the experience causes LF detuning which reduces the laser power, consequently the heat input to the optics is lowered which reduces the rate of temperature rise. This slowing down of the cavity detuning rate causes the final equilibrium to be reached very slowly. This is the probable explanation of the output

behaviour after 20 minutes and up to 1 hour which has increased power fluctuations compared with the ultimate performance.

The frequency drifts of the lasers after switch on was measured by the heterodyne technique and Figure 4.23 shows fractional frequency drift during the first hour. By comparison with a line centre stabilized laser, the freerunning laser was switched on electrically, set to line centre (zero beat frequency) and then left to drift. The experiment was performed many times and these results show some typical frequency excursions. Two cases are shown for similar lasers, a compact CO_2 laser (cavity length 35 cm) and the sequence band laser (cavity length $\sim$ 110 cm). Initially (1 minute) the drift rate is slow; it subsequently increases and ultimately reduces (after 20 minutes) in agreement with the hypotheses due to the amplitude measurements. The initial slow drift suggests that when the laser is constrained near line centre (< 0.5 MHz) the drift rate is small but between 1 MHz and $\sim$ 10 MHz off line centre the drift rate is large and then reduces again (possibly due to equilibrium temperature being achieved in the optics). This low drift rate is observed for the subsequent period $\sim$ 5 MHz/hour. This value has been observed over long runs of several hundred hours to be an upper limit for drift. The compact laser drifts $\lesssim$ 25 MHz or one half line signature segment in the first hour, whereas the longer cavity drifts $\sim$ 6 MHz which is again about one half line signature segment. A similar resonator length change ΔL is required in both cases; where L_1 = 35 cm and L_2 = 110 cm

$$\Delta L_1 = \Delta L_2 = \frac{L_1 \Delta f_1}{f_o} = \frac{L_2 \Delta f_2}{f_o} \simeq -0.3\ \mu m \quad \ldots (4.3)$$

where f_o is the laser frequency and Δf_1 and Δf_2 are the drift ranges for the two cavities. The sign of this initial frequency change was found empirically to be a decrease, therefore, the cavity is shortened by $\sim$ 0.3 μm in the first hour. Assuming that only the output coupler surface was expanding from the mounting plane (in these particular lasers the total reflector is mounted with the reflecting surface in the zero expansion plane) $\sim 3^{o}$ K temperature

increase of these components would be sufficient to cause a length shortening 0.3 μm. Calculation of the temperature rise of the components other than the coupler (e.g. laser tube) due to the laser beam heating is non-trivial because of the combination of several conduction losses, but a simple calculation of linear conduction shows that beam heating of the output coupler is a sufficient mechanism for this initial 'warm up' drift (thermalization).

The short term drift (1 μs to 1 ms period) was investigated by the heterodyne technique and Figure 4.24(a) shows the difference frequency signal of the two compact CO_2 lasers. This timescale is equal or shorter than the diffusion time of particles to the tube walls and the collisional relaxation time of the upper laser level and this definition of short term is used in this work. Over 20 measurements with observation times in the range 500 μs to 1 ms showed a mean peak frequency excursion of 10.5 ± 1.8 kHz/ms.

A useful (and simple) definition of laser stability[132,133] is just the inverse of the fractional frequency drift with a fixed time period

$$S_f(t) = f_L/\Delta f_L(t) \quad \ldots\ldots\ldots\ldots\ldots\ldots (4.4)$$

where f_L is the averaged laser frequency over time t and Δf_L is a measure of the frequency fluctuation over the observation period t. The wavelength stability S_λ is equivalent due to the fundamental relationship

$$\lambda/\Delta\lambda = - f/\Delta f \quad \ldots\ldots\ldots\ldots\ldots\ldots (4.5)$$

but operationally frequency stability was measured by electronic heterodyne techniques and is used here exclusively. According to this definition the short term stability of these oscillators S_L is found to be

$$S_L(0.5 \text{ ms}) \geq 2.7\ (\pm 0.5) \times 10^9 \quad \ldots\ldots\ldots (4.6)$$

The major assumption (discussed in 3.42) is the independence of the oscillators; the use of diffuse reflectors has made optical coupling problems insignificant, however, some sympathetic drifts may still occur due to the

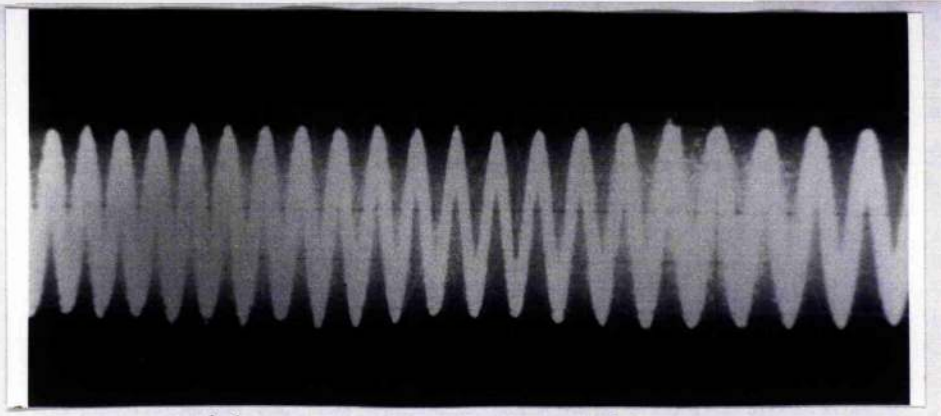

(a) | 100 μs |

Fig. 4.24 The difference frequency Δf of two compact lasers as displayed on a storage oscilloscope and detected by a Plessey LBC LTT photovoltaic detector. In photograph (a) the difference frequency changes from $\sim$ 16 kHz (LHS) to $\sim$ 25 kHz (RHS) over this period. Trace (b) shows that for times $\sim$ 5 μs the difference frequency change is $<<$ 1 MHz. Trace (c) shows Δf one laser stabilized where f_{mod} = 720 Hz and the modulation phase varies from $\pi/4$ to $3\pi/4$.

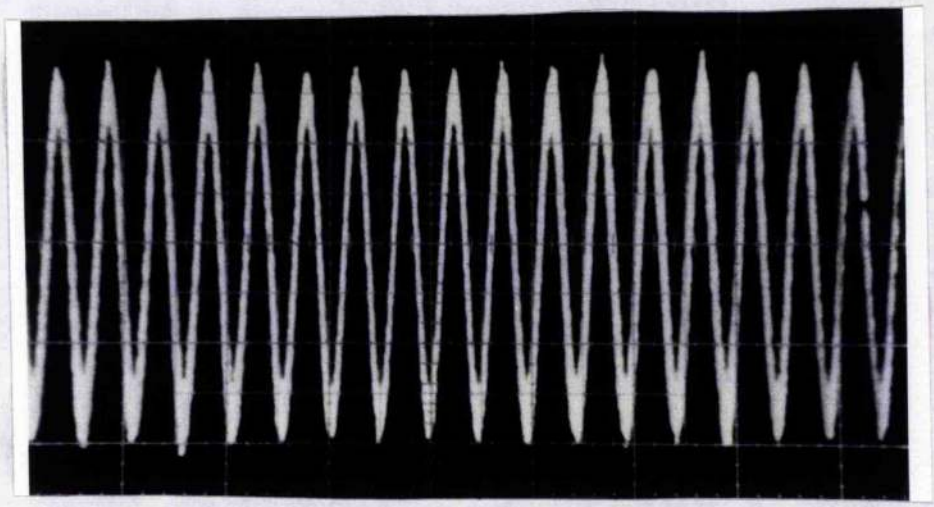

(b) | 20 μs |

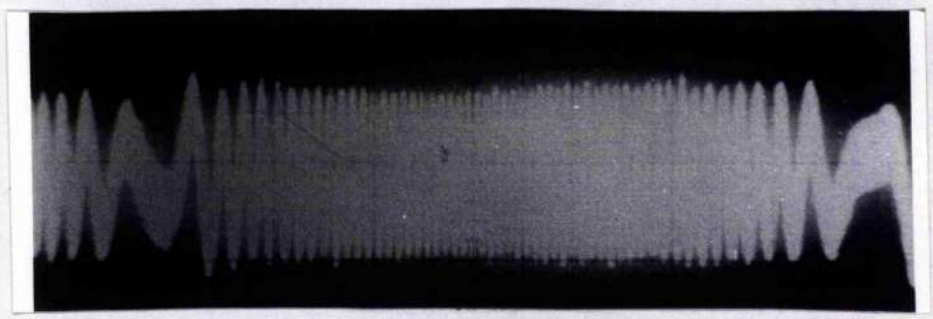

(c) | 100 μs |

shared environment.[128] The fact that two oscillators are being compared suggests a reducing factor (÷ 2) in the stability calculation; this has not been used in this work and the '$\lesssim$' inequality will be used to denote that the drift of each oscillator is probably less than the figure quoted or the stability greater ($\gtrsim$).

Figure 4.24(b) shows a shorter time difference frequency signal from a similar experiment. The conclusion of such an experiment is not particularly useful because several cycles of beat are needed for measurement which requires the beat frequency $\sim$ 5 MHz and from this photograph S (20 μs) $>>$ 10^7. A microwave or fast switching frequency counter is required to make accurate measurements of this parameter.

The medium term stability, 5 s to 1 minute, was investigated by the heterodyne technique by studying the drift of two unstabilized lasers over this period (after thermalization). Figure 4.25 shows mode jitter width 1.3 ± 0.17 MHz (for 20 measurements) over 5 seconds, drifts of $\lesssim$ 1 MHz in 30 and 60 seconds. Both lasers were operating < 10 MHz from line centre.

The two major instability influences noticed were draught effects (intentional draught caused a $\sim$ 5 kHz in 1 ms excursion) and power supply induced frequency jitter. This effect is an important source of instability[134] (see Figure 4.22) which will be treated further in this chapter. By minimizing the PSU $\Delta i/i$ and carefully draught shielding peak excursions widths of 5.1 ± 2.0 kHz corresponding to S (1 ms) $\gtrsim$ 5.5 (± 2) x 10^9 were measured; the residual value of frequency changes was largely due to the power supply ripple induced frequency jitter which can be reduced by improved PSU filtering.

By applying a small dither (2 V) to one laser and stabilizing it at line centre and heterodying this laser with another freerunning oscillator (at line centre) a storage oscillograph shown in Figure 4.24(c) was observed where the dithered oscillator is frequency swept from the relative frequency values of 0 to $\sim$ 300 kHz in 0.3 ms and for the modulation frequency of 720 Hz (approximately sine wave) this represents $\sim$ 1/4 cycle ($\sim \pi/2$) passing through a maximum frequency excursion point (from $\sin \phi = \pi/4$ to

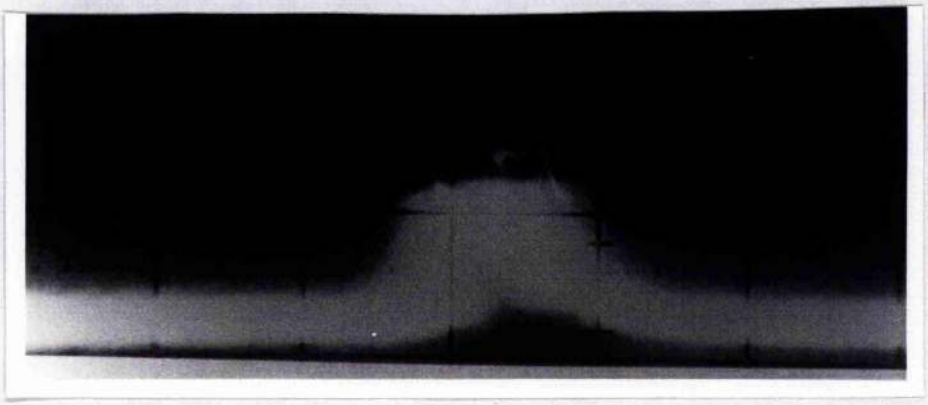

Fig. 4.25 (a) Laser heterodyne signals received with the Plessey LTT detector. The centre graticule displays a 5 MHz difference frequency, the horizontal scale is 1 MHz/division with 300 kHz resolution. For a 5 s exposure the mode jitter width was 1.3 ± 0.17 MHz.

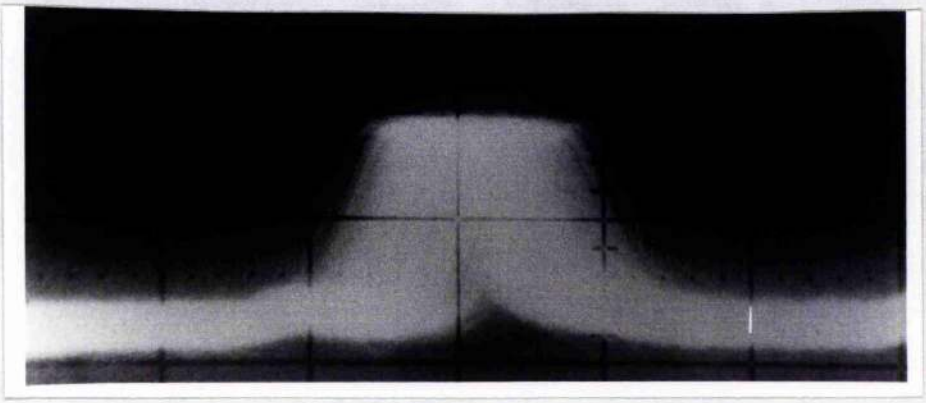

(b) As (a) after 30 seconds.

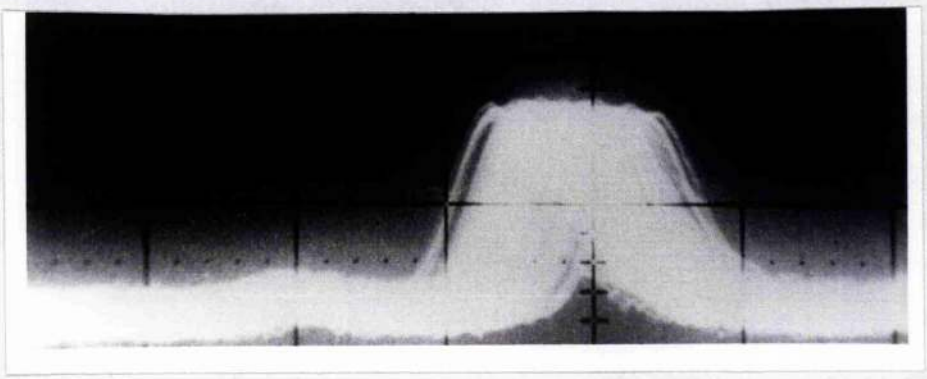

(c) As (a) after 60 seconds.

$3\pi/4$). The total modulation induced frequency deviation is $2\sqrt{2}$ x 300 kHz = 850 kHz peak to peak or 300 kHz rms.

This factor (modulation deviation) is an important parameter in the feedback loop gain; it is the PZT reference modulation which determines the amplitude of the error signal for a given laser optogalvanic transfer function (dependent on gain profile slope, laser total gain, mixture of gases, etc.). It was found (see 3.13) that the PZT tubes were polarity independent and linear over a wide extension range and that stacks were linear to a good degree although the polarity equivalence (+ or - drive either extension or contraction) is not so well understood. Figure 4.26 shows the difference spectrum for the two compact lasers (fitted with Lansing stack PZT's) where one was modulated with 3 V and 16 V peak to peak compared with no applied modulation. The full width Δf of the heterodyne spectrum gave the peak to peak frequency deviation used to calibrate the PZT's over a wide frequency range. A spectrum analyzer effectively scans a tuned receiver at a known rate for a chosen time and reception bandwidth (i.f.). When a single slow linear scan records an ac dithered difference frequency ($\sim$ 10 MHz) (see 4.26(c)) many coincidences of signal frequency and reception frequency occur. In this case the i.f. frequency was 100 kHz and because the ac dither is sufficiently fast the spectrum analyzer 'sees' a number of signals separated in frequency space. The number of channels with non zero (above noise) voltage values represents the number of coincidences. The channels are discrete because the Marconi TF2370 is a digital device (from the display point of view). The number of non zero channels found in one sweep (time fixed t_s) is equal in 4.26(b) and (c) but is not countable in (b) due to the 100 kHz resolution set by the i.f. But the coincidences are resolved in 4.26(c) where n = 28 during 3/10 of the scan time equivalent to 94 in t_s seconds. This count is simply related to the laser modulation frequency f_{mod} by the following relation

$$f_{mod} = \frac{3.33n}{2t_s} \simeq 500 \text{ Hz} \quad \ldots\ldots\ldots\ldots\ldots (4.7)$$

(a)

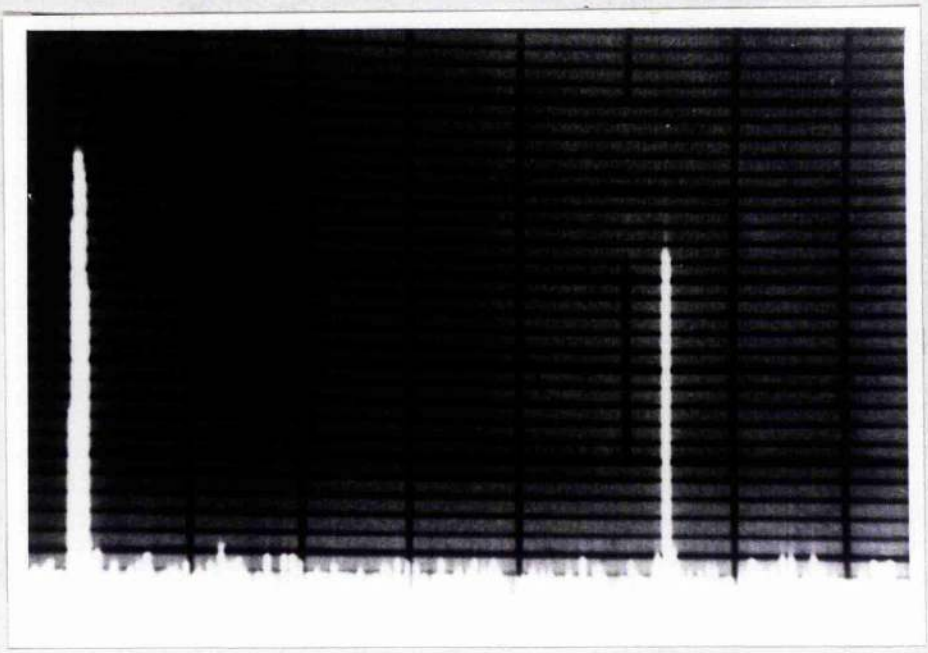

Fig. 4.26 The effect of PZT modulation on the spectral output of a compact CO_2 laser. The heterodyne signal of two similar lasers is shown and the zero frequency marker is visible at the left. Frequency (horizontal) scale is 2 MHz/major division. The vertical scale is linear and relative. The spectrum analyzer (Marconi TF2370) scan time is ∿ 50 ms, and a Plessey LBC detector was used with a diffuse reflector. Photograph (a) shows the heterodyne signal with neither laser modulated and photograph (b) shows the signal with one laser modulated by ∿ 3 V at 520 Hz. Photograph (c) (overleaf) shows the spectrum where one laser is modulated at ∿ 16 V at 520 Hz.

(b)

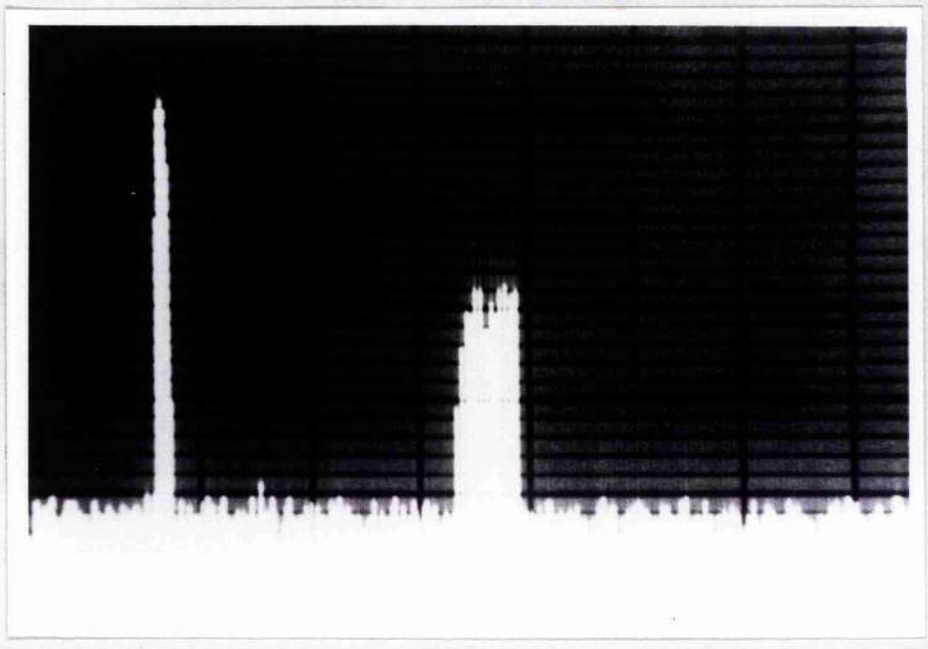

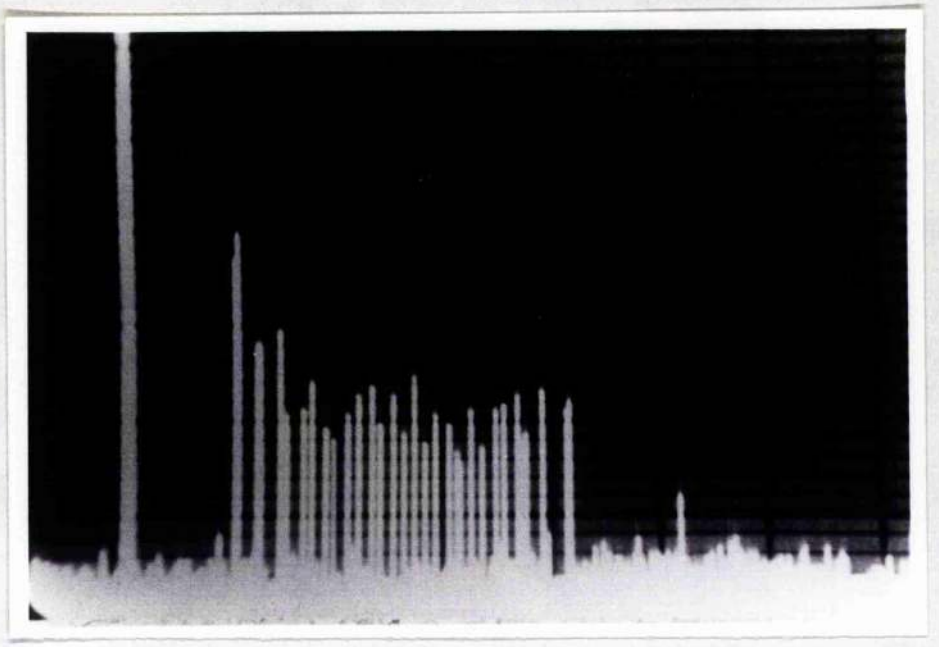

Fig. 4.26 (c)

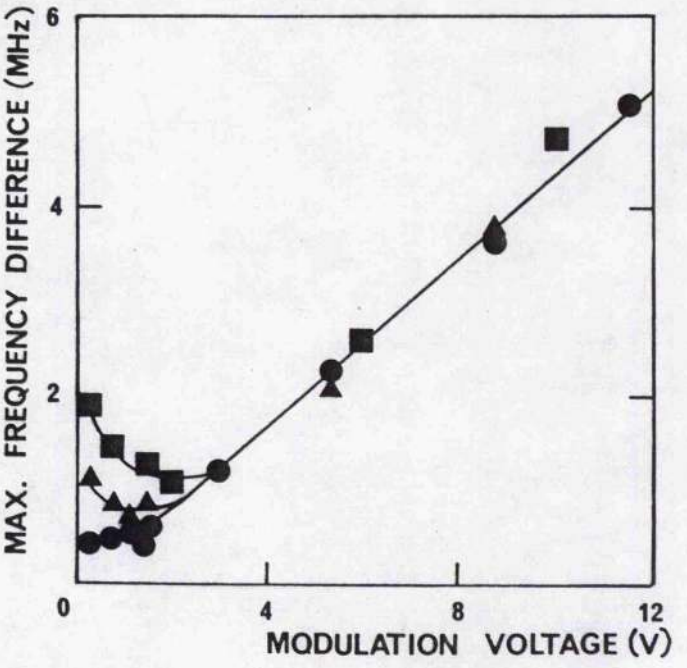

Fig. 4.27 The peak difference frequency of two compact lasers shown as a function of modulation voltage. Above 4 V, the modulation broadened regime occurs where the induced frequency modulation was greater than the 1 s drift. For 1 s (●) observation time (∿ servosystem integration time constant) the minimum frequency difference of 400 kHz was overcome by modulation at ∿ 2 V. For a 30 s observation time (▲) the stabilization gave an improvement over passive performance with a modulation of 1.5 - 2.5 V. For a 3 min. observation time (■) a frequency difference ∿ 1 MHz was found when the optimum modulation was applied. Both lasers were stabilized by OGE to 10P(20) line centre.

for the scan time t_s = 0.1 s. The actual modulation frequency was 520 Hz.

Both lasers were stabilized, initially with a large PZT modulation voltage, to 10P(20) line centre and the ac gain optimized to saturate the PSD input (no tuned preamplifier) and the dc gain optimized for a 'tight' lock without 'hunting' instability. The integrator time constant was set to 1 s and the PZT modulation successively reduced for both lasers (independently) and the resulting maximum frequency difference (Δf) changes measured. Figure 4.27 shows the experimental results for three observation times (averaged on the spectrum analyzer). For modulation above 4 V peak to peak the Δf value increases linearly with voltage, reflecting the linearity of the PZT stacks. This modulation broadened regime occurs when sufficient error signal is detected for the servo to lock. The coincidence of the longer observation times (30 s, 3 minutes) with 1 second time is due to the stabilizing effect of the servomechanism; i.e. above 4 V modulation the 1 second stability is preserved up to 3 minutes (with no degradation). This correspondence was seen over many hours. The lock may be lost when the cavity has drifted so far that the high voltage amplifier has reached a limit (0 V or 1 kV). The divergence for longer observation times shows that below $\sim$ 2.5 V modulation, servo instability and ordinary drift occur and this gives frequency jitter up to $\sim$ 1 MHz in 3 minutes. The zero volt modulation case shows the unstabilized passive performance discussed previously and from these measurements the minimum required modulation is 1.5 V. Because the integrator has a 1 s time constant no improvement of stability for 1 s observation can be expected by active stabilization, but over 3 minutes by choosing $\sim$ 3 V modulation an improvement from 2 MHz drift to 1 MHz (of known FM) modulation width occurs. The actual drift of this broadened spectrum was found to be much less than the envelope width for 2 V modulation and approximately equal for 0.5 to 1 V. For application of these lasers it must be remembered that the modulation broadening does indeed degrade the spectral width of the laser output but that this FM component is determined and predictable and can sometimes be removed or

ignored.

Figure 4.28 demonstrates typical long term stability of the OGE stabilized laser. After half an hour of thermalization the servo was locked for both lasers at 10P(20) line centre and photograph (a) taken of the heterodyne spectrum; after 1 hour photograph (b) was taken and the maximum difference frequency changed by $\lesssim$ 200 kHz corresponding to a long term stability S (1 hour) $\geq$ 1.6 ($\pm$ 0.5) x 10^8. The modulation broadened spectrum was $\lesssim$ 1.7 MHz full width.

The frequency resettability is an important parameter for stable sources; it is closely related to frequency stability. The frequency resettability (R_f) is defined[133] as a quality factor describing the precision of reset after perturbation

$$R_f = \frac{f_o}{\Delta f_n} \qquad \ldots\ldots\ldots\ldots\ldots\ldots \quad (4.8)$$

where f_o is the desired set frequency and Δf_n is the standard deviation of n trials of reset to f_o. Accordingly, in this system either one or both lasers can be interrupted and if the initial difference frequency (of the two lasers) $f_o = 0$ then the <u>mean</u> difference frequency will return for n trials to $f_1, f_2, \ldots, f_n$ after n reset trials. Because of the modulation broadening of the difference frequency (half width f_{mod}), the variance frequency error (Δf_n^2) is

$$\Delta f_n^2 = \frac{\sum_{S=1}^{n} \ell_S (f_S - \bar{f} - f_{mod})^2}{\sum_{S=1}^{n} \ell_S} \qquad \ldots\ldots\ldots\ldots \quad (4.9)$$

(and the standard deviation is the square root) of the variance ℓ_S is the frequency (<u>statistically</u>) of the frequency difference f_S observations and $\bar{f}$ is the mean difference (or fixed offset). The resettability is given by

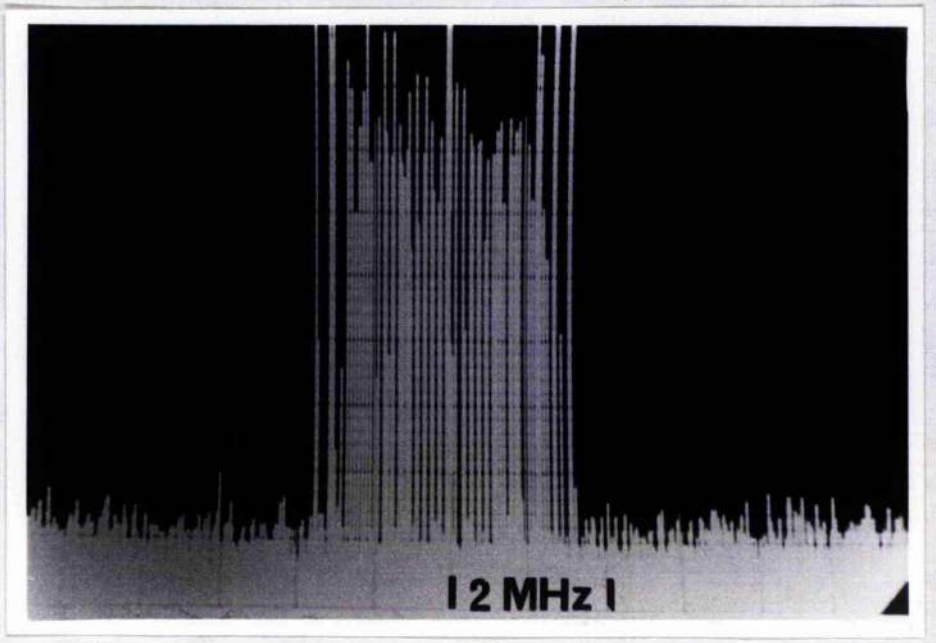

(a) After 1½ hours warm up stabilizer switched on.

Fig. 4.28 Heterodyne signal from the two OGE stabilized (10P(20) line centre) compact CO_2 lasers. The centre line shows zero frequency. The modulation was 3 V at frequencies of 520 Hz and 720 Hz. The heterodyne signal was detected with the LBC LTT detector and Marconi TF 2370 spectrum analyzer. The vertical scale is linear ∿ 1 V from detector amplifier and the time for the single frequency scan was 0.1 s. The frequency resolution was 50 kHz.

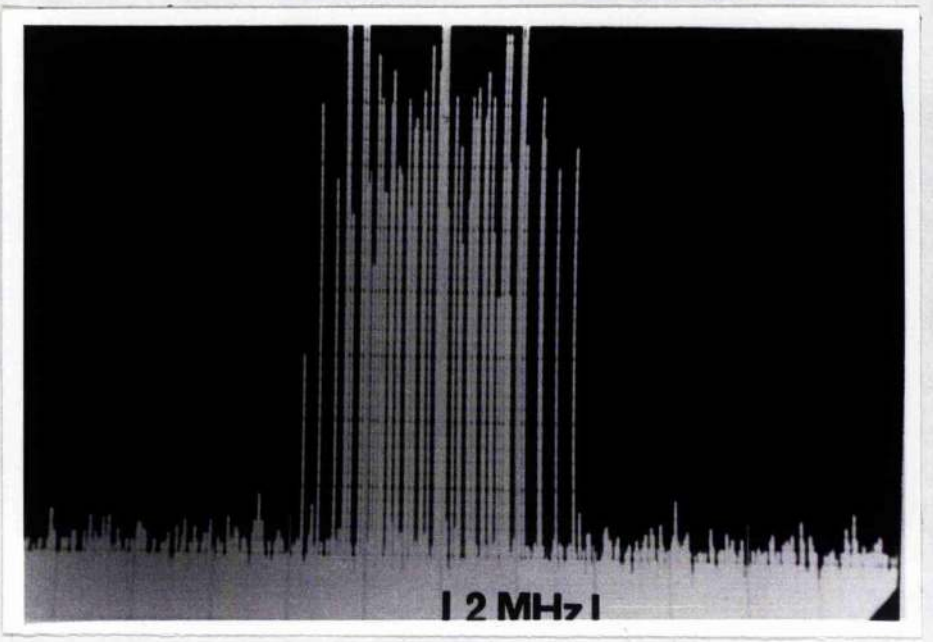

(b) One hour after (a).

$$R_f = \sqrt{\frac{\sum_{S=1}^{n} \ell_S}{\sum_{S=1}^{n} \ell_S (f_S - \bar{f} - f_{mod})^2}} \; f_o \qquad \ldots\ldots\ldots\ldots \quad (4.10)$$

In practice, the resolution of spectrum analyzer is sometimes a limiting factor in the calculation of resettability.

One resettability trial of the locked lasers is demonstrated in Figure 4.29 where the system performance limit was achieved and the lasers 10P(20) line centre stabilized with $\sim$ 400 kHz modulation. In the upper spectrum the frequency difference spectrum was constrained to 400 kHz during 1 s averaged spectrum analysis. The feedback loop was subsequently broken for both lasers. Over the succeeding 5 minutes the difference frequency spectrum drifted to mean value $\sim$ 4 MHz and when the feedback loop was closed the lasers were driven back to line centre (by the servomechanism) and the difference frequency spectrum returned to near zero as shown in the lower photograph. The difference spectra differ by < 100 kHz and this is a simple measure of the resettability of the stabilized lasers.

After careful optimization (with draught shields fitted and after thermalization) resettabilities were measured for the compact lasers for differing values of dc gain (Figure 4.210). Most values of gain are consistent with a good resettability but very low gain (loose lock) results in slow hunting and high gain in oscillation which is reflected in an imprecision of locked frequency during reset. All values must be treated for two systems as previously.

Analyses of long term output power fluctuations show between 0.2 and 1% maximum deviation of which the largest component is periodic ($\sim$ 40 min) and has been identified as the thermocirculator thermostat cycle. As the discharge wall temperature cycles through $\pm$ 1.5 K the laser gain was modulated, resulting in output power fluctuations which do not give first order frequency changes (hence the feedback loop cannot compensate for

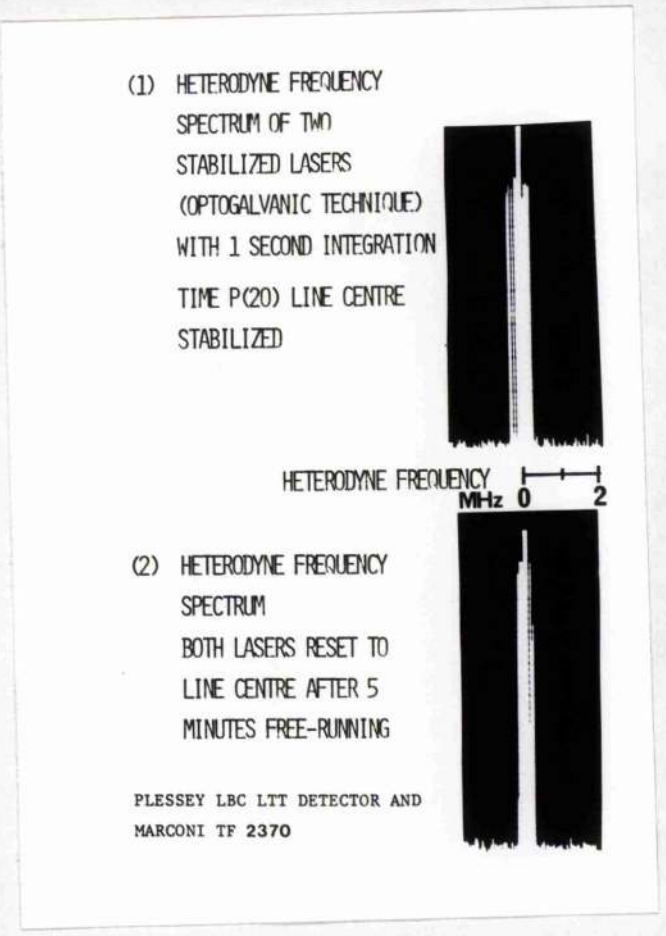

Fig. 4.29 A resetability test of the compact CO_2 lasers.

Gain (dB)	R_f
10	3.5×10^6
20	5.5×10^7
30	1.8×10^8
40	1.9×10^9
50	3.5×10^8
60	1.9×10^7
70	3.1×10^6

Fig. 4.210 Table showing resetability (R_f) of the compact CO_2 stabilized lasers as a function of dc amplifier gain when operating 10P(20) line centre at an output power $\sim$ 7 W.

them). Figure 4.211 shows the comparative output stability (A) (passive and active) for a medium gain laser line 10P(14) and (B) the long term stability (10 hours) of 10P(20) with a compact laser stabilized by OGE. The periodic coolant cycle can be clearly seen and could be removed by using tap water cooling. Tap water cooling unfortunately introduces discontinuous power changes during long operation as the temperature changes at specific times during the working day (possibly due to central heating cycles). Figure 4.212 shows two weeks of operation and the discontinuous changes (not seen with thermocirculator) are clearly shown.

The system performance limitations can be summarized as follows

1. Power supply current ripple and the resulting frequency (and amplitude) jitter is the major stabilization channel noise.
2. Wall cooling presents a problem (amplitude fluctuations) and ultimately coolant bubbling can produce broadening of the output spectrum.
3. The broad nature of the frequency discriminant feature (pressure broadened) of the CO_2 line determines the error signal.
4. The intentional modulation broadening of laser output can reduce absolute stability.

The possibility of using a sharper OGE discriminant feature (standing wave saturation resonance)[65] was investigated and will be described in Chapter 9; the avoidance of modulation broadening requires the frequency modulation of the reference rather than the laser oscillator[64]. The use of a stark shifted gas absorption[135] to modulate a small fraction of the laser has been used but only optical detection has been utilized so far to generate the error signal. It may be possible to use an external (to the laser) low pressure OGE cell with a sharper discriminant as described in 8.1 as long as discharge noise problems are overcome.

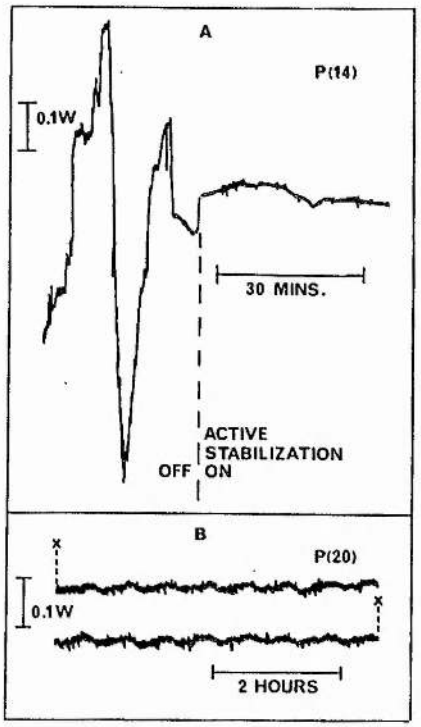

Fig. 4.211 (A) Comparison of 10P(14) OGE stabilized output power (compact laser) with freerunning passive stability with a mean power of 6.6 W. (B) Long term power stability of 10P(20) with laser OGE stabilized for ten hours continuous operation at a mean power of 7.7 W.

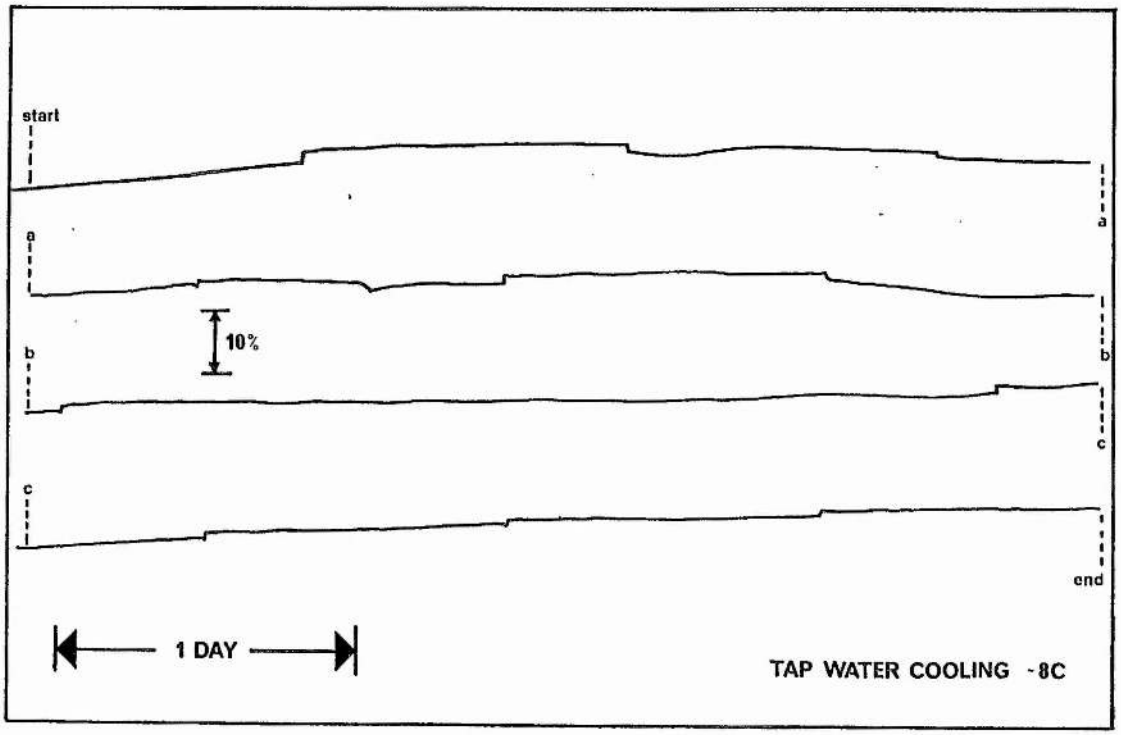

Fig. 4.212 Output power of a compact laser with slow flowing tap water cooling (unstabilized) over a period of 2 weeks, showing discontinuous power changes once or twice a day.

A modulation broadened limit $\sim$ 400 kHz to 1 MHz has been set so far by the above restrictions of the broad discriminant and consequent modulation. The power supply and cooling noise are systematic and their investigation by monitoring of the heterodyne signal in real time provided simple investigation of these phenomena.

The laser mode jitter on the 10 ms to 1 s (transitional) time scale is controlled mostly by environment (acoustic, vibrational, thermal, draughts, electric and magnetic fields), power supply ripple, coolant bubbling and thermocirculator pump vibration. The environmental factor is minimized by the construction and situation of the laser head. However, in these experiments the power supply and coolant contributed noticeably to the laser mode frequency jitter.

Figure 4.213 shows the difference frequency spectrum of two lasers (unstabilized) taken with a 2 second exposure. A 420 kHz full width was measured with a thermocirculator (manufactured by Churchill) compared to $\sim$ 120 kHz when cooled with slow flowing tap water. This residual $\lesssim$ 120 kHz mode jitter width is due largely to the Edinburgh Instruments 183 power supplies used which have a peak to peak current ripple of 50 μA (0.1% rms Figure 3.212).

Excitation changes caused varying heating of the laser gas which perturbs the pressure and refractive index (and electron density). This effect was measured (Figure 4.214) by tuning the laser frequency by adjusting current and measuring the heterodyne frequency difference (compared to a stabilized laser). The current (and pressure) dependent mode frequency shifts were investigated carefully and found not to be dependent on mode frequency within the gain profile, as shown previously by Mocker.[136] The actual value of current and pressure tuning varied between 500 kHz/mA and 3 MHz/mA and between 2 MHz and 8 MHz/torr depending on composition and gas pressure.[137] For the compact lasers with a typical 26 torr filling, a current tuning factor $\partial f/\partial i$ of 2.8 MHz/mA was measured at 10 mA which results in a ripple induced frequency jitter Δf

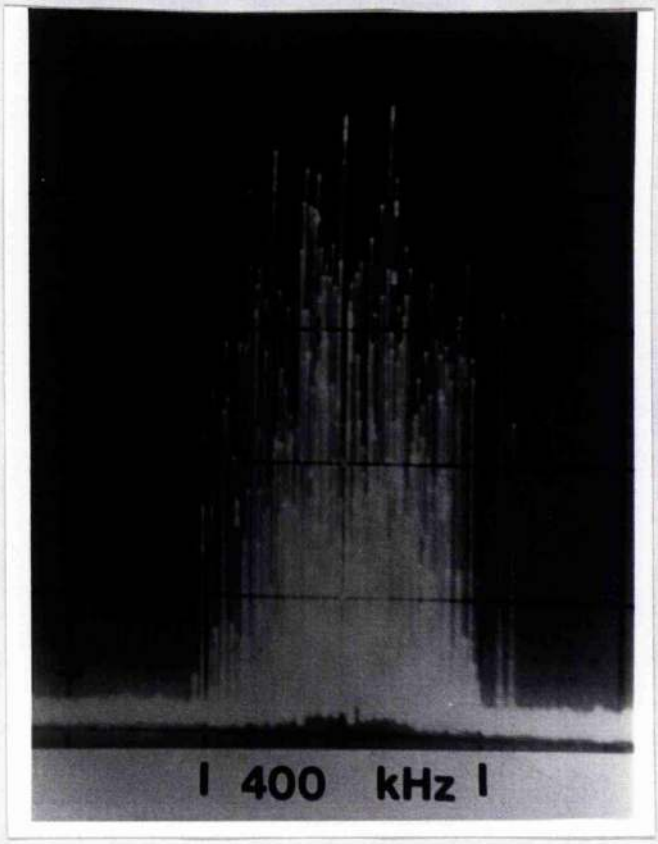

Fig. 4.213 (a) Difference frequency spectrum (unstabilized 10P(20) transition) with one laser offset 10 MHz. The horizontal scale is 200 kHz/division and 10 kHz resolution and 2 s exposure. Laser (1) was cooled with a thermocirculator (Churchill) and excited with an EI 183 power supply. Laser (2) was cooled with a thermocirculator (E.M. scope) and excited by an Irvin C1096.

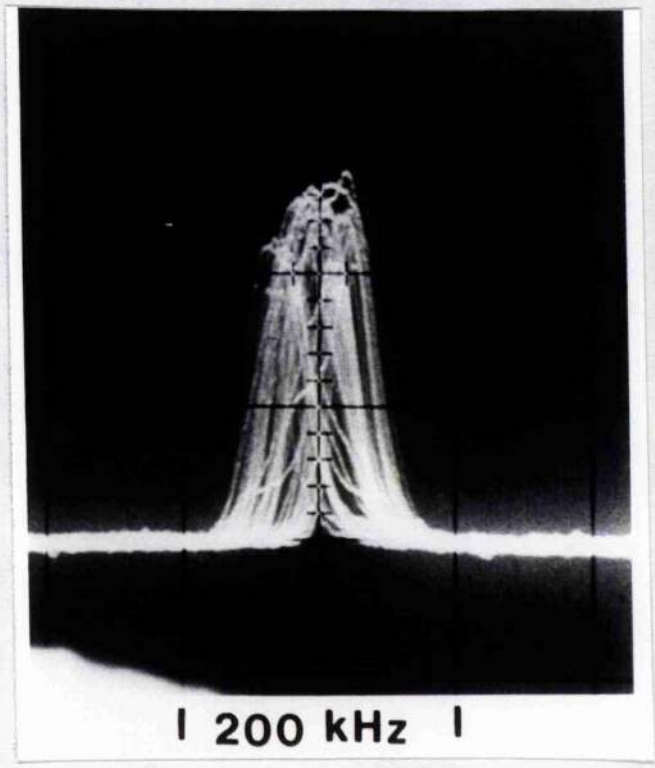

(b) as (a) but tap water cooled, slow flowing. Horizontal scale is 100 kHz/division with 30 kHz resolution.

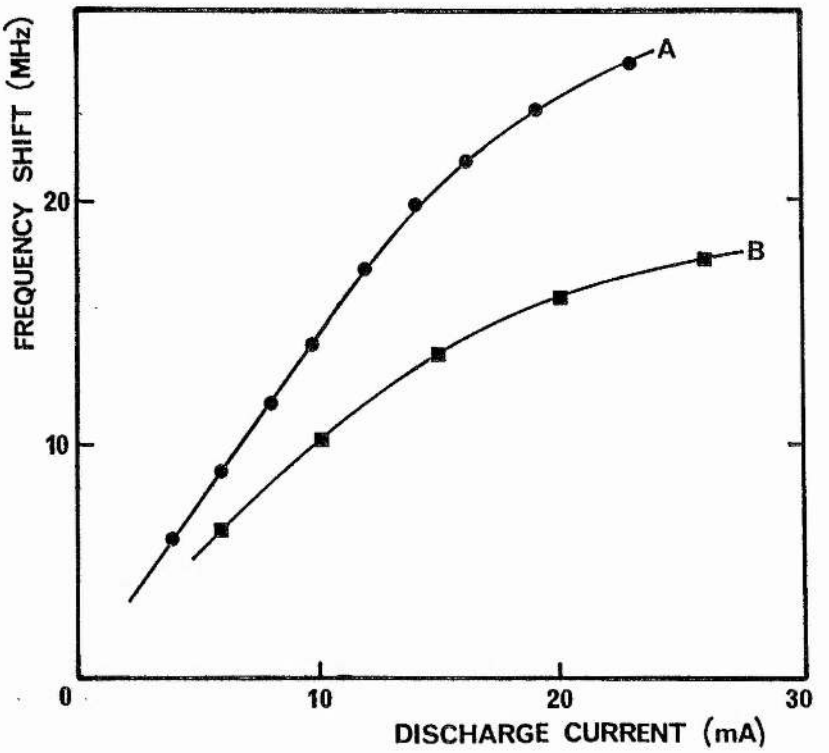

Fig. 4.214 The current dependence of laser mode frequency (normalized to i = 0) for (A) the compact CO_2 laser 1 Xe, 3 CO_2, 4 N_2, 12 He (torr) and (B) the smaller sequence band laser, 50 cm amplifier and 1.1 m resonator length 1.5 Xe, 1 CO_2, 3 N_2, 10 He (torr). Typical standard deviation of shifts is 0.3 MHz.

$$\Delta f = \frac{\partial f}{\partial i} \Delta i = 140 \text{ kHz} \quad \ldots\ldots\ldots\ldots \quad (4.11)$$

which could account for the majority of the residual broadening. Excitation with the Irvin C1096 power supply in cv and the modified EI 183 supply resulted in a spectrum width of 105 kHz consistent with the predicted (from 4.11) 140 kHz width.

4.3 STABILIZATION WITH OFFSET LOCKING

The lasers were also stabilized off line centre by adding a determined quantity of reference signal (ac) into the PSD input. This generated a fixed dc output which required an error signal of the same value but opposite sign to attain null point which the servo seeks.

In general, offset locking produces poorer stability because although a well defined offset signal can be presented to the PSD, any change in laser parameters will vary the OGE discriminant feature and the error signal voltage for a given frequency will change. As a result, a new frequency will be found where these voltages (error and offset) sum to zero. The beat frequency spectrum of two compact lasers was observed when one was stabilized at 10P(20) line centre (conventionally) and the other was offset by - 18 MHz from line centre by adding $\sim$ 5 mV ac reference into the input. The drift over 1 hour was $\lesssim$ 100 kHz which corresponds to a long term stability S (1 hour) $\gtrsim 2.8 \times 10^8$.

A - 21 MHz offset was introduced by the offset control to one laser and it was stabilized with reduced gain for two hours; Figure 4.31 shows the difference spectrum at t = 0, 30 minutes, 60 minutes and 120 minutes respectively. With the modulation set to introduce 3.5 MHz full width servo hunting of $\sim$ 350 kHz was observed and the offset laser drifted $\lesssim$ 0.5 MHz over two hours corresponding to S (2 hours) $\gtrsim 6 \times 10^7$. The servo hunting could not be completely removed. Stabilization at the extreme edge of the signature segment (25 to 30 MHz offset) resulted in poor stability locks, servo hunting ($\sim$ 0.1 to 10 Hz dependent on gain) and ultimately line changing.

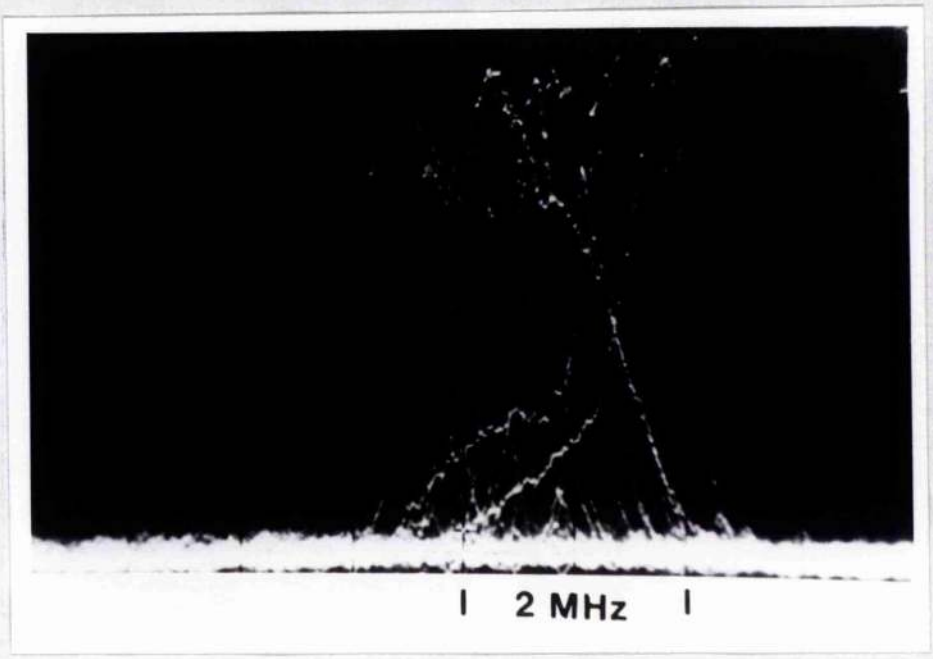

Fig. 4.31 (a) Offset laser difference frequency spectrum. One laser stabilized at - 21 MHz with respect to 10P(20) line centre, with modulation 4.0 V at 220 Hz. Horizontal scale is 1 MHz/division, 300 kHz resolution freerun trigger 0.1 s.

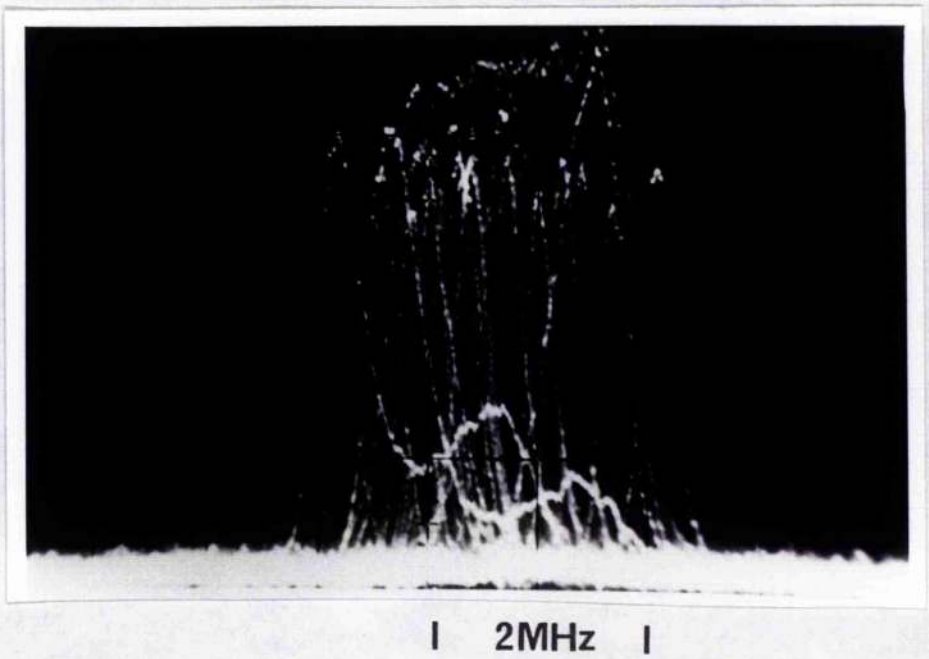

(b) As (a) after 30 minutes.

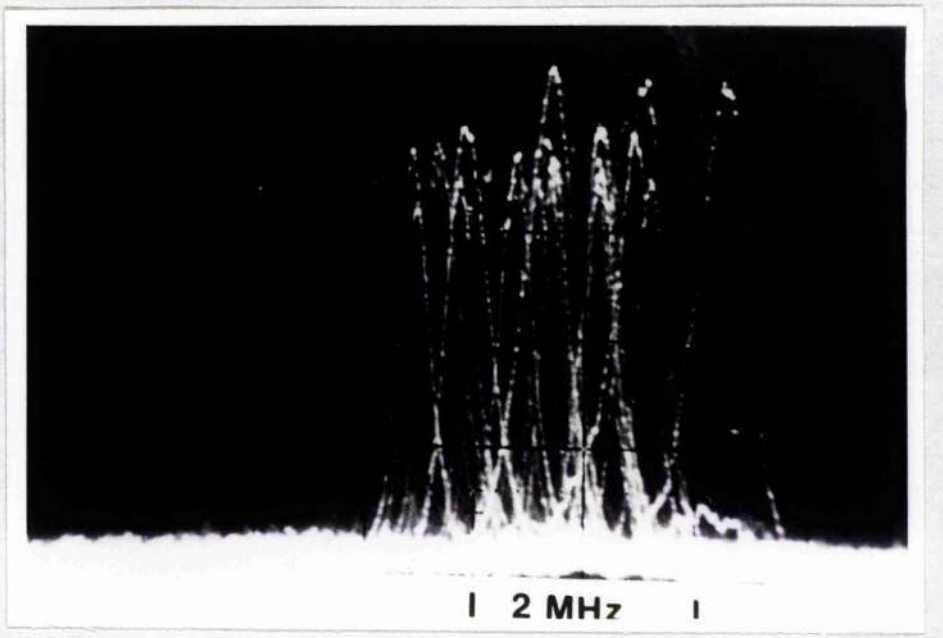

Fig. 4.31 cont. (c) As (a) after 60 minutes.

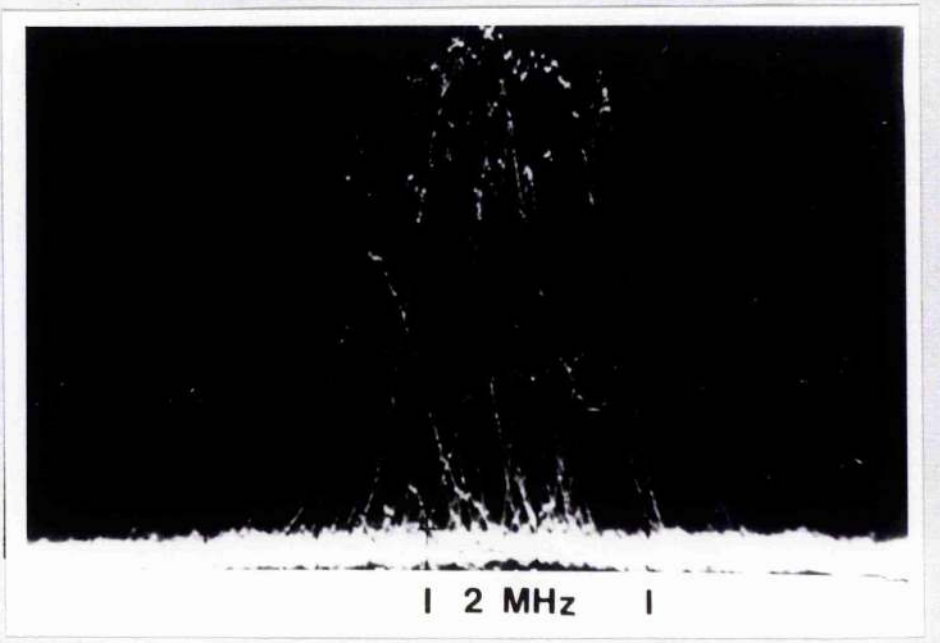

(d) As (a) after 120 minutes.

4.4 SEQUENCE CO_2 LASER STABILIZATION

The 9 to 11 μm ($00^02 \rightarrow [10^01, 02^01]_{I,II}$) transitions exhibit a smaller optogalvanic effect and the measurements of these effects is given in detail in 5.1. Although the sequence CO_2 laser is both lower power and less efficient it is of interest for optical pumping, spectroscopy, atmospheric transmission including pollution monitoring and vibrational temperature measurement.[118,138]

The smaller (50 cm amplifier, 110 cm total length) stable sequence band laser was OGE stabilized on several different 00^02 rotational transitions by signature selection and the amplitude and frequency stability was found to be very similar to that achieved with the fundamental transition OGE stabilization of the compact lasers. Sequence band lasers are noticeably less stable than fundamental band CO_2 lasers due to thermal problems resulting from the intracavity hot (400 C) CO_2 absorber used to suppress the ordinary transitions. Figure 4.41 shows the sequence laser output power unstabilized compared with the laser OGE stabilized (as in 4.2) on P17, P21 and P23 lines. The different power levels show the range of gains of different lines; the improvement is from $\sim$ 10% to $\sim$ 0.5%. By observation of the PSD, output error signals equivalent to greater than 300 kHz (10 mV), were never observed and the inferred frequency stability was S (1 hour) $\geq 3 \times 10^7$.

Unfortunately, no heterodyne experiments were possible because two sequence lasers were never available simultaneously but all experimental indications show a comparable resettability, response time and stability performance equal to the conventional OGE stabilization of fundamental transitions. The tuning range of the longer cavities was less and offset locking was restricted to 8 MHz.

4.5 HIGH POWER LASER STABILIZATION

The high power ($\gtrsim$ 43 W) sealed CO_2 laser described in 3.13 was used,

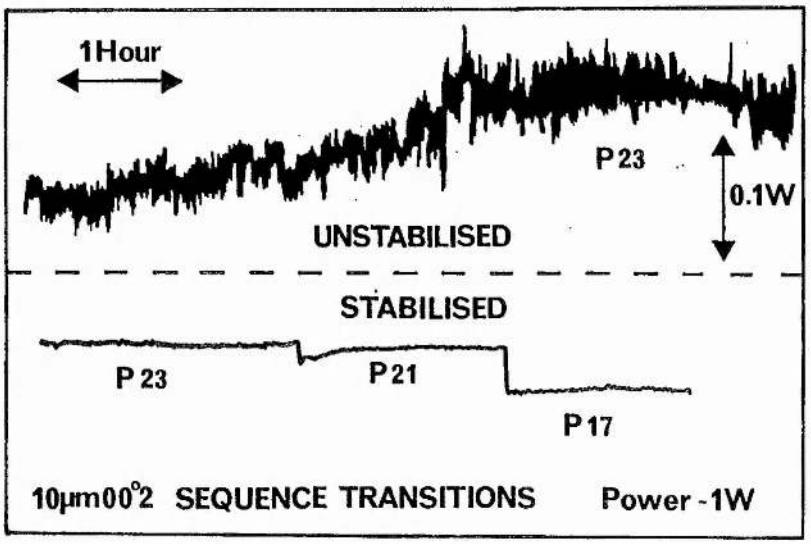

Fig. 4.41 Output power stability of sequence band laser with and without OGE stabilization. The mean power level was 1 W, and all transitions were in the 10 μm band.

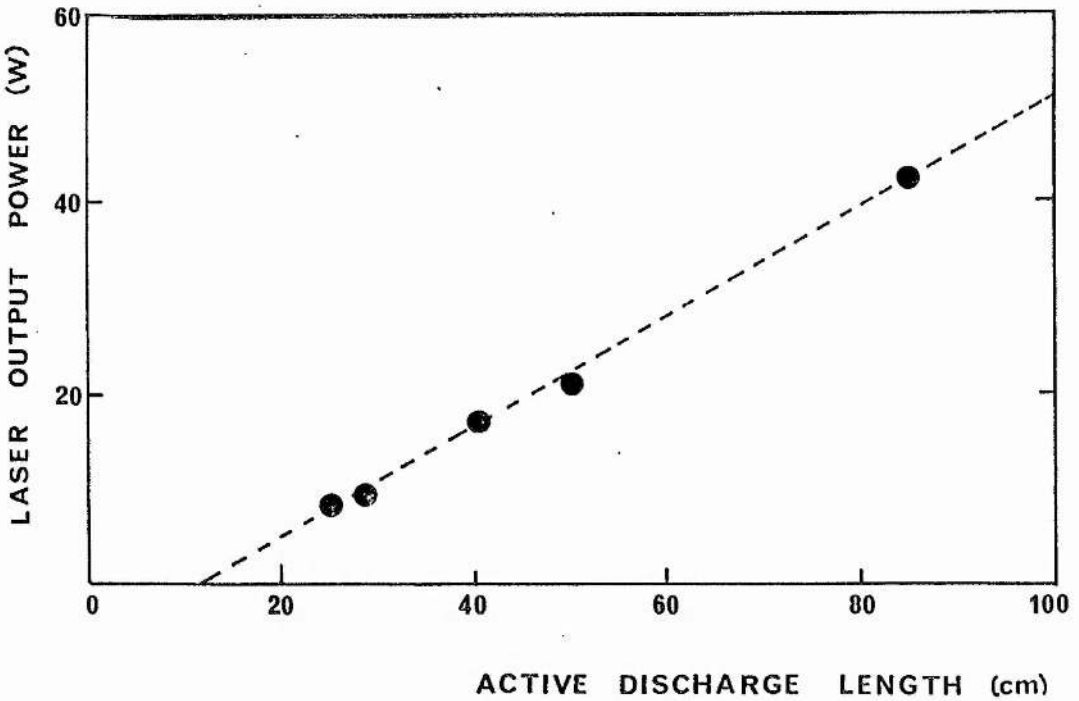

Fig. 4.51 Output power (with optimized output coupler) generated by a sealed laser with internal diameter 8 - 10 mm for 26 torr filling of 1 Xe, 3 CO_2, 4 N_2, 18 He when single mode is optimized at 10P(20) line centre. The output couplers used were (90% for 35 cm, 80% for 50 cm and 60 or 70% for 80 and 85 cm).

with the two sequence lasers to measure the suitability of OGE stabilization for more powerful lasers. Because the laser gain/unit length is constant for a given medium the amplifier tube (and resonator) must be longer for higher output powers. Figure 4.51 shows the output power extracted from the lasers used in this experiment as a function of length. These lasers show the highest powers per unit length to date of any published data on sealed low pressure lasers. An empirical expression of output power P

$$P \sim 22L + 12L^2 \quad (W) \qquad \ldots\ldots\ldots\ldots\ldots\ldots \quad (4.12)$$

where L is the amplifier length has been evaluated by Browne & Smith[139] in 1974, of the most effective sealed CO_2 lasers constructed at St. Andrews University and previously reported in the literature. Some improvement (up to 20%) has been achieved here and this was probably due to

1. Better optical optimization - particularly output coupler reflectivity
2. High reflection coefficients of total reflectors
3. Careful choice of tube diameter
4. Careful optimization of gas composition.

A new empirical rule from the maximum single mode output power P can be suggested from these experiments

$$P \sim 57.3\ (L-0.11) \qquad \ldots\ldots\ldots\ldots\ldots\ldots \quad (4.13)$$

where P is in watts and length is in meters. This equation exhibits the familiar laser threshold condition where 11 cm is the minimum gain length required to overcome the cavity losses. No report could be found of lasers of this type oscillating with gain lengths shorter than this figure. The absolute length limit 1.2 to 1.5 m for signature selection was not exceeded by any of these oscillators and they are strictly comparable in construction; the high power laser was carefully designed and constructed for an improved passive stability. The smaller sequence band laser (50 cm amplifier) was

improved by more stable optical mounting, new discharge tube and better draught shielding, in order to be used as a stable partner for heterodyne experiments.

The short term passive stability was S (1 ms) $\geq$ 6.1($\pm$ 0.6) x 10^9 and the transitional passive stabilities were S (1.5 s) $\geq$ 2.5 $\pm$ 0.4 x 10^8, S (5.0 s) $\geq$ 2.9($\pm$ 0.8) x 10^8, S (12 s) $\geq$ 1.6($\pm$ 0.6) x 10^8 and S (60 s) $\geq$ 9.1($\pm$ 0.8) x 10^7. Heterodyne output from the HP 8557A spectrum analyzer is shown in Figure 4.52 for 5 s and 12 s.

The long term (hours) passive frequency stability of the high power was measured by the heterodyne method and the reference laser was stabilized at line centre. During the measurement the modulation was switched off and the loop broken; the PSD output error was observed during the measurements. This technique is necessary to remove the modulation broadening of the difference spectrum and reference shifts of < 500 kHz assured. When the loop is closed again any measurable correction can be seen both in the difference spectrum and the PSD output. Multiple trials of this technique resulted in a reference shift compared to a third laser (compact stabilized) of $\leq$ 200 kHz.

Figure 4.53 shows the difference spectrum obtained as above; the reference laser was stabilized to 10P(22) line centre and the high power laser set at + 6 MHz with respect to line centre. The offset line centre drift rate was $\leq$ 2.3 MHz/hour. For six trials S (1 hour) $\geq$ 1.4 ($\pm$ 0.3) x 10^7. This improvement of stability over shorter systems is due, of course, partly to development, improved design and careful construction but there is an improvement in passive stability just due to length as previously described.

Figure 4.54 shows the empirical values of stability for the laser cavity lengths (in all cases construction is comparable but not identical). Some intermediate lengths were obtained by removing the hot cell from the sequence lasers and situating the output coupler nearer to the discharge tubes. The improvement of passive stability is considerable and clearly demonstrates why laser manufacturers supply longer lasers when stability performance is a customer requirement. This order of stability can be simply achieved by

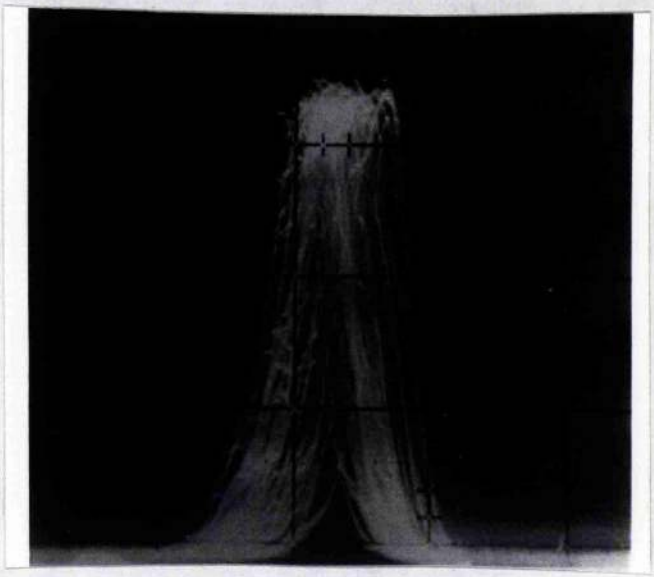

200 kHz

(a) 5 s averaged difference spectrum

Fig. 4.52 Difference frequency spectrum of high power laser (output power ∿ 35 W) and modified sequence laser (output power ∿ 15 W). Tap water cooling was used. The HP8557A spectrum analyzer and LBC 600 LTT detector were used to detect both beams scattered off a diffuse reflector. Resolution was 30 kHz and both lasers were freerunning. The centre line represents 3 MHz difference frequency.

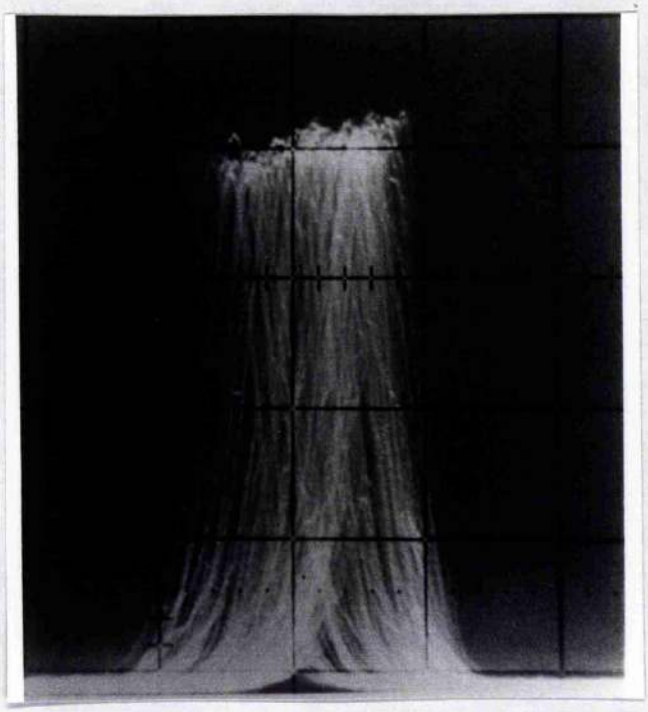

200 kHz

(b) 12 s averaged difference spectrum

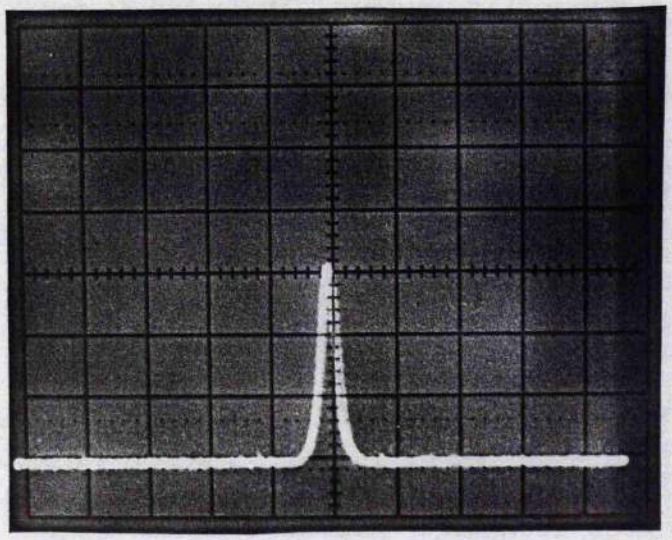

Fig. 4.53 (a) Beat spectrum of reference laser (unmodulated) and high power laser (power ∿ 40 W). Centre line is + 6 MHz with respect to 10P(22) line centre. The horizontal scale is 1 MHz/division and the resolution is 300 kHz.

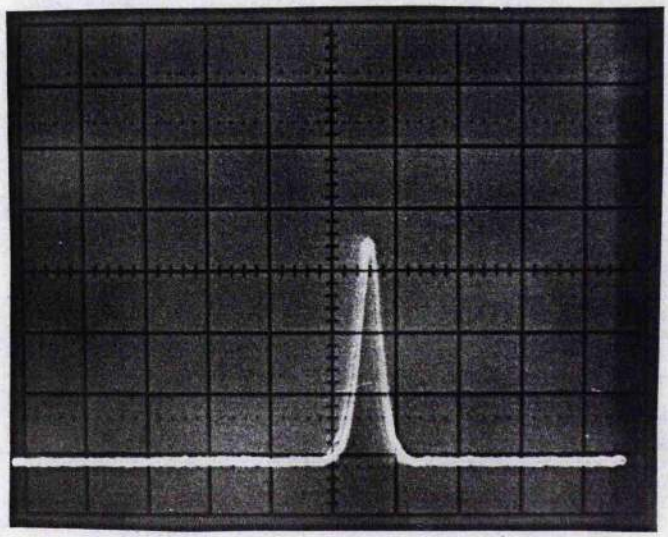

(b) As (a) after 15 minutes freerun.

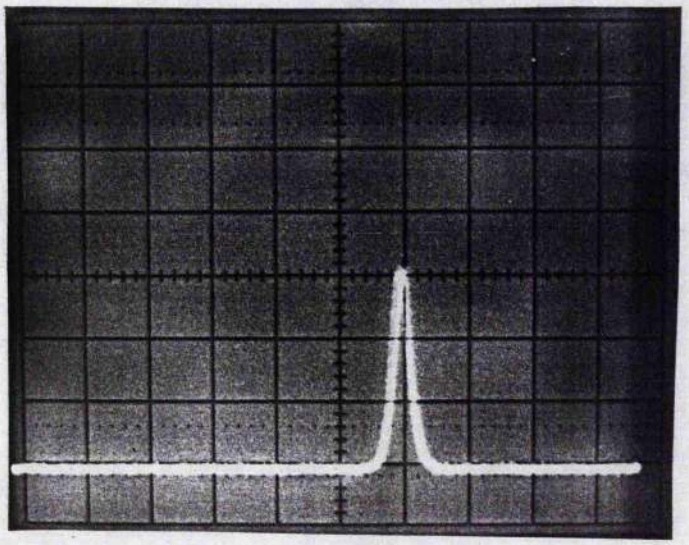

(c) As (a) after 30 minutes freerun.

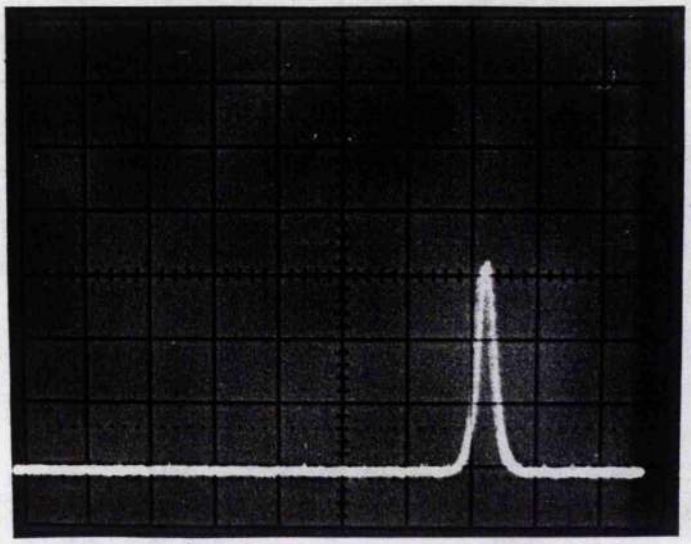

Fig. 4.53 continued (d) As (a) after 60 minutes freerun. Total shift = 2.3 MHz.

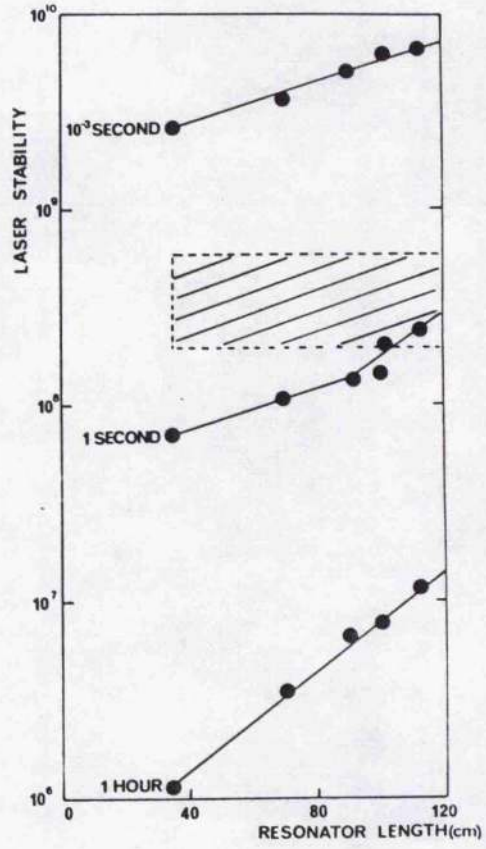

Fig. 4.54 The sealed laser passive stabilities S(1 ms), S(1 s) and S(1 hour) increase with increasing length (experimental points) and the OGE stabilized (response time $\sim$ 0.1 s) performance for long periods (> 1 hour) shown as a dashed box.

active stabilization (OGE or otherwise) with shorter lasers and performance investigation of a miniature cavity (minimum) ∿ 10 cm may provide more information on the thermal behaviour of the optical system.

The high power laser was stabilized in a similar manner to lasers previously described with one important exception. The discharge was double (two floating anodes and one shared high voltage cathode) and excited by two EI 183 matching power supplies. This arrangement does not allow any terminal to be earthed and the parallel capacitive coupling scheme was not satisfactory due to oscillatory behaviour. Transformer coupling (Figure 3.226) was used for one arm of the discharge (a Ferromag 10 kV isolation transformer 1:1 ratio with 50 mA primary capability and a 20 kHz bandwidth was supplied by Ferromag part no. FM3931), and active stabilization was simply achieved.

Due to the improved long term passive stability more care was required in the heterodyne stability measurements. The reference laser (modified sequence band laser) was carefully OGE stabilized to line centre and compared with a compact laser OGE stabilized 5 MHz off line centre. This difference frequency was checked when measurements of the high power laser were not being made and this difference spectrum was observed not to drift more than 100 kHz. Figure 4.55 shows a six hour OGE stabilization test of the high power laser (37 W). The long term stability of these higher power lasers when OGE stabilized was S (1 hour) $\geq 5.6\ (\pm\ 1.5) \times 10^{8}$.

In summary, the optogalvanic stabilization proved to be a most useful technique for stabilizing small conventional cw CO_2 lasers, CO_2 sequence band lasers and higher power CO_2 lasers giving impressive stability improvements of up to two orders of magnitude in the laser intensity and more than six orders of magnitude improvement in frequency stability (of signature tuned lasers which change lines). Additionally, due to the OGE technique's insensitivity to vibrational and acoustic interference (the distributed detection element is coincident with the laser amplifier) and since it avoids the use of an infrared detector which degrades either beam quality

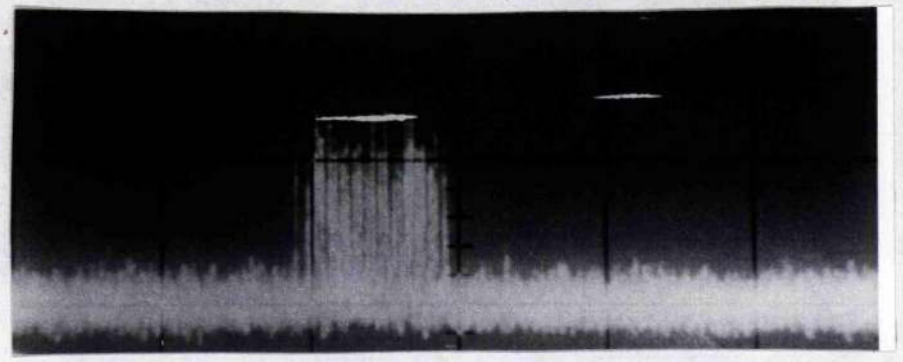

(a) Stabilizer switched on after 1 hour warm up

Fig. 4.55 OGE stabilized high power laser, output power 37 W difference spectrum when heterodyned with modified reference laser stabilized at 10P(20) line centre and compared with a third stabilized laser. The reference source was reproducible to better than 100 kHz. The horizontal scale is 1 MHz/division. The resolution is 30 kHz. The drift over 6 hours $\lesssim$ 150 kHz.

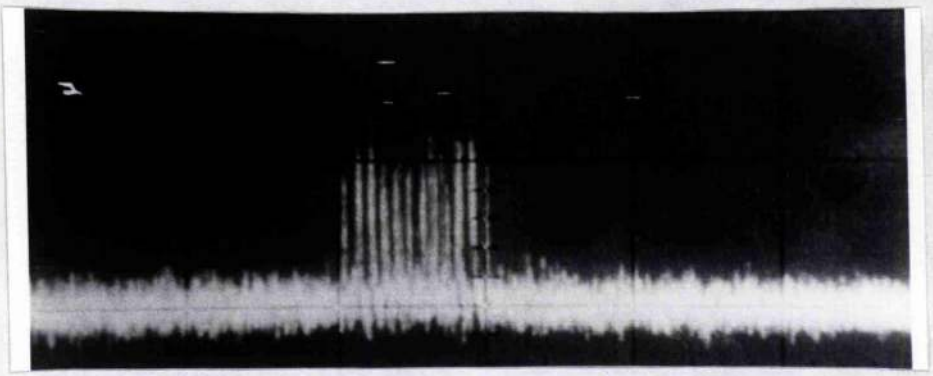

(b) As (a) after 3 hours

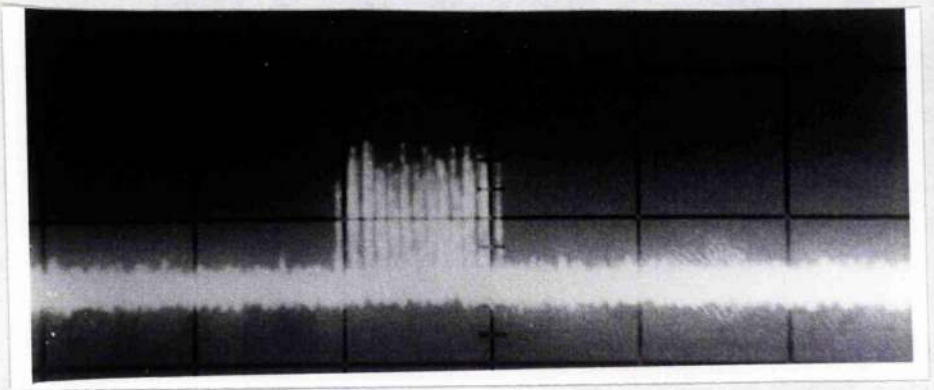

(c) As (a) after 6 hours

or power (or both), OGE stabilization was found to be a suitable, cost effective and consistent method of improvement for efficient, sealed CO_2 lasers.

5.0 OPTOGALVANIC MEASUREMENTS IN SIMILAR VIBRATIONAL SYSTEMS

Investigation of the optogalvanic effect due to the perturbation of other vibrational level populations in CO_2 laser discharges and of similar kinetic processes in other molecular systems is important

1. For the fundamental understanding of the precise kinetics of laser discharges
2. To test the gas temperature perturbation theory
3. For technological reasons such as detection and stabilization.

In these experiments the CO_2 (00^02 - $[10^01, 02^01]_{I,II}$) sequence band laser induced OGE and CO (5.3 μm) molecular laser optogalvanic effects were measured.

The CO molecular laser has both a higher theoretical efficiency and less dependence of output power on cavity length than the CO_2 laser;[140] additionally, the 5 to 6 μm wavelength is often technologically preferable to the CO_2 10 μm wavelength. It has been shown[141] that genuine single line operation can be obtained under carefully controlled conditions and in principle, due to the high efficiency and stable electric discharge, the laser should be a good candidate for optogalvanic stabilization.

5.1 CO_2 (00^02 - $10^01, 02^01_{I,II}$) SEQUENCE BAND LASERS

The sequence band lasers constructed for these experiments are described in 3.12 and produced single mode output powers in the range 0.5 to 1.5 W. This lower beam power resulted in the majority of OGE experiments having to be performed within the laser cavity (where the beam irradiance is much higher). In this chapter the measurement of the OGE signals is

compared to the $00^0 1$ regular band signals in both frequency, amplitude and phase.

The sequence laser has been previously adequately described[138,142] and the relevant set of energy levels are displayed in Figure 5.11. Due to the essentially harmonic structure of the CO_2 vibrational energy levels the $00^0 2$ and $00^0 3$ (upper laser level) transitions have very similar energies; because of slight anharmonicity there are frequency shifts of these laser lines relative to the regular laser band.

In the $00^0 2$ sequence band laser, stimulated emission results in $00^0 2$ depletion and the lower level ($10^0 1$, $02^0 1$) population relaxes via V-V processes to $01^0 1$ and then via V-T processes to the ground state. The fractional populations of the $00^0 n$ levels due to N_2 and CO resonant pumping always results in a lower population of the $00^0 2$ level than the $00^0 1$ level for all realistic laser asymmetric stretch mode vibrational temperatures ($< 10^4$ K). The resultant $00^0 2$ sequence band laser gain is always lower[118] and consequently laser output powers are lower from small sealed devices.

The sequence laser fitted with a 50 cm amplifier and 1 m cavity produced ten signature selectable $00^0 2$ P branch 10 μm lines at output powers 0.1 to 1.0 W and the available output spectrum of $00^0 2$ and $00^0 1$ laser emission is compared in Figure 5.12. The precise strength of each laser line varies due to the wavelength dependent, reflectivity of the mirrors, window absorption, etc., but in general the band centre lines $00^0 1$ P(18) and P(20) and $00^0 2$ P(19) were strongest although the $00^0 2$ P(11) line showed strong laser emission. This laser could be optogalvanically stabilized on any of these lines and the performance of the active stabilization is described in 4.4 and 5.3.

The operating characteristics of this sequence laser were investigated to assess the suitability of scaling up the system to provide high single mode power ~ 25 to 50 W. Typical output powers for a $00^0 2$ high gain mixture 1 CO_2, 3 N_2, 16 He (torr) is shown in Figure 5.13 where the discharge current has been varied and the output coupler reflectivity maintained at 95%. The

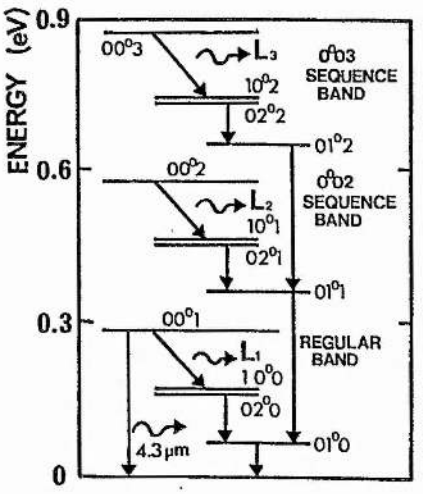

Fig. 5.11 A simplified diagram showing some of the CO_2 vibrational energy levels. The laser transitions of the regular and sequence bands are shown by the diagonal arrows. Some relaxation processes, 00^01 spontaneous fluorescence and V-V-T processes are shown as downwards pointing arrows.

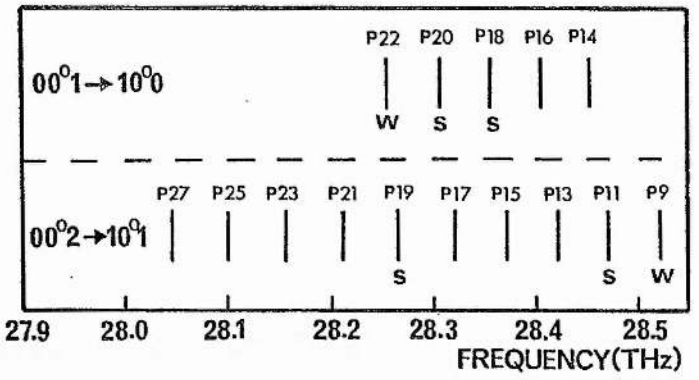

Fig. 5.12 The set of vibrational-rotational laser transitions available by cavity tuning from the 1 m long cavity, 50 cm amplifier sequence band laser. The upper half demonstrates the transitions observed with the Optical Engineering spectrum analyzer with the laser hot cell evacuated. The lower half shows the transitions similarly observed with the hot cell filled with 40 torr CO_2 at 350 C. The particularly strong lines and weak lines are marked by s and w respectively, 1.5 Xe, 0.6 CO_2, 1.8 N_2, 19 He.

non-optimized 00^01 laser power is shown for comparison; when this laser was optimized for 00^01 operation (1 Xe, 3 CO_2, 4 N_2, 12 He torr) the maximum output power was 14 W. The 00^01 oscillation shows the characteristic output power peak at $\sim$ 14 mA corresponding to a current density 7 mA/cm^{-2}. This approximate value was demonstrated in Figure 3.112. The maximum 00^02 output occurred, however, at a lower current $\sim$ 6 mA (3 mA cm^{-2}). Reduced optimum current for 00^02 operation was observed for all mixtures associated with expected lower electrical efficiencies $\sim$ 1 to 3%.

The regular band sealed lasers of this type of construction are known[143] to have output powers per unit length which saturate at pressures 28 to 35 torr (slightly dependent on mixture) in this tube diameter range. This output saturation is demonstrated in 5.14; in contrast the 00^02 laser output peaked at 16 torr and decreased sharply and oscillation ceased at > 25 torr. The 00^01 regular oscillation continued to oscillate at higher pressures above 50 torr. Ultimately, discharge constriction occurred and the discharge became unstable. The narrow range of operating conditions for 00^02 oscillation could be due to the marginal gain of the system (maximum gain $\simeq$ minimum losses). Because 00^02 gains are highest for high asymmetric stretch mode vibrational temperatures (better population of upper laser level) gas mixtures are required which are consistent with this requirement. Low CO_2 content has been shown both experimentally and theoretically[118,138] to produce high vibrational temperatures and the results of this work are consistent with that hypothesis. The ratio of 2 to 3:1 N_2 to CO_2 was required for 00^02 oscillation whereas 2 to 1:1 was optimum for regular operation. This lower CO_2 content means that the equilibrium CO_2 dissociation (which is current dependent) can cause a rapidly reducing CO_2 concentration at higher currents. This mechanism can account qualitatively for both the rapidly reducing 00^02 output power and the considerably reduced efficiencies at moderate currents. Previously gas heating theories have been invoked to explain CO_2 00^01 laser power deterioration at higher currents; if this is the case, then power reduction should not be seen in medium and fast rate

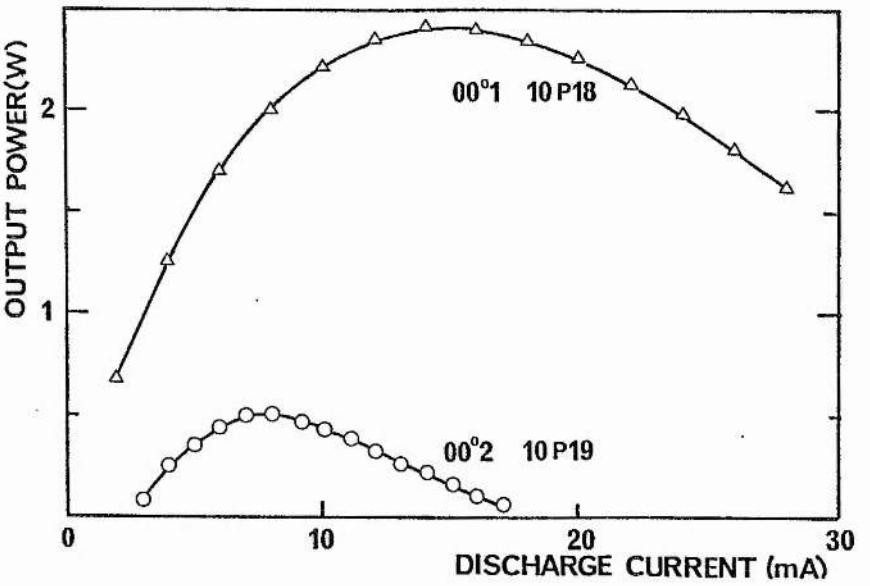

Fig. 5.13 Typical performance of a short (50 cm amplifier) sealed CO_2 laser. The gas mixture and pressure and laser output coupler were optimized for $00^0 2$ operation. The variation of single mode output power with discharge current is shown. The gas composition was 1 Xe, 1 CO_2, 3 N_2, 12 He.

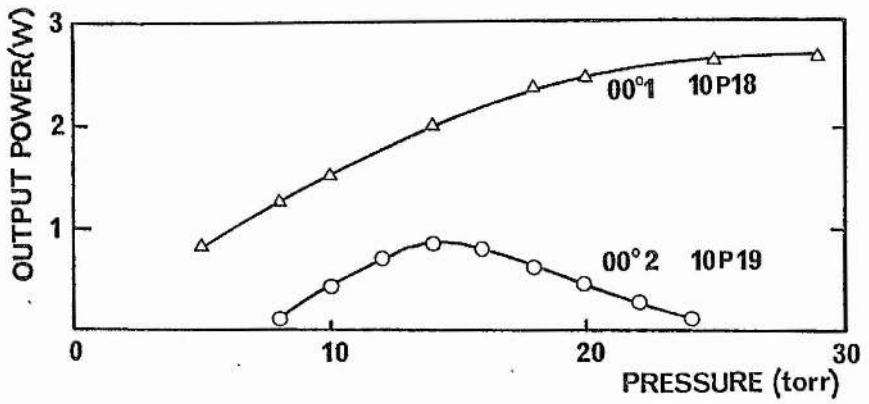

Fig. 5.14 Typical performance of the sequence CO_2 laser described in Fig. 5.13. The variation of single mode output power with total laser amplifier pressure is shown for 15 mA discharge current.

flowing gas lasers but this could be the consequence also of lower dissociation). The gas heating theory cannot be discounted altogether because deliberate heating of the walls to 50 C (from 0 C) can readily reduce the $00^0 1$ output power by 50%. The equivalent increase of axial temperature can be achieved by increasing the P/L by approximately 2 W/cm in this case. It is assumed that the temperature rise modifies thermally relevant energy level populations and alters relevant temperature dependent rates in the discharge. The fact that $00^0 2$ power reduction is more marked than the $00^0 1$ where thermal lower level population could be invoked as the major mechanism strongly suggests that the gas heating theory is not adequate. The relative merits of these theories will be discussed later in this chapter during discussion of the efficacy of Xe addition.

The three main components of the sequence laser are

1. CO_2 - N_2 - He - ? amplifier
2. CO_2 hot cell absorber
3. CO_2 fluorescence cell discriminator

The first has been briefly described already although more careful analysis will be required to explain the detailed OGE results. The second component is the filter required to eliminate regular laser lines and the third is a discriminator which can be used to unambiguously determine the band of oscillation. The second and third components are now to be described.

5.11 HOT CO_2 ABSORPTION OF RESONANT LASER RADIATION

A frequency selective filter is required for CO_2 sequence laser operation to attenuate regular lines so that the gain is lower than for the required sequence line. In the case of signature selected lines the absorber must attenuate the whole CO_2 $(00^0 1 \rightarrow [10^0 0, 02^0 0]_{I,II})$ laser band and not appreciably attenuate the closely spaced (in frequency) sequence lines. This criterion is met most simply with suitably heated CO_2. Grating selected lasers only require the attenuation of one neighbouring CO_2 line (within the bandwidth of the grating $\sim$ 3 to 10 GHz); NH_3 absorption of 10P(20) has been

used.[144] Alternatively, the use of cavities which are highly wavelength selective can be used without an absorbing filter[145] for particular high gain $00^0 2$ lines that have wavelengths sufficiently different to the closest (frequency) $00^0 1$ neighbour. Unstable return to $00^0 1$ oscillation can occur due to cavity drift.

For these experiments powerful single mode lasers were required in order to investigate the optogalvanic perturbations and hot CO_2 intracavity cells were investigated as suitable selection filters.

From practical requirements, several constraints upon hot cell construction and operation can be identified:

1. Strong selective absorption of regular CO_2 lines (dependent on gas temperature and pressure)
2. Avoidance of undue cavity heating and expansion
3. Overall cavity length restriction $\sim$ 1 to 1.5 m for signature selection
4. Choice of suitable optical components, window, materials and cell construction.

The construction of such a hot cell has previously been described by Berger, Seimson and Reid[146] which utilized a Nichrome heater in a vacuum jacket surrounding a quartz tube. This resulted in an outside temperature of $\sim$ 40 C. The mechanical details of the structure result in some uncertainty of absorption length due to the length temperature profile. The absorption of CO_2 laser radiation (regular band) was found to be independent of pressure above about 30 torr in agreement with earlier spectroscopic results.[147]

Several simple and similar structures were investigated for these experiments both inside and outwith laser cavities and the most useful layout used is shown diagramatically in Figure 5.111 with the associated temperature profiles for one and two heater windings. Miniature water jackets were included separating the heated area from the windows and several heater

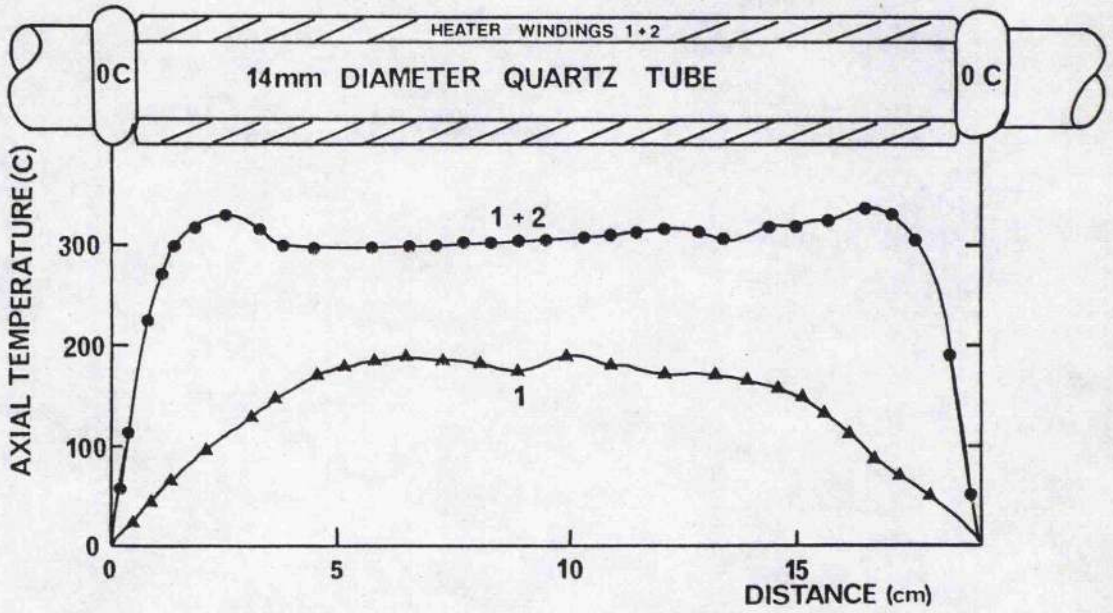

Fig. 5.111 The temperature variation with length due to (1) a single 0.15 Ω/cm nichrome tape winding of constant pitch, 3 turns per cm and (2) with two isolated windings in parallel, the outer as in (1) and the inner wound with a non-uniform pitch as shown in Fig. 5.112 which selectively heats the ends. The heater was supplied with 10 V rms and the atmospheric air temperature measured with a Cr/Al thermocouple placed inside the tube. There is some error introduced due to heat lost down the thermocouple wire by conduction. Excitation with 24 V rms produced the maximum centre temperature of 502 C.

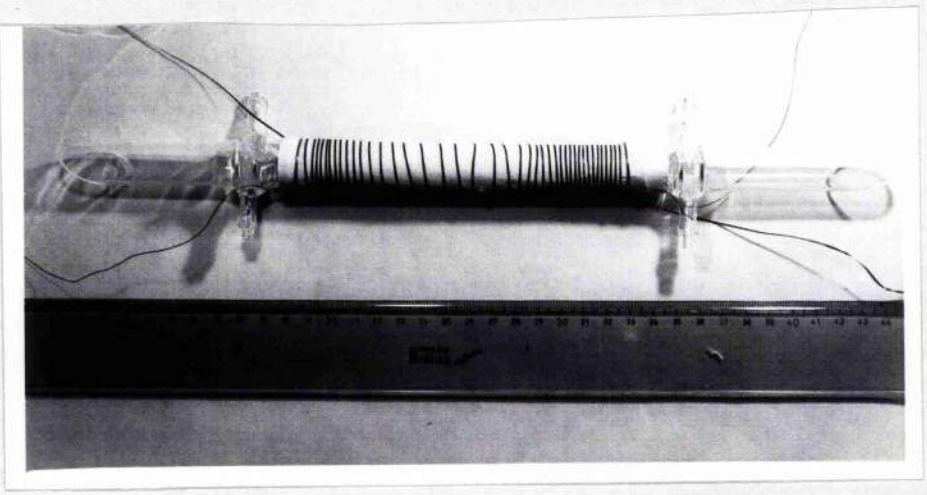

Fig. 5.112 The innermost heater winding of a CO_2 hot absorber cell. The variable winding pitch and small water jackets are clearly seen. Positioning the heater turns closer to the cooling jackets produces higher thermal gradients at the ends.

windings (some non-linear) were required to obtain a 'flat top' temperature profile with length (Figure 5.112). A heater vacuum jacket was not used and the heating element was encased in thermally insulating ceramic wool and wrapped with aluminium heat reflecting foil. Thermocouples were attached to the outside of the quartz tube; the temperature with length profile was investigated in air at atmospheric pressure. Berger et al found little difference in such temperature/length profiles between air at 760 torr and CO_2 at 30 torr.

The hot CO_2 cell must suppress both 10 μm and 9 μm regular bands for signature selection; the intracaivty absorption is minimum for the 10 μm P transitions whereas the laser gain is maximum.[148] As a result, providing that the 10 μm transitions are suppressed no other $00^0 1$ lines will oscillate. All measurements of absorption were made therefore at 10P(18) and 10P(20) when the hot cell was being evaluated. As the CO_2 temperature (translational) increases the rotational Boltzmann distribution shifts to higher J values (for example P(40) has increased absorption relative to P(18)). From these considerations we can test the fundamental criteria for the estimation of the hot cell length, a parameter of considerable practical interest. It is required that

1. There is a net loss per pass for all $00^0 1$ lines or at least
2. The net gain per pass $00^0 2$ is greater than the net gain of the regular band (i.e. little or no $00^0 2$ absorption)
3. Some compensation is to be made in order to avoid low J value, regular laser oscillation.

Previous estimations of length[146] suggested lengths between 0.2 and 0.25 of the amplifier length, the latter figure giving occasional regular oscillation at low J value $00^0 1$ transitions. Absorption/gain ratios of 0.2 to 0.3 were investigated in these experiments by fitting several cells, and the 'flat top' temperature profile has decreased the real length of the

absorbing filter. Use of a single KCL brewster window to separate the hot CO_2 absorber and the laser amplifier was found to be an important step because the cavity losses are reduced.

Typical operating pressures and temperatures for a 50 cm amplifier, 15 cm absorber laser are shown in Fig. 5.113. As the CO_2 temperature is increased (200 to 500 C) the minimum required pressure to hold 00^02 laser action reduces to approximately 10 torr. To recover 00^02 sequence oscillation once regular oscillation has occurred higher pressure for a given temperature is required; for example, to stop 00^01 10P(20) oscillation in this case at 400 C a pressure of 25 torr was required. This 'hysteresis' phenomena has also been observed by Seimson[149] and is an example of the effect which has recently become known as optical bistability.[150,151] Optical bistability is defined as the existence of two stable states of an optical system for a given set of input conditions. It is possible to identify which state (00^02 or 00^01) the laser is in by the transition pressure (or temperature) when a discontinuous output power change occurs. For example, if the power change occurs at 25 torr then the system is 00^01 going to 00^02, however, if the power change occurs at 12 torr the system is 00^02 going to 00^01. In this sense, the sequence band laser system has a memory of its present state (either 00^01 or 00^02) and two possible states which can be discriminated (by the transition pressure for a given temperature, or vice versa).

By probing a hot CO_2 cell of the described construction with a 5 W laser beam and by defining the heated length to be the points where the temperature falls by 25% (say from 400 to 300 C) absorption coefficient measurements were made for two lengths and a series of pressures and temperatures. The probe beam parameters and the laser intracavity beam parameters were comparable in profile and diameter but the power density was reduced by a factor of 4 to 10.

The absorption coefficient at 500 C (a maximum practical operating temperature) of pure CO_2 was found to vary from 2×10^{-3} cm^{-1} at 1 torr

to $\sim 2 \times 10^{-2}$ cm^{-1} at 100 torr as shown in Figure 5.114. The combined Doppler and collision broadening has been demonstrated extensively previously[152] and the purpose of this investigation was to both optimize the sequence laser design and to make accurate quantitative measurements for the particular beam parameters used in these lasers (rather than a conventional spectroscopic measurement). At low pressures (a few torr) and densities the absorption line is Doppler broadened and the line centre absorption coefficient $A(\lambda_o)$ is given by

$$A(\lambda_o) = \frac{-1}{8\pi} \frac{\lambda_o^3}{c\tau_{21}} \left[\frac{Mc^2}{2\pi kT}\right]^{\frac{1}{2}} \left[N_2 - \frac{g_2}{g_1} N_1\right] \quad \ldots (5.1)$$

where Mc^2 is the rest mass, g_2/g_1 the level degeneracy ratio and T is the gas temperature. In this low density limit the absorption is directly proportional to density (because populations (N_2, N_1) increase linearly with density); the radiation transition lifetime τ_{21} can be directly measured because all the other parameters are known.

At higher pressures (> 5 torr) the absorption is collision broadened and the absorption coefficient $A(\lambda_o)$ is

$$A(\lambda_o) = \frac{-1}{8\pi} \frac{\lambda_o^2}{\tau_{21}\nu_c} \left[N_2 - \frac{g_2}{g_1} N_1\right] \quad \ldots\ldots (5.2)$$

where the constants are as previously but ν_c is the optical broadening collision frequency. For gas in thermal equilibrium both populations N_2 and N_1 and the collision frequency are proportional to density and consequently the absorption coefficient becomes independent of pressure.

This measurement shows that for CO_2 at 500 C the Doppler broadened absorption coefficient is equal to the collision broadened coefficient for a pressure of approximately 8 torr. The saturated absorption coefficient of interest in this application is 2% cm^{-1} in good agreement with previous reports in the literature.[153,154,155,156] It is clearly shown that there is little advantage in operating the hot cell at pressures above 30 to 40 torr. If the pressure is increased too much the CO_2 absorption collision broadening ($\sim$7.6 MHz/torr) ultimately means that the

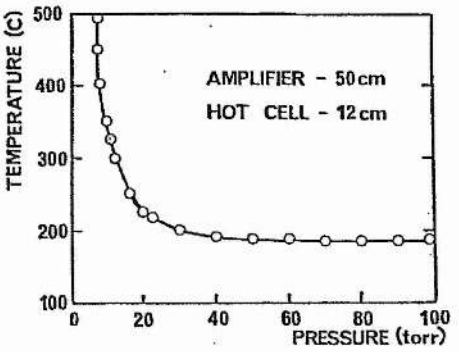

Fig. 5.113 Typical operating characteristics for the hot CO_2 absorber showing the transition to 00^01 oscillation from 00^02 (by lowering pressure) with rising temperature. The line represents the boundary condition. All values of pressure and temperature above the line stop 00^01 oscillation.

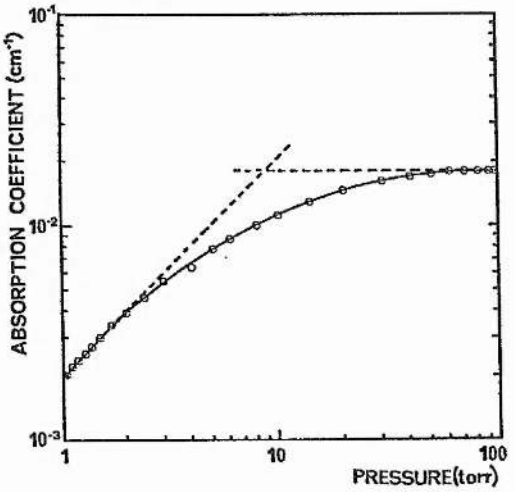

Fig. 5.114 The variation of CO_2 absorption coefficient with pressure for a hot cell at 500 C. The probe laser was line centre stabilized to 10P(18) and the probe power was 5 W for a single mode beam of 1/e diameter of 4.7 mm.

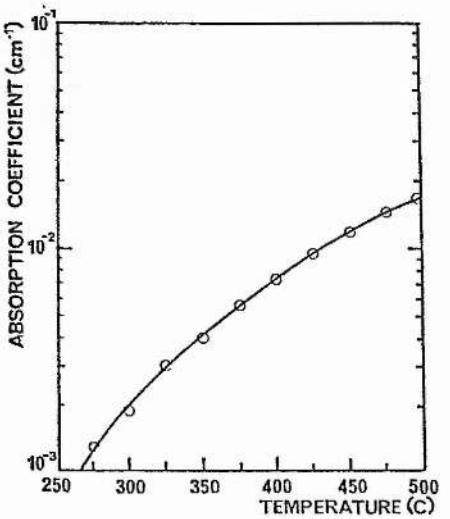

Fig. 5.115 The variation of CO_2 absorption coefficient with cell temperature for 30 torr. The other conditions are as described above.

neighbouring $00^0 2$ lines are also attenuated.

The rise of absorption due to temperature for collision broadened CO_2 is due to the increased thermal population of the lower laser levels. Figure 5.115 shows the measured increase in absorption coefficient from $\sim 10^{-3}$ cm^{-1} at 550 K to $\sim 2 \times 10^{-2}$ cm^{-1} at $\sim$ 780 K for 30 torr pressure. Absorption coefficients lying below this curve were measured for all lower pressures following the form described in 5.114. There is some advantage in using hotter cells for short cavities and within the constraints imposed by cavity dimensional stability the temperature could be increased further.

The 10P(18) transition was chosen as a representative mean band centre line rather than 10P(20) due to the latter's energy coincidence with the 10R(23) $01^1 1 - 11^1 0$ hot band transition (energy difference 0.01 cm^{-1}) which leads to anomalous absorption values.[149,156,157]

A calculation on the basis of these measurements may be attempted to predict the length of absorber needed in order to satisfy the differential gain criterion, i.e. that the $00^0 2$ adjacent laser line gain ($\alpha_{00^0 2}$) is greater than $00^0 1$ laser gain ($\alpha_{00^0 1}$) minus the single pass absorption. For a 500 C, 30 torr absorber an absorption coefficient (α^1) of 2×10^{-2} cm^{-1} is expected and the necessary absorption length L_2 is by eliminating the exponentials

$$L_1 (\alpha_{00^0 1} - \alpha_{00^0 2}) < \alpha^1 L_2 \quad \ldots\ldots\ldots\ldots (5.3)$$

or

$$L_2 > \frac{L_1}{\alpha^1} (\alpha_{00^0 1} - \alpha_{00^0 2}) \quad \ldots\ldots\ldots\ldots (5.4)$$

where L_1 is the amplifier length.

The saturated laser gains are known from experiments by Reid and Seimson, Smith and Mellis and experiments performed for this purpose during this work. Gain ratios of $00^0 1$ band to $00^0 2$ band in the range 3 to 5 : 1 have been measured for sealed lasers depending on precise gas mixture. The $00^0 1$ to $00^0 2$ laser gain ratio was 3:1 for the particular optimized gas

mixture used here. Assuming[158] $\alpha_{00^0 1} = 0.35 \times 10^{-2}$ cm^{-1} and $\alpha_{00^0 2} = 0.12 \times 10^{-2}$ cm^{-1} then the minimum length absorber required would be approximately 6 cm. This length needs to be increased by $\sim$ 25% to account for the end (albeit sharp) temperature profile (see Figure 5.111) and additionally $\sim$ 30% to avoid low J value $00^0 1$ oscillation. A required minimum length of $\sim$ 9 cm or 18% of the amplifier length is predicted somewhat shorter than the Berger[146] empirical rule. Three hot cell lengths (one of which was split into halves) were used in the two sequence lasers; for 450 C and 30 torr CO_2. No $00^0 1$ rejection occurred with a hot cell 12% of the amplifier length. With a hot cell 22% of the amplifier length all $00^0 1$ lines except $00^0 1$ 10P(12) and 10P(8) were rejected. With a 25% hot cell length only 10P(12) was available in the $00^0 1$ band simultaneously with some sequence lines; it could be eliminated by suitably lowering the discharge current. The longest hot cell (28% of the amplifier length) was successful in providing complete rejection of the $00^0 1$ lines for a temperature of 450 C with a 30 torr CO_2 filling.

There is only poor agreement empirically with the above prediction ((5.4)) because in practice $L_2/L_1 \gtrsim 0.25$ was required for good to complete rejection. This may be due to some saturation of absorption due to the higher intracavity power (rather than probe beam) and due to simultaneous oscillation and rapid line switching effects which have not been considered. Additionally, the ratio of laser gains can be higher than the assumed values due to dissociation mixture balance and other effects. Because in practice the oscillation will always be somewhat away from optimum $00^0 2$ conditions the $00^0 1$ gain increases preferentially and should be compensated by increased absorbing power.

5.12 CO_2 $00^0 1$ FLUORESCENCE CELL DISCRIMINATOR

The function of this component was to unambiguously identify $00^0 1$ laser transitions. Absorption by room temperature CO_2 of regular CO_2 laser transitions is a resonant process ($\left[10^0 0, 02^0 0\right]_{I,II} - 00^0 1$); for low pressures

of CO_2 the absorption line is not collision broadened and has a line width $\sim$ 40 MHz. Following absorption of laser photons relaxation from the increased 00^01 population occurs to re-establish the equilibrium population fraction (determined by the temperature of the gas). Relaxation by spontaneous emission in V-R bands occurs (see Figure 5.11) and this has a characteristic band centre wavelength of 4.3 μm. The optogalvanic detection of $([10^00, 02^00]_{I,II} - 00^01)$ absorption for stabilization and discrimination will be presented in Chapter 9 and the use of narrow standing wave saturation resonances for OGE and optical detection investigated. The rotational splitting that results in the various J value transitions ensures resonant absorption of each 00^01 laser transition by the low pressure absorbing gas.

However, in general, sequence transitions have different frequencies which are statistically unlikely to overlap with the 00^01 resonant absorption lines. At 10P band centre the line spacing $(f_n - f_{n-1})$ is $\sim$ 55 GHz and the bandwidth for pressures below $\sim$ 1 torr Δf is $\sim$ 40 MHz. The probability (P) of a coincidence giving 4.3 μm fluorescence for 00^02 radiation presuming that the anharmonic shift of 00^02 relative to 00^01 is $>> \Delta f$ (it is $\sim$ 10 GHz) is given by

$$P \leq \Delta f / f_n - f_{n-1} \leq 10^{-3} \quad \ldots\ldots\ldots\ldots \quad (5.5)$$

which is insignificant because only ten or so lines are available in the signature. The inequality represents the possible false discrimination due to a positive fluorescence signal for 00^02 photons. By noting the specific laser power, improvement of the discriminating power by a factor $\sim$ 10 to 10^2 is achieved (with calibrated 4.3 μm photon yield). This discriminator system should be capable of identifying (see Figures 5.122 and 5.123) 00^01 radiated power with detection of sequence lines erroneously for only 1 in $\sim$ 10^4 to 10^5 lines.

It is possible to calculate the spontaneous emission flux per unit solid angle for a given experimental geometry[159] and it is well known[65,66] that the yield is particularly small and synchronous detection is usually

used. The spontaneous emission probability is small, (at 0.1 torr $\sim 10^{-5}$ cm^{-1}) and as a result the following considerations can be identified

1. The probing 00^01 laser beam is only very slightly attenuated .
2. The asymmetric stretch mode vibrational temperature is approximately the wall temperature, therefore, 000 is well populated whereas 00^01 has a very small population .
3. The $(10^00, 02^00)_{I,II}$ level set is only slightly populated but significantly more populated than $(10^01, 02^01)_{I,II}$ set.
4. Rotational equilibriating processes exist which reduce the fluorescence transition probability.
5. The CO_2 detecting gas is optically dense for the 4.3 μm photons and substantial reabsorption occurs.

The conclusion to be drawn from these observations is that the collected photon flux at 4.3 μm will be small.

Initially a discriminator cell was constructed which was of large diameter $\sim$ 2.5 cm and only small signals (< 1 μV for 1 W laser beam) could be obtained with a 77 K cooled InSb detector. A smaller diameter discriminator cell was constructed which minimized the distance from the interaction region to the KCl detector window ($\sim$ 5 mm). The fluorescence wavelength was identified by using a series of optical filters with different passbands placed between the detector and the source. It was established that the received wavelength lay between 3 and 7 μm and that the radiation was due to resonant absorption in CO_2 (substituting the CO_2 with N_2 produced no signal).

The dependence of 4.3 μm fluorescence intensity on pressure was

investigated to find optimum operating conditions for the discriminator. Figure 5.121 shows the fluorescence signal detected with the nitrogen cooled InSb detector using a 4 mm Ge filter over the pressure range 20 mtorr to 50 torr.

The results show a significant difference to those of Woods and Jolliffe[160] where nearly saturated output was measured $\sim$ 0.1 torr. The $00^0 1 \rightarrow 000$ yield should at low pressure increase with pressure as the ($10^0 0$, $02^0 0$) populations increase for a given temperature. Additionally, however, the reabsorption of the 4.3 μm photons is a resonant absorption process and the sheath of gas surrounding the interaction region becomes optically thick at higher pressures. There is qualitative agreement with this description but prediction of the exact peak fluorescence pressure (in this case at 4.5 torr) depends strongly on geometry (including beam parameters, divergence, profile, etc.). Fluorescence cells of this type are usually operated at pressures 0.1 → 0.6 torr so that saturated standing wave resonances (Lamb dips) can be observed for frequency reference (see Chapter 9). However, for sequence/regular band discrimination higher pressures can be used. Indeed there is some advantage in using higher pressures from the aspect of linearity (higher saturation). Figure 5.122 shows the 4.3 μm fluorescence signal increasing with increasing laser probe power. Some non-linearity is observed at 0.6 torr; the laser absorption significantly depletes the ($10^0 0$, $02^0 0$) population at powers of 5 to 10 W (20 to 40 W/cm^2). It is useful to use the discriminator as a measure of $00^0 1$ laser power when <u>mixed</u> $00^0 2/00^0 1$ laser outputs are being monitored and a strongly saturated fluorescence response (occurs at pressures below 0.2 torr) is not particularly useful. The frequency shifts of the $00^0 2$ lines (compared with $00^0 1$) can be seen directly with the Optical Engineering spectrum analyzer near 10 μm band centre. The shifts are all larger ($\sim$ 40 GHz) than the resolution of the system ($\sim$ 3 GHz); this has been illustrated in Figure 5.12.

The fluorescence photon yields are a function of rotational quantum number. The dependence of fluorescence intensity on transition J values

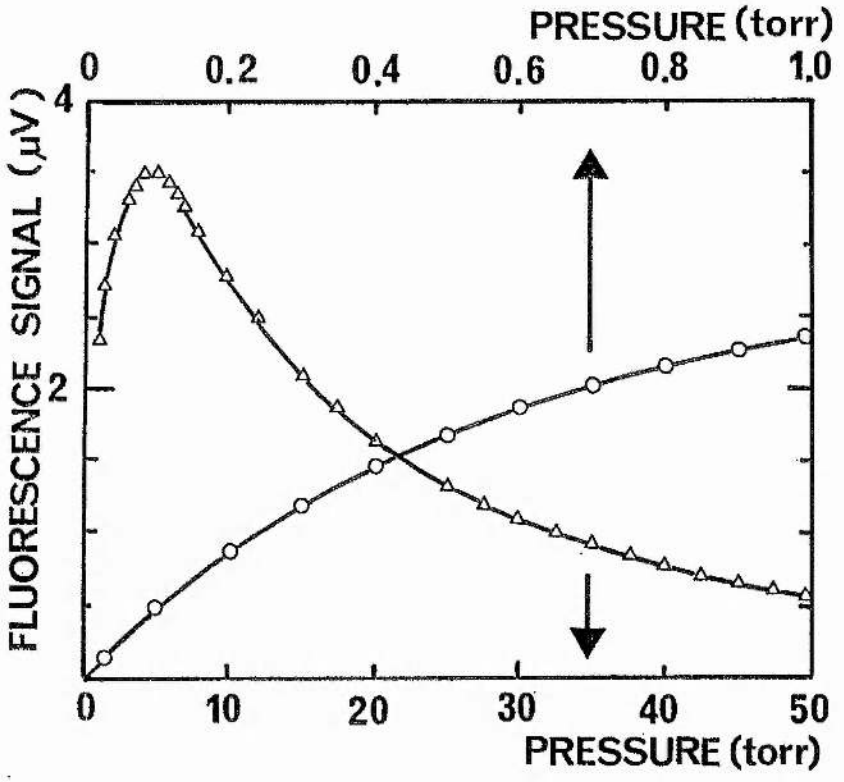

Fig. 5.121 $00^0 1$, 10P(22) fluorescence signal detected with RPY37, an InSb detector, Ge filter and X100 Brookdeal preamplifier. The probe beam, stabilized at line centre, had a power of 700 mW, and was positioned off axis close to the side window.

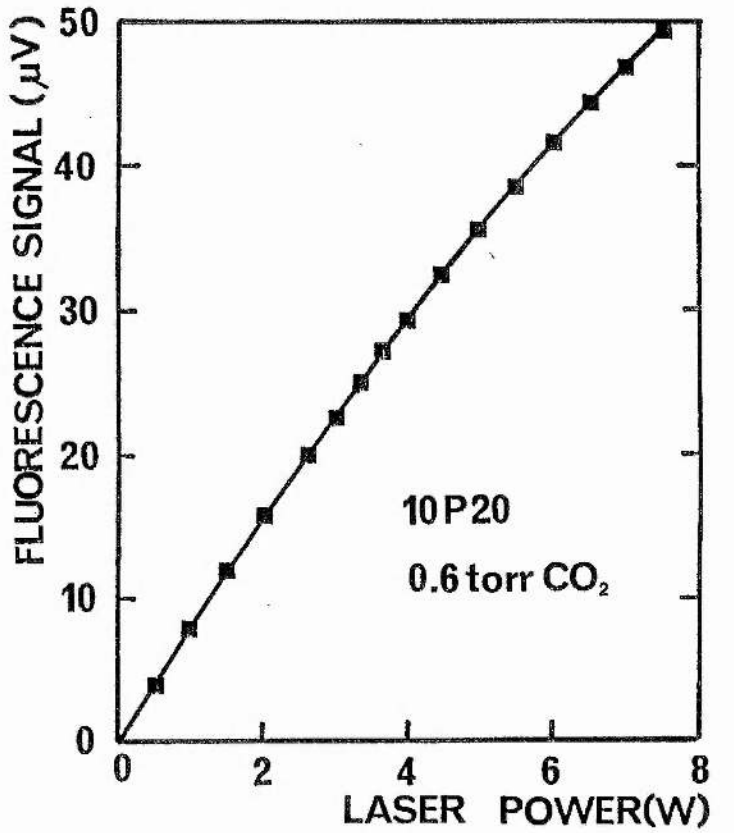

Fig. 5.122 $00^0 1$, 10P(20) fluorescence signal (as above) for 0.6 torr CO_2 using a compact laser to provide the probe beam.

were measured for the 10P band. A Boltzman distribution of the $00^0 1$ rotational sublevels was observed. This is due to the rapid rotational thermalization rate ($\sim$ 0.1 μs) which is very much faster than the $00^0 1$ relaxation rate ($\sim$ 1 ms). For a temperature of $\sim$ 300 to 400 K the Boltzman distribution peaks at P(20). A reduction of $00^0 1$ fluorescence to 30% of the 10P(20) value was measured at 10P(12) and a reduction to 50% of the 10P(20) value at 10P(26).

5.2 THE ADDITION OF Xe TO CO_2 SEQUENCE LASER AMPLIFIERS

The relatively low output power/unit length and efficiency of the $00^0 2$ sequence laser required experiments to improve the operating conditions so that small (< 1 m) devices may provide sufficient and maximized output power. Figure 5.21 shows how the optimum ratio of N_2/CO_2 was established over the practical current range. The N_2/CO_2 ratio of 2 to 3:1 was found a reasonable criterion for $00^0 2$ rather than the 1 to 2:1 ratio for $00^0 1$ for mixtures that are He rich (i.e. He/CO_2 ratio > 10:1). However, low He concentration mixtures have considerably reduced gain and ratios lower than $\sim$ 6:1 did not oscillate with output coupler reflectivities less than 95%. This gas composition (1:3:80, CO_2, N_2, He) for the 50 cm amplifier is in reasonable agreement with Reid and Siemsen's optimum[138,149] where it has been found that higher ratios of He/CO_2 than in the regular laser were optimum for flowing systems. However, in the flowing case lower He concentrations were tolerated (optimum $\sim$ 5:1 He/CO_2).

By using the two CO_2 sequence lasers with split discharges and three output couplers (98%, 95%, 94%) the output power for the optimum mixture 1 CO_2, 3 N_2, 10 He could be evaluated for the four lengths. The minimum amplifier length with 98% coupler is $\sim$ 40 cm and 1 W can be extracted from 50 cm. For 80 cm output power of $\sim$ 1.5 W has been achieved so far and approximately 3 W should be available.[158]

Figure 5.22(a) shows in the upper part how the <u>total</u> single mode laser output power varies as the hot cell pressure is increased for a

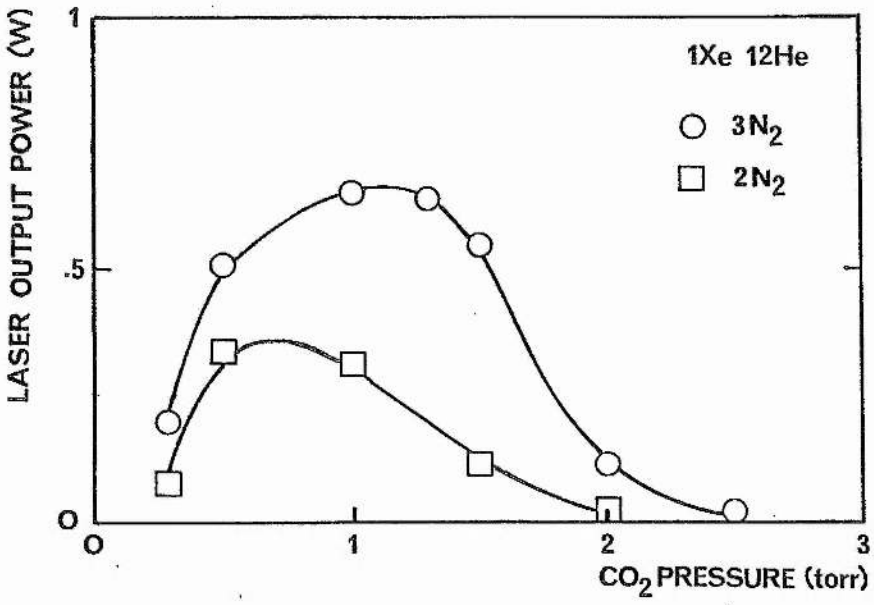

Fig. 5.21 The maximum single mode $00^{0}2$ output power available from the sealed 50 cm amplifier CO_2 sequence band laser (see Fig. 3.01 (b) and chapter 3.12) with optimization of current and selection of the output coupler (94%, 95%, 98%). The gas mixtures consisted of 12 torr He and 1 torr Xe with N_2 and CO_2 concentration as shown.

temperature of 350 C. A distinct discontinuity of power occurs at ∿ 25 torr. The 4.3 μm ($00^0 1$ - 000) fluorescence signal decreases (Figure 5.22(b)) in accordance with reducing $00^0 1$ laser power and the cut off of regular band oscillation occurs at 30 torr. From this information and the calibration of the fluorescence cell the $00^0 1$ and $00^0 2$ optical power contributions can be calculated and this is shown in Figure 5.22. The onset of $00^0 2$ oscillation is sharp and rises to a plateau value as the $00^0 1$ output is extinguished. For a narrow range of conditions both $00^0 2$ and $00^0 1$ oscillation can occur and this region was identified with the minimum in the output power curve (Figure 5.22(a)).

The addition of a small quantity of Xe, as used in the sealed regular band laser, resulted in considerable improvements in performance (up to 75% in output power, 50% in efficiency). However, if 1.5 torr Xe is added (see Figure 5.23) to the mixture of 1 CO_2, 3 N_2, 10 He then the plateau value of sequence band output power is increased from 0.25 W to 0.48 W. The decreasing $00^0 1$ power with increasing CO_2 absorbed pressure is essentially unchanged. The ability of Xe to assist in the maintenance of $00^0 2$ output power and efficiency is shown in Figure 5.23. Additions of more than 10% Xe decrease output power and less than 2% have little effect. Subsequently, this observation has been verified by investigations of Siemsen[161] who found similar increases for larger lasers of up to 80% and detailed gain experiments by Smith and Mellis[158] and Siemsen[161] have shown that additions of ∿ 5% Xe result in a small signal gain (α_0) increase for all slow flow rates. Increases of small signal gain in sealed systems due to Xe addition were not found by Siemsen and some beneficial effects other than dissociation control were suggested. Recent investigation by Mellis[158] has shown that sealed laser equilibrium CO_2 dissociation is considerably modified by Xe addition. Investigations of the dissociation ($2\ CO_2 \rightarrow 2\ CO + O_2$) rate constant k_d have shown that Xe, Kr, D_2 and H_2 all reduce k_d (and indeed ∿ 0.05 torr residual H_2 is beneficial in this respect). However, Siemsen has observed that all those gases other than Xe reduce the small signal gain. However, 5% Xe

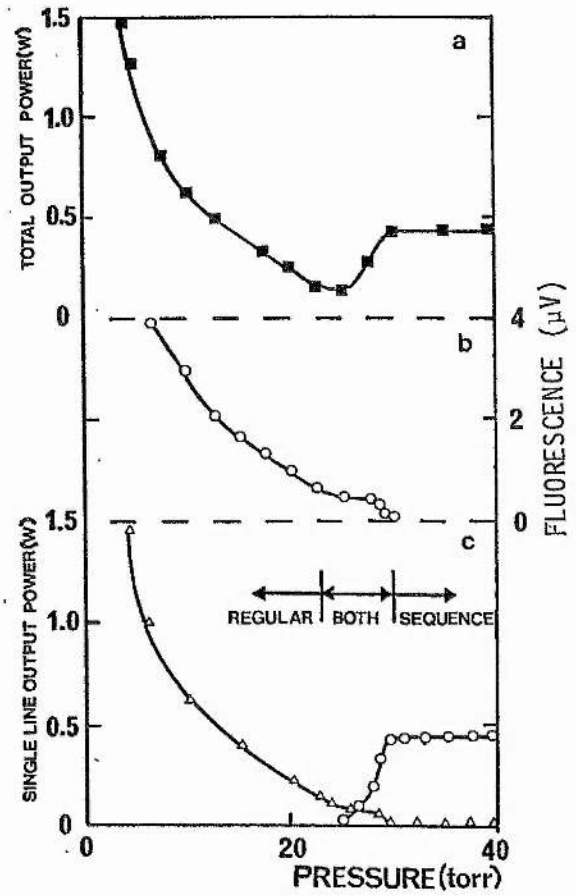

Fig. 5.22 Laser output power, 4.3 μm fluorescence signal and calculated regular and sequence power contributions with the variation of CO_2 hot cell pressure. The hot cell temperature was 350 C and the amplifier gas mixture was 1 Xe, 1 CO_2, 3 N_2, 12 He (torr).

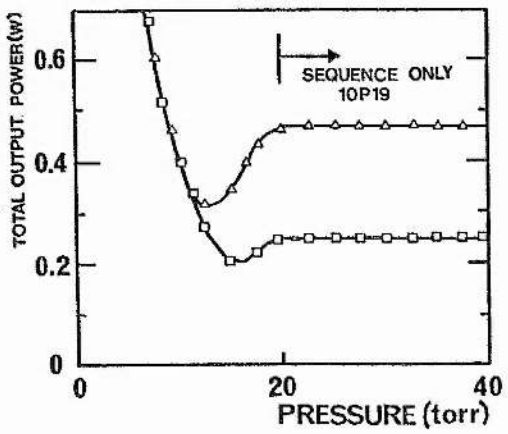

Fig. 5.23 The total laser output power variation (all $00^0 2$ above 20 torr) with the variation of hot cell pressure with conditions as above except the hot cell temperature was 400 C.

addition at high flow rates (∿ 1 L/min) gives gains close to the dissociation free case. Xe has a low ionization potential and a large crosssection for high energy electrons which otherwise are significant in dissociation. The result of the modified electron kinetics (changes in mean free path, lifetime and energy distribution) could improve the pumping mechanism or result in a larger fraction of energy being coupled to the asymmetric stretch mode. This would directly lead to the increase in electrical efficiency seen. But more significantly the change in electron kinetics could modify the CO_2 dissociation which is electron density and energy dependent. Alternatively, the small magnitude of the changes in small signal gain seen by Siemsen may be most significant because they occur in sealed oscillators (lower gain); very small changes in gain can cause larger variation of output power; also electron density changes could alter the saturation intensity as well as small signal gain which is not necessarily the most significant parameter in assessing oscillator output powers.

5.3 00^02 SEQUENCE BAND OPTOGALVANIC EFFECT

The first CO_2 00^02 sequence band optogalvanic measurement was made in these experiments and it has been described how the effect was used to stabilize a laser oscillator (Chapter 4.4). Initial experiments confirmed that the phase of optogalvanic signals in the low frequency regime < 300 Hz were the same as for the 00^01 laser by chopping (on and off) the radiation field and measuring the voltage and current changes. For constant current excitation the voltage across the discharge tube increased with increasing laser power at low frequencies (< 2 kHz) whereas it decreased at high frequencies for both 00^01 and 00^02 oscillation. Similarity with constant voltage excitation the circuit current was decreased and the tube voltage increased at low frequencies (< 2 kHz) for both 00^01 and 00^02 laser operation, whereas at high frequencies the circuit current increased and the tube voltage decreased with increasing laser power. The high frequency effect (described in Chapter 6), therefore, shows complete agreement in phase. By using

sinusoidal ac perturbation by PZT length modulation and phase sensitive detection the difference in the phase of 00^02 and 00^01 OGE signals at frequencies < 500 Hz were seen not to exceed $\pi/10$. Optogalvanic signal decay at frequencies greater than $\sim$ 800 Hz was observed consistent with the 00^01 situation (Figure 4.15) for both cc and cv excitation. A full high frequency optogalvanic spectrum up to 100 kHz was observed and no significant difference to the 00^01 case could be detected.

The amplitude of the 00^02 OGE signals was smaller than the regular band in all situations investigated which included the maximum operating range of pressure and current. A convenient representation of the optovoltaic shift for a dc on/off perturbation is to consider the increased discharge power (voltage change multiplied by current) brought about by switching the laser beam on from the non-oscillating state. The power change is not circuit dependent as other schemes are (see 3.2) and it is approximately constant over a wide range of excitation; therefore, it provides a good measure of any other parametric change occurring in addition to the optogalvanic perturbation. This concept will be used extensively in Chapters 7 and 8. Figure 5.31 shows the increased discharge power ΔP_{in} due to a laser field within the cavity that produces an output power P_{out} of 0 to 0.5 W. Previously, Figure 4.12 showed how the discharge voltage varied at cc for a change of laser output power. This representation showing the input electrical power perturbation which is the cc multiplied by the voltage shift has a similar form.

Because the pair of transitions 00^01 and 00^02 have different gains, the cavity losses (ξ) have to be set to different values, by different degrees of misalignment, for the same output power. For example, with full alignment of the output coupler, the 00^01 10P(20) maximum output power was $\sim$ 1.8 W whereas the 00^02 10P(23) maximum power was approximately 0.7 W so to obtain 0.7 W from the 00^01 transitions rather more loss has to be introduced. The optogalvanic signal is predicted to be linearly dependent on the losses factor (equation (7.28)). For an oscillator kept otherwise the same (mode,

excitation, diffraction losses, etc.) the ratio of the losses factor is just equal to the ratio of the saturated laser gains. Another way of describing this is as follows:- for a high gain transition (i.e. $00^0 1$) the number of photons produced per unit volume is greater than for a low gain transition. For the same irradiance and output power some of the high gain line photons must be given up deliberately; this is achieved experimentally by partial mirror misalignment. The ratio of the energy wasted per round trip is just N_1/N_2 where N_1 and N_2 are the photon creation rates per unit volume. For the same equilibrium beam irradiance the ratio of losses must be equal to this. Additionally, of course, the ratio of photon creation rates is just equal to the ratio of saturated laser gains α_1/α_2, therefore,

$$\frac{\alpha_1}{\alpha_2} = \frac{N_1}{N_2} = \frac{\xi_1}{\xi_2} \qquad \ldots\ldots\ldots\ldots\ldots\ldots \quad (5.6)$$

Taking the standard formulation of the laser gain (or absorption)[162] for a pressure broadened line

$$\alpha = \frac{g_2 A_{21}}{8\pi^2} \left[\frac{N_2}{g_2} - \frac{N_1}{g_1}\right] \frac{\lambda}{(\Delta\nu)} \qquad \ldots\ldots\ldots\ldots \quad (5.7)$$

where A_{21} is the spontaneous transition probability and N_1 and N_2 are the lower and upper level populations, the g factors are the degeneracies, λ is the line centre wavelength and $\Delta\nu$ is the optical broadening coefficient which will all be equal for $00^0 1$ and $00^0 2$ lines of close wavelength apart from the population differences and the transition probabilities, hence the ratio

$$\frac{\alpha_1}{\alpha_2} = \frac{\Delta N_1}{\Delta N_2} \frac{(A_{21})_1}{(A_{21})_2} \qquad \ldots\ldots\ldots\ldots\ldots\ldots \quad (5.8)$$

where ΔN_1 is the population inversion $(N_2 - N_1)$ of the $00^0 1$ transition and $(A_{21})_1$ is the $00^0 1$ transition probability, etc. The ratio of the transition probabilities has been measured by Reid et al[163] to be close to 2 (predicted by simple harmonic oscillator model) and for the 9.4 μm bands the transition probabilities, which are the square of the quantum mechanical matrix

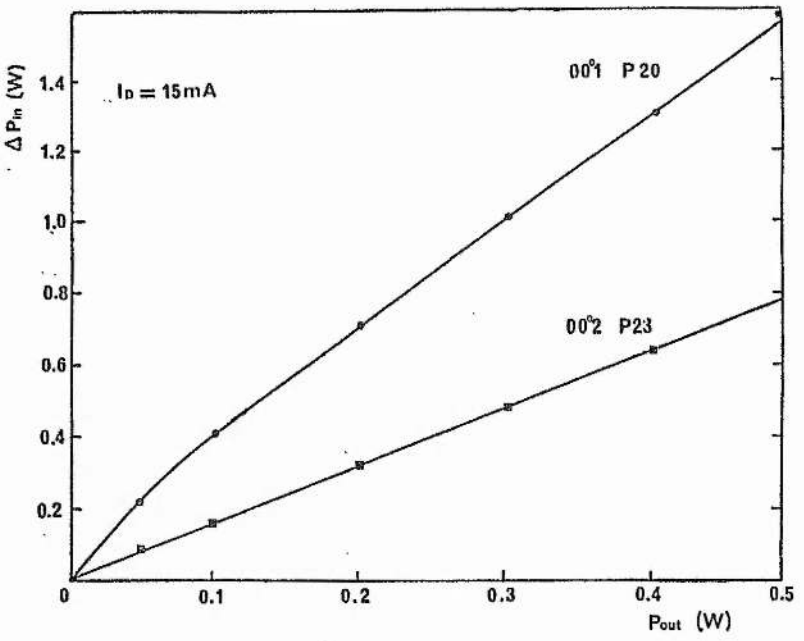

Fig. 5.31 Variation of changed input power (ΔP_{in}) with adjusted laser output power (P_{out}) for 15 mA cc excitation during 00^02 and 00^01 oscillation. The laser cavity was 1 m long, with a 50 cm amplifier and optimized 00^02 mixture at 16 torr.

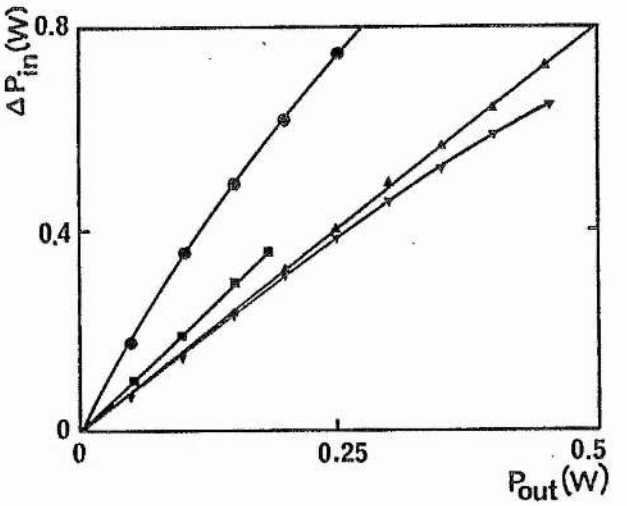

Fig. 5.32 The effect of increasing discharge current (increasing discharge temperature) for 00^02 sequence band OGE. The discharge power variation ΔP_{in} for a given laser output power is shown for (▼) 10 mA, (▲) 15 mA, (■) 20 mA 00^02 10P(23) oscillation and 10 mA (●) 00^01 10P(20) oscillation. The gas composition was 1.5 Xe, 1 CO_2, 3 N_2, 12 He (torr) with a 50 cm amplifier and 95% reflectivity output coupler.

elements, (μ) were found to be

$$\left[\frac{\mu_2}{\mu_1}\right]^2 = \frac{(A_{21})_2}{(A_{21})_1} = 1.89 \quad \ldots\ldots\ldots\ldots \quad (5.9)$$

Consequently, because the measured linewidths are equal

$$\frac{\alpha_1}{\alpha_2} = \frac{1}{1.89}\,\frac{\Delta N_1}{\Delta N_2} \quad \ldots\ldots\ldots\ldots\ldots\ldots \quad (5.10)$$

and because the optogalvanic response (ΔP) is just linear with losses factor from (5.1)

$$\frac{\Delta P_1}{\Delta P_2} = \frac{\xi_1}{\xi_2}\,\frac{1}{1.89}\,\frac{\Delta N_1}{\Delta N_2} \quad \ldots\ldots\ldots\ldots\ldots\ldots \quad (5.11)$$

The ratio of population difference is just a function of the asymmetric stretch vibrational temperature if the lower laser level differences is ignored. This appears to be a valid assumption because the populations are known to be small and good predictions of behaviour can be obtained whilst not taking account of this parameter.[118] For the current densities and mixtures used the vibrational temperature is $\sim$ 2500 K to 3000 K for a sealed laser and this directly gives a fractional upper laser level population ratio N_{002}/N_{001} of between 3.5 and 4.[118] If the lower populations are presumed to be zero then

$$\frac{\Delta P_1}{\Delta P_2} = \frac{1}{1.89}\,\frac{N_{002}}{N_{001}} \sim 1.6 \text{ to } 2.0 \quad \ldots\ldots\ldots \quad (5.12)$$

It can clearly be seen from Figure 5.31 that a 10 mA excitation current optogalvanic ratio $\Delta P_1/\Delta P_2$ is 1.8.

Figure 5.32 shows the variation of optogalvanic ratios over the full operating current range; the $00^0 2$ optogalvanic change is greater for high currents (20 mA) compared to currents 10 to 15 mA. An excitation power increase also causes an increase in optogalvanic perturbation (due to increasing gas temperature - see Chapter 8 for details). At optimum currents the perturbation will be relatively large due to the maximized gain which results in a higher loss being required for a given output beam power. By

comparing only the maximum output power for a given current, equal values of losses factor are observed and hence the slope differences show only the gas temperature differences due to P/L changes. For this low pressure mixture the P/L increases from ∿ 1.5 W/cm to 2.5 W/cm for a current increase from 10 mA to 20 mA. The corresponding increase in the predicted ΔP (from (7.28) and (7.29)) using Shields and Smith's[164] empirical temperatures (see Chapter 8) is a factor of ∿ 25%; the actual increase is 27%.

The exact ratio of power changes $\Delta P_1/\Delta P_2$ will for a laser oscillation, be equal to the ratio of saturated laser gains. The effect of laser action will be to reduce ΔN and it is possible that ΔN_{oo2} will be reduced more or less than ΔN_{oo1} for a given output beam (ΔP_{out}) due to the lower pumping rate and other factors. For very low beam irradiances (output powers ∿ 50 mW) when the cavity is considerably misaligned then the stimulated emission de-excitation mechanism is small compared with the collisional relaxation processes. Because the ratio $\Delta P_1/\Delta P_2$ obtained in this regime is similar in value to the ratio over most of the operating range it seems that any difference in saturation parameter is not particularly significant.

5.4 CO MOLECULAR LASER OPTOGALVANIC EFFECT

The CO laser exhibits considerable kinetic differences to the CO_2 laser, however, it is electrically efficient (∿ 10 to 20%) and can generate high cw output powers per unit length (∿ 20 W/m). As a result, the optogalvanic perturbation is expected to be large because of gross electrical perturbations occurring due to the large laser radiation field within the discharged volume.

The CO vibrational excitation is due to the electron impact with the CO molecules which populates the lower vibrational levels. Vibrational-vibrational-translational (V-V-T) collisions distribute the excitation to higher levels and the vibrational population equilibrium is determined by both V-T and V-V-T relaxation of high energy levels. The CO vibration is anharmonic so that relaxation of the higher levels is reduced and population of the levels ∿ 5 to ∿ 15 are approximately equal.

Multimode CO laser output usually occurs on a large number of $v + 1 \rightarrow v$, $J - 1 \rightarrow J$, P band V-R transitions (wavelength in the 5 μm region). If grating line selection is used then output on a few closely spaced lines occurs[141] and the output power per unit length is reduced from $\sim$ 20 W/m to $\sim$ 1 W/m. The reduction in power and efficiency is due to the nature of the transitions in the vibrational system which are usually a series of cascades of approximately equal energy transitions with a loss of one rotational and one vibrational quantum.

Room temperature cooling can be used for efficient sealed CO lasers[109] as long as careful mixtures and hydrogen free, high vacuum systems are used. The beneficial addition of Xe[165] and O_2[166] to CO and He mixtures results in the particular high gain mixture of 0.1 torr O_2, 1.4 torr CO, 2.5 torr Xe and 25 torr He being used in these experiments. The discharge v-i characteristic is shown in Figure 5.41. The perturbed characteristic for 2, 4, 6, 8 and 10 W output beam is also shown. The total cavity losses include 5% output coupling. The excitation consisted of a cv power supply with 200 kΩ ballast to each tungsten anode and 200 kΩ to the copper cathode; the split discharge total length was 90 cm.

The optogalvanic perturbation is large for cv excitation even though the circuit gain amplification factor is low compared to CO_2 (due to the flatter nature of the v-i characteristics at the optimum current). The gas amplification factor can be determined approximately; when a 10 W beam is extracted from the cavity the laser discharge voltage at 16 mA increases from 2.9 kV to 3.53 kV (with beam on) with a current reduction of 0.7 mA. This current change will, at most, increase the discharge voltage by 50 V (from the v-i characteristic). The amplification factor was, therefore, approximately 1.08. The voltage shift can be treated as a cc power change (because the gas amplification factor is approximately unity) and then compared (Figure 5.42) to the CO_2 case; this comparison results in the same order of magnitude optogalvanic effect. The exact comparison of magnitude could not be made because the precise losses of the CO laser cavity were

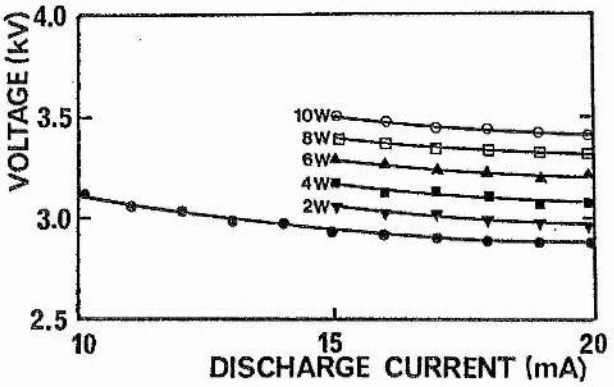

Fig. 5.41 The variation of discharge voltage (one 45 cm segment) with discharge current for different laser output powers selected by varying the misalignment of the 95% Ge output coupler. The gas composition was 1.4 CO_2, 2.5 Xe, 0.1 O_2, 22 He (torr).

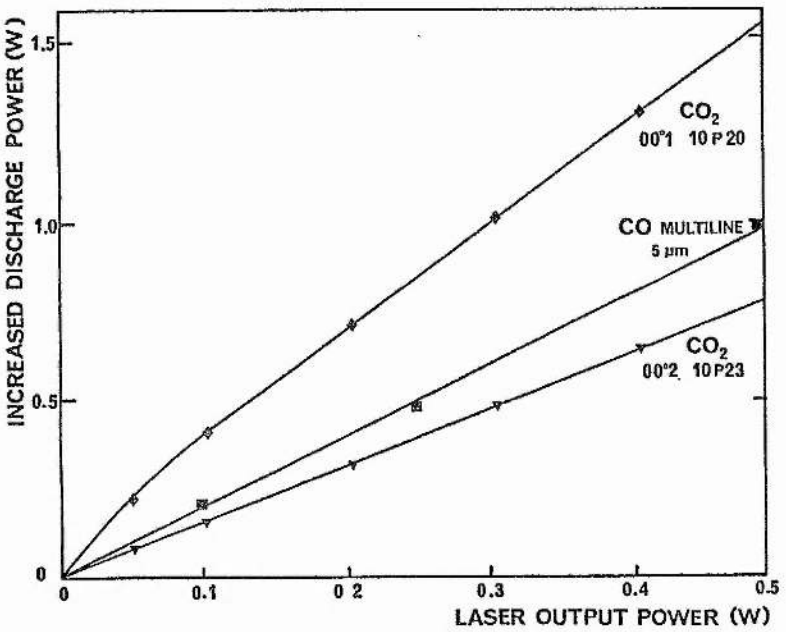

Fig. 5.42 The variation of increased discharge power ΔP_{in} for the 90 cm active length CO laser described above and the 50 cm CO_2 sequence band laser.

unknown. Assuming 7% total cavity losses and taking the power perturbation during full alignment, the CO effect is of similar magnitude to the CO_2 $00^0 1$ effect because the minimum losses factor of the sequence 5 W CO_2 laser (including Brewster windows) was $\sim$ 20%. The doubled discharge of the CO laser gives twice the voltage (power) change but the reduction of a factor of 2 to 3 in the minimum losses compensates for this. The consideration of cavity losses is included in the theory, elucidated in Chapters 7 and 8.

The V-V rate coefficients for CO laser discharges have been calculated by Lightman and Fisher.[167] Assuming a mean vibrational level $\nu = 10$ the rate $k_{VV} \sim 1.5 \times 10^{10}\ s^{-1}$ $(\nu \rightarrow \nu - 1)$. The number density (N) of the $\nu = 10$ vibrational population has been calculated by Davies, Roberts, Smith and Thompson[168] and measured by Lightman and Fisher[168] to be $\gtrsim 10^{14}$, a suitable experimental value for $\nu \rightarrow \nu - 1$ is $N_{\nu 10} = 1.5 \times 10^{14}\ cm^{-3}$. The limiting time during which the upper laser level can re-establish equilibrium by collisions due to radiation is just given by

$$t_{\nu=10} = k_{VV}\, N_{\nu 10} \sim 2 \times 10^{-4}\ s$$

In other words, as in the case of CO_2 laser upper level $(00^0 1)$ relaxation, any changes in gas heating cannot occur in the CO laser gas faster than $\sim$ 200 μs; in the CO_2 laser the limiting time was found to be approximately 0.5 ms (see Chapter 6).

The investigation of the OGE spectrum used signal pick off by transformer coupling (Figure 3.226) to a double discharge Edinburgh Instruments PL3. The PZT was driven with 4 V rms (producing amplitude modulation $\sim$ 0.1 to 0.5% rms) and the laser was emitting 0.5 W. Figure 5.43 shows the OGE spectrum which was attenuated at low frequencies due to the feedback circuit of the cc power supply (EI 183D). The current fluctuation caused by optical amplitude modulation fell rapidly at frequencies above 4 kHz and was no longer detectable above 10 kHz, in good agreement with the 200 μs prediction by vibrational kinetics. The phase at 8 kHz was delayed by $\pi/2$ rad relative to frequencies below 2 kHz which were of the same phase (rising laser power →

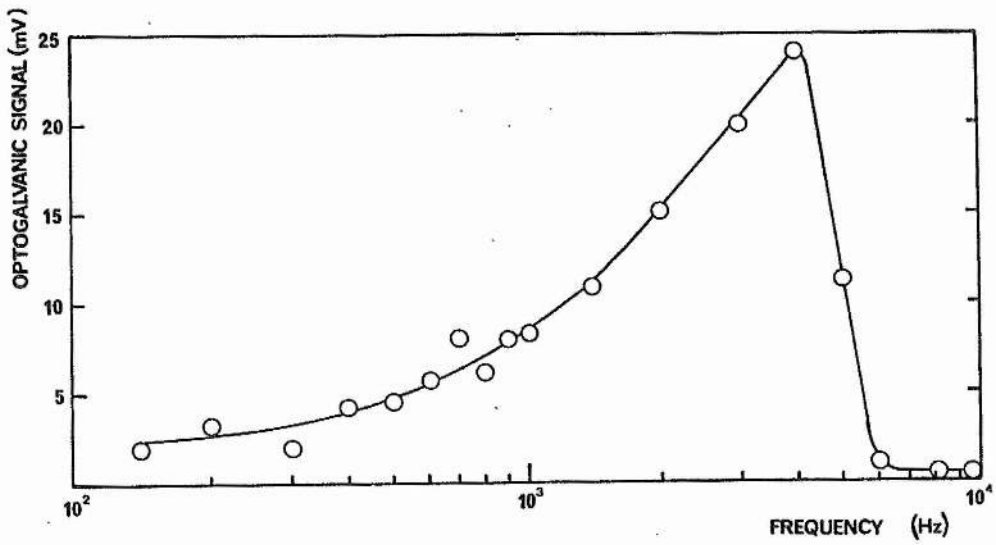

Fig. 5.43 The effect of cavity length modulation frequency on the OGE discharge perturbation in the CO laser. The signal was transformer coupled and is shown as the voltage across the 1:1 secondary. The discharge conditions were 20 mA with a cc supply, 1.6 m cavity and a 30 torr gas mixture (0.8 CO, 1.0 Xe, 5.5 N_2, 23 He) at - 20 C.

rising voltage). No high frequency effects above 10 kHz could be found even by increasing the PZT drive by a factor of 25. The response of the PZT tube is known to extend above 20 kHz, therefore, it was concluded that no high frequency signals $\lesssim$ 50 kHz could be measured. This was consistent with the CO_2 analysis because the lower laser relaxation route analogous to T_L has the same relaxation rate in the CO case as the upper laser route (T_U) and, therefore, the two frequency band behaviour should not be observed (see Chapter 6). Some of the low frequency signal decay 500 Hz to 3 kHz may not be due to the power supply feedback but could be kinetic in origin; this could be investigated with a more flexible power supply facility which was not available at the time this experiment was performed.

6.0 HIGH FREQUENCY OPTOGALVANIC EFFECT IN CO_2 LASER DISCHARGES

This section will describe the first direct experimental evidence of the optogalvanic effect at frequencies above 4 kHz in CO_2 laser discharges and presents a detailed kinetic explanation for two distinct process regimes for the low pressure range, 5 to 30 torr. The low frequency signal regime, $f < 2$ kHz is due to the effect so far investigated and the high frequency regime 5 to 100 kHz is explained in terms of another kinetic pathway involving the lower laser complex which relaxes at a more rapid rate. Stabilization with modulation frequencies in this regime is described and certain advantages including faster servo response times and improved signal to noise ratio can occur.

The higher frequency effect is smaller in amplitude and experimentally difficult to investigate due to the lack of simple modulation techniques in this frequency band. Some particularly small signals were also received above 100 kHz but could not be characterized by phase with the equipment available. This very high frequency effect is not likely to be due to gas temperature changes or indeed any momentum exchange effect, but could be due to the very small ionization effect which is normally swamped by the much larger gas temperature effects at lower frequencies.

In order to use a gas temperature explanation for the discharge perturbations some knowledge of the propagating pressure wave in the gas is required. It is necessary initially to know that the radially propagating changes of density can take place sufficiently quickly for the re-establishment of a new number density equilibrium and temperature profile during the modulation half cycle (see Chapter 7.1). The sufficient time (t_{min}) for a new equilibrium to be established across the diameter is approximately

$$t_{min} \sim r/v_s \sim 0.5\ \mu s \quad \ldots\ldots\ldots\ldots\ldots \quad (6.1)$$

where r is the radius and v_s is the speed of sound. In this situation the gas ballast pressure is not necessarily varying and the volume ratio used in calculating the size of the effect is reduced. If the maximum critical distance is to the most distant part of the system (reservoir), then the minimum time is $\sim$ 1 to 2 ms. Providing the reduced volume ratio is recognized, the gas temperature changes are allowed due to the radial propagation of number density changes up to rates of $\sim$ 200 kHz sufficient for the bandwidth of the observed high frequency effect.

The exact acoustic resonance frequencies are of interest because any such modes could result in maxima or minima of the OGE spectrum. Fortunately, the modes are simply calculated because of the cylindrical geometry which is well known in acoustics (e.g. musical instruments).

The wave equation can be used to consider harmonic dependency with time and it may be written in terms of the velocity potential Φ

$$\Phi = \psi\ e^{i\omega t} \quad \ldots\ldots\ldots\ldots\ldots\ldots \quad (6.2)$$

where ω is the angular frequency. For cylindrical wavefronts and assuming a cylinder which is infinitely long it is necessary to only consider waves with rotational symmetry; two components of Φ are zero valued

$$v_\phi = \frac{\partial \Phi}{\partial \phi} = 0 \quad \ldots\ldots\ldots\ldots\ldots\ldots \quad (6.3)$$

$$v_z = \frac{\partial \Phi}{dz} = 0 \quad \ldots\ldots\ldots\ldots\ldots\ldots \quad (6.4)$$

and the wave equation can be simplified to

$$\frac{d^2\psi}{dr^2} + \frac{1}{r}\frac{d\psi}{dr} + k^2\psi = 0 \quad \ldots\ldots\ldots\ldots\ldots\ldots \quad (6.5)$$

which is Bessel's equation to the zeroth order. The solution of this equation is well presented in standard texts.[169] The solution gives modes determined by three mode numbers (lmn) and their frequencies are denoted ω_{lmn}. The Bessel coefficients are simply evaluated by the theory of cylindrical functions and the main symmetrical radial mode which is of interest here, f_{100}, is given by

$$f_{100} = \frac{C_o \beta_1}{2\pi} = \frac{3.8317}{2\pi}\frac{C_o}{r} \quad \ldots\ldots\ldots\ldots \quad (6.6)$$

where 3.8317 is the $\beta_1 r$ product of the first Bessel coefficient and the radius, and C_o is the speed of sound in the gas. Succeeding radial modes f_{200}, f_{300}, etc. are simply related by β_2, β_3, etc.

The speed of sound for particular gas mixtures was not evaluated but the He value is known. (The laser gas mixture is typically 80% He). The velocity of sound C_o is simply

$$C_o = \sqrt{\frac{K\,p}{\ell}} \quad \ldots\ldots\ldots\ldots\ldots\ldots \quad (6.7)$$

where K is specific heat, p is the pressure and ℓ the density. Hence, the velocity of sound (ideal gas) does not depend on pressure at constant temperature since according to Boyle's law the density is directly proportional to pressure; the p/ℓ ratio is therefore constant. Strictly, in this application, this may not be valid but insofar as it is only necessary to identify the approximate frequencies of the lowest modes this is not important. The sound velocity for He at 300 K is 965 ms^{-1} (for CO_2 = 259 ms^{-1}, N_2 = 334 ms^{-1}) and at 150°C it is 1085 ms^{-1}, using the linear approximation. Hence,

$$f_{100} \sim \frac{3.83}{2\pi} \times \frac{1085}{4\times10^{-3}} \sim 200 \text{ kHz}$$

as simply shown in equation (6.1) and successive values occur

$$f_{200} \sim 300 \text{ kHz}, \; f_{300} \sim 400 \text{ kHz}, \text{ etc.} \quad \ldots\ldots \quad (6.8)$$

Any minima due to radial standing acoustic waves should not occur below $\sim$ 200 kHz. The crucial experimental minima is at $\sim$ 2 kHz and radial acoustic standing waves cannot account for this. The lowest longitudinal standing wave resonance occurs at $\sim$ 1 kHz sufficiently close to the major OGE minimum. However, this minimum longitudinal acoustic should not fall to zero because there is still a considerable radial ballast volume (due to the small optical mode filling factor $\sim$ 0.25) and only a considerable reduction of signal could be predicted at frequencies much higher than this, i.e. $\lesssim$ 20 kHz (see section 7.4). The optogalvanic minima attributed to kinetic effects at $\sim$ 2 kHz falls to < 2% of the maximum signals.

The acoustic system is, therefore, adequate to support number density changes up to $\sim$ 100 kHz within the radiating volume and some reduction of the signal magnitude at frequencies $\gtrsim$ 20 kHz is predicted by the reduction of ballast volume for rapid changes of number density.

6.1 DETAILED MOLECULAR KINETIC THEORY OF HIGH FREQUENCY OPTOGALVANIC EFFECT IN CO_2 LASER DISCHARGES

The kinetic perturbation mechanism for connecting the modulation of the laser cavity length (at frequency f) with the resultant discharge current (or voltage or both) fluctuation has been described qualitatively in Chapters 2 and 4.1; the quantitative theory will be presented in the next chapter. The effect so far described is summarized in the upper part of Figure 6.11. The radiatively stimulated transitions (shown as $h\nu$ laser) from the $00^0 1$ upper laser level compete directly with the otherwise dominant V-V-T relaxation process

$$CO_2\,(00^0 1) + M \rightarrow CO_2\,(n,m^0,o) + M + T_U$$

where M represents all the possible collision partners CO_2, CO, O_2, N_2, He, Xe and minority species. The energy factor T_U represents the surplus energy given by the exothermic process to translational energy (i.e. the sum kinetic energy of all the molecules).

Both de-excitation processes, leading to either $h\nu_{LASER}$ or T_U energy loss, transfer the CO_2 excited population to a closely coupled group of levels which have been labelled 010 in Figure 6.11 for convenience. This population (010) rapidly relaxes by collisional processes to the ground state giving up all of the vibrational energy as translational energy (shown as T_L in 6.11). It is important to notice and distinguish these two routes of energy exchange.

The left hand side of the lower part of Figure 6.11 shows the simplified explanation of the conventional low frequency effect which was introduced in Chapter 4.0. When the laser field intensity <u>increases</u> (for a quasi-equilibrium change or small ac perturbation) by improved alignment or cavity length modulation at frequency f (driving the cavity mode <u>towards</u> a laser line centre), T_U will <u>decrease</u> because more 00^01 population is removed by $h\nu$ laser photon induced transitions. To summarize, there are relatively fewer V-V-T collisional relaxations and T_U decreases. The energy exchange via T_L is unaltered because all the population still flows through the 010 group and the total pump rate to the 00^01 level is constant for both halves of the modulation cycle. Consequently, there is a net decrease in the transfer of energy to the gas (T_U decreased, T_L unaltered at the modulation frequency f when the laser field is increasing; the localized number density in the radiating volume is increased and the discharge impedance increases. The current is subsequently modulated at frequency f out of phase (π radians) with the radiation field and decreases for cc excitation; the current is in phase with the amplitude modulation of the radiation field for cc operation.

The roll-off of the OGE in the 1 to 2 kHz region can be explained in terms of the upper state V-V-T relaxation process rate. For the gas mixtures

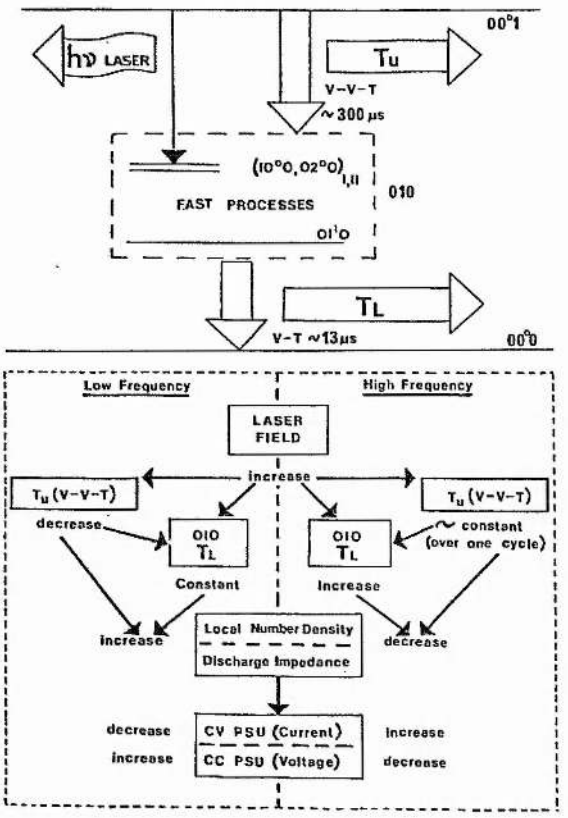

Fig. 6.11 Simplified energy level diagram (upper) for the CO_2 laser and the OGE process diagram (lower) in two modulation process regimes.

(1) UPPER LASER LEVEL $00^0 1$

OPERATING GAS FILL 2 Xe + 2 CO + 3 CO_2 + 5 N_2 + 16 He (torr)

(a) $T_{gas} = 37.3 \frac{p}{L} + T_{wall}$ (EMPIRICAL SHIELDS AND SMITH)

$= 37.3 \times \frac{55}{33} + 278$

$T_{gas} = 340$ K

(b) DEACTIVATION CONSTANTS FOR $00^0 1$ LEVEL

$k_{Xe} = 30$; $k_{CO} = 240$; $k_{CO_2} = 340$; $k_{N_2} = 130$;

$k_{He} = 86$ ($s^{-1}torr^{-1}$), $k_{H_2O} = 3.3 \times 10^4$

(SOURCES, MOORE ET AL, CHEO, TAYLOR ET AL, AND OTHERS)

multiplying by partial pressure of constituents

60 + 480 + 1020 + 650 + 1370 = 3580

(c) LIFETIME $\tau_{00^0 1} = \frac{1}{3580} = 0.3$ ms

(2) LOWER LASER LEVEL COMPLEX $01^0 0$

OPERATING GAS FILL 2 Xe + 2 CO + 3 CO_2 + 5 N_2 + 16 He (torr)

(a) $T_{gas} = 340$ K

(b) DEACTIVATION RATES FOR $01^0 0$ LEVEL

$k_{Xe} = 44$; $k_{CO} = 400$; $k_{CO_2} = 200$; $k_{N_2} = 4$;

$k_{He} = 4000$ ($s^{-1}torr^{-1}$), $k_{H_2O} = 10^5$ to 10^6

86 + 8000 + 600 + 2000 + 64000 = 75000

(c) LIFETIME $\tau_{01^0 0} = \frac{1}{75000} = 13$ μs

Fig. 6.12 Calculation of CO_2 laser level lifetimes.

used here it is a simple matter to calculate the relaxation time of the $00^0 1$ level by collisional de-excitation (see Figure 6.12). For a mixture of 3 torr CO_2, 4 torr N_2, 1 torr Xe and 18 torr He and assuming 30% CO_2 dissociation, and rate constants for a gas temperature of 370 K the $00^0 1$ relaxation rate is predicted to be $\sim$ 3100 s^{-1} giving a relaxation time t_{001} against collisional relaxation of $\sim$ 300 μs. Therefore, as the cavity length modulation frequency is increased the $00^0 1$ population fluctuations at f should reduce as $f \rightarrow 1/2\ \tau_{001}$ or $f \sim 1650$ Hz as has been previously observed here (see Chapter 4) and by others.[45,46,53] Thus the f frequency modulation component of energy transfer to molecular translational motion ($T_U(f)$) also becomes small and the number density, discharge impedance and current fluctuations at frequency f are reduced.

However, if $f \gtrsim 1/2\ \tau_{001}$, T_L acquires a modulated component at frequency f. Although the laser field stimulated transitions 001 $\rightarrow$ 010 are still modulated at frequency f, due to the field amplitude modulation, the f modulation of the V-V-T 001 $\rightarrow$ 010 transition is less ($\rightarrow 0$ as $f \gg 1/2\ \tau_{001}$) and hence the arrival rate of 010 population is not the same for the two halves of the f modulation cycle and the 010 population fluctuates, modulating T_L. Or to express it in another manner, when the modulation frequency is low, each half of the modulation cycle f represents a kinetic equilibrium state (constant pumping and equilibrated relaxation process), but with the increase in f the V-V-T process is too slow to re-establish and maintain an equilibrium over the cycle period. So as seen on the right hand side of the lower part of Figure 6.11, as the laser field changes so although T_U remains unaltered, now T_L increases as the field increases, leading to a number density decrease and hence a current increase. Thus the current response is now (high f) in phase with the cavity length modulation.

As the cavity length modulation frequency increases to become comparable with $1/2\ \tau_{001}$ so $T_U(f)$ decreases and $T_L(f)$ acquires a non-zero value, resulting in an optogalvanic signal phase change. But $T_L(f)$ will

in turn decrease as $f \rightarrow 1/2\ \tau_{010}$, where τ_{010} is the V-T collisional relaxation rate of the 010 group, which for this gas mixture was calculated to be $\sim$ 13 μs, hence when $f \rightarrow 40$ kHz.

6.2 HIGH FREQUENCY DETECTION OF OGE SIGNALS

Some early reports by Gower and Carswell[50] and Aoki[49] showed some high frequency current oscillations in low pressure absorbing/amplifying CO_2 discharges undergoing pulsed optical perturbations; Kindl[43] hypothesized that at least two time constants would be necessary to fully describe the low frequency chopped cw OGE signal. Measurement of the effect above $\sim$ 2 to 4 kHz was not achieved until this work and this was probably largely due to the following reasons:

1. Pulse response relaxation is difficult to interpret.
2. Intracavity chopping at rates above $\sim$ 500 Hz is physically difficult.
3. Large amplitude perturbations at higher frequencies lead to laser Q switching.

The general scheme adopted here for high frequency detection in oscillators was to use small amplitude ($\sim$ 1 to 5%) modulation which produces small optogalvanic effects maintaining a quasi-equilibrium state of the laser populations and discharge. Some pulsed investigation was attempted and Figure 6.21 shows the effect on an oscillator discharge caused by applying an amplified pulse to the PZT (slew rate 1 V/800 ns) (from a Farnell double pulse generator with 100 W class B valve amplifier). The slow nonlinear voltage ramp at the right hand side of the trace shows the optogalvanic signature being recorded at a rate $\sim$ 500 Hz as shown in Figure 4.13. Several turning points in the current corresponding to laser power maxima and minima are visible. During the rapid decreasing ramp in PZT voltage (left side of photograph) the signature is again demonstrated at a rate of $\gtrsim$ 8 kHz ($T \sim 100$ μs) for thirteen tuning points in 2 ms.

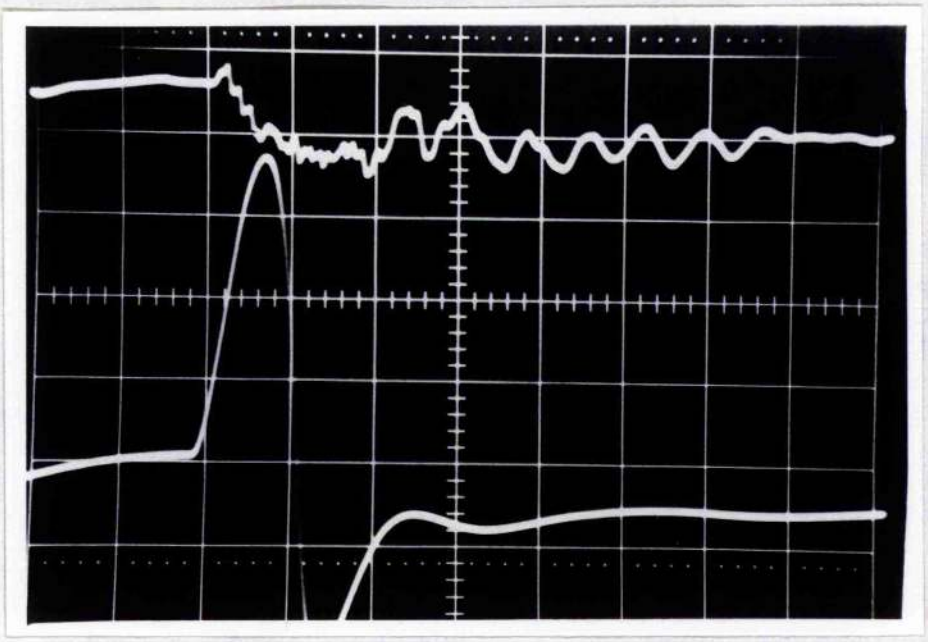

Fig. 6.21 Upper trace shows the optogalvanic signal from a series 10 kΩ resistor for the compact laser with 0.5 V/major division for a 10 mA constant current excitation. The time axis (horizontal) was 2 ms/major division and the lower trace shows the voltage applied to the PZT with 200 V/major division. A Farnell dual pulse generator feeding a 50 Ω load into a Mullard 100 W class B valve amplifier into 100 Ω load was used to drive the Lansing PZT. The output power changes were monitored with a pyroelectric detector and were ∿ 28%.

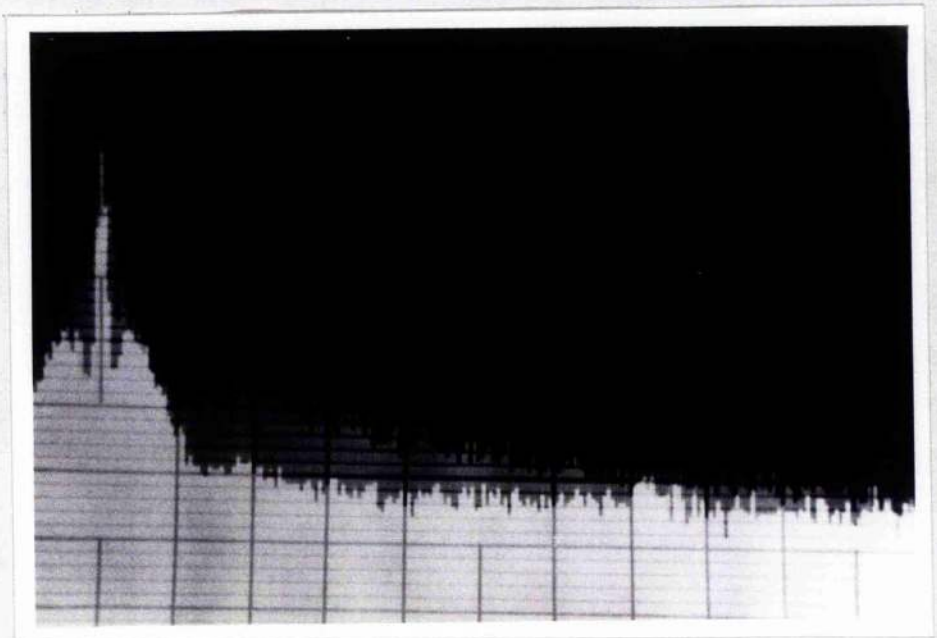

Fig. 6.22 Spectrum of laser discharge noise (white) and OGE signal (grey) up to 100 kHz (10 kHz/major division). The vertical scale is logarithmic 10 dB/major division and the zero frequency marker is clearly shown at the left.

There is additionally a delay ∿ 0.6 ms after the PZT voltage ramp commences before the high frequency signature begins. The amplitude is smaller than the slow ramp case by a factor of ∿ 2:1. The signal to noise ratio is high in this experiment (see extremities of OGE trace) because the perturbations are whole signatures (∿ 30% amplitude) and because optimum discharge current has been chosen.

Another good demonstration of the high frequency signals was achieved by modulating the laser with a 10 Hz square wave applied to the PZT with an amplitude of ∿ 50 V. Because the harmonic structure of the resulting high modulation is rich in harmonics (particularly odd) and because the slope of the laser line profile is non-linear (nearly parabolic) a whole OGE spectrum can be observed in real time (Figure 6.22). The white envelope is the discharge and modulation electrical current noise taken with the beam off and the darker envelope is the current signal with the beam on. The low frequency effect ∿ 1 kHz can easily be seen in the left hand side major division near the zero marker. The signal from 2 kHz to ∿ 8 kHz is lost in the noise and then increases to reach a maximum at ∿ 20 kHz. Because the modulation harmonics are reducing with frequency the high frequency pass band is selectively attenuated at higher frequencies. However, the signal is still larger than the noise up to ∿ 94 kHz. This particular PZT has a strong resonance at ∿ 12 kHz shown by the response peak. This gives preliminary evidence of improved signal to noise in the high frequency band and the possibility of using PZT resonances for modulation with lower power amplifiers.

The detailed investigation of the high frequency effect was achieved by using small ac perturbations of the cavity length which was initially adjusted by setting the dc bias voltage on the PSD so that the cavity mode was at the maximum slope of a signature segment. The best exact setting was found to be midway between the power minimum intersection of two transitions and the peak of a high gain transition such as 10P(20). This length position allows the maximum amplitude modulation without intersecting

the maximum or minimum point. Cc and cv supplies were used and the variation of tube voltage and current monitored with a spectrum analyzer, storage oscilloscope and PSD. The cc supply permits less current fluctuation below frequencies of 400 Hz and consequently lower voltage fluctuations result due to the reduced gas amplification factor. Additionally, instrumental phase changes of low frequency current perturbations occurred due to both power supply feedback limitations and anomalous phase changes caused by PZT dc level shifting with increasing frequency (modulation second harmonic distortion). This produces predominantly 2f signals close to line centre and line changing length values. These effects when coupled together result in a broad OVE resonance at $\sim$ 600 Hz as observed by Scholtz[125] who has designed a circuit to linearize the output signal. However, by systematic investigation using several lasers and PZT translators with different known resonances only one significant phase change was observed at $\sim$ 2 kHz coincident with the signal minimum.

Figure 6.23 shows the OGE signal for cv excitation (i.e. current perturbation $\Delta i/i$) which is opposite in phase to the radiation field at low frequencies, but steadily decreasing in amplitude as the frequency increases and reaches a near zero minimum at 2 to 3 kHz for the particular mixture, current, etc. shown. The current fluctuation also occurs at higher frequencies, but with reversed phase (i.e. in phase with the radiation modulation). A maximum amplitude is reached in the 10 to 20 kHz region before the signal decreases and disappears at $\sim$ 100 kHz. The behaviour near the crossover suggests subsidiary maxima and minima. The separate phase curve shows how the phase reversal extends from $\sim$ 1 to 3 kHz.

This behaviour is in good agreement with the $1/2\ \tau_{001}$ low frequency decay at 1.5 kHz and the $1/2\ \tau_{010}$ high frequency decay at 40 kHz. The predicted phase reversal occurs as predicted in 6.1 and a low frequency effect delay of 0.6 ms has been measured which correlates well with the time for the collisional relaxation from 001, i.e. the communication time for $00^{0}1$ population fluctuation to affect the gas translational temperature.

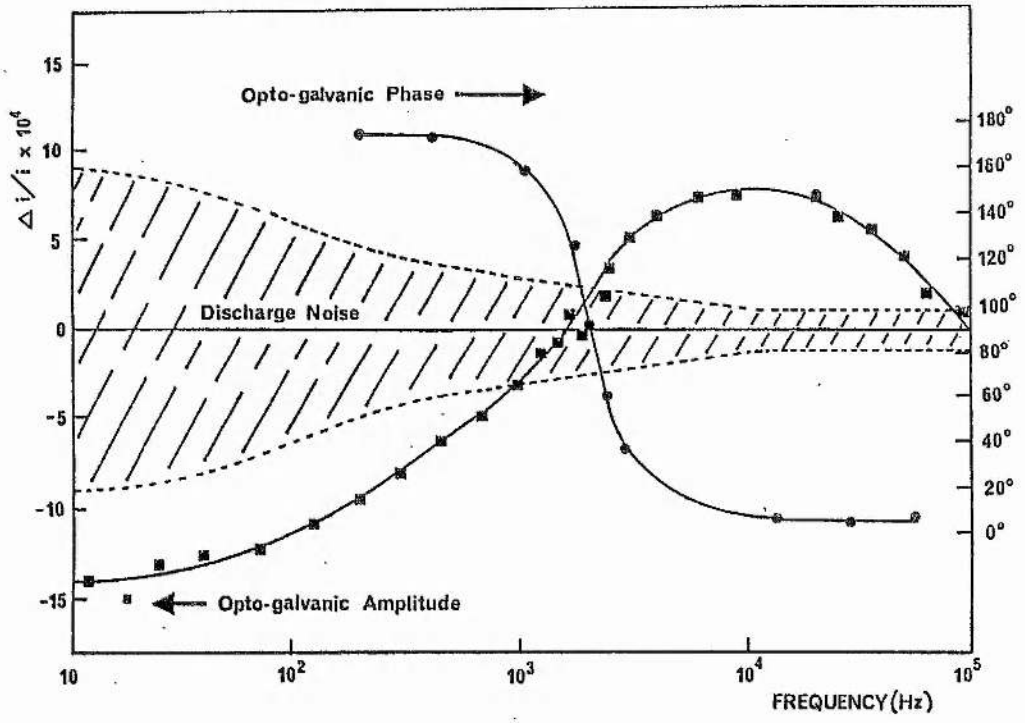

Fig. 6.23 Variation of OGE signal $\Delta i/i$ and OGE phase with length (100 nm) modulation frequency for the CO_2 laser with cv excitation. The dashed lines show the envelope of the amplitude of the power supply harmonics noise induced current fluctuations $\Delta i/i$ for a typical commercial power supply, as measured with a HP 3580A audio frequency spectrum analyzer.

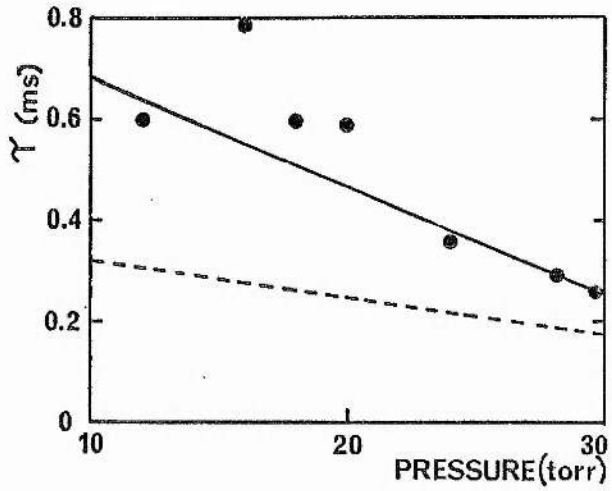

Fig. 6.24 OGE minimum frequency (f) represented as $\tau = 1/2f$ compared with calculated time constant for $00^0 1$ relaxation rate with variation of the total pressure change of the amplifying discharge. The experimental results are shown as (●). The H_2O free calculation is shown as a solid line and with 0.05 torr H_2O is shown as a dashed line. The gas composition is the same as in Fig. 6.12.

The variation of the OGE signal null and high frequency decay with operating pressures and current were investigated. No strong dependence of the low frequency decay ($\sim$ 2 kHz) on current was observed but a small shift towards a lower frequency phase turnover at high current of > 20 mA was found. The effect was $\lesssim$ 400 Hz for a 10 mA increase and it could be due to the increased CO content due to the increased equilibrium partial pressure; the CO de-excitation rate for $00^0 1$ is high $\sim$ 240 s^{-1}. Additionally, the increased P/L results in increased gas heating and because all of the rates are temperature dependent, the level lifetime will vary in a complicated manner.

However, total pressure increase did result in a large increase of null frequency corresponding to an increased de-excitation rate. Figure 6.24 shows how the null time constant (1/2f) shifts close to the value predicted with no H_2O or H_2 content. The experiment was repeated with a heated palladium tube to reduce H_2 partial pressure and no change in the null time constant was observed. This suggests that the residual H_2O content in these lasers is low (<< 0.1 torr). No increase of the high frequency roll-off (80 kHz) could be observed with increased pressure, but with reduction of laser pressure to 10 torr some shift to low frequencies was observed.

The high frequency plasma oscillation seen by Gower and Carswell[50] (discussed in 2.3) corresponds well in frequency to the peak of the high frequency effect. The resonant nature of this bandpass function may give rise to ringing at $\sim$ 50 kHz when strong impulsive (TEA pulse) excitation occurs. Similarly, in the low frequency passband when certain excitation conditions exist (see Figure 4.15 and Scholtz and Schiffner[125]) a peaked response may occur. This ringing behaviour was not observed in these experiments; it may only be apparent with very intense pulses.

6.3 ACTIVE STABILIZATION OF CO_2 LASERS BY HIGH FREQUENCY OGE STABILIZATION

The lasers and electronic feedback systems used for high frequency stabilization are as previously described for low frequency stabilization,

except that the PZT is driven via a capacitative mixer from a low impedance ac source capable of supplying high voltages and a lower impedance dc source for cavity correction. The modified circuit is shown in Figure 6.31. In some cases twin PZT's were used so that isolation of the ac dither from the dc correction signal was achieved.

The improvement of amplitude stability, which for a passive cavity drifts $\sim$ 10 to 20% per hour, is evident in Figure 6.32. A high modulation frequency of 14.6 kHz was used and with suitable feedback gain intensity fluctuations were reduced to $\lesssim$ 0.3% for 10P(20) line centre stabilization. The ac preamplifier was set to have a low frequency roll-off at $\sim$ 8 kHz to reduce the large noise fraction contributed in the low frequency band and servo response times of between 50 and 100 ms were achieved, consistent with a 'tight lock' providing < 0.5% intensity jitter. The long term stability remains as in the low frequency case and $\lesssim$ 0.3% stability was observed over 8 to 10 hour periods. Offset locking with deviations up to $\pm$ 15 MHz was used and this produced little noticeable degradation of intensity stability.

Frequency stability was assessed in detail by beating two independently stabilized lasers together, in some cases one or both lasers were stabilized off line centre by offsetting the PSD operating point with a known ac input signal at the reference frequency. Over long periods (up to 4 hours) the frequency drift was less than 50 kHz (compared with greater than 20 MHz unstabilized) and the frequency resettability (after the feedback loop had been opened) was always better than 100 kHz.

At all times low frequency jitter of 100 to 400 kHz appeared due primarily to the power supply ripple of 1 to 5 V rms which consequently perturbed the optical cavity length by modulating the discharge refractive index with the predominantly 100 Hz ripple. This can be avoided along with reduced water vibration broadening by the techniques discussed in Chapter 4.

The higher modulation reference frequencies used result in the capability of faster collection of error data and faster length correction.

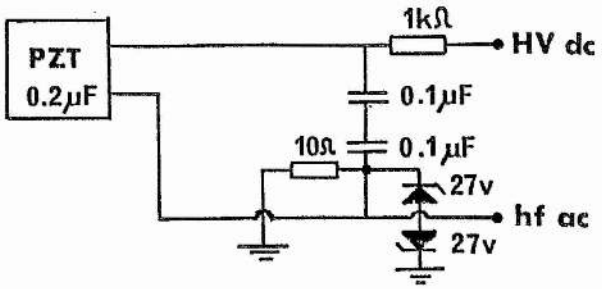

Fig. 6.31 Modified modulation circuit for high frequency modulation (up to 100 kHz).

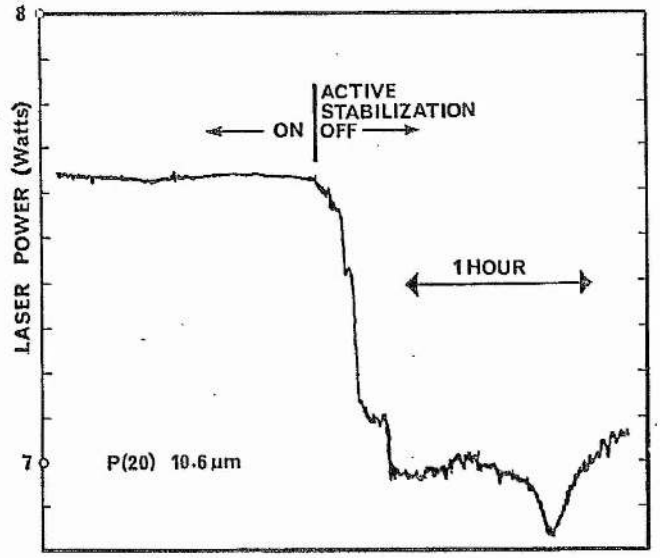

Fig. 6.32 Comparison of CO_2 laser single mode power with high frequency OGE active stabilization with passive stabilization only, for a compact sealed laser.

The dc drive to the PZT (0 to ∿ 1 kV) used for cavity correction requires a high slew rate into the capacitive element; the Burleigh PZ81 (see 3.2) has a good specification in this respect but either a suitable matching circuit of faster drive capability will be required to improve the servo response beyond 50 to 100 ms. Additionally, a minimum amount of post detector integration is required for a given PSD and use of more linear lower noise (perhaps digital) PSD's may provide considerable improvement. The low frequency stability could not achieve much useful stabilization below 1 s and the fastest useful response with the high frequency system was 50 ms. The table shown in Figure 6.33 shows the 30 s frequency jitter width for various limiting time constants for the system and a comparison with the low frequency case is given.

By constructing systems with 1 to 2 orders of magnitude improvement which critically damped time constants of 1 to 10 ms, correction of the laser frequency jitter due to the power supply ripple and water vibration should be possible. Additionally, reduction of acoustic interference in the audio frequency band (up to 100 to 1000 Hz) will be achieved. This improvement will depend on faster electronic drive for ac modulation and dc correction and perhaps improved PSD specification (dynamic range). Increasingly, lasers are being used not only in optical laboratories but in less controlled environments and rejection of vibration and acoustic interference is necessary. Even commercial antivibration surfaces permit substantial vibration at low frequencies (up to 100 Hz) which cannot be corrected with most stabilization systems (time constant $\gtrsim$ 1 s). This high frequency OGE stabilization method can satisfy the requirements of fast error correction and has an inherently low susceptability to microphony due to the distributed discharge detector.

7.0 THEORY: DISCHARGE POWER PERTURBATIONS

This chapter presents a simple optogalvanic perturbation model of CO_2 laser discharges with considerable predicative power that shows how the

τ_L	Δf_{30}
LF OGE 1 s	620 kHz
HF OGE 1 s	740 kHz
300 ms	780 kHz
100 ms	1.6 MHz
50 ms	2.1 MHz
30 ms	5.3 MHz
10 ms	NO LOCK

Fig. 6.33 The 30 s frequency jitter widths (Δf_{30}) for the high frequency stabilized compact laser for various feedback loop time constants (τ_L). The ac and dc gain has been optimized in each case. The laser was stabilized to 10P(20) line centre and the output power was ~ 8 W. A low frequency OGE jitter width is shown for comparison; the modulation details are as described for Fig. 6.32.

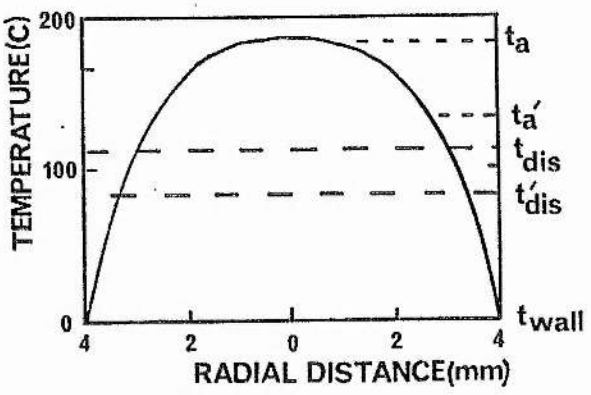

Fig. 7.11 Radial temperature profile of the laser discharge. The mean discharge temperature t_{dis} is reduced to t_{dis}' (by kinetic cooling) when the radiation field is switched on.

optogalvanic effect in a CO_2 laser discharge depends on input excitation, gas pressure, composition and temperature; the comparison of the predictions with experiments will be presented in Chapter 8. In Chapter 2 a brief description of the gas temperature explanation was given as extant from the work of Brooks,[52] Smith and Brooks[53] and originally Rigden and Moeller.[40] In Chapter 4 a more detailed kinetic description was presented in order to explain the solution of the stabilization problem by positive column optogalvanism. It is the purpose of this whole chapter to provide, for the first time, a precise quantitative temperature perturbation model, and the first section (7.1) describes some of the features of the physical system and some simplifications. Subsequently in 7.4 a discussion of the limitations imposed by these simplifications and other considerations will be given.

7.1 SUMMARY OF THE CO_2 LASER KINETICS

The CO_2 asymmetric stretch mode is pumped by resonant N_2, CO and CO_2 V-V transfer and by direct electron impact. In a laser discharge normal relaxation for this mode population is dominated by V-V-T exothermic processes

$$CO_2(00^01) + M - CO_2(n,m,o) + M + T$$

which result in gas heating due to the translational (kinetic) component T; here M represents all possible collision partners CO_2, CO, N_2, He, Xe and T is the excess kinetic energy supplied to the gas. Stimulated emission from the discharged volume removes energy directly from the asymmetric stretch system (see Figure 6.11) and reduces the number of V-V-T transitions supplying kinetic energy to the gas (kinetic cooling). The change in translational energy (and the resultant modified temperature profile) is simply related to the electrical input power via the perturbation in the number density (due to kinetic cooling) of electron collision partners. Figure 7.11 shows the form of the radial temperature profile which is

approximately parabolic[170,171] with some typical values for a low pressure laser discharge. The axial temperature (t_a) is maximum and the wall temperature (t_{wall}) is fixed by the coolant. The mean difference of these temperatures, t_{dis} varies with any change of translational (kinetic) energy.

Assume initially a very simple (sealed) system where a discharged volume is totally radiating stimulated photons (see Figure 7.12(a)). The emerging flux of energy results in a kinetic cooling of the gas which, because the number of molecules and the volume are constant (N per cc), causes a reduction in pressure. For cc excitation the voltage will not change with a radiation change to the first order and there will be no thermal optogalvanic effect because the number of collision partners will remain the same. There may, of course, be a smaller effect because the change in momentum of the molecules can alter the energy exchanged by electron collisions.[60]

A further degree of complexity is shown in Figure 7.12(b). The cross-section of the discharge again has a uniform current density (A) but only a part is radiating with a uniform beam irradiance (B). The volume B will have a reduced number density and the remaining volume will have a suitably increased number density as B starts to radiate (in order to conserve the number of particles). The result will be no optogalvanic effect as in the previous case because the average number density of collision partners over the area is constant. The momentum exchange effect will be reduced.

Another increase in complexity is demonstrated in Figure 7.12(c) where only a part of the total volume (D) is uniformly discharged (C) and all of that volume is radiating. The consequence of this structure is a large optogalvanic effect because the number density change of collision partners is maximized, however, the precise amplitude will depend on the ratio C/D, i.e. the active to dead volume ratios. The experimental apparatus used here has (due to the gas reservoir) a D:C volume ratio of > 30 and the ballast volume D can initially be considered to be infinite. The most physical description of the laser oscillators requires a further degree of

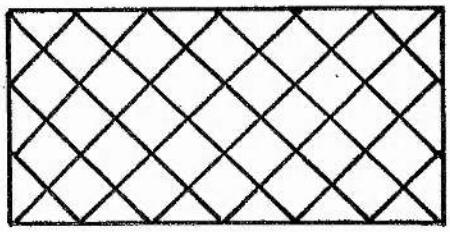

(a) Fully and uniformly discharged and radiating volume $\Delta N = 0$, no optogalvanic effect

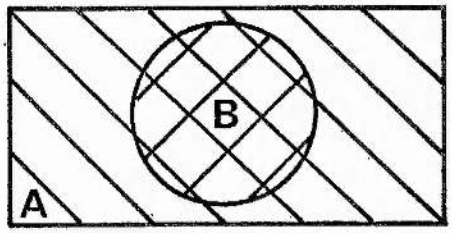

(b) Fully and uniformly discharged volume (A) partially radiating (B) ΔN_A and $\Delta N_B \neq 0$ but $\Delta N_{AV} \sim 0$, no optogalvanic effects

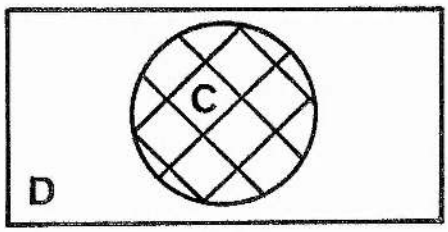

(c) Coincident partial uniform discharge and radiating volume (C) $\Delta N_C \neq 0$, large optogalvanic effects

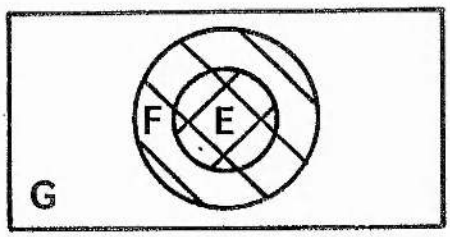

(d) Partial uniform discharge (F) which is partially filled with uniform radiating field (E) $\Delta N_F \neq 0$, large optogalvanic effects reduced by factor E-F/G.

Fig. 7.12 Simple diagramatic representation of the physical geometry of the laser amplifiers whilst radiating.

complexity; part of the total volume (G) is uniformly discharged (F) and only part of this (E) is uniformly radiating. The local number density (E) increases with radiation but the remaining (F-E) discharge number density decreases only by a factor (F-E/G). Hence, the cross-section averaged number density change is proportional to E-(F/G) which results in a small OGE dependent on the ratio of the volumes E, F and G.

Practically, it is not possible to assume that the beam is radiating from the total discharge volume because the TEM_{oo} mode has a form which results in the majority ($\sim$ 90%) of the photon flux emanating from the 1/e beam radius volume and the tube is designed (for optical reasons) to have an aperture of $\sim$ 1.5 times the 1/e beam diameter (see Figure 3.115). This correction is simply made by assuming the partially discharged volume is partially radiating and the assumption of uniform irradiation and discharge can still be made by taking average values of current density, number density, temperature and beam irradiance as shown in Figure 7.11(b).

Optically induced modifications of translational energy (temperature) which result in number density changes can be averaged out in this way only because the changes are quasi-equilibrium, i.e. this analysis would not be valid for pulsed systems. If the translational energy is reduced (say), then the local irradiated number density increases (isobaric kinetic cooling) and consequently the electron collision frequency increases because the number of possible electron collision partners increases. Collisions with neutrals is the major electron energy loss process in a weakly ionized molecular discharge and, therefore, as the number of collisions increases the electrical input power increases (for cc excitation).

7.2 POWER PERTURBATION THEORY FOR CO_2 LASER OSCILLATORS

Consider one electron in the positive column of a CO_2 laser discharge. The energy gained by the electron per second E_g due to the accelerating electric field E is

$$E_g = E\, e\, v_d \quad \ldots\ldots\ldots\ldots\ldots\ldots \quad (7.1)$$

where e is the electronic charge and v_d is the electron drift velocity. For an electron density of n_e electrons per cc the energy gained per second per unit volume of discharge is

$$E_g' = E\, e\, v_d\, n_e \quad \ldots\ldots\ldots\ldots\ldots\ldots \quad (7.2)$$

The positive column current density j is given by

$$j = e\, n_e\, v_d \quad \ldots\ldots\ldots\ldots\ldots\ldots \quad (7.3)$$

and hence from (7.2) and (7.3) the gained electron power density is

$$E_g' = E\, j \ (W\ cm^{-3}) \quad \ldots\ldots\ldots\ldots\ldots\ldots \quad (7.4)$$

Now consider the energy lost by a single electron; this will be proportional to the number of collisions n_{coll} and the energy lost per collision E_{coll}. The energy lost per second is, therefore, given by

$$E_l = n_{coll}\, E_{coll} \quad \ldots\ldots\ldots\ldots\ldots\ldots \quad (7.5)$$

However, for an electron density of n_e the energy lost per cc by the electrons due to collision with neutral partners is

$$E_l' = n_e\, n_{coll}\, E_{coll} \quad \ldots\ldots\ldots\ldots\ldots\ldots \quad (7.6)$$

Collision with molecules is the dominant energy loss process for electrons and assuming that the energy loss per collision is constant (a reasonable approximation see Smith and Brooks[53]) then any change of electron energy loss is primarily due to a change in the number of collisions which occur. The number of collisions is directly proportional to the number density of all the possible collision partners (n) for a simple two body process. Hence

$$\frac{\Delta E_l'}{E_l'} = \frac{\Delta n}{n} \quad \ldots\ldots\ldots\ldots\ldots\ldots \quad (7.7)$$

where $\Delta n/n$ is the fractional number density change. This equality requires that both n_e and E_{coll} remain constant and the total number of gas molecules is constant during the perturbation (molecular number density is conserved in a sealed laser). For a cw molecular discharge the electron energy gained due to the accelerating electric field equals the energy lost by collisions. Hence, in fractional terms

$$\frac{\Delta E_g'}{E_g'} = \frac{\Delta E_1'}{E_1'} = \frac{\Delta n}{n} \quad \ldots\ldots\ldots\ldots\ldots\ldots \quad (7.8)$$

The gas pressure (p) is related to number density n by

$$p = \frac{1}{3} n m \bar{v}^2 \quad \ldots\ldots\ldots\ldots\ldots\ldots \quad (7.9)$$

Hence, the number density in terms of <u>mean</u> molecular translational energy (T) is

$$n = \frac{3p}{m\bar{v}^2} = \frac{3p}{2T} \quad \ldots\ldots\ldots\ldots\ldots\ldots \quad (7.10)$$

The total number change dn, by differentiation is

$$dn = \frac{\partial n}{\partial P}\bigg|_T dp + \frac{\partial n}{\partial T}\bigg|_P dT \quad \ldots\ldots\ldots\ldots \quad (7.11)$$

If the non-irradiated volume is large compared to the radiating volume then the pressure remains approximately constant and $dp \simeq 0$. The first term of (7.11) is negligible compared to the second term. Hence, the isobaric approximation is valid

$$dn = \frac{\partial n}{\partial T} dT = -\frac{3p}{2T^2} dT \quad \ldots\ldots\ldots\ldots \quad (7.12)$$

For a small finite number density perturbation Δn in fractional terms

$$\frac{\Delta n}{n} = -\frac{\Delta T}{T} \quad \ldots\ldots\ldots\ldots\ldots\ldots \quad (7.13)$$

where T is the mean translational energy of each molecule in the gas and ΔT is the change brought about by a number density change Δn.

Now when the CO_2 laser field is switched on by appropriate cavity

alignment a beam irradiance I ($W\ cm^{-2}$) is set up. An energy creation and loss equation can be set up for the whole radiating volume

$$\frac{\partial E}{\partial t} = N\ h\ \nu\ LA - I\ \frac{\xi}{2}\ A = 0 \quad \ldots\ldots\ldots\ldots \quad (7.14)$$

where the first term is the photon creation and the second term is the energy lost from the whole system (N is the generated photon number ($s^{-1}cm^{-3}$) and LA is the radiating volume). The losses factor ξ takes into account the output beam, reflection and absorption losses associated with the optics, and loss due to the tube aperture. For a cw beam the power creation and loss are equal, hence

$$I = \frac{2N\ h\ \nu\ L}{\xi} \quad \ldots\ldots\ldots\ldots\ldots\ldots \quad (7.15)$$

The energy removed by photons per unit volume per second (ℓ') is given by

$$\ell' = N\ h\ \nu = \frac{I\xi}{2L}\ (Js^{-1}cm^{-3}) \quad \ldots\ldots\ldots\ldots \quad (7.16)$$

This energy is removed directly from the vibrational asymmetric mode of the CO_2 population. Competing relaxation from this mode occurs via V-V-T processes which result in an equilibrium translational energy stored in the gas. When the laser field is switched on this process is reduced and the stored translational energy and gas temperature reach new equilibrium values.

Empirically, it is found[165,172] that the discharged gas translational temperature, (t_{gas}) for a laser discharge of this kind is given by

$$t_{gas} = t_w + t_{dis} = t_w + m\ \frac{P}{L} \quad \ldots\ldots\ldots\ldots \quad (7.17)$$

where t_w is the wall temperature, t_{dis} is the increased axial temperature due to the discharge, m is a constant precisely dependent upon the gas pressure and composition approximately 40 to 70 for the range of input powers per unit length 1 to 3 W/cm, and P/L is the electrical input power per unit length. Expressing this as the unit volume gas translational energy

$$T_{gas} = \frac{3}{2}\ nk\ (t_w + m\ \frac{P}{L}) \quad (J/cm^3) \quad \ldots\ldots\ldots\ldots \quad (7.18)$$

As the stimulated emission removes Q (W) from the CO_2 asymmetric stretch mode translational energy is removed from the gas (via the V-V-T processes) and a change in gas translational energy occurs

$$\Delta T = \frac{3}{2} \frac{n k m}{L} Q \quad \ldots\ldots\ldots\ldots\ldots\ldots \quad (7.19)$$

The fractional change of translational energy is given then simply from the previous two equations

$$\frac{\Delta T}{T} = \frac{m Q}{L (t_w + m P/L)} = \frac{m Q}{L t_w + mP} \quad \ldots\ldots\ldots \quad (7.20)$$

The total energy removed by photons from the whole discharge is from equation (7.16)

$$Q = - v \ell' = \frac{- I \xi V}{2L} \ (W) \quad \ldots\ldots\ldots\ldots\ldots \quad (7.21)$$

where $V = \pi L r_b^2$, the partial discharge volume is assumed to be uniformly radiating (r_b is the 1/e beam radius > 80% of the beam lies in this volume); therefore, by substituting into (7.20)

$$\frac{\Delta T}{T} = \frac{-\pi r_b^2 \xi I}{2(L t_w/m + P)} \quad \ldots\ldots\ldots\ldots\ldots \quad (7.22)$$

It is known from equation (7.14) that there is a simple relationship between fractional number density and fractional translational energy changes, and letting A be the beam cross-sectional area (πr_b^2)

$$\frac{\Delta n}{n} = - \frac{\Delta T}{T} = \frac{A \xi I}{2(L t_w/m + P)} \quad \ldots\ldots\ldots\ldots\ldots \quad (7.23)$$

The electrical input power fluctuation $\Delta P/P$ due to the laser irradiance I set up in the oscillator cavity is in fractional terms

$$\frac{\Delta P}{P} = \frac{\Delta E_g'}{E_g'} = \frac{\Delta n}{n} \quad \ldots\ldots\ldots\ldots\ldots\ldots \quad (7.24)$$

from equation (7.4) and (7.8). Experimentally, only voltage and current parameters are easily measurable and these discharges have a negative

differential positive impedance characteristic.[170] If the current i is allowed to vary (as in conventional cv series ballast excitation) then the input power fluctuation is a function of the external circuit.[53] Cc excitation removes the gas amplification factor G (see Chapter 3.211) which magnifies the perturbation (during cv operation). Although large signals are observed in the OGE mode with cv operation and judiciously selected ballast resistance (slightly larger than discharge impedance) the channel noise is also amplified and either constant S/N or reduced S/N with increasing G at low currents is observed (see Chapter 8.2).

Experimentally then, beam irradiance (I) is set by varying the cavity alignment (part of the losses factor ξ) where the current (i) is maintained constant by using a cc power supply at many selected values and the change in the resultant tube voltage (v) is measured. Microscopically, holding the tube current constant corresponds to controlling the product of electron density and drift velocity (equation (7.3) but individually these parameters are allowed to change. However, from (7.4) this power perturbation theory is general and valid for any power perturbation providing the gas amplification factor G is considered. The experimental case where i is constant is additionally the most simple to evaluate. The electrical input power fluctuation $\Delta P/P$ is numerically equal to the fractional change of gained electron power density (see equation (7.4), (7.7) and (7.8)), and this in turn is equal to the fractional number density change (7.8), therefore,

$$\frac{\Delta P}{P} = \frac{\Delta E_g'}{E_g'} = \frac{\Delta n}{n} = \frac{A\,\xi\,I}{2(L\,t_w/m + P)} \quad \ldots\ldots\ldots \quad (7.25)$$

The electrical input power change ΔP (W) is, therefore, for cc excitation

$$i\Delta v = \Delta P = \frac{A\,\xi\,I}{2(L\,t_w/Pm + 1)} \quad \ldots\ldots\ldots \quad (7.26)$$

Experimentally, the laser radiation field was adjusted by a fixed misalignment of one of the cavity mirrors; this corresponds to changing ξI. As the loss ξ is varied from minimum ($\sim$ 25%) to maximum $\sim$ 50%, beam irradiance falls to

zero (discussed in Chapter 8); the ξI product overall is a rapidly reducing function with misalignment. The optically induced discharge power perturbation is then measured as a function of the laser output beam power P_{out} from which the beam irradiance I can be calculated from first principles

$$I = \frac{(1 + R)\, P_{out}}{(1 - R)\pi r_b^2} \quad \ldots\ldots\ldots\ldots\ldots\ldots \quad (7.27)$$

where r_b is the beam radius and R is calibrated output coupler reflectivity. The electrical input power perturbation ΔP in terms of beam irradiance for linear power per unit length or more generally for the temperature of the discharged gas is given by

$$\Delta P = \frac{r_b^2\, \pi\, \xi\, I}{2(L\, t_w/Pm + 1)} = \frac{r_b^2\, \pi\, \xi\, I}{2(t_w/t_{dis} + 1)} \quad \ldots\ldots \quad (7.28)$$

where $t_{dis} = m\, P/L$ or in terms of laser output power

$$\Delta P = \frac{(1 + R)\, \xi\, P_{out}}{2(1 - R)(L\, t_w/Pm + I)} = \frac{(1 + R)}{2(1 - R)} \cdot \frac{\xi\, P_{out}}{(t_w/t_{dis} + 1)} \quad (7.29)$$

Equations (7.28) and (7.29) predict a linear dependence of discharge excitation perturbation on beam irradiance (and output beam power) for a given ξ; the proportionality constant is then a function of losses (including output coupler reflectivity), wall temperature and excitation (P/L) or discharge temperature. In some experiments the losses factor ξ was varied deliberately (by misalignment) and occurred simultaneously with changes in irradiance and the ξI product is usually a suitable parameter as long as certain precautions are taken (see Chapter 8).

7.3 POWER PERTURBATION THEORY OF CO_2 AMPLIFIERS AND ABSORBERS

When a discharge external to the laser oscillator is illuminated by resonant CO_2 laser radiation, similar and smaller changes of input power occur and the sign of this perturbation is either positive or negative depending on whether stimulated emission or absorption occurs. Neglecting

spontaneous emission, the beam irradiance (I) is a function of length in the discharge and normal exponential attenuation/gain (shown as - or +) occurs

$$\frac{dI}{dZ} = \pm \alpha I_Z \quad \ldots\ldots\ldots\ldots\ldots\ldots \quad (7.30)$$

where Z is the discharge length co-ordinate. Integrating the absorption/gain over length Z gives

$$I_Z = I\, e^{\pm \alpha Z} \quad \ldots\ldots\ldots\ldots\ldots\ldots \quad (7.31)$$

where I is the incident probe beam irradiance. The conservation of energy requires that

$$\frac{dI}{dZ} = - \ell = \alpha I_Z \quad \ldots\ldots\ldots\ldots\ldots\ldots \quad (7.32)$$

where ℓ is the power (per unit volume) absorbed or lost due to the radiation field by the asymmetric stretch system as before.

$$\ell = \mp \alpha\, I_Z = \mp \alpha I\, e^{\pm \alpha Z} \quad \ldots\ldots\ldots\ldots \quad (7.33)$$

Therefore, the <u>total</u> energy supplied or lost to the gas (Q) translational system by absorption or stimulated emission respectively, is given by

$$Q = \pi r_b^{\,2}\, L \frac{dI}{dZ} = \mp \pi r_b^{\,2}\, L\, \alpha I\, e^{\pm \alpha L} \quad \ldots\ldots \quad (7.34)$$

where L is the positive column discharge length and α (cm^{-1}) is the gain or absorption coefficient. Substituting this energy change into the general equation (7.20) evaluated in 7.2; the fractional power perturbation is

$$\frac{\Delta P}{P} = - \frac{\Delta T}{T} = \pm \frac{\pi r_b^{\,2} L \alpha e^{\pm \alpha L}\, I}{(L\, t_w/m + P)} \quad \ldots\ldots\ldots \quad (7.35)$$

or in terms of the discharge input power change for input power per unit length or more generally in terms of the discharge temperature

$$\Delta P = \pm \frac{\pi r_b^{\,2} L \alpha e^{\pm \alpha L}\, I}{(L\, t_w/mP + 1)} = \pm \frac{\pi r_b^{\,2} L \alpha e^{\pm \alpha L}\, I}{(t_w/t_{dis} + 1)} \quad \ldots\ldots \quad (7.36)$$

For short sealed discharges (tube length < 10 cm) the laser gain was always found (by optical methods) to be $\lesssim 5\%$ and typical absorption for low pressure CO_2 was < 2%. For simplicity in analysis a reasonable approximation in this limit is to let $e^{\alpha L} = 1$ and, therefore,

$$\Delta P \sim \pm \frac{\pi r_b^2 \, L \, \alpha \, I}{(t_w/t_{dis} + 1)} \quad \ldots\ldots\ldots\ldots \quad (7.37)$$

and, as previously, there is a linear beam irradiance dependence.

7.4 LIMITATIONS OF POWER PERTURBATION THEORY AND SOME SYSTEM DEPENDENT EFFECTS

Several simplifications have been made in this chapter and some elucidation is necessary in order to interpret the experimental data. The first major simplification is geometric; a mean temperature due to discharge heating is assumed and consequently a mean number density, constant, across the tube diameter is required. This value is assumed to be 60% of the axial temperature. Similarly, the laser beam is treated as a mean irradiance by dividing the total optical power by the area described by the 1/e radius circle. In the real laser axial beam modes were selected (near gaussian) and no control or measure of the radial number density or temperature was available. These simplifications result in some dependency on the optical system in the case of the oscillator and the probe beam parameters for the external cell. The beam profile varied along the discharge and changed diameter with differences in radii of curvature, and position of the mirrors. The output beam radius was measured in the near field with the beam profile monitor at the position where it entered the external cell. The internal cell beam radius was calculated by standard formulae[5,6] from the resonator optical parameters.

A more fundamental approximation occurs due to the physical effect. As the laser starts to oscillate a deficiency of V-T 00^01 de-excitation

processes results in kinetic cooling of the gas. The axial number density increases and the electrical impedance rises. For cc excitation the electrical input power rises subsequently causing an increased heating of the gas (due to the greater P/L). This process opposes the first order effect and a balance is reached causing a small reduction of the effect. For series ballast cv excitation the increased discharge impedance (Z) results in decreased current with consequently increased discharge voltage (multiplied by the amplification factor G). The precise input power change depends on the value of ballast resistance (R_b) and if $R_b \simeq Z$ then the power change is minimum. High ballast resistance $R_b >> Z$ results in cc behaviour as described above. If $R_b < Z$ then unstable operation occurs (see chapter 3.21).

The assumption has been made throughout this work that the rate of supply of energy (pumping rate) to the $00^0 1$ upper laser level is not substantially changed by variation of the degree of stimulated emission. In principle, as the number of stimulated emission transitions increases the $00^0 1$ population may be expected to decrease resulting in even less V-T and V-V-T de-excitation events. The major mechanism is due to the stimulated emission rate being substantially faster than any other de-excitation rate. The pumping rate of the $00^0 1$ level is determined, due to vibrational mixing, by the total pumping rate of at least the first six vibrational modes ($00^0 1$ to $00^0 6$). The population of each level is determined by the vibrational temperature and therefore the $00^0 1$ population is 'stabilized' against de-excitation changes. The energy flowing through both routes (V-V-T and stimulated emission) in summation remains the same.

No account has been taken in this theory of the momentum exchange changes used first by Lobov[60] to explain the optogalvanic effect. The close correspondence of this theory with experiment suggests that for discharges with excitation currents in the range 5 to 50 mA (for 8 mm diameter) the momentum exchange effect is probably small compared to the number density change. However, as previously noted by Smith and Brooks some deviations consistent with the momentum exchange theory occur at low currents. It

should be possible to include a momentum dependent term into the theory[52,53] but it was not found necessary to explain these experimental results which relate to the excitation regime where efficient laser action occurs (10 to 30 mA).

For small non-irradiated (ballast) volumes (V_B), i.e. when $V_B \lesssim Lr_b$ (where r_b is the beam filled volume) the allowed number density changes are reduced because the gas has insufficient volume in which to expand into. The ratio of V_B:L $r_b \gtrsim 30$ was maintained in the oscillator experiments which should account for not more than 5% signal reduction for dc and low frequency ($\lesssim$ 100 Hz) perturbations. In practical terms the optogalvanic effect is reduced by two factors. The main ac signal reduction is due to the $00^0 1$ relaxation time and secondly, at very high frequencies $\gtrsim$ 20 kHz the signal is reduced by the $01^0 0$ relaxation time and also due to the smaller available ballast volume determined by the speed of sound. The effect of this volume reduction will be system dependent and may be less noticeable in larger diameter discharge tubes.

The particular dominant high frequency reduction effect will be determined by pressure which adjusts the $01^0 0$ relaxation time limitation. The 'acoustic' time constant due to the available ballast volume reduction will become important at f $\gtrsim$ 20 kHz and will essentially be independent of pressure. This is the reason why the high frequency signals f $\gtrsim$ 20 kHz are smaller than the low frequency (f < 100 Hz) signals (see Figure 6.23). There is no fundamental reason to expect the T_L kinetic coupling to produce a smaller effect.

7.5 POWER PERTURBATION THEORY SUMMARY

A precise qualitative theory has been developed based on the 'gas temperature explanation' first expounded by Rigden and Moeller. The theory ignores, for simplicity, momentum exchange changes[60] which may become important for low excitation[53]. The electrical input power change expressed fractionally as $\Delta P_{in}/P_{in}$ has been shown to be directly dependent on number

density changes ($\Delta n/n$). For certain physical constraints (such as constant number and large ballast volume) this fractional number density change is exactly equal to the fractional kinetic energy change ($\Delta T/T$) otherwise expressed by the fractional gas temperature change. The gas temperature (t_{dis}) can be measured or calculated for various excitations (P/L), pressures and compositions. By using simple optical resonator considerations (concerning 'losses', etc.) the gas temperature change due to a loss or gain of photon energy (Q) has been used to evaluate the change of number density and consequently the change of electrical input power (ΔP_{in}). The following section (Chapter 8) investigates the specific empirical measurements made in order to verify or refute this theory.

8.0 EXPERIMENTAL: DISCHARGE POWER PERTURBATIONS

Variation of the laser irradiance within a CO_2 laser oscillator results in a change of the discharge voltage (Δv) for a cc (i). The input power change ($\Delta P = i\Delta v$) has been predicted (Chapter 7) to be

$$\Delta P_{in} = \frac{\pi r_b^2 \xi I}{2(t_w/t_{dis} + 1)} = \frac{(1 + R) \xi P_{out}}{2(1-R)(t_w/t_{dis} + 1)} \qquad (8.1)$$

Figure 8.01 shows the measured input power change (ΔP_{in}) due to a variation of laser output power (P_{out}) achieved by varying the alignment of the output coupler. This technique involves varying the cavity loss ξ but initially, an average ξ value will be assumed; this will be treated more carefully subsequently.

The laser beam was switched on to off and the full tube voltage measured with a DVM (and high voltage probe with input impedance > 100 MΩ) for a wide range of constant currents. The table shown in Figure 8.02 lists the values of the appropriate experimental parameters used in the experiment that are required for comparison of the theoretical prediction (8.1).

Assuming nominal values of t_{dis} and ξ of 120 C and 0.3 respectively, then the average input power fluctuation should be (from equation (8.1)) for an average loss situation

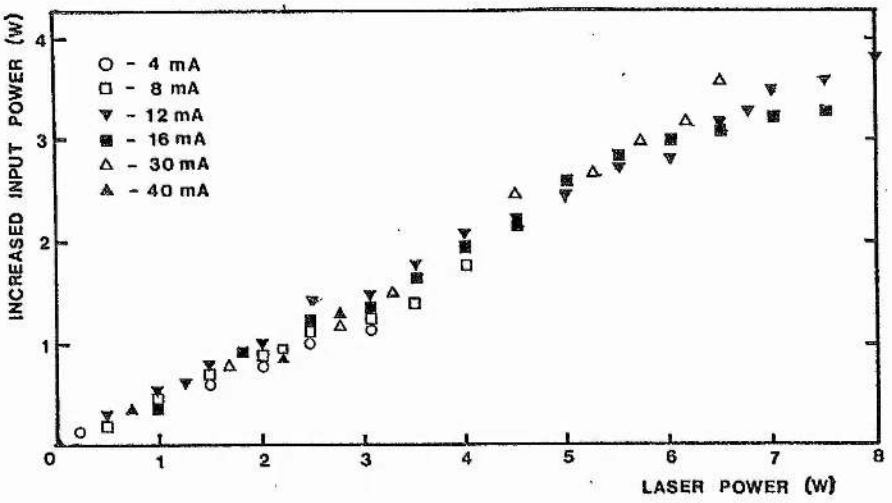

Fig. 8.01 Variation of electrical input power (ΔP_{in}) due to changes of laser output power (P_{out}) caused by output coupler misalignment for a laser as described in the table 8.02. The solid line shows the approximate prediction $\Delta P_{in} = 2.8\xi P_{out} = 0.6\ P_{out}$ for the average loss case. The gas mixture was 1 Xe, 3 CO_2, 4 N_2, 16 He torr.

t_w = 280 K	ξ = 0.15 to 0.4 approximately
R = 0.9	with output coupler loss 10%, fixed
L = 25 cm	reflector loss 3%, Brewster window and
$t_{dis} \sim$ 120 K	aperture loss = 2%; misalignment
r_b = 0.2 cm	(deliberate) loss 0 - 25% laser fully
	on to fully off.

Fig. 8.02 The parameters of the experimental laser required for the theoretical prediction (Fig. 8.01) of the laser induced power perturbation.

$$\Delta P_{in} \sim 0.02\ \xi\ I \sim 2.8\ \xi\ P_{out} \sim 0.6\ P_{out} \quad . . \quad (8.2)$$

This average slope factor ($\Delta P_{in}/P_{out} \sim 0.6$) is in good general agreement with the experimental data (the precise values vary with ξ and P/L). The data points for the maximum laser output power (low ξ) for a particular excitation current giving a lower $\Delta P_{in}/P_{out}$ slope factor than the data points for low output powers (high ξ). Equation (8.1) predicts an input power perturbation which is lower for the fully aligned case (due to low ξ). The 16 mA experimental points, for example, show a slope reducing at full power ($\sim$ 8 W) in reasonable agreement with the estimated ξ change (Figure 8.02). The maximum misalignment results in a total cavity round trip loss slightly less than the gain which is approximately known for these discharges. The maximum loss required to stop oscillation would be (for 25 cm length) $\sim$ 0.3 to 0.4 and the minimum loss due to output coupling (10%) fixed reflection loss ($\sim$ 3%) and Brewster windows and aperture loss ($\sim$ 2%) was approximately 0.15. This range of ξ results in the reduction of $\Delta P_{in}/P_{out}$ slope for well misaligned case $\xi \sim 0.3$ at $\sim$ 1 W to the well aligned case ($\xi = 0.15$) at $\sim$ 6 W from $\Delta P_{in}/P_{out} = 0.8$ to $\Delta P_{in}/P_{out} = 0.4$. Figure 8.03 shows a linear dependence of ξ upon P_{out} and ΔP_{in} calculated using (8.1). Previously, the reduction of ΔP_{in} for the low ξ (fully aligned case) was noted in Figure 4.02a and an empirical measure of minimum ξ will be obtained in section 8.1 where output coupler reflectivity variation is discussed. The simple linear approximation of the variation of ξ from $\sim$ 0.15 fully aligned to $\sim$ 0.3 when laser action ceases is, however, adequate for an approximate evaluation of ΔP_{in} for these lasers with the experimental parameters shown in Figure 8.02. In practice, the loss factor ξ will vary in a complicated manner dependent on the nature of the resonator (aperture, etc.).

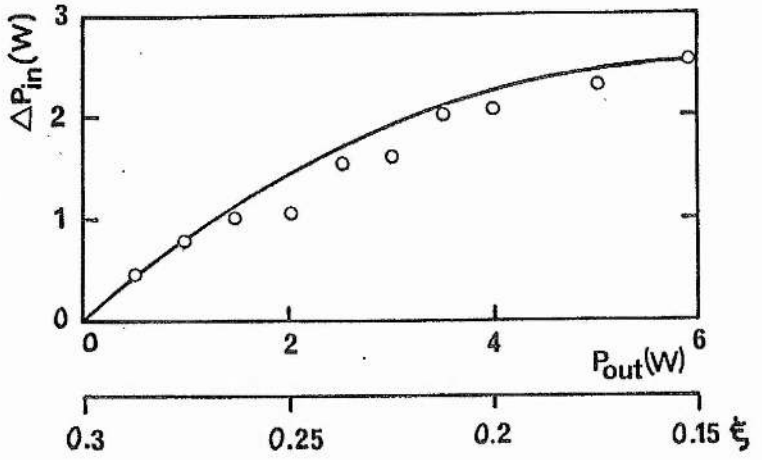

Fig. 8.03 The increased discharge input power (ΔP_{in}) experimentally determined by adjustment of the output coupler alignment. The theoretical prediction of the input power change is calculated assuming a linear variation from 0.15 minimum loss to 0.3 maximum loss. The gas mixture was 1.5 Xe, 3 CO_2, 4 N_2, 15 He (torr).

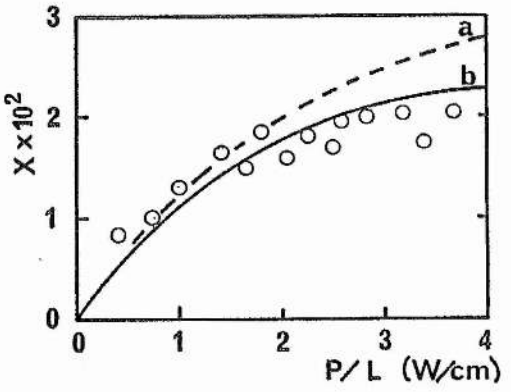

Fig. 8.11 The variation of both predicted X coefficient and experimental $\Delta P/\xi I$ (equal to X) with discharge excitation P/L for a laser mixture of 15-15-20-50, Xe-CO_2-N_2-He at 20 torr (o). Curve (a) shows the predicted X value using Laderman and Byron[173] calculated values of t_{dis} and curve (b) shows X values calculated using t_{dis} values measured by Shields and Smith[164] (t_{dis} = 0.6 t_{axial}).

8.1 DISCHARGE POWER PERTURBATIONS IN CO_2 LASER OSCILLATORS

When optogalvanic perturbations occur within an efficient CO_2 laser oscillator the effect is particularly large and proportional to the high beam irradiance within the cavity (typically > 200 W cm^{-2}). The variation of the power perturbation has been shown to be dependent on cavity alignment but it is also in general, dependent on all the discharge parameters. The $\Delta P_{in}/\xi I$ slope factor $\left[\pi r^2_b/2(t_w/t_{dis} + 1)\right]$ will be named X (optogalvanic coefficient) in this chapter, and this coefficient (which is approximately 0.02, see equation (8.2)) varies with operational parameters such as gas pressure, composition and excitation (which all directly alter t_{dis}) as well as with wall temperature and output coupler reflectivity. In this section changes of X due to these parameters are demonstrated experimentally and compared to theoretical predictions.

The increase of excitation (P/L) results in an increase of gas temperature of the discharge (t_{dis}) for fixed pressure and composition. Figure 8.11 shows predicted values of X for variation of P/L for the full practical laser range, up to 4 W/cm. The X value was calculated from equation (8.1) using (a) Laderman and Byron's[173] calculated discharge temperatures and (b) Shields and Smith's[164] empirical values. The experimental gas mixture had a lower fraction of helium but was comparable.

The best agreement with the theory is achieved with the Shields and Smith empirical temperatures used with equation (8.1); however, an adequately good agreement can be achieved with the linear approximation with a heating constant m equal to 50 to 60 cm $W^{-1}K$ (see equation (7.18)). The experimental temperature results of Waszink and van Vliet[174], Maksimov, Sergienko and Slovetskii[175] and Schwartz and Margalith[176] provide very similar values of X over this range of excitation. The X coefficient will be precisely dependent on mixture which will be discussed later, however, this comparison (Figure 8.11) establishes how X rises with excitation (as t_{dis} increases) and because t_{dis} does not rise as rapidly above 1.5 W/cm, X begins to saturate resulting in a saturated value of the discharge power

perturbation with higher values of P/L (corresponding to higher currents); this results in a saturated value of $X \sim 2 \times 10^{-2}$ above 1.5 W/cm.

Historically, due to measurement techniques, the fractional voltage change, $\Delta V/V$ or equivalent $\Delta Z/Z$ (impedance change) rather than power change, has been presented by authors;[34,57] the calculated power change (ΔP_{in}) can be translated into $\Delta V/V$. In Figure 8.12 the fractional voltage change has been normalized to 1 W output power (by using the fully aligned case and dividing the voltage change by the output power) from the 25 cm discharge CO_2 laser with 90% output coupler. Although the current voltage product change (ΔP_{in}) rises slowly with increased excitation (discharge temperature increase), the fractional voltage change decreases (with increasing current) because the discharge power increase for a given laser output power is approximately constant above 10 mA (due to the saturation of X with P/L above 1.5 W/cm). A constant t_{dis} (kinetically cooled) requires a discharge power change which is constant for a given beam irradiance and because t_{dis} only rises slowly with current (and saturates at $i \gtrsim 15$ mA) the voltage change ΔV reduces (whilst the current rises) resulting in an approximately constant input power change. However, the discharge voltage reduces with increasing current but this decrease is less marked at currents $\gtrsim 12$ mA where the differential impedance slope with current (dZ/di) tends to zero (see Figure 4.11). Hence, the $\Delta V/V$ fractional change is a reducing function with respect to current for a constant laser output power, gas composition, etc., with two distinct slope regimes: high for $i \lesssim 10$ mA and low for $i \gtrsim 10$ mA. An alternative, more microscopic, explanation is that with increasing current (or P/L) the discharge temperature t_{dis} rises and the fixed kinetic cooling due to a particular photon loss produces a number density change $\Delta n/n$ which produces a given t_{dis} decrease. Proportionally, this temperature decrease with respect to the quiescent t_{dis} value is less for higher currents (temperatures). The fractional changes (for a given photon output) are, therefore, higher for low currents as previously observed by Smith and Brooks[53] and Lawler[34] and the theory presented so far predicts the experimental

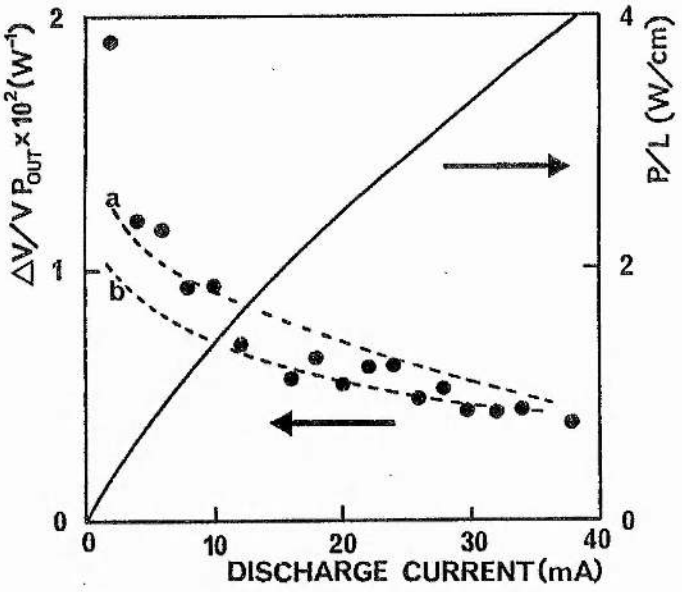

Fig. 8.12 The variation of fractional voltage change $\Delta V/V$ for unit output power (P_{out}) as the excitation current varies up to 40 mA; the P/L varies up to 4 Wcm^{-1} over this range. Curve (a) shows the prediction of equation (8.1) for $\xi = 0.15$ and curve (b) $\xi = 0.2$. ξ was adjusted by varying the output reflectivity R. The data points are for a gas mixture of 3 Xe, 3 CO_2, 4 N_2, 10 He (torr) and the laser was used fully aligned.

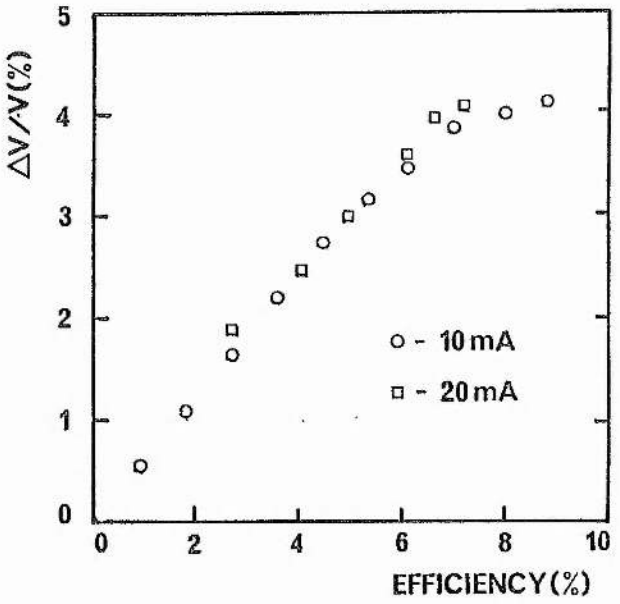

Fig. 8.13 The empirical variation of laser efficiency with the fractional voltage change for 10 and 20 mA. The laser had a 25 cm discharge 90% output coupler and a gas mixture of 1 Xe, 3 CO_2, 4 N_2 and 16 He (torr). The efficiency was reduced by output coupler misalignment.

results (Figure 8.12) closely. The parameters v, i and P_{out} are directly measured and the Δv has been calculated from (8.1) for two losses factors $\xi = 0.2$ and 0.25.

The dependency of the fractional laser voltage change on efficiency (η) is shown in Figure 8.13. The fractional voltage change $\Delta v/v$ is, for cc excitation, equal to the fractional impedance change $\Delta Z/Z$, and the fractional input power change $\Delta P_{in}/P_{in}$. The laser efficiency is simply the output power per unit input power (P_{out}/P_{in}). The ratio of $\Delta v/v$ to η is just X (1 + R)/(1 - R) from the theory

$$\Delta P_{in}/P_{in} = \frac{(1 + R)}{(1 - R)} X\left[P_{out}/P_{in}\right] \quad \ldots\ldots\ldots \quad (8.2)$$

because from (8.1) the $\Delta P_{in}/P_{out}$ relationship has been evaluated in Chapter 7. This correspondence results in an average $\Delta v/v$ versus η slope of $\sim$ 0.6 in analogy to the ΔP_{in} versus P_{out} plot in Figure 8.01. The exact ratio varies with alignment and a slope reduction for high efficiency is seen (when ξ is low valued).

The $\Delta P_{in}/\xi I$ measurements shown in Figure 8.14 show that the X coefficient increases with increasing laser pressure (for a given mixture) in accordance with the theoretical prediction. As the pressure is increased for a given constant excitation current the discharge impedance increases due to the increased number density of electron collision partners. The effect is an increased P/L for a given current due to the voltage rise. This increased P/L causes an elevation of discharge temperature which can occur in a different manner to the previous analysis because the thermal conductivity of the gas changes with pressure. The prediction from 8.13 due to the P/L change described above is shown in 8.14. The increase in X was found to be larger than that predicted which can be interpreted that t_{dis} is higher at higher pressures for a given P/L although elementary reasoning suggests that it could be lower because the higher pressure gas should have a higher thermal conductivity. Other secondary effects also may alter the results, e.g. pressure increases may alter CO_2 dissociation

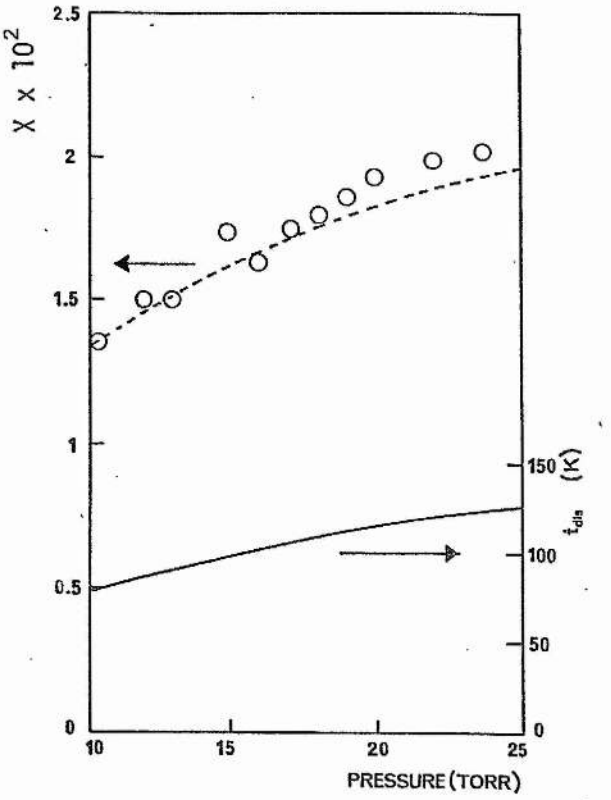

Fig. 8.14 The variation of $\Delta P/\xi I$ (experimental O) and the predicted X value for a variation of laser gas pressure. The variation of mean discharge temperature t_{dis} due only to the increased P/L subject to pressure increase is shown. These values have been used to calculate the X values shown by the dashed line; the gas mixture was 6% Xe, 6% CO_2, 12% N_2, 80% He.

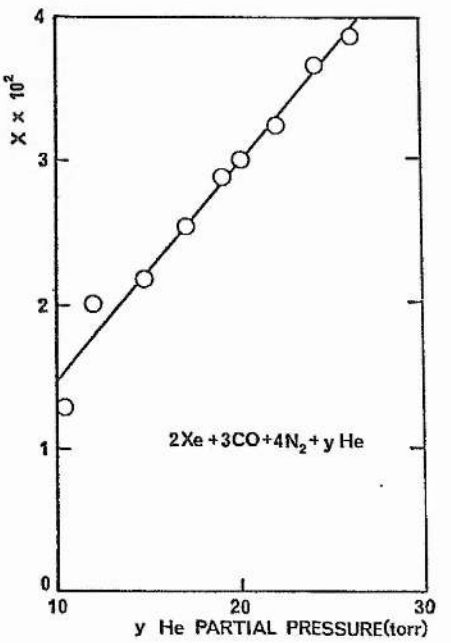

Fig. 8.15 The variation of $\Delta P/\xi I$ (experimental) = X with the variation of He partial pressure for the laser described in 8.02 with 2 Xe, 3 CO_2, 4 N_2 (torr) and a variable partial pressure of helium - y.

and the effect of residual H_2 (which is an important factor in sealed discharges) may be reduced. The overall agreement of experimental results and theory is good considering only simple considerations of temperature and power change have been used.

The dependency of X on the composition of the laser gas mixture falls into two parts; the largest variation with composition is due to changes of the ratio of the polyatomic population (CO_2, N_2, CO, etc.) to the atomic He concentration and the dependency of X on the CO_2:N_2 or CO_2:CO concentration ratios.

The helium concentration dependent variation of X is shown in Figure 8.15; the X coefficient rises markedly with increasing He partial pressure for cc (10 mA) excitation. The theoretical analysis of this situation is complex; there are at least three separable effects: (a) the excitation (P/L) for fixed i will rise with overall gas pressure increase and, therefore, X will increase (as in Figure 8.14), (b) an isobaric (constant total pressure) helium concentration change (for a given current) will result in a change of P/L, and hence change X and (c) the discharge temperature (t_{dis}) for a given P/L will be higher for He lean rather than He rich mixtures due to change of thermal conductivity resulting in a reduced X. This experimental result shows a large order increase of X with He content and a large order change due to strong dependence of t_{dis} or He fraction. The helium content dependence explains the lower experimental values of $\Delta P_{in}/\xi I$ shown in Figure 8.11 where the calculated X value was for mixtures with higher helium concentrations.

No significant dependence of X on CO_2:N_2 or CO_2:CO concentration ratios was found over the laser operating range. Additionally, the optogalvanic coefficient X was found to be identical for Xe-CO_2-CO-He mixture and Xe-CO_2-N_2-He mixtures where the partial pressures of He were maintained and the partial pressures of CO and N_2 were equivalent. Figure 8.16 shows how the increased power input ΔP_{in} increases with laser output power as the cavity alignment is improved. The presentation shows the variation for a

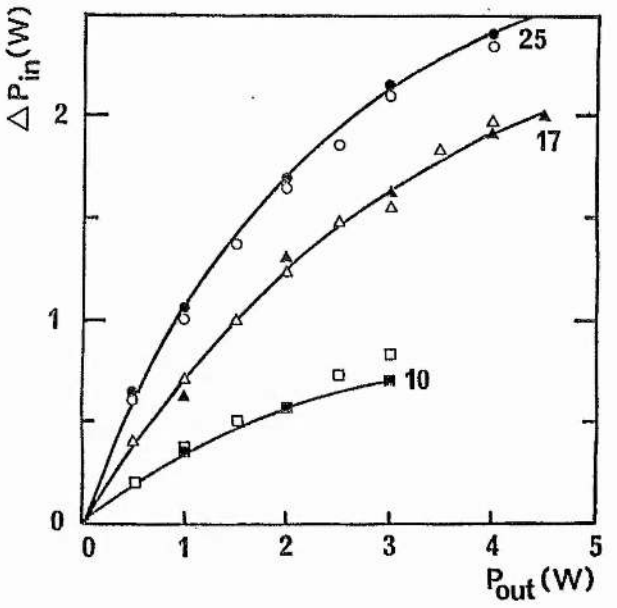

Fig. 8.16 The variation of discharge input power ΔP_{in} with the variation of laser output power which was varied by adjustment of the output coupler alignment. The open points (○ △ □) represent the empirical results for the mixture 1 Xe, 3 CO_2, 4 N_2, y He where y = 10, 17 and 25 torr. The solid experimental points (● ▲ ■) display the ΔP_{in} variation for a N_2 free mixture consisting of 1 Xe, 3 CO_2, 4 CO, y He (torr).

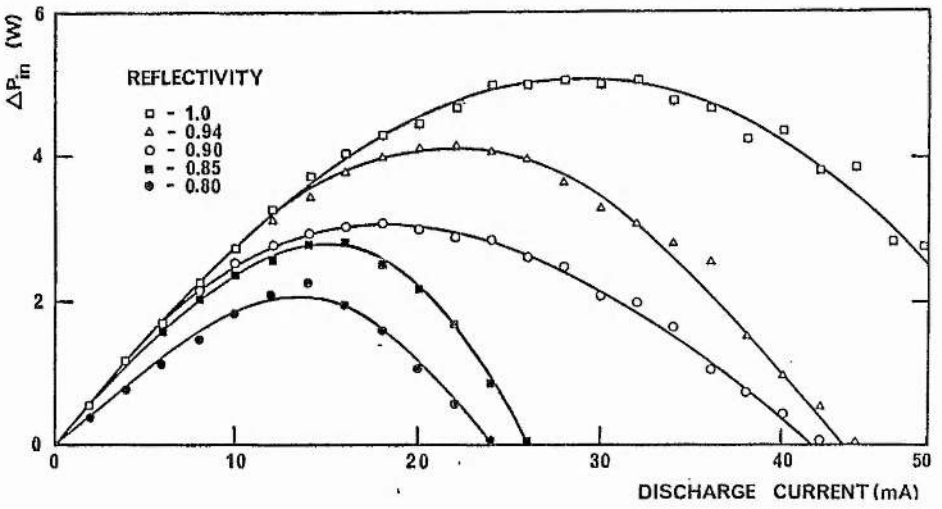

Fig. 8.17 The variation of the increased input power (ΔP_{in}) due to laser oscillation for a fully aligned laser over the full operating current range for different output coupler reflectivities. The laser details are given in the caption of Fig. 8.18.

mixture with N_2 or CO for different He concentrations. This behaviour of CO substituted for N_2 cannot be adequately explained by the ionization theory[57] which requires a specific nitrogen excited state (B_3) to couple the laser induced $00^0 1$ population changes with fluctuations of ionization. This behaviour was expected from the theory because no major thermal changes are known to take place for substitutions of CO or N_2 for CO_2 in laser discharges. The thermal properties of the discharge are dominated by the large quantity of He present.

Variations in the input power perturbations due to changing the output coupler reflectivity are shown in Figure 8.17. For fixed operating conditions, mixture, pressure, excitation and alignment changes in reflectivity result in changes of the beam irradiance as well as changes in ξ. By using a series of reflectors 99% (total reflector), 98%, 95%, 94%, 90%, 85% and 80% and measuring the output power and input power change, the cavity losses were measured for the 25 cm active discharge lasers described in Chapter 3.1. The laser output power and beam irradiance measured during this experiment has been presented in Figure 3.113. Higher reflectivities allow laser oscillation to occur over a wider range of excitation because a lower gain can be tolerated due to the lower cavity losses. The optogalvanic effect also provided the facility of measuring the laser irradiance when no output beam was present (due to total reflectors forming the optical cavity).

The ΔP_{in} values (Figure 8.17) can just be considered as $X\xi I$ where ξ has changed with output coupler reflectivity (to a small extent) and X varies with increasing discharge temperature (as shown in Figure 8.14). The ΔP_{in} axis represents (approximately) beam irradiance and this increases straightforwardly with increasing coupler reflectivity; the output power, however, peaks for 90% reflectivity (as shown in Figure 3.113). The excitation required for optimum irradiance increases with increased output reflectivity from 15 mA for 80% coupler to 30 mA for total reflector ($\sim$ 99%). This must reflect the effect of the increased stimulated emission energy

fraction (compared to other relaxation processes) due to the larger beam irradiance I. When the output coupling is large (R ≃ 0.8) then the beam irradiance (I) can never become large because the loss processes (which increase with excitation) become comparable to the stimulated emission at lower currents. When lower coupling is used (R ≃ 1.0) then the beam irradiance is considerably higher and the increased stimulated emission dominates over the loss processes for higher currents. The maximum beam irradiance occurs at higher currents because the beam irradiance rises simply with improved pumping. The relevant loss processes (apart from the beam) are likely to be V-V-T and V-T processes and super elastic electronic collisions.

The losses factor can be established from (8.1) to be

$$\xi = \frac{\Delta P_{in}}{P_{out}} \frac{(1 - R)}{(1 + R)} \frac{\pi r_b^2}{X} \quad \ldots\ldots\ldots\ldots \quad (8.3)$$

and the minimum resonator losses minus the reflectivity of the output coupler calculated ($\xi_o = \xi - (1 - R)$). Figure 8.17 shows the calculated total ξ for the compact laser design and the ξ_o cavity loss had an average value of 0.082 ± 0.025 which gives a value for the 0.9 reflectivity output coupler of the fully aligned loss $\xi_{min} \simeq 0.182$, this calculated value using empirical data is in reasonable agreement with the estimated $\xi_{min} \simeq 0.15$.

The discharge temperature profile is directly related to the wall temperature (t_w) and it has been shown[177] that a change of wall temperature Δt results in a shift of Δt in the axial temperature (t_a).

$$t_{w1} = t_{w2} + \Delta t; \; t_{a1} = t_{a2} + \Delta t \quad \ldots\ldots\ldots \quad (8.4)$$

The wall temperature was varied experimentally by adjusting the cooling water temperature (by setting cooler thermostat) over the range 270 K to 320 K and the fully aligned 25 cm laser had the fully on to off OVE signal measured with a DVM. Figure 8.19 shows the comparison of the $\Delta P/\xi I$ experimental values with the calculated X value from equation (8.1). The laser tube was excited with a total input power of 56 W. The expected t_{dis} value lies in

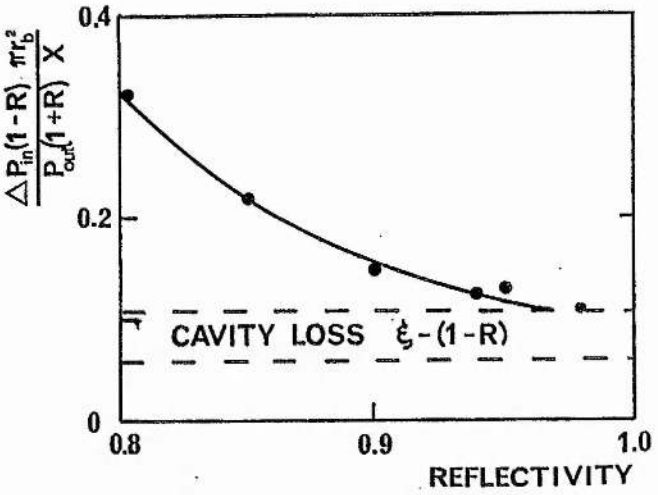

Fig. 8.18 The calculated losses factor $\xi = \frac{\Delta P_{in}}{P_{out}} \frac{(1-R)}{(1+R)} \frac{\pi r_b}{X}$ as a function of reflectivity from the empirical results shown in Fig. 8.16. The cavity loss (neglecting output beam) $\xi - (1 - R)$ was found to be 0.082 ± 0.025 and is shown by the dashed box. The laser consisted of an 8 mm diameter discharge tube 25 cm active length filled with 3 Xe, 3 CO_2, 4 N_2, 10 He (torr). The laser is described more fully in section 3.11.

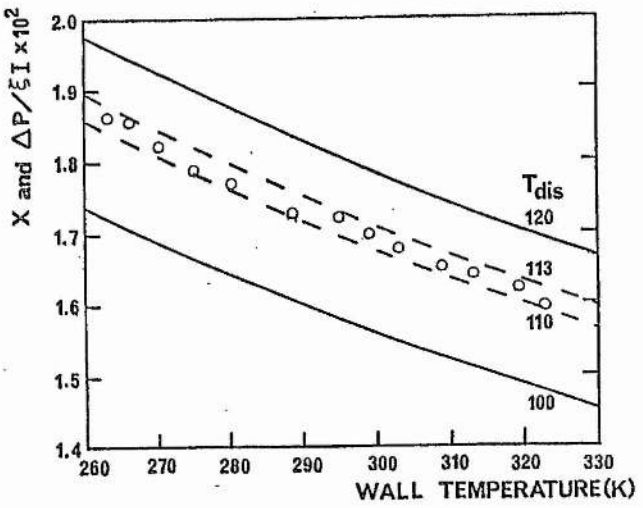

Fig. 8.19 The calculated X variation and measured $\Delta P/\xi I$ with the variation of wall temperature from 260 K to 330 K. The experimental points (o) are consistent with a mean discharge temperature of 111.5 ± 2 C.

the range 80 to 100 for this value of P/L (m $\sim$ 50) and this mixture (1 Xe, 2.5 CO_2, 3.6 N_2, 15 He torr). The curves show the calculated X value for t_{dis} = 100, 110, 113 and 120 C; a good agreement between theory and experiment was observed and a useful relative measure of discharge temperature (t_{dis}) can be made this way.

8.2 EXPERIMENTAL: POWER PERTURBATION OF CO_2 AND CO_2-N_2-He DISCHARGES PROBED BY CO_2 LASER RADIATION

Extensive investigation of optogalvanic phenomena in CO_2 laser discharges external to the oscillator has been achieved by Smith and Brooks[52,53]; measurements of ac pressure changes (Δp) and current changes (Δi) were correlated and shown that changes in density of the gas due to kinetic cooling and heating (with stimulated emission and absorption of photons) cause discharge parameter changes including sidelight intensity, current and voltage in discharges external to the laser oscillator. It is the purpose of this section to present new experimental evidence and compare this with the theory presented in Chapter 7. Sealed CO_2 and laser mixture discharges have been investigated and the dependence of the electrical power changes due to laser absorption and amplification on discharge length, pressure and excitation measured. The direct comparison of the oscillator and small signal amplifier perturbations demonstrates the universality of the theory.

The external cell experiments reported here were of an exploratory nature and precise experiments would be required to determine the variation of the optogalvanic effect with gas composition, etc. as described in 8.1. Compared with the oscillator perturbations the power changes in external discharges are smaller; typical probe beam irradiances of < 100 W cm^{-2} were used. The probe lasers were adjusted (using the profile monitor) to provide a near Gaussian beam (TEM_{oo}) and the gas cells were constructed with approximately the same internal diameter quartz tubes as the laser sources. The CO_2 probe beam was chopped at 16 Hz and stabilized at laser line centre of 10P(20); the OGE discharge tubes had a platinum side arm cathode and

multiple tungsten point anodes which allowed eight different discharge lengths to be chosen. The total tube voltage was split by a 10:1 potential divider with total resistance of 100 MΩ and the 10% voltage fed via a suitable coupling capacitor (0.1 μF, 2 kV) to a Brookdeal 9502 lock-in amplifier. Typically, integrator time constants of 0.1 to 10 s were used. A comparison of the measured perturbations in CO_2 and laser mixture (CO_2-N_2-He) discharges is shown in Figure 8.21. The fractional power perturbation for four different gases for variation of the probe beam irradiance is demonstrated for one excitation condition (10 mA).

Absorption was determined in cases (c) and (d) and gain in cases (a) and (b) by the polarity of the effect; this was confirmed by optical measurements with the LTT detector. A change of sign between absorption and gain is anticipated by the theory and the derived relationship (from (7.37)) is just

$$\Delta P_{in} \simeq \pm \frac{\pi r_b^2 \, L \, \alpha \, I}{(t_w/t_{dis} + 1)} \quad \ldots\ldots\ldots\ldots \quad (8.5)$$

or in fractional power terms

$$\frac{\Delta P_{in}}{P_{in}} \simeq \pm \frac{\pi r_b^2 \, \alpha \, I}{(t_w/t_{dis} + 1) \, P_{in}/L} \quad \ldots\ldots\ldots \quad (8.6)$$

where the - sign (lower half of 8.21) represents absorption and + sign (upper half of 8.21) represents gain. Some quantitative measure of the absorption/gain can be seen immediately from Figure 8.21 but the differences are compressed by the P/L variation due to the large pressure variation. Some saturation of the low pressure (CO_2 0.5 torr) absorption (α) with beam irradiance (I) is evident with probe powers > 20 W/cm^2. This effect is due to the substantial depletion of $10^0 0$ level by absorption population. A low density of CO_2 molecules in any excited state exists for room temperature low pressure CO_2 and the large amount of CO_2 dissociation (for this excitation condition) reduces the CO_2 density by $\gtrsim$ 50%. All other gases (i.e. pure CO_2 at pressures above 8 torr and laser mixtures above 5 torr) were found to be in the small

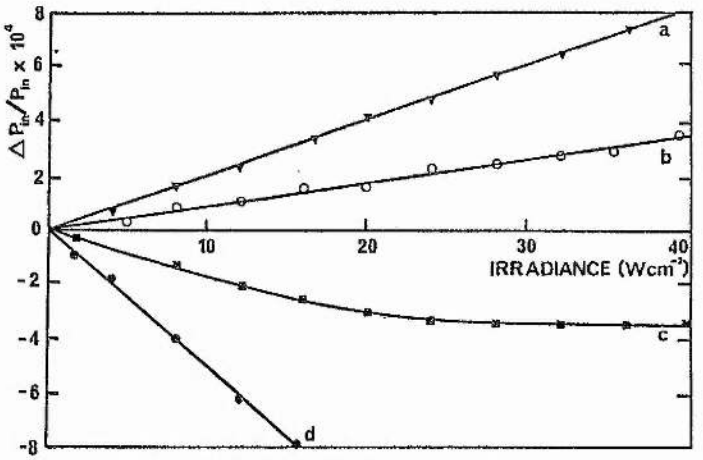

Fig. 8.21 The fractional input power perturbation $\Delta P_{in}/P_{in}$ variation from a variation of probe beam irradiance (10P(20) line centre stabilized) for (a) 3 CO_2, 4 N_2, 12 He (torr), (b) CO_2 3 torr, (c) CO_2 0.5 torr, and (d) CO_2 20 torr all for 10 mA cc excitation.

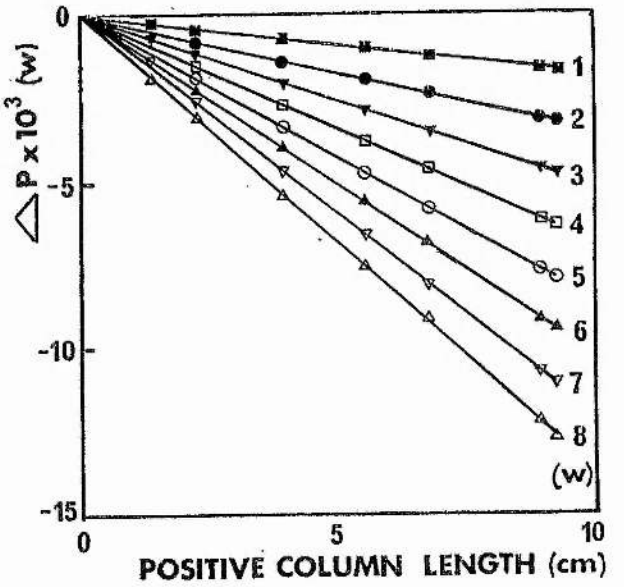

Fig. 8.22 The input power change ΔP_{in} as a function of positive column length for 1 to 8 W probe beam power (8 - 64 W/cm^2).

signal regime (unsaturated) below 100 W/cm^{-2} for sufficient excitation. The optogalvanic technique allows simple electrical measurement of gain/absorption saturation; it is clearly seen here that CO_2 at 3 torr for 10 mA excitation exhibits gain, and this behaviour will be investigated in detail later.

Little saturation of $\alpha(I)$ occurs for higher pressures (> 5 torr) of CO_2 if the crossover excitation from absorption to gain is avoided. Linear dependence of input power change ΔP_{in} with positive column length, probe beam irradiance and absorption coefficient was predicted by (8.4). Figure 8.22 shows the input power change for absorbing CO_2 at 10 torr which was discharged with an input P/L of 0.9 W/cm for many values of probe beam power up to 8 W and varying lengths of positive column. Linearity of both length and irradiance of better than 5% was found. A transverse positive column (orthogonal to the probe beam) produced a power perturbation equivalent to a colinear discharge 8.5 ± 1.2 mm long which was consistent with the estimated discharge thickness (by observing the visible glow). Rearranging equation (8.5) in terms of absorption coefficient the following relationship is obtained

$$\alpha = \frac{\Delta P_{in}}{L P_{LASER}} (t_w/t_{dis} + 1) \quad \ldots\ldots\ldots\ldots (8.7)$$

because $P_{LASER} = I \pi r_b^2$. For a P/L ~ 1, t_{dis} ~ 100 C. A suitable value of absorption is

$$\alpha = 1.7 \pm 0.07 \times 10^{-4} cm^{-1} \quad (8.8)$$

Hot CO_2 absorption measurements with these laser beams have been made and were reported in section 5.11. The room temperature (300 K) and 500 C absorption coefficients at 10 torr are 1.5×10^{-5} and $10^{-2} cm^{-1}$ respectively. These measurements require, for a 50% CO_2 dissociation, a discharge temperature of $\lesssim$ 100 C. The precise value cannot be determined unless the dissociation is accurately known. The absorption was measured optically with the LTT detector and found to be < 0.1% cm^{-1}.

When the tube filling consists only of CO_2, in the pressure range ~ 1

to 20 torr, either gain or absorption can occur dependent upon excitation. Figure 8.23 shows the optogalvanic signal $\Delta i/i$ which for 5 torr CO_2 rises characteristically at low currents (due to the increasing circuit amplification factor $G >> 1$). The transition from absorption to gain occurs as 5 mA discharge current. The optogalvanic phase shows a shift from in phase with the chopped radiation field (at high current) to fully out of phase at low current. The theory predicts that absorption should cause gas heating and consequent decreased discharge impedance and either lower voltage or higher current. When the discharge provides gain the gas is cooled (as in the oscillator case) and the rising impedance causes increased voltage or decreasing current. The optical measurement of gain/absorption confirmed this behaviour; zero net gain occurred at $\sim$ 5.5 mA. The $\Delta i/i$ signal in the low current regime was large but had large noise fluctuations. The 20 torr CO_2 $\Delta i/i$ signal shows gain at currents below $\sim$ 10 mA and the phase change behaviour was similar to the 5 torr case. However, no large absorption signal was seen because the absorption gain transition occurs at a sufficiently high current where the circuit amplification factor G was approximately 1. Large $\Delta i/i$ signals due to gain are seen, however, at comparably low currents $\sim$ 1 mA where $G \gtrsim 10$.

The external cell pressure was varied for cc excitation in order to study how CO_2 discharges behave over a wide pressure range. This experiment was useful in assessing suitable pressure for operating external cells for stabilization error signal sources. Currents from 1 mA to 50 mA were investigated; the 10 mA excitation curve is shown in Figure 8.24. At 0.5 torr the gas was clearly in absorption ($-\pi$ phase with respect to the beam) whereas at 3 torr it was in gain. Such small changes of gain are not easily observed by optical methods and the optogalvanic detection of small changes of absorption or gain provided simple direct measurement over the pressure range 0.2 to 40 torr. Curve A shows the fractional discharge power perturbation ($\Delta P_{in}/P_{in}$) due to a 16 Hz chopped beam (and phase sensitive detection); curve B shows the signal phase. At 10 mA the transitions from

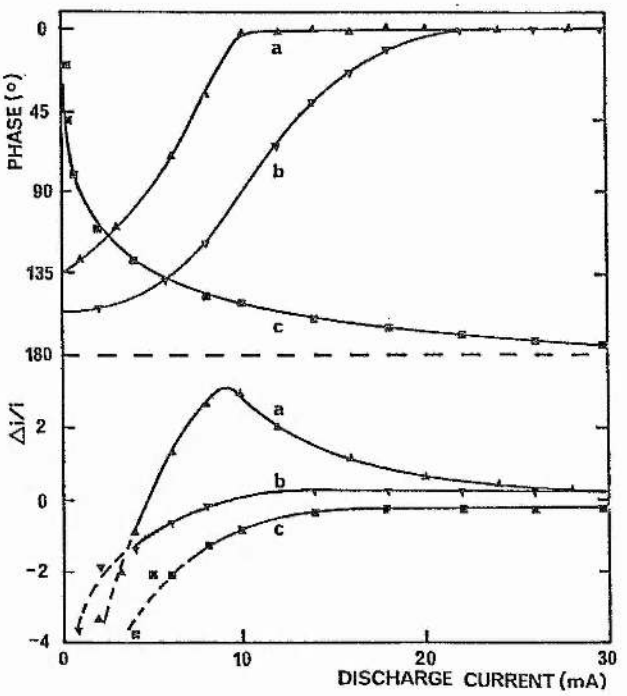

Fig. 8.23 The optogalvanic phase and signal ($\Delta i/i$) as a function of excitation current for cv excitation with 10 kΩ ballast resistance. The signal $\Delta i/i$ has been normalized for 1 m length of positive column and is shown as a percentage. The gas fillings represented are (a) 5 torr CO_2, (b) 20 torr CO_2, and (c) laser mixture 1 Xe, 3 CO_2, 4 N_2, 18 He (torr). The crossover between gain and absorption occurs at ∿ 10 mA and 5 mA for 5 torr and 20 torr CO_2 respectively. The laser mixture is in gain at all currents above 1 mA.

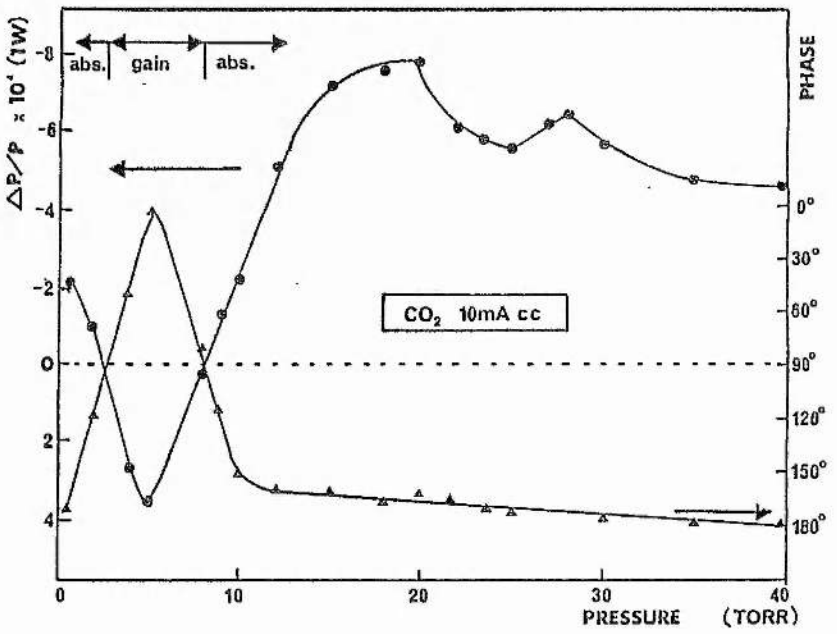

Fig. 8.24 The variation of fractional power change $\Delta P_{in}/P_{in}$ and power change phase with a variation of CO_2 pressure for a laser probe beam of 1 W. The laser was line centre stabilized to 10P(20).

absorption to gain and gain to absorption occur at 8 and 2.5 torr respectively with reducing pressure.

The narrow gain pressure condition is probably due to the selection of a suitable dissociation equilibrium. This will generate both sufficient CO for pumping of the asymmetrical stretch mode population and also maintain a sufficient CO_2 population to be excited into oon levels. Different excitation resulted in a shifted gain band and in general, the gain band is wider and shifted to higher pressures with lower currents. Because the CO is only generated by electrical dissociation in the discharge and the gain pressure band is determined by the precise partial CO pressure the exact behaviour depends on tube geometry.

Early operation[38,39] of cw CO_2 lasers did not utilize N_2 vibrational pumping of CO_2 but depended upon dissociated CO vibrational excitation. The behaviour of CO_2 discharges over a wide pressure change was not studied in detail but optogalvanic behaviour shown in Figure 8.24 shows (a) the expected increase in power perturbation $\Delta P/P$ over the range 10 to 20 torr where the absorption is rising and then saturates due to pressure broadening (Chapter 5) and (b) above the saturation point large variations of the $\Delta P/P$ signal were measured $\simeq -4$ to -8×10^{-4}. These changes were reproduced in two different tubes with excitation above 6 mA. The detailed behaviour (maximum $\sim$ 20 and 30 torr, minimum $\sim$ 26 torr) varied with discharge current and the overall effect was to reduce the $\Delta P/P$ signal at pressures > 30 torr; this decrease was larger for high currents. This effect could be due to constriction of the discharge[178,179] because the positive column glow visually appeared to constrict above 20 torr. Constriction causes changes of input power and radial temperature profile. The fractional power change $\Delta P_{in}/P_{in}$ is sensitive to both these parameters.

From the analysis forming the theory in Chapter 7 and from the similarity of the apparatus it is expected that for a given laser radiation field with fixed discharge conditions (tube radius, mixture, pressure, excitation) the external discharge cell should show the similar input power

perturbations to the oscillator discharge. It is convenient to define a new parameter (P_{LOST}) which is just the power lost to the radiation field by stimulated emission from the discharge. In the oscillator case this is just

$$P_{LOST} = - I \xi/2 A \quad \ldots\ldots\ldots\ldots\ldots\ldots \quad (8.9)$$

in terms of the beam irradiance (I). This quantity is the energy loss term (from (7.4)) due to stimulated emission. In terms of the laser output power (from (7.28)) the lost power is

$$P_{LOST} = - \frac{\xi}{2} \frac{(1 + R)}{(1 - R)} P_{OUT} \quad \ldots\ldots\ldots\ldots \quad (8.10)$$

where R is the output coupler reflectivity and P_{OUT} is the laser output beam power. Similarly for the external discharge (amplifier) the lost power (from (7.34)) is

$$P_{LOST} = - \pi r_b^2 L \alpha I e^{\alpha L} \quad \ldots\ldots\ldots\ldots \quad (8.11)$$

where the beam irradiance is I, discharge length L and gain coefficient α. Expressed in terms of the input laser beam power (probe beam)

$$P_{LOST} = - \alpha L P \quad \ldots\ldots\ldots\ldots\ldots\ldots \quad (8.12)$$

where the approximation $e^{\alpha L} = 1$ has been used. For short amplifiers the approximation is valid to better than 5%.

With the proviso that P_{LOST} is likely to be larger for oscillators compared to small signal amplifiers it is expected from the theory that the relationship between the input power change ΔP_{in} and the power lost P_{LOST} should be preserved for the two situations (i.e. oscillator and small signal amplifier). The exact relationship of these quantities is first for the oscillator (from (7.29))

$$\Delta P_{in} = \frac{(1 + R)}{2(1 - R)} \frac{\xi P_{OUT}}{(t_w/t_{dis} + 1)} = (t_w/t_{dis} + 1)^{-1} P_{LOST} \quad (8.13)$$

and for the amplifier from (7.37)

$$\Delta P_{in} = \frac{\pi r_b^2 L \alpha I}{(t_w/t_{dis} + 1)} = (t_w/t_{dis} + 1)^{-1} P_{LOST} \quad . . . \quad (8.14)$$

because the laser beam power $P = \pi r_b^2 I$ by definition of the beam irradiance. The constant of proportionality relating ΔP_{in} and P_{LOST} is the gas temperature term which is central to this theory $(t_w/t_{dis} + 1)^{-1}$; it is dependent on excitation, pressure mixture and wall temperature, and the value for typical laser discharges lies in the range $0.5 < (t_w/t_{dis} + 1)^{-1} < 0.8$. This temperature factor is not gain dependent because the gain parameter is either explicit in the amplifier equation or implicit in the oscillator equation (equal to the losses factor). The experimental measurement of this quantity is shown in Figure 8.25 for a gas mixture of 1 Xe, 3 CO_2, 4 N_2, 16 He torr with 10 mA excitation and a wall temperature of 280 K. The solid line represents the theoretical prediction based on the value of discharge temperature t_{dis} = 110 C. The close correspondence of both the oscillator and amplifier values with the theoretical slope show the considerable power and precision of the power perturbation theory that has been developed. The agreement of the theory (Chapter 7) with experimental evidence has been established over approximately four orders of magnitude for both the laser oscillator and external gain cell.

9.0 STANDING WAVE SATURATION RESONANCES OF THE CO_2 10.6 μm TRANSITIONS IN AN INTRACAVITY CO_2 CELL

When low pressure CO_2 absorbs a sufficiently high intensity resonant CO_2 laser standing wave the resulting $00^01 \rightarrow 00^00$ fluorescence will be saturated. At the transition line centre the saturated 10 μm absorption (and the resultant 4.3 μm fluorescence) can exhibit a Lamb dip[180] which can be used as a narrow frequency discriminant for laser stabilization. Conventionally, the CO_2 Lamb dip has been detected by optical means with a 4.3 μm photodetector such as InSb or Au:Ge[160] and in these experiments it has been detected for the first time electrically by the optogalvanic effect.

The HeNe laser was the first laser to be stabilized by locking the laser

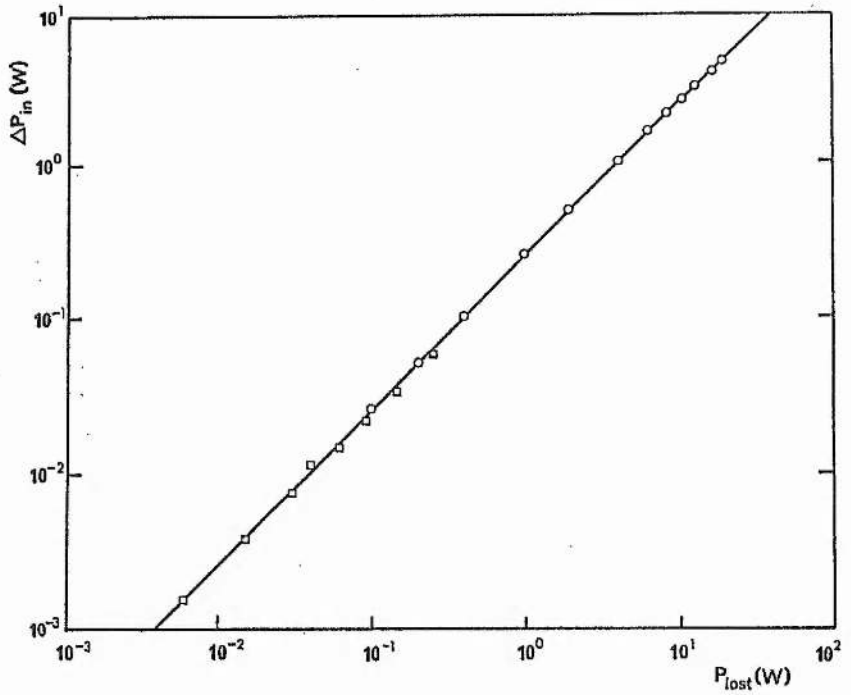

Fig. 8.25 The variation of input power change ΔP_{in} due to stimulated emission in a CO_2 laser oscillator (o) and small signal amplifier (□). The gas composition was 1 Xe, 3 CO_2, 4 N_2, 16 He (torr) and the discharge current was 16 mA. The small signal gain was optically measured to be 5 x $10^{-3}cm^{-1}$ and this value was used to calculate P_{LOST} for the 9.3 cm amplifier. The laser discharge used a 25 cm active length and a 90% reflectivity output coupler. The solid line represents the calculated values from equations (8.13) and (8.14) developed from the power perturbation theory presented in chapter 7.

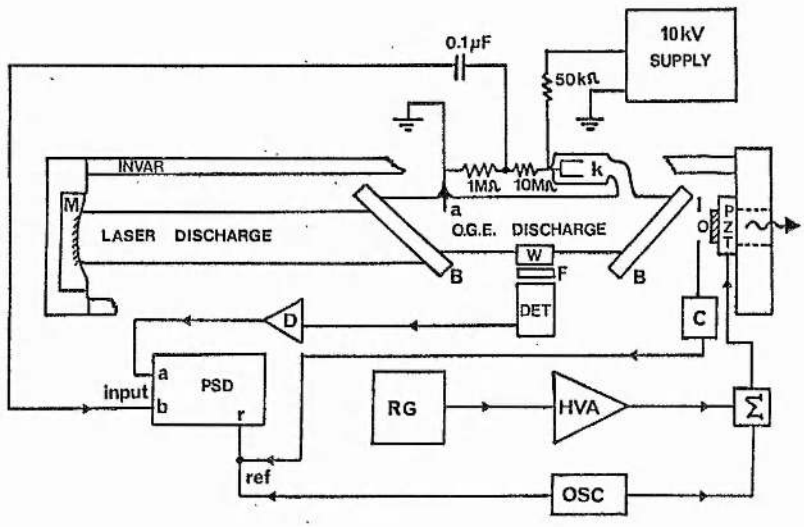

Fig. 9.01 The experimental apparatus used to detect $00^{0}1$ - 000 fluorescence and low pressure OGE by insertion of an intracavity gas cell in a stable CO_2 laser. The components are as follows: (PSD) - Brookdeal 9502 lock-in amplifier, (D) Brookdeal X100 preamplifier, (DET) Mullard RPY37 InSb 77 K photodetector, (F) Ge filter, (B) KCl Brewster windows, (W) Calcium Aluminate window, (RG) 300 s linear ramp generator, (HVA) Burleigh PZ81 high voltage amplifier, (Σ) mixer, (OSC) variable frequency ac source, (PZT) Lansing piezoelectric translator, (O) output coupler Ge or ZnSe 85%, 90% or 98%, (M) gold total reflector, (a) discharge anode, (k) discharge cathode.

cavity to a Lamb dip[181] and other absorptive gases with accidental frequency coincidence have been used for stabilization[182,183,184,185]. The use of saturated resonances in gases other than CO_2 has been successful[186,187] but if each of the CO_2 lines is to be stabilized then the use of CO_2 as a saturated absorber is required. At room temperature there is a small thermal lower laser level population which is excited into the upper laser level (00^01) by resonant absorption; subsequently, enhanced $00^01 \rightarrow 00^00$ spontaneous fluorescence occurs (in all the V-R lines due to the close rotational coupling). Tuning a laser across its gain profile results in a doppler line profile being generated by optical detection of the $00^01 \rightarrow 00^00$ yield.

The absorption lineshape at low pressures is predominantly doppler (velocity) broadened; the natural absorption frequency of a molecular transition is doppler shifted due to the translational velocity of the particular molecule. As a narrowband laser source is tuned across the absorption line, sets of molecules of different velocities are selected (for absorption) from the Maxwellian velocity distribution and their initial state population is depleted (if the laser beam is sufficiently intense). For a standing wave beam (which can be constructed from two travelling waves in opposite directions) only the set of molecules with zero velocity component along the axis will absorb both direction beams. This results in the standing wave saturation effect first described by Lamb which produces a narrow absorption minima occurring at the line centre of the absorbing transition.

The major reasons given for using these saturated resonances for stabilization references are the fact that the spectral feature is not significantly pressure broadened and because relatively good signal to noise ratios (for the $00^01 \rightarrow 00^00$ signal) have been achieved by simple optical construction. The absorption cell is usually operated in the pressure range 5 mtorr to 0.8 torr with a laser power of $\sim$ 1 mW to 1 W (see Chapter 5). The laser irradiance cannot be too high because this can introduce power broadening of the dip; consequently, the use of an external detection system (with forward and reflected beam) may be indicated for high power, high

efficiency lasers. The specific technological applications of the OGE system would be to provide improved stability of the existing conventional system or more significantly, the OGE stabilization of a CO_2 waveguide laser to a narrow frequency spectral feature;[188] recently a CO_2 waveguide laser with a wide gain profile (∿ 500 MHz) has been OGE stabilized[189] to laser line centre using a similar (non-saturated) system following the description in the publications reporting this work (Appendix 2).

Figure 9.01 shows the experimental system used here to investigate the saturated absorption signals (4.3 μm spontaneous emission and OGE). The secondary intracavity gas cell was constructed in a similar manner to the external cell described in Chapter 8 and like the lasers it was constructed of quartz with a Pt tubular side arm cathode, tungsten anode and fitted with KCl Brewster windows at either end and an infrared glass side window for viewing the sidelight. A liquid nitrogen cooled InSb detector was used with an intracavity chopper and Brookdeal 9502 lock-in amplifier. The PZT which mounted the laser output coupler (reflectivity 85% to 98%) was fed with a dc ramp voltage (linearity better than 5%) with which could be mixed a small ac signal. When ac length modulation was used, this signal provided the PSD reference signal and the beam chopper was removed.

The laser signature was readily detected by ramping the resonator length and observing the total 3 to 5 μm sidelight. Figure 9.02 shows two peaks 10P(20) and 10P(14) in the signature both exhibiting Lamb dips with a 0.2 torr CO_2 filling at 20 C. The Lamb dip full width at half depth was measured to be 2.7 ± 0.52 MHz at this pressure. The laser frequency scan rate was 400 kHz/s and the PSD integration time constant was 1 s; this results in ∿ 500 kHz spectral resolution. For 1 s integration the PSD output S/N was 5 dB and the Lamb dip depth was ∿ 3% for an intracavity power of 25 W. For a constant intracavity power level the dip broadened and became shallow when the cell pressure was increased disappearing at ∿ 0.75 torr. Figure 9.03 shows the effect of pressure change on the Lamb dip parameters. The relative depth decreases and the width increases with

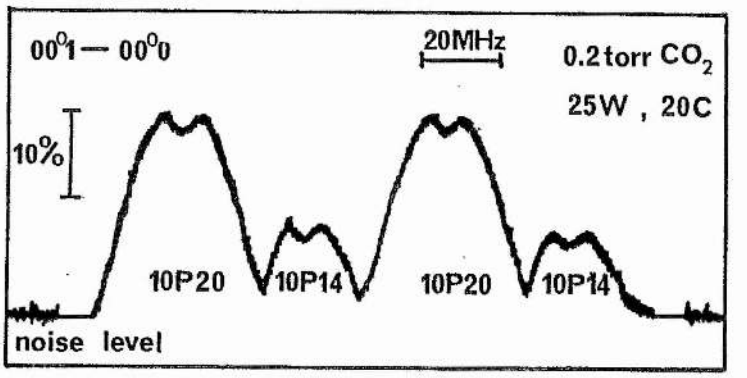

Fig. 9.02 00^01 - 00^00 saturated resonance spectra obtained by linearly translating the laser length twice by 2.7 μm. The total laser length was 1.2 m and the peak intracavity power was ∿ 25 W.

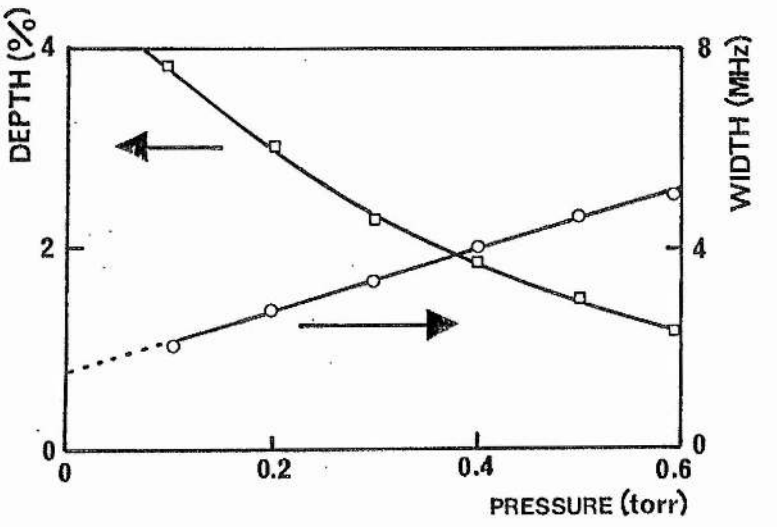

Fig. 9.03 The variation of the $00^01 \rightarrow 00^00$ fluorescence Lamb dip parameters (depth and width) with the variation of CO_2 cell pressure for a 25 W beam with a 1/e radius ∿ 2.2 mm.

pressure in line with predictions of previous workers[190]. The Lamb dip pressure broadening was 4.5 MHz/torr (34 kHz/Pa) in reasonable agreement with other investigators such as Freed and Javan (3.7 MHz/torr) and Woods and Jolliffe (11.6 MHz/torr). The extrapolated zero pressure dip width was $\sim$ 1.5 MHz. The power broadening for the 25 W beam appears to be small $<$ 1 MHz by comparing the observed dip widths to the 'zero power' value given by Woods and Jolliffe. The resolution of the experiment was not sufficient to measure this parameter; a reasonable upper limit would be 50 kHz/W.

The purpose of demonstrating these features of the $00^01 \rightarrow 00^00$ flourescence stabilization system here is to provide a detailed baseline for comparison of the OGE system described in 9.1. The laser could be stabilized by the fluorescence technique to either the Lamb dip (at pressures below 0.6 torr) or to the peak (for pressures between 2 and 0.8 torr) with time constants limiting the servo response to greater than 10 seconds. No improvement over the conventional OGE system was observed and the considerably inferior signal to noise ratio resulted in an amplitude stability of $\sim$ 2%. Some improvement may be made by using a hollow metallized reflector mounted on the discharge tube to direct more light into the small detector. The system used here was not adequate to provide sufficient low noise signals. It is known[128,160,191] that the technique is a difficult one requiring considerable preparation. Freed and O'Donnell[192] suggested that careful experimental refinement was necessary to improve the signal to noise ratios; this was also the conclusion of this experiment. It was possible here, however, to measure beam frequencies and identify transitions (Chapter 5.12) but to detect small amplitude modulation (as required for active stabilization) integration times (10 to 100 s) were required.

In general, the laser line centre frequency corresponded well to the Lamb dip centre frequency. The laser stabilized as above at the Lamb dip of 10P(20), 10P(14) and 10P(26) showed a maximum mean difference frequency when compared with a conventional OGE line stabilized laser of - 0.8 MHz. The

averaged frequency difference was 640 ± 720 kHz; the laser line centre being high frequency with respect to the Lamb dip. The difference between the Lamb dip centre and laser line centre is small (< 1 MHz) and no strong dependence on excitation or pressure could be found.[193]

9.1 OPTOGALVANIC DETECTION OF 9 TO 11 μm V-R TRANSITION STANDING WAVE RESONANCES

Using a low pressure discharge to detect radiation results in two major problems: the low energy absorption implying small optogalvanic perturbations and the increased discharge noise apparent at pressures below 1 torr. This section will deal largely with the detection of high intensity chopped beams in order to describe the operating characteristics of this new system and then show some preliminary attempts at Lamb dip OGE stabilization.

It was shown in Chapter 8 (see Figure 8.24) that low pressure CO_2 discharges are weakly absorptive and a small negative optogalvanic signal occurs due to the kinetic heating of the gas. It has also been shown that for low pressures ($\lesssim$ 0.5 torr) the absorption (and hence OGE) saturates at moderate laser beam powers (< 100 W). Figure 9.11 shows the voltage change in the intracavity gas discharge (at 0.6 torr) due to the absorption of the laser beam. The voltage change for a fixed current (5 mA) is presented; this excitation produced the maximum signal to noise ratio. The saturated value occurs for $\Delta V \sim 0.5$ V corresponding to a fractional power perturbation $\Delta P_{in}/P_{in} = 2 \times 10^{-4}$ which is 50% lower than expected from Figure 8.21. The experimental results in Chapter 8 used a 16 Hz chopping frequency. The OGE was found to decrease in value for frequencies above $\sim$ 100 Hz, for this pressure of CO_2, and the 16 Hz value comparing the external cell with internal cell agreed to within 10%. This empirical low frequency reduction suggests that the 00^01 relaxation time $\tau_{001} \sim$ 10 ms. Assuming 50% CO_2 dissociation and a gas temperature of 100 C the relaxation time of 00^01 level was calculated to be 6 ms; the decay frequency $f \rightarrow \frac{1}{2}\tau_{00^01}$ was calculated to be 150 Hz. CO_2 pressures down to approximately 0.5 torr produce relatively

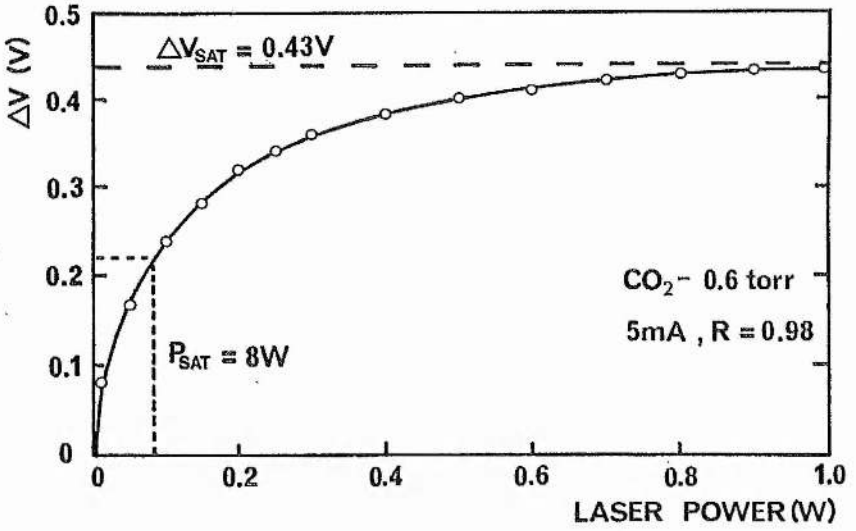

Fig. 9.11 The variation of the optically induced voltage change ΔV with the variation of the laser output power up to 1 W. The output coupler reflectivity was 98%, therefore, intracavity standing wave power varies up to $\sim$ 100 W. The saturation voltage change for a 5 mA current was 0.43 V and the half saturation voltage ($\Delta V_{SAT}/2$) and standing wave power (P_{SAT}) were 215 mV and 8 W for 0.6 torr CO_2 pressure. The laser beam was chopped at 220 Hz and a Brookdeal 9502 lock-in amplifier was used for detection.

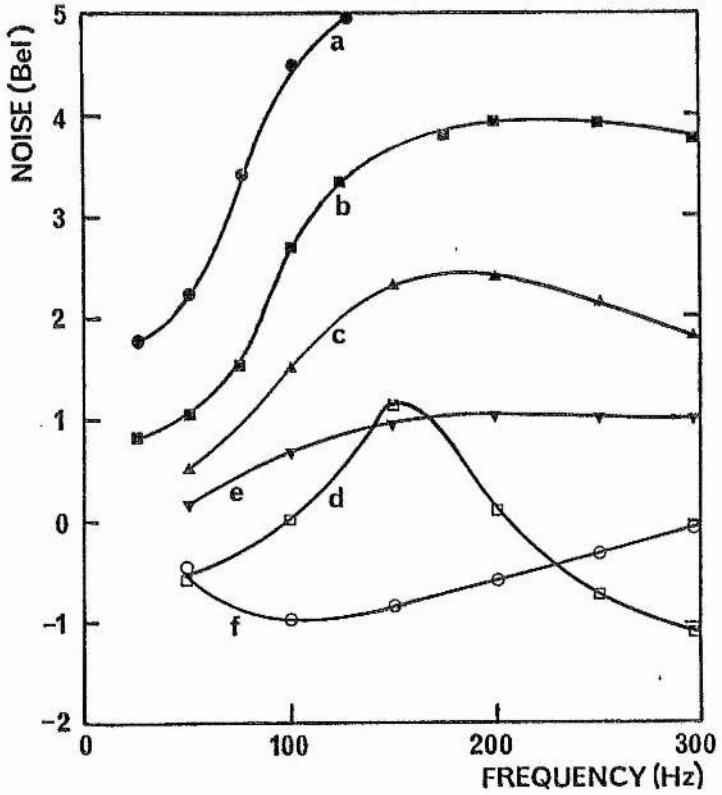

Fig. 9.12 The variation of the noise voltage spectra received into a 1 MΩ resistance from the intracavity discharge tube with various gas fillings. The logarithmic scale is referred to the undischarged noise level. The curves represent the following conditions, (a) 0.1 torr CO_2, (b) 0.2 torr CO_2, (c) 0.3 torr CO_2, (d) 0.5 torr CO_2, (e) 2 torr CO_2, (f) 0.2 torr CO_2 + 0.3 torr N_2 all discharged at 2 mA.

quiet dc discharges with this electrode geometry and with the laser fitted with a 98% output coupler the laser absorption transition is well saturated with 1 W output power. The half saturation standing wave power was 8 W corresponding to an output power of 80 mW.

OGE laser signatures can be obtained with these conditions and they show no Lamb dips at pressures above 0.8 torr. This was expected at these pressures because detection of the 4.3 μm fluorescence dip above 0.6 torr was difficult although CO_2 dissociation occurs, resulting in ∿ 50% CO_2 loss, it appears that the dip broadening due to the O_2 and CO was sufficient to prevent the presence of a Lamb dip.[194] The CO_2 pressure cannot be reduced significantly below 0.6 torr because striations form, and the electrical discharge exhibits severe electrical noise in the audio frequency band.

The problem of electrical noise in low pressure molecular discharges is complicated and sparsely dealt with in the literature. There has been considerable investigation of HeNe laser discharges[195,196,197] and the major interest has been the correlation of the electrical noise with output beam modulation[198]. The nature of the previous investigations resulted in inconclusive evidence due to the variety of discharge geometries (configurations). The general conclusion is, however, that striations must be avoided in order to maintain a low noise discharge and that the relative noise figure increases with decreasing pressure in the range 0.05 to 0.5 torr. Several authors[199] studying CO_2 have also observed that a threshold current (for a given pressure) exists above which noise is markedly increased. This threshold current shifts to lower values for lower pressures. Typical values in these experiments were 4 to 10 mA depending on pressure and composition. Additionally, all currents below ∿ 0.5 mA for the low pressure (< 1 torr) CO_2 discharges were particularly noisy in the very low frequency band < 50 Hz; large noise spikes ∿ 1 to 10 V occurred at irregular intervals. This behaviour may have been due to the power supply and ballast excitation circuit.

The threshold current for 1 torr CO_2 was ∿ 3 mA and all measurements

were made with 1.0 mA < I_{dis} < 5 mA (i.e. in the low noise current window). Figure 9.12 shows noise measurements of the various discharges made with the HP8557 audio frequency spectrum analyzer. The mains harmonic noise usually dominates and the curves between the harmonic points are in some cases higher than the narrow bandwidth noise values. For this excitation condition (2 mA cc) there is a clear increase of noise as pressure decreases in the usable OGE detection bandwidth (10 to 500 Hz). For example, the 0.1 torr noise at 100 Hz is 50 dB higher than 2.0 torr. The noise value in this figure is taken relative to the undischarged noise received with the cell screened in an aluminium box. Figure 9.13 shows how for 2 torr (similar to 9.12(e)) the noise increases by up to 10 dB over the whole band.

In some cases, however, the received noise decreases when the discharge is running (9.12(d) and 9.12(f)). This reduction of noise can be understood in the following way. The cathode is floating (the anode is earthed at the psu) when the cell is undischarged. Mains related and other electromagnetic radiation was received and typical hum voltages at 100 Hz are $\sim$ 10 μV to 1 mV. When the discharge is running, a low impedance ($\sim$ 100 kΩ) exists between the electrodes. If the power supply ripple and 'discharge fluctuations' are small compared to the pickup then a noise reduction due to the lower source resistance would be recorded. There may also be some antiphase discharge fluctuation component.

In the case of a particularly quiet discharge and psu this noise reduction behaviour can be observed (even in 20 torr laser discharges). In this limit OGE S/N will be very high and the $\gtrsim$ 0.5 torr OGE was found to have acceptable S/N for the generation of good signatures with integration times of a few seconds. There is a general peak of noise in the 100 to 500 Hz band which shifts to higher frequencies and broadens as the pressure decreases below 1 torr. The 0.5 torr noise spectrum shows a 150 Hz peak of mains related noise. Additionally, there is a striation related noise band $\sim$ 5 to 20 kHz which shifts frequency and bandwidth with pressure in the range 0.05 to 0.3 torr.

It is demonstrated in 9.12 that additions of N_2 can produce large reductions of noise at low total pressures. By utilizing approximately 1:1 mixtures of CO_2:N_2, reductions of at least 20 to 30 dB at all pressures below 0.8 torr were obtained. Buffering the CO_2 with He or Xe conversely, increased noise by 30 and 10 dB respectively for a 1:1 mixture at 0.5 torr total pressure.

Some investigation of the noise spectrum outside the 50 to 500 Hz regime was attempted. Firstly, as long as currents are carefully chosen, noise does not rise substantially below 50 Hz down to $\sim$ 5 Hz; the resolution of the spectrum analyzer made lower frequency investigation unreliable. Likewise, low noise behaviour up to 50 kHz was observed for suitable (2 mA, 0.2 CO_2, 0.3 N_2) discharges apart from some oscillatory bands ($\sim$ 10 kHz). Because the OGE bandwidth is restricted for the low frequency effect to an upper limit of $\sim$ 300 Hz the noise spectrum at higher frequencies was not investigated. An OGE signal at high frequencies related to the $01^{o}0$ V-T process (see Chapter 6) should be observable but it was not possible experimentally to chop the radiation field faster than $\sim$ 300 Hz. Small signal ($\sim$ 2%) ac modulation did not produce sufficiently large OGE signals at these frequencies to make quantitative measurements.

In order to achieve both a stable low noise discharge at a sufficiently low pressure for the detection of a Lamb dip a CO_2:N_2 gas mixture has been indicated. The excitation conditions required for the lowest noise operation suggest a value below the noise threshold ($\lesssim$ 6 mA for this pressure) and above a critical value ($\sim$ 0.5 mA) set by the power supply current control system. Additionally, the equilibrium CO_2 dissociation must not be too large and in this respect lower values of P/L are favoured. With the Pt cathode a reasonable estimate of the equilibrium dissociation for 1 to 2 mA current is $\sim$ 50%. When N_2 is added the upper laser level is more efficiently excited and, therefore, the gas can either be in gain or only weakly absorptive. Figure 9.14 shows the optogalvanic spectrum obtained by repetitive length scanning across the peak of 10P(20) at various pressures.

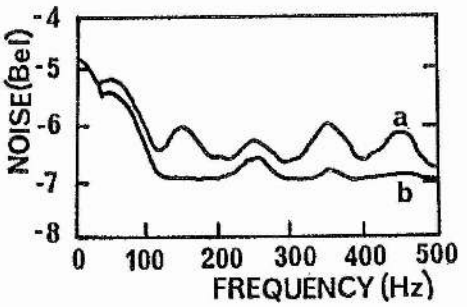

Fig. 9.13 The noise spectrum for 2 torr CO_2, both discharged at 2 mA (a) and undischarged (b). The resolution was 30 Hz and the voltage referred to 1 mV into 1 MΩ.

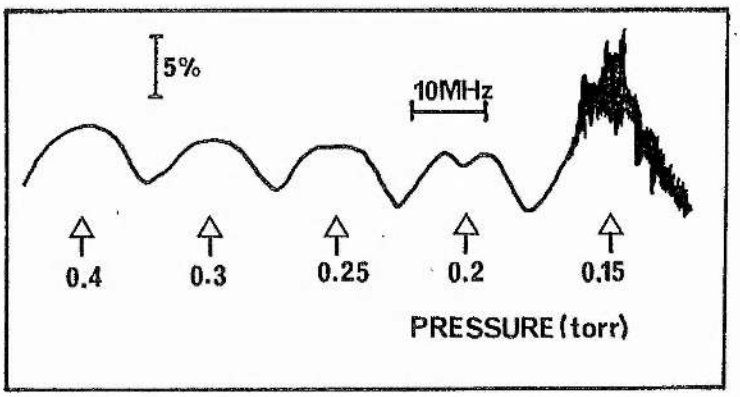

Fig. 9.14 Various optogalvanic spectra of 10P(20) line centre at pressures of 0.15 to 0.4 torr of 1:1 CO_2; N_2 mixture.

No Lamb dip was observed with the CO_2:N_2 total pressure down to 300 mtorr. At 250 mtorr the peak was noticeably flattened and a pronounced dip was visible below 220 mtorr. At 200 mtorr the dip was 3 MHz wide at half depth and 2% deep. Reducing the pressure below 200 mtorr resulted, at this current (2 mA), in markedly increased noise (greater by $\sim$ 40 dB). Some reduction ($\sim$ 15 dB) of this noise was achieved by setting the current to $\sim$ 0.7 mA. The optimum total pressure for Lamb dip detection was found to be 0.2 torr and the excitation for the best S/N was $\sim$ 1.0 mA (P/L $\sim$ 0.4 Wcm^{-1}).

In order to stabilize a laser only small amplitude length modulation is required and to investigate the feasibility of OGE Lamb dip stabilization, a 4 V pk-pk 20 Hz sine wave was mixed with the 0 to 1 kV dc ramp voltage. The tube voltage change was detected with a lock-in amplifier referenced to this 20 Hz signal. The integrated output of the PSD in this case was the first differential of the discharge voltage (discriminant) which is zero valued for power tuning points; it is this voltage null that the stabilizer servomechanism seeks. Figure 9.15 shows the discriminant of the 10P(20) peak at 0.2 torr shown in Figure 9.14. The in phase signal at the modulation frequency will be proportional to the slope of the gain profile at the fixed operating point, tending to zero at the dip centre and the two intracavity power maxima. Three distinct zero values are shown in Figure 9.15. The central zero crossing is the centre of the Lamb dip. The ac modulation signal produced approximately $\sim$ 700 kHz FM deviation; typical ac tube voltage signals of 0.1 to 1 mV were received and amplified by 60 dB using the Brookdeal 9502 and preamplifier. The time constant was 10 s. The PSD output clearly shows the phase change over at the centre of the Lamb dip. The laser was tuned from - 4 to + 4 MHz and as a result the whole line shape slope is not shown, this length scan was achieved in 500 s.

Attempts to stabilize the laser at the centre of the Lamb dip directly were not successful because rapid perturbations occurred which resulted in the servomechanism locking to a minimum between two line segments.

If a low pressure CO_2 OGE cell is to be used as a stabilization reference in preference to conventional OGE stabilization the following considerations must be made. Typical Lamb dip parameters (at 100 W beam power) are 3 MHz width (Δf_a) and 1 to 3% depth. The equivalent power change for line centre stabilization (for 25 torr laser discharge) occurs with approximately 4 MHz frequency shift. The Lamb dip is full width however, therefore, the comparative pressure broadened line centre frequency shift (Δf_b) is 8 MHz. The Lamb dip discriminant advantage factor (F_1) is just given by the ratio of the frequency shifts.

$$F_1 = \frac{\Delta f_b}{\Delta f_a} = (8.0/3.0) \sim 2.7 \quad \ldots\ldots\ldots \quad (9.1)$$

For the waveguide CO_2 laser where the pressure broadening is much greater this factor is considerably larger[135,200,201] (the typical line width is 500 MHz (at $\sim$ 100 torr)) and the comparative frequency shift for 1 to 2% power reduction is 30 MHz. The discriminant advantage (F_1) is now

$$F_1 = (60/3) \sim 20 \quad \ldots\ldots\ldots\ldots\ldots\ldots \quad (9.2)$$

The other major consideration is the error signal to noise ratio. Firstly, at low pressures (0.2 to 0.6 torr) the OGE signal is much smaller ($\lesssim$ 10%) and the noise is increased <u>at best</u> by 8 to 10 dB at the optimum modulation frequency $\sim$ 175 Hz. The signal to noise ratio factor F_2 which is a measure of the ability to stabilize using the error signal source is given by the ratio of S/N values for the two cases (i.e. low pressure CO_2 and laser mixture)

$$F_2 = \frac{S/N_{(0.2\ \text{torr})}}{S/N_{(25\ \text{torr})}} \sim 0.05 \text{ or } -40 \text{ dB} \quad \ldots\ldots \quad (9.3)$$

A suitable measure of comparison of the two systems is the figure of merit (G) consisting of the product of the S/N factor F_2 and the discriminant factor F_1. Firstly, comparing the case of 25 torr laser line centre versus Lamb dip stabilization

$$G = F_1F_2 = 2.7 \times 0.05 \sim 0.14 \quad \ldots\ldots\ldots (9.4)$$

and hence the performance should be $\sim$ 7:1 in favour of line centre stabilization. Otherwise a longer integration time constant is required (empirically $\geq$ 10 times was needed) for the same information retrieval. As a result a better passive stability design would be indicated in order to reach the same ultimate performance. Taking the case of the waveguide laser and assuming the signal to noise factor F_2 is the same as in the 25 torr case

$$G = 20 \times 0.05 = 1 \quad \ldots\ldots\ldots\ldots\ldots (9.5)$$

indicating that the performance would be similar for both the Lamb dip stabilization and line centre stabilization. In practice, the discharge may well provide a different S/N ratio. The discharge noise could have a different value at high pressure and the OGE signal could be higher for larger values of gain and efficiency. This would suggest that there may be some small advantage in using Lamb dip detection. However, due to the considerable increase in complexity it is probably not a practical development.

For stabilization of the waveguide laser, advantage can be made of the improved discriminant width (F_1) and a high signal to noise ratio factor (F_2) by using a low pressure OGE cell with pressures $\gtrsim$ 0.5 torr and using the narrower line centre peaks rather than Lamb dips. Figure 9.16 shows a laser signature detected with the OGE cell filled with 0.2 torr CO_2, 0.3 torr N_2. Each line peak shows a fall of 1 to 2% over approximately 2 MHz giving an F_1 value of $\sim$ 32 with a good signal to noise ratio (because the pressure is above the limit for striations) yielding an F_2 value $\sim$ 1. In this case, with low pressure rather than high pressure line centre stabilization an advantage factor G = 32 is indicated. This could provide a large improvement of active stabilization performance for the waveguide laser.

The OGE saturated resonance signals received down to pressures of 200 mtorr (when suitably discharged with N_2 added) produced slightly better S/N than the InSb 4.3 μm flourescence signals. In general, neither signals were adequate for high grade stabilization, although the utilization of line centre

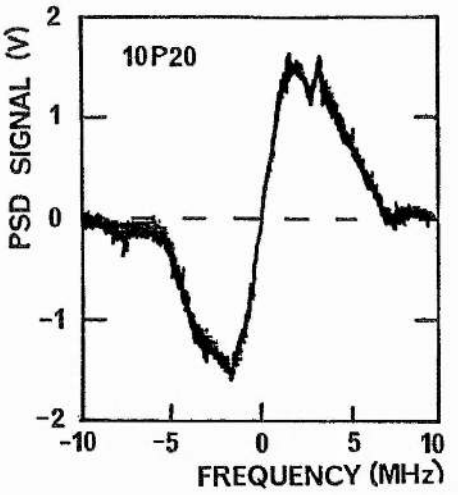

Fig. 9.15 The first differential (discriminant) of the OGE 10P(20) signature shown in Fig. 9.14 for 0.2 torr pressure. The discriminant was detected by applying a small (4 V) ac modulation to the PZT during ramp length translation using a Brookdeal 9502 lock-in amplifier to detect the synchronous voltage changes for across the discharge.

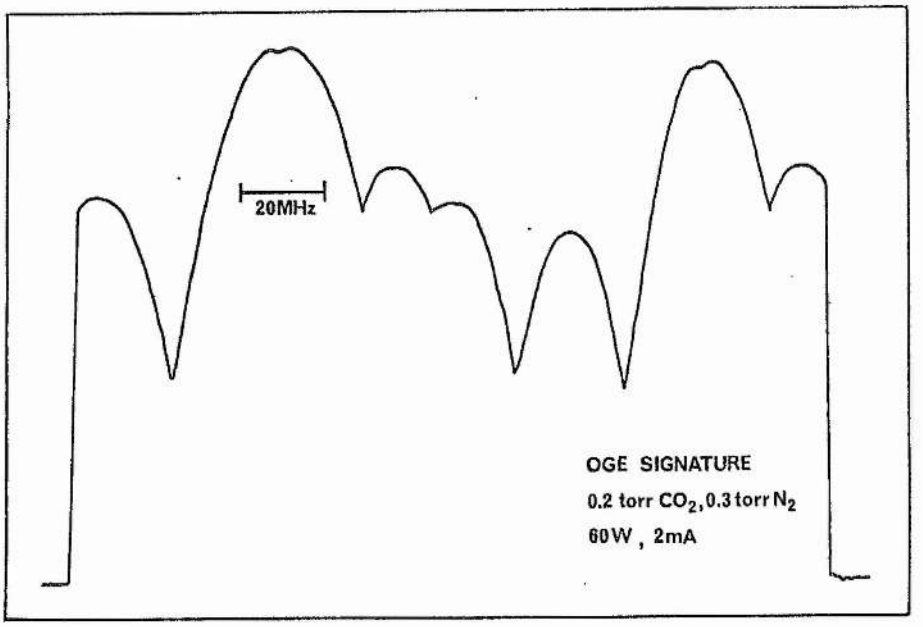

Fig. 9.16 OGE signature obtained with low pressure intracavity cell. The larger peaks are 10P(20) and apparently show very small Lamb dips.

stabilization in the secondary low pressure discharge by OGE techniques provided a sufficiently good signal for stabilization which was comparable with the laser discharge line centre signal. These saturation resonance experiments were intended to be essentially exploratory in order to find if low pressure discharge OGE signal sources would be useful. A more thorough investigation of the noise problem and a much better developed laser system would be required to complete the measurements. However, from this study sufficient data has been collected to show that this low pressure OGE system is not likely to provide a good signal source with dc excitation.

10.0 CONCLUSIONS

The CO_2 laser optogalvanic effect (OGE) provides fundamental kinetic information about the laser discharge and has several major technological applications including optical detection and stabilization. The discharge power perturbation model presented (Chapter 7) relates the change of optical beam power to temperature variations of the discharge and subsequently, determines directly the change of electrical discharge characteristics. These predictions have been compared to electrical measurements made with various CO_2 laser oscillator amplifiers, external amplifier/absorber cells and secondary intracavity gas cells. Considerable experimental evidence for supporting the theory has been collected by varying all the major operational parameters: excitation, cooling pressure, gas mixture and output coupler alignment and reflectivity. The prediction of electrical perturbation has been shown to agree (Chapter 8) with empirical data over almost four orders of magnitude change in beam intensity and the dependence of OGE on wall cooling can be modelled over a wide temperature range to $\sim$ 10 C. No other theory offered so far can predict qualitatively all the behaviour observed. The reduced OGE due to $00^0 2$ sequence band laser beams has been predicted and measured and demonstrates that the ratio of the upper laser level populations for $00^0 1$ to $00^0 2$ levels is approximately 4.

The variation of the electrical properties of the discharge (due to changing beam irradiance) provided some direct electrical measurements of absorption/gain saturation and the relaxation lifetimes of the $00^0 1$ and $01^1 0$ levels. These perturbation results give secondary evidence supporting existing measurements. More fundamentally, the temporal response of OGE in CO_2 gives important primary evidence supporting the (gas temperature) power perturbation model. A new high frequency effect has been discovered, explained and used to stabilize lasers with a fast closed loop response.

A high degree of stability has been achieved using a simple stable resonator (without dispersive components) and a suitable OGE feedback loop to provide stable outputs of 5 to 40 W with amplitude changes $\lesssim$ 0.5%, long term (hour) frequency stabilities of $\lesssim$ 50 kHz and a resettability of better than 400 kHz. To summarize, OGE stabilization has provided impressive stability improvement for small CO_2 oscillators giving up to two orders of magnitude improvement in the laser intensity fluctuations and over six orders of magnitude improvement of frequency stability.

10.1 FUTURE INVESTIGATIONS

It is the intention of this section to point directly to areas which could be investigated in order to more precisely test the power perturbation theory and to extend the application of the ideas presented here. The three major areas for work of primary importance are

1. The careful measurement of dc discharge noise dependent on gas composition, excitation and reception frequency band. The discovery of low noise conditions would extend the low pressure investigations.
2. Accurate thermocouple measurements of gas temperature dependent on radial position, gas composition, pressure and excitation. This will allow more precise testing of the power perturbation theory for various compositions (e.g. He concentration change).

3. Development of a phase sensitive detection scheme for the bandwidth 100 kHz to 10 MHz.

The OGE stabilization system developed during this work and described here has been used to assist CO_2, far infrared laser pumping by controlled offset locking[202] and injection locked TEA lasers.[189] The stabilization scheme is currently being used to actively stabilize a hybrid TEA laser,[203] CO_2 waveguide lasers[189, 204] as well as conventional lasers.[205] The possibility of using the electrical error signal to correct resonator alignment (as well as length) by using a microprocessor based system should also be investigated. This technique could automatically select the highest gain line (10P(20)) from a laser signature after one or two scans through. As the utilization of RF discharges increases due to their inherent quietness and stability analogous RF, OGE techniques detecting VSWR changes from the discharge load could be used in a control system to stabilize and programme laser outputs.

BIBLIOGRAPHY

1 Avtonomov V.P., Antropov E.T., Goldina N.D., Gorelik A.V., Sobolev N.N., Ostapchenko E.P. and Troitskii Y.T., Sov.J.Quantum Electron. 3, 345 (1974)

2 Smith P.W., IEEE J.Quantum Electron. QE-1, 343 (1965)

3 Claspy P.C. and Pao Y., Appl.Opt. 10, 136 (1971)

4 Schiffner G., IEEE J.Quantum Electron. QE-8, 877 (1972)

5 Fox A.G. and Li T., Bell Syst.Tech.Journ. 453 (1961)

6 Kogelnik H. and Li T., Appl,Opt. 5, 1550 (1966)

7 Foote P.D. and Mohler F.L., Phys.Rev. 26, 195 (1925)

8 Meissner K.W. and Graffunder W., Ann.der Phys. 84, 1009 (1927)

9 Penning F.M., Phil.Mag.S.7.11, 961 (1931)

10 Meissner K.W. and Pierson R.M., Phys.Rev. 92, 896 (1959)

11 Penning F.M., Physica 8, 137 (1928)

12 Kenty C., Phys.Rev. 80, 95 (1950)

13 Bridges W.B., J.Opt.Soc.Am. 68, 352 (1978)

14 Townshend J.S. and McCallum S.P., Proc.Roy.Soc.A124, 543 (1929)

15 Pike E.W., Phys.Rev. 49, 513 (1936)

16 Pike E.W., Ph.D. thesis, Princeton (1934)

17 Meissner K.W. and Miller W.F., Phys.Rev. 92, 896 (1953)

18 Green R.B., Keller R.A., Luther G.G., Schenck P.K. and Travis J.C., Appl.Phys.Lett. 29, 727 (1976)

19 Kravis S.P. and Haydon S.C., J.Phys.D: Appl.Phys. 14, 151 (1981)

20 Green R.B., Keller R.A., Luther G.G., Schenck P.K. and Travis J.C. U.S. Patent PB-288605 (1978)

21 Goldsmith J.E.M. and Lawler J.E., Contemp.Phys. 22, 235 (1981)

22 King D.S. and Schenck P.K., Laser Focus 51 (1978)

23 Garscadden A., Bletzinger P. and Friar E.M., J.Appl.Phys. 35, 3432 (1964)

24 Garscadden A. and Adams S.L., Proc.IEEE 54, 427 (1967)

25 Schiffner G. and Seifert F., Proc.IEEE 53, 1657 (1965)

26 Weaver L.A. and Freiberg R.J., J.Appl.Phys. 37, 1528 (1966)

27 Weaver L.A., Contract AF19 (628)-3307 Sci.Rep. 4 (1966)

28 Bennett W.R., Kindlmann P.J. and Mercer G.N., Appl.Opt.Supp. 2, 34 (1965)

29 Waksberg A.L. and Carswell A.I., Appl.Phys.Lett. 6, 137 (1965)

30 Freiberg R.J. and Weaver L.A., J.Appl.Phys. 38, 250 (1967)

31 Klein M.B., Bridges W.B. and Halsted A.S., unpublished, Hughes Res. Lab., Malibu, California (1965)

32 Dunn M.H. and Maitland A., Proc.Phys.Soc. 92, 1106 (1967)

33 Pepper D.M., IEEE J.Quantum Electron. QE-14, 971 (1978)

34 Lawler J.E., Phys.Rev. A22, 1025 (1980)

35 Erez G., Lavi S. and Miron E., IEEE J.Quantum Electron. QE-15, 1328 (1979)

36 Lawler J.E., IEEE J.Quantum Electron. QE-14, 971 (1978)

37 Webb C.E., Inst.Phys.Conf.Ser. 29, 1-28 (1976)

38 Patel C.K.N., Phys.Rev. 136, 1187 (1964)

39 Patel C.K.N., Sci.Am. (August 1968)

40 Rigden J.D. and Moeller G., IEEE J.Quantum Electron. QE-2, 365 (1966)

41 Parks J.H. and Javan A., Phys.Rev. 139A, 1351 (1965)

42 Carswell A.I. and Wood J.I., J.Appl.Phys. 38, 3028 (1967)

43 Kindl H., Leeb W. and Schiffner G., Proc.IEEE 56, 781 (1968)

44 Cheo P.K., J.Appl.Phys. 38, 3563 (1967)

45 Schiffner G., J.Opt.Soc.Am. 61, 650 (1971)

46 Schiffner G., private communication

47 Gower M.C. and Carswell A.I., Appl.Phys.Lett. 21, 556 (1972)

48 Taylor R.L. and Bitterman S., Rev.Mod.Phys. 41, 26 (1969)

49 Aoki T., J.Appl.Phys. 9, 1249 (1970)

50 Gower M.C. and Carswell A.I., J.Appl.Phys. 45, 3922 (1974)

51 Vesley V., Plasma Phys. 3, 149 (1964)

52 Brooks M., Ph.D. thesis, St. Andrews (1976)

53 Smith A.L.S. and Brooks M., J.Phys.D: Appl.Phys. 12, 1237 (1979)

54 Kerecman A.J., Jacobs H., Lo Cascio C., Brand F.A. and Novick G., IEEE J.Quantum Electron. QE-5, 474 (1969)

55 Crane R.A., Can.J.Phys. 47, 2785 (1969)

56 Bleekrode R., IEEE J.Quantum Electron. QE-5, 57 (1969)

57 Nowicki R. and Pienkowski J., J.Phys.D: Appl.Phys. 15, 1165 (1982)

58 Aoki T., Yamada C. and Katayama M., Japan.J.Appl.Phys. 10, 332 (1971)

59 Gebhardt F.G. and Smith D.C., Appl.Phys.Lett. 20, 129 (1972)

60 Lobov G.D., Shtykov V.V., Bogatkin V.I. and Drugov L.C., Radio Eng. Elect.Phys. 16, 968 (1971)

61 Skolnick M.C., IEEE J.Quantum Electron. QE-6, 139 (1970)

62 Rabinowitz P., Keller R. and Latourrette J.T., Appl.Phys.Lett. 14, 376 (1969)

63 Basov N.G., Belenov E.M., Danileiko M.V. and Nikitin V.V., Sov.Phys. JETP 33, 66 (1971)

64 Goldberg M.V. and Yusek R., Appl.Phys.Lett. 18, 135 (1971)

65 Freed C. and Javan A., Appl.Phys.Lett. 17, 53 (1970)

66 Woods P.T. and Jolliffe B.W., J.Phys.E. 9, 395 (1975)

67 Thomason W.H. and Elbers D.C., Rev.Sci.Instrum. 46, 409 (1975)

68 Thomason W.H. and Elbers D.C., Laser Focus (November 1975)

69 Hart K. and Siemsen K.J., private communication

70 Massig J.H., IEEE J.Quantum Electron. QE-13, 29 (1977)

71 Jacobs H., Kerecman A.J. and Schumacher J., J.Appl.Phys. 38, 3412 (1967)

72 Stefanov V.J., J.Phys.E. 3 (1970)

73 Witteman W.J., IEEE J.Quantum Electron. 5, 92 (1969)

74 Pao Y.H., ed. Opto-acoustic Spectroscopy and Detection, Academic Press (N.Y.)

75 Kreuzer L.B., J.Appl.Phys. 42, 2934 (1971)

76 Kreuzer L.B. and Patel C.K.N., Science 173, 45 (1971)

77 Kreuzer L.B., Keynon N.D. and Patel C.K.N., Science 177, 347 (1972)

78 Whinnery J.R., Chem.Res. 7, 225 (1974)

79 Bailey R.T., Cruickshank F.R., Pugh D. and Johnstone W., private communication

80 Jackson W.B., Amer N.M., Boccara A.C. and Fournier D., Appl.Opt. 20, 1333 (1981)

81 Boccara A.C. and Fournier D., Opt.Lett. 5, 377 (1980)

82 Brassington D.J., J.Phys.D: Appl.Phys. 15, 219 (1982)

83 Green R.B.; Keller R.A., Luther G.G., Schenck R.K. and Travis J.C., IEEE J.Quantum Electron. QE-13, 63 (1977)

84 Marr G.W. and Wherrett S.R., J.Phys.B. 5, 1735 (1972)

85 Turk G.C., Travis J.C., Devoe J.R. and O'Haver T.C., Anal.Chem. 50, 817 (1978)

86 Lawrence E.O. and Edlefsen N.E., Phys.Rev. 34, 233 (1929)

87 Mohler F.L. and Boeckner C., J.Res.Nat.Bur.Stand. 3, 303 (1929)

88 Freundenberg K., Z.Phys. 67, 417 (1931)

89 Popescu D., Ann.Phys.LPZ 18, 103 (1966)

90 Popescu D., Rev.Romaine Phys. 11, 925 (1966)

91 Lampert M.A. and White A.D., Elect.Commun. 30, 124 (1953)

92 Farmat N.H., Proc.IEEE 52 (1964)

93 Kopeika N.S., Galore B., Stempler D. and Heimenrath Y., IEEE Trans. on Microwave Theory and Techniques, MTT-23, 843 (1975)

94 Severin P.J.W., Philips Res.Rep.Suppl. 2 (1965)

95 Kopeika N.S., Proc.IEEE 63, 981 (1975)

96 Kopeika N.S. and Rosenbaum J., IEEE Trans.Plasma Science PS-4, 51 (1976)

97 Eytan G., Kopeika N.S. and Kushelevsky A.P., IEEE Trans.Plasma Science PS-6, 261 and 314 (1978)

98 Allen A.D., Found.Phys. 7, 609 (1977)

99 Macdonald A.D., Microwave Breakdown in Gases, Wiley (N.Y.) 24 (1966)

100 Ben-Amar A., Shuker R. and Erez G., Appl.Phys.Lett. 38, 763 (1981)

101 Shuker R., Gallagher A. and Phelps A.V., J.Appl.Phys. 51, 1306 (1980)

102 Molnar J.P., Phys.Rev. 83, 933 (1951)

103 Molnar J.P., Phys.Rev. 83, 940 (1951)

104 Krish H., Z.Phys. 208, 322 (1968)

105 Haydon S.C. and Williams O.M., J.Phys.D. 11, 1859 (1981)

106 Miron E., Smilanski I., Liran J., Shimon L. and Erez G., IEEE J.Quantum Electron. QE-15, 194 (1979)

107 Drawin H.W., Euratom-CEA Rep. EUR-CEA-FC 383 (1967)

108 Thomas W.R.L., J.Phys.B: Atom.Molec.Phys. 2, 551 (1969)

109 Smith A.L.S. and Browne P.G., J.Phys.D: Appl.Phys. 7, 1652 (1974);

see also 139 for deliberate Pt catalysts

110 Carbone R.J., IEEE J.Quantum Electron. QE-3, 373 (1967)

111 Taylor F.M., Lombardo A. and Eppers W.C., Appl.Phys.Lett. 11, 180 (1967)

112 Witteman W.J., Appl.Phys.Lett. 11, 337 (1967)

113 Rosenberger D., Phys.Lett. 21, 520 (1966)

114 Mellis J., private communication

115 Fahlen T.S., Appl.Opt. 12, 2381 (1973)

116 Technical Bulletin 108: E7 epoxy adhesive, Techkits, P.O. Box 105, Demarest, New Jersey 07627, U.S.A.; see also Peele J.R. and Whitney W.T., Rev.Sci. Instr. 40, 1114 (1969).

117 Avtonomov V.P., Antropov E.T., Sobolev N.N. and Troitskii Y.V., Sov. J.Quant.Electron. 2, 300 (1972)

118 Mellis J. and Smith A.L.S., Opt.Commun. 41, 121 (1982)

119 Specification sheet for Vernitron PZT 5H material, Vernitron Ltd., Thornhill, Southampton SO9 5QF

120 Varwig R.L., Sandstrom R.L. and Wang C.P., Rev.Sci.Instrum. 52, 200 (1981)

121 Duxbury G., private communication

122 Vinculum Manual: Handbook for twin laser control unit M.65, Vinculum Services, 40A Kneesworth Steet, Royston, Herts. SG8 5AQ

123 Maggs P., private communication

124 Siemsen K.J., private communication

125 Scholtz A.L. and Schiffner G., Appl.Phys. 21, 407 (1980)

126 Shotton K.C. and Rowley W.R.C., NPL Quantum Metrology Report QU-28 (1975)

127 Wallard A.J. and Wilson D.C., J.Phys.E. 7, 161 (1974)

128 Freed C., Proc. of 31st Annual Freq.Control Symp. 592 (1977), U.S. Army Electronics Ind. Assoc., Washington D.C.

129 Bullis R.H., Nighan W.L., Fowler M.C. and Wiegand W.J., AIAA Journal 10, 407 (1972)

130 Nicholls R., Nature 226, 353 (1970)

131 Rowley W.R.C. and Wilson D.C., Appl.Opt. 11, 475 (1972)

132 Birnbaum G., Proc.IEEE 55, 1015 (1967)

133 Heard H.G., Laser Parameter Measurements Handbook, Wiley

134 Freed C., IEEE J.Quantum Electron. QE-4, 404 (1968)

135 Hall D.R., Jenkins R.M. and Gorton E.K., A Frequency Stabilized cw Waveguide CO_2 Laser, J.Phys.D: 11, 859 (1978)

136 Mocker H.W., Appl.Phys.Lett. 12, 20 (1968)

137 Work carried out with Wood A. and Vass A., Physics Department, Heriot Watt University, Edinburgh, Scotland

138 Reid J. and Siemsen K.J., J.Appl.Phys. 48, 2712 (1977)

139 Browne P.G. and Smith A.L.S., J.Phys.D. 7, 2464 (1974)

140 Aleinov V.S. and Masychev V.I., Sov.J.Quantum Electron. 9(7), 915 (1979)

141 Smith A.L.S. and Murray G., Opt. & Laser Tech. 307 (1981)

142 Reid J. and Siemsen K.J., Opt.Commun. 18, 211 (1976)

143 Smith A.L.S. and Moffatt S., unpublished

144 Siemsen K.J. and Reid J., Appl.Opt. 17, 3523 (1978)

145 Reid J. and Siemsen K.J., Appl.Phys.Lett. 29, 250 (1976)

146 Berger W., Siemsen K.J. and Reid J., Rev.Sci.Instrum. 48, 1031 (1977)

147 Arie E., Lacome N. and Rossetti C., Can.J.Phys. 50, 1800 (1972)

148 Murray E.R., Kruger C.H. and Mitchner M., J.Chem.Phys. 62, 388 (1975)

149 Siemsen K.J., private communication

150 Bowden C.M., Optical Bistability, Plenum (N.Y.) (1982)

151 Miller D.A.B., Laser Focus (April 1982)

152 Abrams R.L., Appl.Phys.Lett. 25, 609 (1974)

153 McCubbin T.K., Darone R. and Sorrell J., Appl.Phys.Lett. 8, 118 (1966)

154 Devir A.D. and Oppenheim U.P., Appl.Opt. 8, 2121 (1969)

155 Gerry E.T. and Leonard D.A., Appl.Phys.Lett. 8, 227 (1960)

156 Leonard R., Appl.Opt. 13, 1920 (1974)

157 Munjee S.A. and Christiansen W.H., Appl.Opt. 12, 999 (1973)

158 Mellis J., private communication

159 Ochkin V., Lebedev Institute, Moscow, USSR, private communication

160 Woods P.T. and Jolliffe B.W., J.Phys.E. 9, 52 (1976)

161 Siemsen K.J., Appl.Opt. 19, 818 (1981)

162 Mitchell A.C.G. and Zemansky M.W., Resonance Radiation and Excited Atoms, Cambridge University Press (1972)

163 Reid J., Shewchun J. and Garside B.K., Appl.Phys. 17, 349 (1978)

164 Shields H. and Smith A.L.S., J.Appl.Phys. 48, 4807 (1977)

165 Murray G.A., Third National Quantum Electronics Conference, Brighton (1978)

166 Murray G.A. and Smith A.L.S., J.Phys.D. 14, 1745 (1981)

167 Lightman A.J. and Fisher E.R., J.Appl.Phys. 49, 973 (1978)

168 Davies A.R., Roberts S.A., Smith K. and Thomson R.M., Res.Rep. 118 University of Leeds (October 1978)

169 Merhaut J., Theory of Electroacoustics, McGraw Hill (1981)

170 Ecker G. and Zoller O., Phys.Fluids 7, 1996 (1964)

171 Cohen I.M. and Whitman A.M., Phys.Fluids 16, 307 (1973)

172 Shields H. and Smith A.L.S., unpublished

173 Laderman A.J. and Byron S.R., J.Appl.Phys. 42, 3138 (1971)

174 Waszink J.H. and van Vliet J.A.J.M., J.Appl.Phys. 42, 3374 (1971)

175 Maksimov A.I., Sergienko A.F. and Slovetskii D.I., Sov.J.Plasma Phys. 4(2), 194 (1978)

176 Schwartz J. and Margalith E., J.Appl.Phys. 45, 4469 (1974)

177 Beyts H. and Smith A.L.S., private communication

178 Rogoff G.L., Phys.Fluids 15 (1931)

179 Eletskii A.V. and Smirnov B.M., Sov.Phys.Tech.Phys. 15, 1308 (1971)

180 Lamb W.C., Phys.Rev. 134A, 1429 (1964)

181 Barger R.I. and Hall J.L., Phys.Rev.Lett. 22, 4 (1969)

182 Wallard A.J., J.Phys.E. 6, 793 (1973)

183 Rowley W.R.C. and Wallard A.J., J.Phys.E: Sci.Instrum. 6, 647 (1973)

184 Wallard A.J., J.Phys.E: Sci.Instrum. 5, 926 (1972)

185 Wallard A.J., IEEE Trans. of Instr. & Meas. IM-23, 532 (1974)

186 Gorokhov Y.A., Kompanets O.N., Letokhov V.S., Gerasimov G.A. and Posudin Y.I., Opt.Commun. 7, 320 (1973)

187 Kompanets O.N., Kukudzhanov A.R., Letokhov V.S. and Mikhailov E.L., Sov.J. Quantum Electron. 3, 293 (1974)

188 Degnan J.J., Appl.Phys. 11, 1 (1976)

189 Kavaya M.J., Menzies R.T. and Oppenheim U.P., IEEE J.Quantum Electron. QE-18, 19 (1982)

190 Szoke A. and Javan A., Phys.Rev. 145, 137 (1966)

191 Freed C., Proc. of 29th Annual Symp. on Frequency Control, Atlantic City 330 (1975)

192 Freed C. and O'Donnell R.G., Metrologia 13, 151 (1977)

193 Mocker H.W., Appl.Phys.Lett. 16, 20 (1967)

194 Borde C. and Henry L., IEEE J.Quantum Electron. QE-4, 874 (1968)

195 Suzuki T., IEEE J.Quantum Electron. QE-5, 132 (1969)

196 Cole J.H., Appl.Opt. 19, 1023 (1980)

197 Privalov V.E., Sov.Phys.Tech.Phys. 16, 1324 (1972)

198 Ezekeil S., IEEE J.Quantum Electron. QE-3, 417 (1967)

199 Shofner F.M., Kreikebaum G., Carlson T.B. and Bray C.W., IEEE J.Quantum Electron. QE-7, 215 (1971)

200 Mocker H.W., S.P.I.E. 92, 129 (1976)

201 Conder P.C., Jenkins R.M., Roper V.G., Parcell E.W., Redding J.R. and Spencer T.W., A Compact Rugged CO_2 Waveguide Laser, RSRE Report (1981)

202 Wood R.A., Vass A., Pidgeon C.R. and Firth W.J., Opt.Commun. 35, 105 (1980)

203 Scott G., Ph.D. Project, University of Strathclyde, Glasgow

204 California Laser Corporation, Stabilization System 81D specification sheet, 1070 Commerce Street, San Marcos, California 92069, U.S.A.

205 Edinburgh Instruments Ltd., Stabilization System 209 specification sheet, Riccarton, Currie, Edinburgh EH14 4AP

GENERAL REFERENCES

Von Engel A., "Ionized Gases", 2nd ed. Oxford Clarendon Press (1965)

Penner S.S., "Quantitative Molecular Spectroscopy and Gas Emissivities", Addison-Wesley, U.S.A. (1959)

Cherrington B.E., "Gaseous Electronics and Gas Lasers", Pergamon Press, U.S.A. (1979)

APPENDIX I NOTATION, CONVENTIONS AND UNITS

The energy levels and infrared transitions of the CO_2 molecule are defined in the following manner. Unless specified, the transitions are vibrational-rotational and not electronic (i.e. non-ionized CO_2 molecules are involved). The vibrational state described as (l, m, n) refers to the symmetric stretch mode, bending mode and asymmetric stretch mode quantum numbers.

The CO_2 laser system involves transitions between states characterized not only by the vibrational quantum numbers but also by the molecular rotational quantum numbers J and M. An eigenstate of the molecule is specified as (l, m, n, J, M) where the rotational quantum numbers J and M determine the rotational state of the molecule. Two kinds of transition are allowed by the selection rules denoted, as P and R for $(J \rightarrow J + 1)$ and $J \rightarrow (J - 1)$ respectively. In this work, the transitions are described by their wavelength band as either 9 or 10 μm and by the kind of transition either P or R. Therefore, 10P(20) means the $J \rightarrow J + 1$ transition with $J = 20$ upper level quantum number in the 10 μm band. The laser transitions have two lower level sets $10^0 0$ and $02^0 0$ which are sufficiently close in energy terms for Fermi mixing to occur. The group of laser transitions resulting from these levels are referred to as $(00^0 1 - 10^0 0, 02^0 1_{I,II})$ which includes all transitions due to these levels exclusively. Higher level laser action with transitions such as $(00^0 2 - 10^0 1, 02^0 1_{I,II})$ are discriminated in the text by describing them as $00^0 2$ 10P(18), etc. Where no prefixed energy level is shown this is to be interpreted as a $00^0 1$ transition and these are sometimes referred to as regular band transitions; similarly, the high energy level transitions due to $00^0 3$, $00^0 2$, etc. are referred to as sequence band transitions.

All pressures measured are expressed in the units torr which has a value of 133 Pa, otherwise MKs SI units have been adopted exclusively, apart from some use of cm (10^{-2} m) for length. All pressures over the range 0.1 torr to atmosphere were measured with MAT differential capacitance manometers

which provide absolute pressure measurements not referred to a certain gas. Some low pressure (ionization guage, mass spectrometer and Pirani) measurements are the N_2 equivalent pressure and this is explained in the text as a relative units scale. All temperatures are given in degrees kelvin or celsius and are in general measured by either chromal alumel thermocouple or Hg-glass thermometer and are to be generally treated with an error of ± 2 K.

Laser beam power was measured with several radiation thermopiles (laser power meters) all of which were referred to one CRL 201 laser power meter supplied with manufacturer (NBS traceable) calibration which was compared with three power meters (during these experiments) supplied by Edinburgh Instruments, Peter Knowles of St. Andrews University Physics Department, and F. Cruickshank of Strathclyde University Chemistry Department, all these had calibration which was NBS or NPL traceable. The result showed this CRL meter (the in-house standard) to read an average - 2.5% (with a worst comparison value of 4%) over the range 1 to 30 W.

All laser gains and absorptions are expressed as α in the sense of $I = I_0 e^{\alpha Z}$ where Z is the beam propagation coordinate. Unless otherwise stated α is to be interpreted as a saturated value rather than a small signal value whence it is denoted as α_0. No radial variations of α are considered.

APPENDIX II PUBLICATIONS PERTAINING TO THIS WORK

1. "Optogalvanic Stabilized CO_2 Laser", A.L.S. Smith and S. Moffatt, Opt.Commun. 30, 213 (1979).
2. "High Frequency Optogalvanic Signals and CO_2 Laser Stabilization", S. Moffatt and A.L.S. Smith, Opt.Commun. 37, 119 (1981).
3. "Optogalvanic Laser Stabilization", S. Moffatt and A.L.S. Smith, Laser Advances and Applications, Proceedings of the Fourth National Quantum Electronics Conference, ed. B.S. Wherret, Wiley (1979).
4. "Recent Advances in CO_2 and CO Laser Stabilization Using the Optogalvanic Effect", S. Moffatt and A.L.S. Smith, Proceedings of the Fifth National Quantum Electronics Conference, Hull University (1981).

OPTO-GALVANIC STABILIZED CO_2 LASER

A.L.S. SMITH and S. MOFFATT
Department of Physics, University of St Andrews, St Andrews, Fife, KY16 9SS, UK

Received 15 May 1979

A compact long-life CO_2-N_2–He-Xe laser has been developed to produce 4–8 W on any one of ten CO_2 $00^\circ1-10^\circ0$ and $00^\circ1-02^\circ0$ transitions, selected by the laser signature technique. Short term (10 μs–10 ms) drift is < 10 kHz and positive column opto-galvanic detection is used in a stabilization feedback loop to produce long term frequency deviation of < 500 kHz on the P(20) line and < 1 MHz on the other lines.

1. Introduction

We report the development of a compact, sealed, CO_2 laser operating at up to 10% conversion efficiency with the laser cavity both actively and passively stabilized to achieve better than three parts in 10^8 frequency stability for the long term (seconds to many hours) and better than three parts in 10^{10} in the short term (10 μs to 10 ms) on any one of ten CO_2 00^01-10^00 and 00^01-02^00 laser transitions. The active stabilization system involves the use of an electronic feedback loop which adjusts the cavity length using the opto-galvanic effect. With an electric discharge excited tube, 25 cm long, the output power stability is better than 1% with more than 8 W on the P(20) 10.59 μm line, and typically 4 to 6 W on the other transitions.

2. The opto-galvanic effect

The cw CO_2 laser is a high efficiency device, and the intensity of the laser radiation field is sufficiently large to cause significant variation in many of the laser and discharge macroscopic parameters when the field intensity changes. Thus, the spontaneous sidelight intensity and its spectral distribution, the gas pressure, discharge current and discharge impedence all change as the internal laser radiation field intensity is altered, for instance, by using an intra-cavity modulator or by changing the resonant cavity alignment. These effects have recently been extensively examined by Smith and Brooks [1,2], and many of the microscopic processes elucidated. Previously, Skolnick [3] noted that the radiation field intensity dependent current fluctuations could be used as the basis of a frequency stabilization system and successfully stabilized a cavity, using additional intra-cavity dispersive elements. In 1975, Thomason and Elbers [4] gave details of the modification of a commercial laser to produce stabilization, but gave no performance details. The laser cavity length is modulated by oscillating the position of one mirror along the cavity axis using a piezoelectric mirror mount at some convenient frequency (~500 Hz). The field intensity is, therefore, modulated at the same frequency as the cavity mode scans across the transition line gain profile. An intensity variation of ~1% is sufficient to significantly (≈0.1%) change the discharge impedence; this impedance change can be detected as current fluctuation (opto-galvanic) or as a voltage variation (opto-voltaic). If the mean mode frequency is lower than the line centre frequency, the phase of the observed impedence fluctuation is opposite to that if the mode frequency is higher than the line centre frequency, and the amplitude of the impedence fluctuation increases with the frequency offset from line centre. Thus, if the impedence fluctuation is measured with a phase sensitive detection system and its integrated output, suitably amplified, applied as a dc correction voltage to the cavity length transducer, the system will maintain the oscillating cavity mode at line centre.

The CO_2 00^01 upper laser level of the asymmetric stretch mode is pumped by both direct electron collision processes and by V-V collisions with $N_2(v = 1)$ electron collision excited molecules. The dominant processes for the relaxation of this level are molecular collisions (mostly V-V-T) and stimulated emission. When considerable energy is extracted from this system by stimulated emission, then energy which would have been coupled to the discharge by V-V-T and V-T processes is lost from the system as radiation, and hence, there is a net cooling of the gas. With a pulsed laser there may also be an initial short term gas heating effect (kinetic heating), but the overall net effect is one of gas cooling [1,5]. The cooled gas has a greater molecular number density (and pressure); the electrons, therefore, collide with heavy particles more frequently and either a larger voltage is required to maintain the same current flowing through the gas, an impedance increase, or a constant potential difference produces a current decrease, likewise an impedence increase. It should be noted that an impendence change is modified by two further effects; first, as the gas number density changes, so not only does the electron collision rate change, but also the energy exchange per collision is altered. Second, if the primary impendence change is allowed to result in a subsequent current fluctuation, then this current change will consequently change the gas heating, causing a secondary impendence change; this latter effect is eliminated with a constant current power supply [1].

Fig. 1 illustrates the macroscopic impedence changes resulting from the microscopic processes, it shows the voltage-current characteristic for the laser (see below) producing 0, 2, 4, 6 and 8 W output power. These power levels were obtained over a wide range of current values by partial misalignment of the resonant cavity, not altering the laser driver circuit. This radiation field intensity dependent impedence component is established in a time comparable with the collisional relaxation time of the 00^01 level, which is ≈ 1 ms.

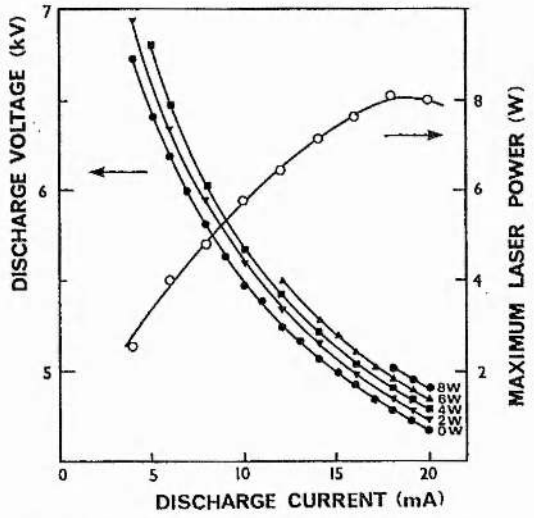

Fig. 1. Variation of discharge voltage with discharge current for different laser output powers and variation of maximum laser output power with discharge current, in a small, sealed CO_2 laser (33 cm discharge length, 25 cm active length), with gas mixture 1 torr Xe, 3 torr CO_2, 4 torr N_2, 16 torr He.

3. Laser design

The compact CO_2 laser head (external dimensions 15 X 15 X 50 cm) shown schematically in fig. 2, utilizes a water cooled quartz laser tube of 8 mm inside diameter and a vacuum system constructed of stainless steel.

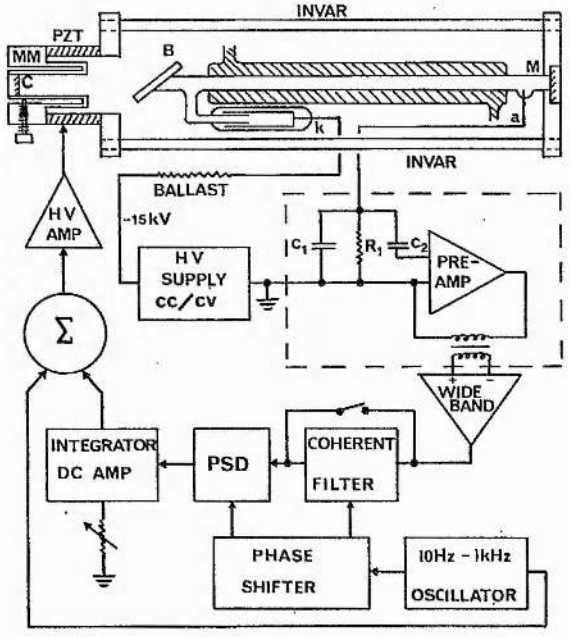

Fig. 2. Schematic of CO_2 laser head and associated feedback circuitry (laser dimensions not to scale). (B) – KCl or ZnSe Brewster window.

The total reflector (M) is a 4 metre radius, gold coated copper mirror, permanently aligned to the axis of the quartz tube. The laser radiation is coupled out of the cavity by a 90% reflecting Ge output coupler (C), fixed to an adjustable mirror mount (MM) with an integral lead zirconate titanate ceramic PZT stack. A discharge is maintained between a nickel point anode and a hollow platinum cathode designed to reduce sputtering, and the total gas volume is 870 cm^3 (including the reservoir).

Passive stability is achieved by the use of a rigid design with invar length control. The total reflector (M) is located in the mid-plane of a machined aluminium block, which is firmly attached to three 25 mm dimaeter invar rods, whereas the output coupler is mounted to the PZT doubly re-entrant, elastically deformable, steel mirror mount assembly (MM), which utilizes an aluminium mounting cup, which expands in the opposite direction to the invar extension so that thermal compensation is achieved. Overall compensation has been found to correspond to a length stability better than 1 μm with a 5 K ambient temperature change, provided no excessive thermal gradients exist. No magnetic, vibrational or acoustic screening is used.

The active stabilization feedback loop utilizes a series resistor (R_1) in the earth supply line as a signal detector (fig. 2). This sensing resistor and its associated filter circuit, narrow band preamplifier and coupling transformer, is located in the electrically screened laser head and provides an output signal related to the cavity length error. The combination of R_1 and C_1 provides a low pass filter response to reduce power supply transients, and is usually adjusted to give a ~1 kHz roll-off. The remainder of the electronic system is assembled from standard units and the final high voltage amplifier supplies both the stable 0 to 1 kV HT voltage for the dc PZT drive and the small ac modulation for length wobbulation.

A total pressure of 20 to 30 torr is necessary to obtain laser power in excess of 6 W from the short discharge length; the optimum gas mix for sealed operation was found to be 4% Xe, 13% CO_2, 17% N_2, 66% He. Although no specific lifetime tests have been made for this system, sealed-off operation with everyday usage has been obtained in the excess of four months, with less than 20% power degradation; details of the CO_2 dissociation control technique can be found elsewhere [6]. Unstabilized laser performance has been monitored for long periods using a radiation thermopile and a pyroelectric detector for power measurements, along with an Optical Engineering CO_2 spectrum analyser for wavelength measurements; apart from the first half-hour warm-up period, during which oscillation on two-vibrational-rotational lines simultaneously can occur in different cavity modes, oscillation on one line usually occurs for a period of several hours (always more than 30 minutes), and a slow drift of output power corresponding to the single cavity mode scanning through a gain profile segment in the laser signature occurs, giving rise to a power fluctuation of typically 10%. The cavity length is sufficiently short so that line competition succeeds in producing single line oscillation for any unique cavity length axial mode, without the need of any extra dispersive element such as a grating or etalon. As the cavity length is changed by slow drift or PZT adjustment, a successive array of about ten individual high gain 00^01-10^00 and 00^01-20^0 laser lines occur, producing a laser signature [7] which is predictable [8]. By correct alignment of the output coupler mirror mount stable axial mode TEM_{00q} operation can be obtained indefinitely, and more than 99% of the output power is always in a single line.

The opto-galvanic technique provides a convenient method of observing the laser signature. Fig. 3 shows an opto-galvanic signature where the cavity length has been scanned 4.4 μm corresponding to a PZT ramp of 500 V. As the intra-cavity power is changed, so is the discharge current, producing a change in potential difference across the sensing resistor R_1. This voltage signal (≈50 mV) shown in the upper trace, is directly

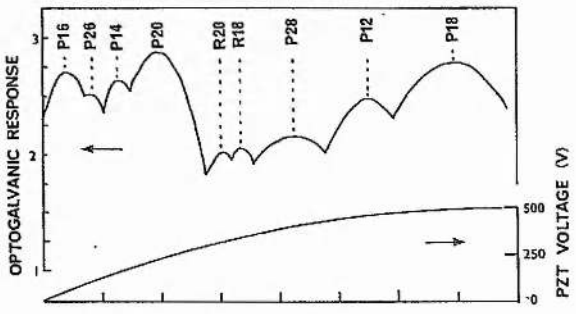

Fig. 3. Tracing of typical opto-galvanic laser signature obtained with a 4.4 μm length ramp (500 V PZT scan, duration ~200 ms). All lines are 00^01-10^00 band. Peak power output P(20) line, 7.0 W.

related to the output power signature: the transition line segments are identified by spectrum analyser.

4. Opto-galvanic stabilization

Fig. 4 shows the discharge impedence fluctuation ($\Delta Z/Z$) caused by switching the internal radiation field on and off, as a function of the laser efficiency (adjusted by misalignment of the cavity). In this instance, the discharge is constant current excited, in order to avoid the aforementioned secondary impedence effect [1,9]. $\Delta Z/Z$ increases with laser conversion efficiency, over the laser operating current range 10 to 30 mA, consistent with the gas cooling theory [1]: consequently (for constant discharge excitation) the impendence fluctuation increases almost linear with output power. When the laser cavity resonance is changed by length modulation rather than misalignment, the output power fluctuation is small (typically 0.1%) and results in a correspondingly small impedence change and a consequent current fluctuation, which are both dependent upon the slope of the gain profile.

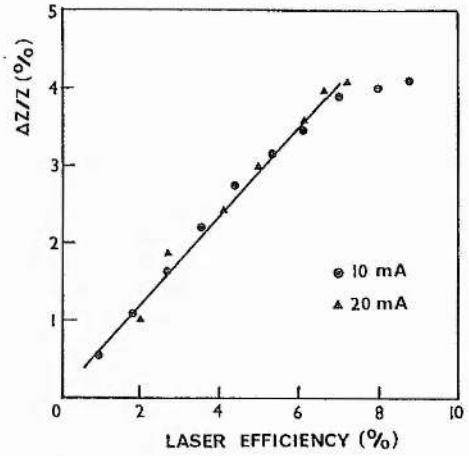

Fig. 4. Variation of impedance fluctuation $\Delta Z/Z$ at 10 and 20 mA discharge currents for change of laser conversion efficiency with gas mixture as in fig. 1.

Fig. 5 shows the opto-galvanic signal ($\Delta i/i$) frequency response (the signal values are typical for off line centre tuning). $\Delta i/i$ is attenuated at higher frequencies (~1 kHz), commensurate with the vibrational

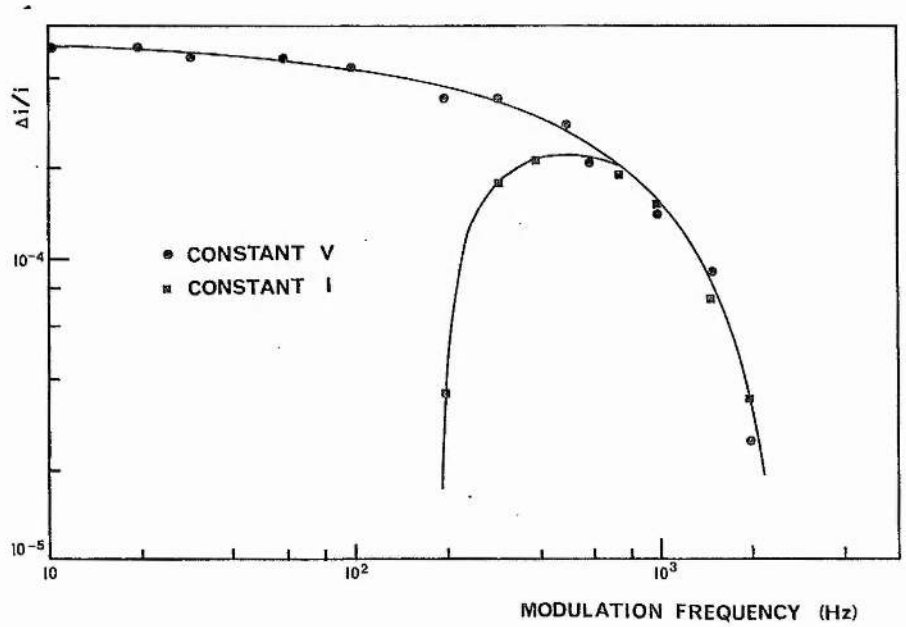

Fig. 5. Variation of opto-galvanic signal $\Delta i/i$ with a change of length-modulation (80 nm) frequency for the CO_2 laser, for both constant current and constant voltage power supply operation.

relaxation time of the $00^0 1$ level as previously predicted [1]. Behaviour at low frequencies is markedly different with constant voltage rather than constant current excitation; a constant voltage power supply permits current fluctuations to occur, whereas a current stabilized supply eliminates current fluctuations. It is usually advantageous to use a constant current power supply in stabilized systems to eliminate long term current changes, and hence, a sufficiently high modulation frequency is required to overcome power supply compensation; in this case, a modulation frequency of between 400 and 750 Hz is most suitable. The particular frequency is chosen to avoid power supply ripple harmonic components as these are the major stabilization channel noise sources.

In order to stabilize at the centre frequency of any transition in the laser signature (which can be opto-galvanically observed as in fig. 3), the cavity length is manually adjusted by varying the dc amplifier operating point until the desired transition is selected; then the feedback loop is closed, initially with a small dc gain, and the PZT modulation reduced to a suitable value (1 to 10 V ac PZT modulation is adequate), as the dc gain is increased. The highest gain line P(20) in the $00^0 1 - 10^0 0$ band can always be identified without external dispersive equipment, because it has the largest amplitude PSD discriminant and the widest signature bandwidth (>100 MHz at 24 torr laser gas pressure). Stabilization of high gain lines P(18), P(20) and P(22) achieves noticeably better stability than the weakest lines (R(20), R(18) etc.)

Stability has been assessed by two methods; first, by heterodyning two similar laser systems, and second, by long term analysis of the single mode output power fluctuations of one laser. The heterodyne experiments consists of mixing the same line output beams of two independently stabilized lasers together in a Lead Tin Telluride detector. With observation times between 10 μs and 10 ms, the mean difference frequency of two free-running lasers changed by less than three parts in 10^{10}. For longer observation times (1–20 s) occasional frequency excursions of up to 200 kHz was measured. With two lasers suitably stabilized (different modulation frequencies), FM sideband beating occurs caused by the modulation generated, frequency difference components of 200 to 400 kHz, which sets a limiting bandwidth of two parts in 10^9 on the absolute laser performance. Difference frequency measurements taken over a series of observations from seconds to several minutes, show a mean drift of less than 500 kHz, when both lasers are P(20) stabilized, and less than 1 MHz (three parts in 10^8) when both lasers are stabilized on any available transition in their signatures. Since the stabilizer servo-mechanisms utilize integrators with time constants which can be adjusted over the range 50 ms to 10 s (typically 0.5 s), the medium term active stability is controllable. However, for times shorter than this, the active stability should be the same as the passive stability and certainly better than one part in 10^8; a figure which is confirmed by secondary evidence from the laser power output stability and the maximum correction signal amplitude in the feedback system.

Analyses of long term power fluctuations show

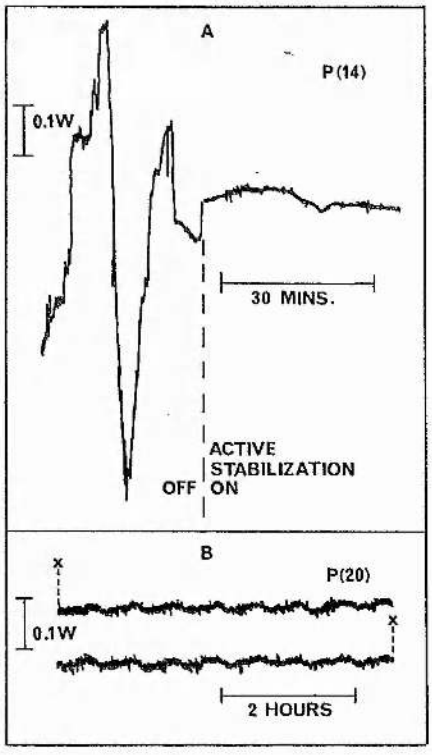

Fig. 6. (A) Comparison of P(14) stabilized output power (opto-galvanic technique) with free-running passive stability, with a mean power of 6.6 W. (B) Long term power stability of P(20) 10.59 μm line with laser stabilized using the opto-galvanic technique, ten hours continuous operation at a mean power of 7.7 W.

between 0.2% and 1% maximum power deviation, of which the largest component is periodic (~40 min), and can be identified with the water thermo-circulator cooling cycle. As the discharge wall temperature is cycled by ±1.5 K the laser gain is modulated, resulting in laser amplitude modulation which is not linked to frequency drift. Fig. 6(A) shows the comparative output stability (passive and active) for a medium gain line, P(14) (00^01-10^00), and 6(B) the long term stability of P(20) with the laser opto-galvanically stabilized.

We have found this opto-galvanic CO_2 system to be particularly insensitive to vibrational and acoustic interference (due to the nature of the distributed detection element), and since it avoids the use of an infra-red detector output beam power or quality is not degraded. Additionally, the signal channel is wavelength insensitive, which is particularly useful for signature observation and the selection and identification of high gain lines. This system is effective simple and inexpensive and particularly suitable for compact, sealed CO_2 lasers.

References

[1] A.L.S. Smith and M. Brooks, J. Phys. D. 11 (1979), in press.
[2] M. Brooks and A.L.S. Smith, J. Phys. D. 11 (1979), in press.
[3] M.C. Skolnick, IEEE J. Quantum. Electron. QE6 (1970) 139.
[4] W.H. Thomason and D.C. Elbers, Rev. Sci. Instrum. 46 (1975) 409.
[5] T. Aoki, C. Yamada and M. Katayama, Jap. J. App. Phys. 10 (1971) 332.
[6] P.G. Browne and A.L.S. Smith, J. Phys. D 7 (1974) 2464.
[7] P.C. Claspy and Y. Pao, Appl. Opt. 10 (1971) 136.
[8] G. Schiffner, IEEE J. Quantum. Electron. QE8 (1972) 877.
[9] S. Moffatt and A.L.S. Smith, to be published.

HIGH FREQUENCY OPTOGALVANIC SIGNALS AND CO_2 LASER STABILISATION *

S. MOFFATT and A.L.S. SMITH
Department of Natural Philosophy, University of Strathclyde, Glasgow G4 0NG, Scotland, UK

Received 22 December 1980

The normal optogalvanic effect used in the stabilisation of CO_2 lasers decreases in amplitude with increase in frequency and disappears at 2–3 kHz. We show that there is also a high frequency optogalvanic effect in CO_2–N_2–He–Xe laser gas mixtures up to ~100 kHz, explain its origin and use it to frequency stabilise a laser with long term (hours) frequency drift of < 50 kHz and frequency re-settability of <100 kHz.

1. Introduction

Large perturbations of the discharge v-i characteristics occur in the CO_2 cw laser due to changes of the radiation field, but have been found to decrease with frequency [1,2] and disappear at 2–3 kHz. These optogalvanic effects (OGE) have been used by several authors [3–5] to stabilise CO_2 lasers and we have reported the performance of such a system [5,6]. We have now observed OGE signals at frequencies up to 100 kHz and actively stabilised lasers with high frequency phase locked loops to provide single mode powers > 8 W with power fluctuations < 0.5% and long term (several hours) frequency stability better than 5 parts in 10^9. Here we show the origin of this high frequency effect and explain the 180° phase change at 1–3 kHz and the signal decay at 40 to 100 kHz.

2. Laser design and system calibration

The sealed CO_2 lasers [5] are of a compact rigid design of invar and have 8 mm bore, 25 cm discharge length quartz tubes with a hollow Pt cathode situated in a side arm; a gold coated 4 m radius total reflector is permanently attached to one end of the tube and the other end is closed by a ZnSe or KCl Brewster window. A 90% flat output coupler is mounted in an elastically deformable mirror mount with an integral lead zirconate titanate ceramic piezo-electric translator (PZT) stack or tube which determines a cavity length of about 35 cm. A small ac voltage (at the chosen modulation frequency, f) is applied to the PZT stack to modulate the cavity length, the resulting OGE discharge current modulation develops an ac voltage across a resistor in the power supply line, and the stabiliser servomechanism (a PSD to determine error signal phase, a pair of integrators and a high voltage DC amplifier) drives the PZT in order to correct cavity length changes and maintain the cavity mode at the centre of the line gain profile of the chosen laser signature segment.

A PZT mirror mount assembly has a complicated mechanical frequency response determined by resonances and drive source capacitive loading. In order to amplitude modulate the laser field by a constant amount (say 1%) as f is varied (over a wide frequency band) each PZT must be calibrated. The most convenient calibration technique is to frequency modulate a laser with the PZT and heterodyne its output beam with a stabilised CO_2 beam in a non-linear wideband detector. We have used a Plessey LBC L.T.T. detector and a HP 8557A spectrum analyzer to determine the laser beat spectrum width from which the PZT length translation is obtained. Typical PZT stack characteristics are a falling HF response –10 dB at 1 kHz, –30 dB at 10 kHz, –40 dB at 20 kHz and –50 dB at 60 kHz with a strong resonance at 45 kHz and a broad resonance at 12 kHz. Using this method we have calibrated

* Supported by UK Science Research Council.

0 030–4018/81/0000–0000/$ 02.50

several PZT's from 10 Hz to 200 kHz, giving response calibration accuracies of ±5% DC–3 kHz, ±10% 3 kHz –10 kHz, and ±20% 10 kHz–200 kHz.

3. The opto-galvanic signal

Constant current dc power supply units are used extensively to excite cw CO_2 lasers and these attenuate low frequency current fluctuations ($\lesssim$ 400 Hz) and tube voltage fluctuations (optovoltaic technique) may be used alternatively [7,8]. Instrumental phase changes of low frequency current perturbations occur due to PSU feedback limitations and some anomalous OGE phase changes can be observed due to dc level shifting with increasing frequency, giving 2f signals as the line centre is approached. However, we have investigated the OGE phase over a wide bandwidth and only one fundamental phase change occurs, at ~2 kHz. Fig. 1 shows that the OGE signal (for constant voltage power supply operation) is opposite in phase to the radiation field modulation at low frequencies (as previously shown by Smith and Brooks [1]), but steadily decreases in amplitude with increase in frequency and disappears at 2–3 kHz. It reappears at higher frequencies, but with reversed phase (in phase with the field modulation) and reaches a maximum amplitude in the 10 to 20 kHz region, before decreasing and disappearing at ~100 kHz. The points near the 2.5 kHz cross over suggest subsidiary amplitude maxima. The separate phase plot shows that the phase reversal extends over the range from ~1 kHz to ~3 kHz.

The discharge noise spectrum envelope (see fig. 1 also) is dominated by power supply unit harmonics which are typically 45 dB greater than background random discharge noise in the band 10 to 100 Hz and 25 dB greater at frequencies 100 Hz to 10 kHz. The noise spectrum shown is typical for a tube as described [5] and shows an increase in background and PSU noise at low frequencies $\lesssim$ 100 Hz when excited by a commercial transistor current regulated supply with a series ballast greater than the tube impedance. There is an improved OGE signal-to-noise ratio in the H.F. band (10–20 kHz) due to reduced PSU harmonics and background noise. Details of discharge noise spectra and optimization of the OGE stabilisation scheme will be published later [8].

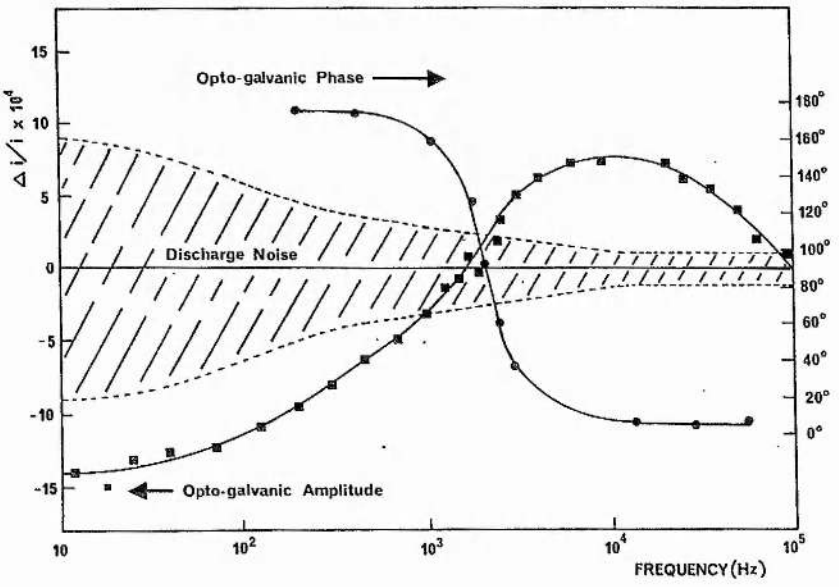

Fig. 1. Variation of OGE signal $\Delta i/i$ and OGE phase with length (100 nm) modulation frequency for the CO_2 laser with constant voltage excitation. The dashed lines show the envelope of the amplitude of the power supply harmonics noise induced current fluctuations $\Delta i/i$ (see text) for a typical commercial power supply, as measured with a HP 3580A audio frequency spectrum analyser.

4. Kinetic perturbation mechanisms

The kinetic perturbation path for connecting the modulation of the laser cavity length (frequency f) with the resulting discharge current perturbation at the frequency f has been described previously [1,5] and is summarised here in fig. 2. From the upper part of the figure we see that the radiation stimulated transitions $h\nu_{\mathrm{LASER}}$ from the upper level compete with the otherwise dominant V-V-T relaxation process.

$$CO_2(001) + M \rightarrow CO_2(n, m, 0) + M + T_U$$

where M represents all the possible collision partners CO_2, CO, O_2, N_2, He, Xe, and T_U represents the surplus energy given by the exothermic process to translational energy. Both processes transfer the CO_2 excited population to a closely coupled group of levels (very rapid vibrational collisions) which are labelled 010

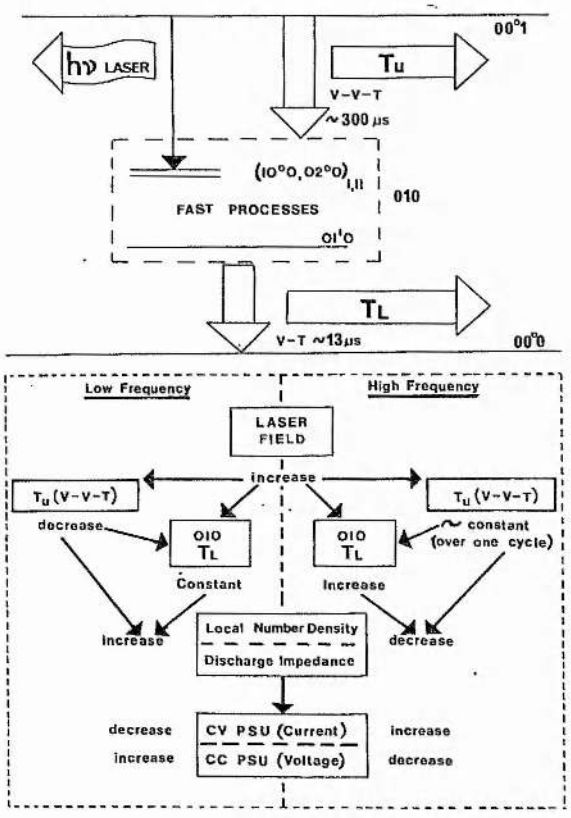

Fig. 2. Simplified energy level diagram for the CO_2 laser and the OGE process diagram in two modulation frequency regimes.

here for convenience. This 010 group then rapidly relaxes by collisional processes to the ground state giving up all the vibrational energy as translational energy T_L.

As shown on the left-hand side of the lower part of fig. 2, when the laser field is increased (cavity length modulation, frequency f, driving cavity mode towards transition line centre), T_U will decrease because more of the 001 population is now removed by $h\nu$ laser photon induced transitions and so there are relatively fewer V-V-T collisional relaxations, hence T_U decreases. T_L is unaltered (all the population still flows through the 010 group and the total pump rate to the 001 level is constant for both halves of the modulation cycle). As a result there is a net decrease in the transfer of energy to the gas (T_U decreased, T_L unaltered) at frequency f; the local number density in the radiation field is increased, the discharge impedance is increased and the current is modulated at f, but out of phase with the modulation field (decrease) for constant voltage power supply operation.

The roll-off of the OGE in the 1 to 2 kHz region can be explained in terms of the upper state V-V-T relaxation process rate. For our gas mixture of 3 Torr CO_2, 4 Torr N_2, 1 Torr Xe and 18 Torr He and assuming 30% CO_2 dissociation and rate constants for an average gas temperature of 370 K, the 001 relaxation rate is predicted to be $\sim 3100\ s^{-1}$ giving relaxation time τ_{001} against collisional relaxation of $\sim 300\ \mu s$. Therefore as the cavity length modulation frequency is increased the 001 population variation at f should become small as $f \rightarrow 1/2\tau_{001}$, or $f \sim 1650$ Hz as observed. Thus the f frequency modulated component of energy transfer to molecular translational motion ($T_U(f)$) also becomes small and the number density, discharge impedance and current fluctuations at frequency f are reduced.

However if $f \gtrsim 1/2\tau_{001}$, T_L acquires a modulated component at frequency f. Although the laser field stimulated transitions 001 → 010 are still modulated at frequency f, due to the field amplitude modulation, the f modulation of the V-V-T 001 → 010 transition is less ($\rightarrow 0$ as $f \gg 1/2\tau_{001}$) and hence the arrival rate of 010 population is not the same for the two halves of the f modulation cycle and the 010 population fluctuates, modulating T_L. Or to express it in another manner, when the modulation frequency is low, each half of the modulation cycle f represents a kinetic equilibrium state (constant pumping and equilibrated relaxation process), but with the increase in f the

V-V-T process is too slow to re-establish and maintain an equilibrium over the cycle period. So as seen on the right-hand side of the lower part of fig. 2, as the laser field changes so although T_U remains unaltered, now T_L increases as the field increases, leading to a number density decrease and hence a current increase. Thus the current response is now (high f) in phase with the cavity length modulation.

To summarise: as the cavity length modulation frequency increases to become comparable with $1/2\tau_{001}$ of the V-V-T relaxation process, so $T_U(f)$ decreases and $T_L(f)$ acquires a non-zero value, resulting in an optogalvanic signal phase change. But $T_L(f)$ will in turn decrease as $f \to 1/2\tau_{001}$, where T_L is the V-T collisional relaxation rate of the 010 group, which for our gas mixture is calculated to be ~13 μs, hence when $f \to 40$ kHz, as is evident in fig. 1.

5. High frequency laser stabilisation

The lasers and electronic systems used for high frequency stabilisation are as previously described for low frequency stabilisation [5], except that the PZT is driven via a capacitive mixer from a low impedance ac source and a high impedance dc source; in some cases twin PZT's have been used.

Fig. 3 shows the laser intensity stability, which for a passive cavity drifts by ~10% per hour. The improvement due to high frequency OGE stabilisation (at a modulation frequency of 14.6 kHz) is evident and intensity fluctuations are reduced to $\lesssim 0.3\%$ when the laser is stabilised at 10.6 μm P(20) line centre. Frequency stability has been assessed in detail by beating two independently stabilised lasers together; in some instances, one laser was stabilised off line centre by a predetermined frequency by adding a known voltage to offset the PSD operating point. Over long periods (several hours) it was found that the frequency drift was <50 kHz (compared with >20 MHz per hour unstabilised) and frequency re-settability (after the feedback loop had been opened) is always < 100 kHz. At all times low frequency jitter of 100–400 kHz is apparent, primarily due to the commercial power supply used having an output ripple of 1–5 V rms, and consequently perturbing the cavity refractive index.

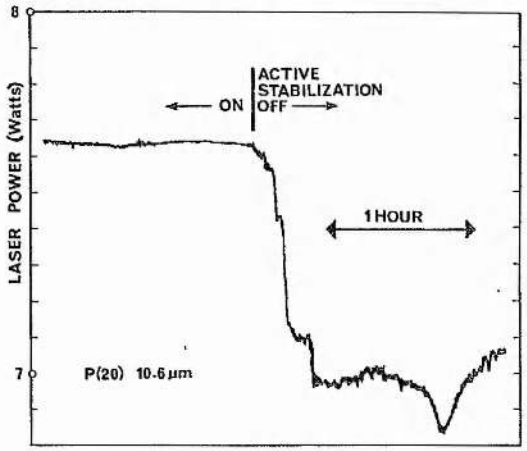

Fig. 3. Comparison of CO_2 laser single mode power with high frequency OGE active stabilisation with passive stabilisation only, for a compact sealed device, as described in section 2.

Higher phase lock loop frequency results in faster response correction; in our case the response time is limited to 100 ms by PZT dc drive and fixed post detector integration. By constructing systems with a response time of 1–10 ms correction of laser frequency jitter due to PSU ripple is possible as well as the reduction of acoustic interference in the audio frequency band (up to 100–1000 Hz). Increasingly, lasers are being used not only in optics laboratories, but also in less controlled environments, and rejection of vibration and acoustic interference is necessary. It is noteworthy that even commercial anti-vibration surfaces permit substantial vibration at low frequencies (up to 100 Hz) which cannot be corrected with most stabilisation systems (~1 s time constant). The OGE stabilisation method can be extended to operate at the higher frequencies necessary and its susceptibility to microphony is inherently low because the distributed discharge acts as the primary frequency error detection element.

References

[1] A.L.S. Smith and M. Brooks, J. Phys. D11 (1979) 1237.
[2] G. Schiffner, J. Opt. Soc. Am. 61 (1971) 650 and private communication.
[3] M.C. Skolnick, IEEE J. Quant. Electron. QE6 (1970) 139.
[4] W.H. Thomson and D.C. Elbers, Rev. Sci. Instrum. 46 (1975) 409.
[5] A.L.S. Smith and S. Moffatt, Optics Comm. 30 (1979) 213.
[6] S. Moffatt and A.L.S. Smith, in: Laser advances and applications, ed. B.S. Wherrett (Wiley, 1980) p. 31.
[7] A.L. Scholtz and G. Schiffner, Appl. Phys. 21 (1980) 407.
[8] S. Moffatt and A.L.S. Smith, unpublished.

Optogalvanic Laser Stabilisation

S. Moffatt *and* A.L.S. Smith*
Department of Physics, University of St. Andrews
**Department of Natural Philosophy, University of Strathclyde*

Introduction

We report the development of a compact, sealed CO_2 laser operating at up to 10% conversion efficiency with the laser cavity both actively and passively stabilised (without an extra dispersive element) to achieve better than 3 parts in 10^8 frequency stability for the long term (seconds to many hours) and better than 3 parts in 10^{10} in the short term (10μs to 10 ms) on any one of 10 CO_2 00^01 - $(10^00, 02^00)_{I,II}$ laser transitions. The active stabilisation system utilises optogalvanic detection and electronic feedback to lock the cavity length to a chosen line centre (in the laser signature). With a quartz discharge tube, 25 cm long and 8 mm diameter the output power stability is 0.2 to 1.0% with more than 8 W on the P(20) 10.6μm line and typically 4 to 6 W on the other transitions.

Optogalvanic Effect

CO_2 laser optogalvanism in the positive column is significantly large because of the large radiation field and high efficiency of the device. Perturbations of the laser field result in changes of the 00^01 level population. There are two major energy routes from the 00^01 level to the lower laser level complex (10^00, 02^00, 01^10, etc.) (a) stimulated emission and (b) V-V-T relaxation. Consequently, in the approximation of constant pumping, changes in the optical field intensity cause compensatory changes in the V-V-T relaxation resulting in fluctuations in the translational energy supplied to the gas. As a result changes in both the

electron collision rate and in the electron exchange per collision produce a net discharge impedance change with a consequent change in voltage, current, or both. These effects have been extensively examined by Smith & Brooks [1] and many of the microscopic processes elucidated. The electronic servo-systems used consist of a series resistance in the power supply earth line for supplying the optogalvanic signal, narrow band ac preamplifier, PSD, integrator, high voltage dc amplifier and PZT length modulator [2].

Negative feedback is produced by modulating the cavity length and seeking a null in the optogalvanic signal at a laser line centre in the signature. The stabilised laser system is particularly insensitive to vibrational and acoustic interference (due to the nature of the distributed detection element), and because it avoids the use of an infra-red detector, output beam power or quality is not degraded. Stability assessments have been made by (a) heterodyne analysis (frequency) and (b) long term power monitoring (amplitude). Fig.1a below shows the difference frequency spectrum of two independently stabilised P(20) lasers; the beat frequency envelope does not exceed 400 kHz from the zero frequency marker. Subsequently both feedback loops were opened and the lasers allowed to drift. After 300 s the lasers were reset by closing the feedback loops (Fig. 1b) and the centre difference frequency returned to within 100 kHz.

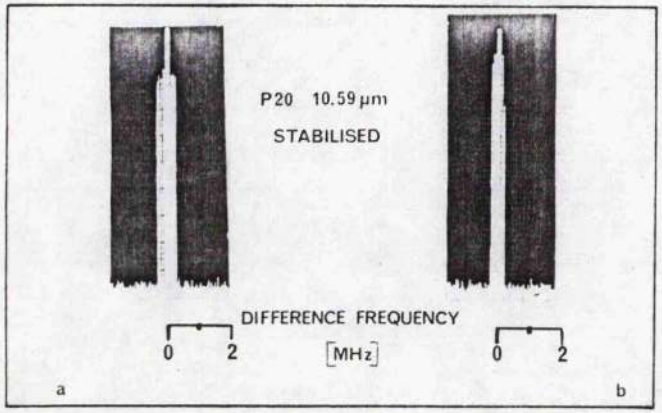

Fig.1

Stabilisation Performance Limitations

The performance limitations of the system consist of (a) the broad nature of the discriminant feature (b) stabilisation channel noise and (c) high frequency signal decay due to the relaxation time of the $00^{0}1$ level. Limitation (a) requires significant laser FM modulation broadening in order to recover a suitable optogalvanic signal. Fig.2 shows the peak difference frequency of two stabilised lasers as a function of modulation voltage. Above a few volts PZT modulation the laser quality is degraded; however, at a suitably small voltage (~1.5V) the laser can be stabilised effectively without degradation beyond its 1 s passive stability (this limitation can be overcome with an optogalvanic cell with a sharper discriminant).

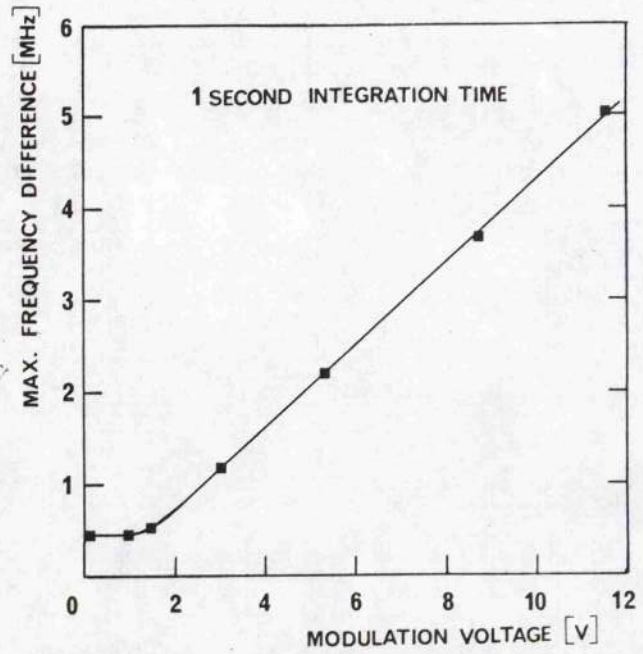

Fig.2

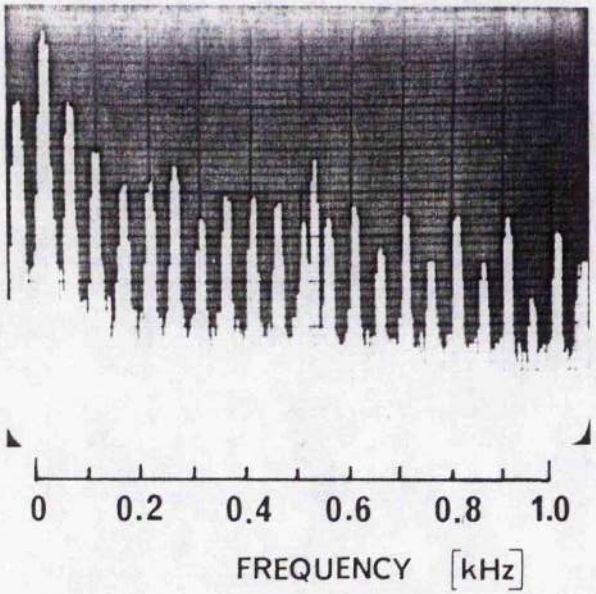

Fig.3

Stabilisation channel noise (b) is usually dominated by power supply harmonics; a typical situation with a constant current power supply is shown in Fig.3. The optogalvanic signal at 520 Hz is observed because it is beyond the feedback response time of the current compensation. This signal has been generated by applying 150 times the typical modulation signal to the PZT in order to illustrate the operating signal to noise ratio (vertical scale 10 dB per main division). Good frequency rejection is required and either a tuned preamplifier or a coherent filter is required before the PSD. Due to the high frequency signal decay which occurs because of the $00^{0}1$ relaxation time of 0.5 to 1 ms (depending on laser gas pressure and composition) a suitable compromise modulation frequency lies in the 400-750 Hz band, for 'constant' current power supplies; the particular frequency is chosen to avoid power supply ripple harmonic components [2].

References

[1] A.L.S.Smith and M.Brooks, J.Phys.D., 12, 1237 (1979).
[2] A.L.S.Smith and S.Moffatt, Opt.Comm., 30, 217 (1979).

Quantum Electronics and Electro-Optics
Edited by P. L. Knight

RECENT ADVANCES IN CO_2 AND CO LASER STABILISATION USING THE OPTO-GALVANIC EFFECT

S. Moffatt and A.L.S. Smith

Department of Natural Philosophy, University of Strathclyde, Glasgow G4 ONG, Scotland, U.K.

INTRODUCTION

The Opto-Galvanic Effect (OGE) is being increasingly used for laser spectroscopy and stabilisation, and in this paper we report three advances in the application of the OGE. Faster response stabilisation of normal band CO_2 laser lines, stabilisation of sequence band transitions and stabilisation of the CO laser.

HIGH FREQUENCY STABILISATION

In the past OGE stabilisation has been found to be most suitable as a long term (~ seconds to hours) frequency control: shorter term stabilisation having been thought to be impossible because of the OGE upper frequency limit at 2-3 kHz (Smith and Moffatt 1979). But recently (Moffatt and Smith 1981) we have shown that there is a high frequency OGE (up to 100 kHz) and we have used a fast response feedback system with time constant as short as 50 ms. Figure 1 shows the variation of the frequency output of a CO_2 laser stabilised with a 6 kHz feedback circuit. This tracing from a photograph shows a laser beat spectrum (500 kHz per division) of two similar systems as the spectrum analyser repeatedly scans over a period of 1 second; clearly the frequency jitter is less than ±500 kHz. Likewise we have found for stabilisation for periods of several hours that the frequency drift is less than 1 MHz.

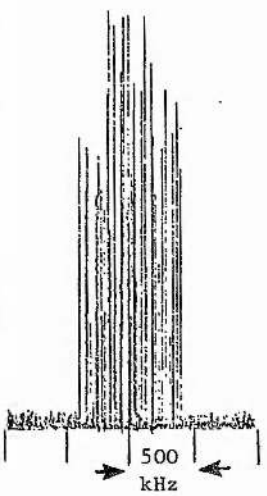

Fig.1. Spectrum analyser output with high frequency OGE (see text).

Using higher phase lock loop frequencies can result in faster cavity correction. Usually when using DC excitation laser frequency jitter (100 kHz to 1 MHz) occurs due to the ripple (~ 100 Hz) input power fluctuation perturbing the cavity refractive index. The reduction of acoustic interference (100 Hz to 1 kHz) is desirable as lasers are being used

not only in optics laboratories but also in less controlled environments where good vibrational and acoustic interference rejection is necessary. Higher phase locked loop frequencies (servosystem time constant ultimately 1 to 10 ms) should greatly reduce these power supply and environmental effects.

SEQUENCE LASER STABILISATION

Although the sequence band ($00^0 2 \rightarrow [10^0 1,\ 02^0 1]_{I,II}$) CO_2 OGE effect is only half the size of the fundamental band ($00^0 1 \rightarrow [10^0 0]_{I,II}$) effect (see Figure 2) and the sequence laser is considerably less powerful, it is of interest for spectroscopy, optical pumping, atmospheric transmission studies and vibrational temperature measurements. We have OGE stabilised a small sequence band laser on several different rotational transitions for periods of several hours and found the amplitude and frequency drift to be very similar to that achieved with the fundamental laser. Sequence band lasers are less stable than fundamental CO_2 lasers due to thermal problems associated with the intracavity hot CO_2 absorber used to suppress the ordinary transitions. Figure 3 compares the amplitude output stability of a sequence laser without stabilisation with one OGE stabilised on the P17, P21 and P23 lines in turn: the improvement is considerable.

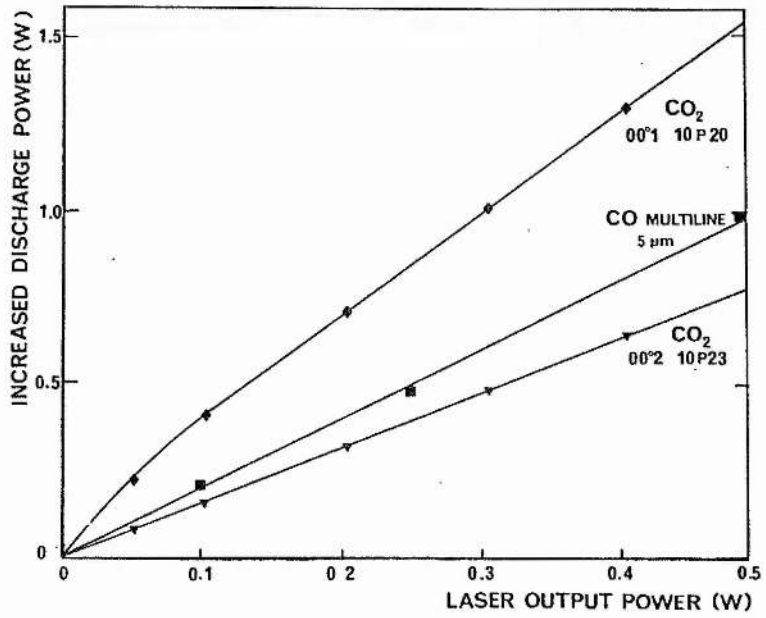

Fig.2. Comparison of size of OGE effects for different laser types (all 6% output coupling, 50 cm active discharge lengths). CO laser 25 mA in 25 torr (1.4 CO, 2.5 Xe, 21.1 He), CO_2 lasers 15 mA in 15 torr (1.0 CO_2 2.5 N_2, 1.5 Xe, 10.0 He).

CARBON MONOXIDE LASER STABILISATION

In many situations the 5-6μm CO laser is preferred to the 10-11μm CO_2 laser because it is more efficient and the laser power output varies less with cavity length fluctuations. Usually the CO laser oscillates on several vibrational-rotational lines, but true single line operation can be obtained under carefully controlled conditions (Smith and Murray 1981).

We have previously shown (Smith and Brooks 1979) that the laser induced discharge impedance change producing the OGE in carbon dioxide is due to temperature induced gas number density changes and the resulting changes of electron collision frequency and cross-section. This is unlike the traditional OGE in atomic systems which is usually assumed to be due to changes in the metastable populations and ionisation rates from relatively high-lying levels. Figure 2 shows that the OGE effect in CO is comparable to that in CO_2 and Figure 4 shows the variation of the amplitude of the OGE with laser field modulation frequency. The low frequency fall-off is attributable to the response rate of the constant current power supply being used, but the rapid decrease at ~4000 Hz is due to the photon-to-discharge impedance coupling process. These results were taken with a typical laser at 30 torr pressure and the associated total V-V-T deactivation time of the vibrational mode at 400 C due to CO collisions with CO, N_2, He and Xe is ~200μs; in good agreement with the experimental result and suggesting the photon-discharge coupling process is temperature induced as in CO_2.

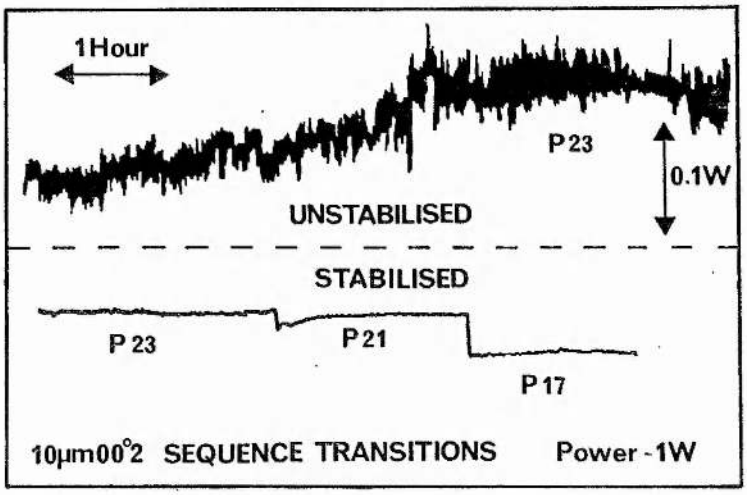

Fig.3. Comparison of stabilised and unstabilised sequence band laser output power. 50 cm discharge tube (1 t CO_2, 2.5 t N_2, 1.5 t Xe, 10 t He) and 15 cm hot cell (CO_2 400 C) in 1 m cavity (4 m full reflector, 6% plane coupler).

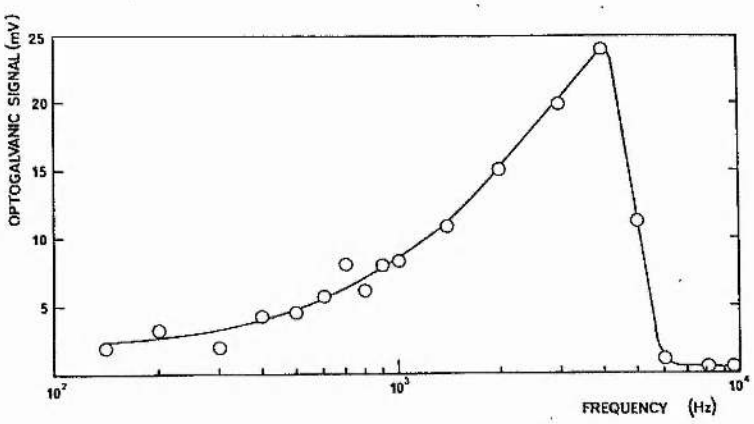

Fig.4. Effect of cavity modulation frequency on OGE discharge perturbation in CO laser. 20 mA discharge with constant current power supply (feed-back to ~400 Hz) with 160 cm cavity and 30 torr gas (0.8 CO, 1.0 Xe, 5.5 N_2, 22.8 He)

REFERENCES

Moffatt, S. and Smith, A.L.S. 1981. Opt. Comm., 37, 119-122.
Smith, A.L.S. and Brooks, M. 1979. J. Phys. D., 12, 1237-1248.
Smith, A.L.S. and Moffatt, S. 1979. Opt. Comm., 30, 213-218.
Smith, A.L.S. and Murray, G.A. 1981. Opt. and Laser Tech. in the press.